UNIVERSITY OF CALGARY

# Quaternary Structure and Sub-cellular Localization of Rat Brain $Na^+/Ca^{2+}+K^+$-exchanger, NCKX2

by

Seunghwa Sally Yoo

A THESIS

SUBMITTED TO THE FACULTY OF GRADUATE STUDIES

IN PARTIAL FULFILMENT OF THE REQUIREMENTS FOR THE

DEGREE OF DOCTOR OF PHILOSOPHY

DEPARTMENT OF BIOCHEMISTRY AND MOLECULAR BIOLOGY

CALGARY, ALBERTA

August, 2008


UNIVERSITY OF
CALGARY

## Abstract

Rat brain $Na^+/Ca^{2+}+K^+$-exchangers (NCKX2) are plasma membrane $Ca^{2+}$ transporters that play a number of important roles in mediating intracellular $Ca^{2+}$ signalling and homeostasis. They are thought to transport one $Ca^{2+}$ and one $K^+$ in exchange for four $Na^+$, the direction of the flux determined by the relative electrochemical gradients of each ion. In this thesis, the quaternary structure and the sub-cellular localization of rat brain NCKX2 were explored in detail. The isolation of detergent-resistant membranes containing lipid rafts/caveolae microdomains from whole rat brain by density floatation and subsequent co-immunoprecipitation experiments demonstrated selective localization of rat brain NCKX2 within lipid raft microdomains likely to be distinct from caveolae. The dimerization of rat brain NCKX2 driven by non-covalent interactions between exchanger monomers was observed, in addition to the formation of higher order oligomeric species with an apparent molecular weight greater than that of the exchanger dimer. The precise oligomeric state and the nature of the higher order oligomers of rat brain NCKX2 remain unclear. Several potential interacting partners of rat brain NCKX2 were identified by mass spectrometric analyses. However, these apparent interactions could not be confirmed in co-immunoprecipitation and immunoblotting experiments, thereby making it difficult to draw convincing conclusions about the physiological relevance of the interactions observed by mass spectrometry. These findings present important new discoveries about the quaternary structure and the sub-cellular localization of rat brain NCKX2, and would be helpful for further studies regarding how the structure of the exchanger relates to its transport function.

**Acknowledgements**

Completion of my degree could not have happened without dedicated, kind, and loving support of my family and friends. My parents' unyielding love and unending support, and my sister's patience and understanding helped me to find my strength and resiliency even in the darkest moments. I thank you and I love you. I would also like to extend my sincere gratitude to Jonathan, my Ph. D. supervisor, for fiercely believing in me and guiding me. Jonathan was a great supervisor, never failing to give me valuable advice in Science as well as in life. His knowledge and wisdom helped me throughout my training. Jonathan also provided me with an excellent opportunity to work with great people, who made my work in the Lytton lab highly enjoyable. They were also instrumental in providing extra help and guidance. These people included Frank Visser, Xiao-Fang Li, YiQian Wang, Jeremy Dunn, Stephen Leach, Xinjiang Cai, and Shirley Chan. I would like to thank my supervisory committee members, Drs. Wayne Chen, Julie Deans, and Mike Walsh, for their expert suggestions, constructive criticism, and helpful guidance. I also thank Dr. Andy Braun for agreeing to be the internal examiner for my thesis defence, and for having been my external examiner for my Ph. D. candidacy examination. I am grateful for Dr. Larry Fliegel from the University of Alberta, who kindly agreed to be my external examiner despite relatively short notice. I would also like to thank the Alberta Heritage Foundation for Medical Research for a valuable studentship they awarded me during the course of my training, and the University of Calgary for providing me everything else I needed to complete my study.

*To Mom, Dad, and Amy,*

*with Love.*

## Table of Contents

## List of Tables

## List of Figures

## List of Symbols, Abbreviations and Nomenclature

| | |
|---|---|
| AMPA | α-amino-3-hydroxy-5-methyl-4-isoxazolepropionic acid |
| ATP | Adenosine 5´-triphosphate |
| BAPTA | Bis-(*o*-aminophenoxy)ethane-N,N,N´,N´-tetraacetic acid |
| BES | N,N-bis(2-hydroxyethyl)-2-aminoethanesulfonic acid |
| Bistris | Bis(2-hydroxyethyl)iminotris(hydroxymethyl)methane |
| BN-PAGE | Blue-Native Polyacrylamide Gel Electrophoresis |
| BSA | Bovine serum albumin |
| $Ca^{2+}$ | Calcium |
| $[Ca^{2+}]_i$ | Intracellular $Ca^{2+}$ concentration |
| CaCA | $Ca^{2+}$/cation transporter |
| CaM | Calmodulin |
| CaMK | $Ca^{2+}$/calmodulin-dependent protein kinase |
| CBB | Coomassie Brilliant Blue |
| CBD | $Ca^{2+}$-binding domains |
| cDNA | Complementary deoxyribonucleic acid |
| cGMP | Cyclic guanosine 3´:5´-monophosphate |
| CHAPS | 3-[(3-Cholamidopropyl)dimethylammonio]-1-propanesulfonate |
| CHO | Chinese hamster ovary |
| CICR | $Ca^{2+}$-induced $Ca^{2+}$-release |
| CNS | Central nervous system |
| CuPhe | 1, 10-phenanthroline-complexed copper |
| DMSO | Dimethyl sulfoxide |
| DNA | Deoxyribonucleic acid |
| DTT | Dithiothreitol |
| EDTA | Ethylenediaminetetraacetic acid |
| eNOS | Endothelial nitric oxide synthase |
| EPSP | Excitatory postsynaptic potential |
| ER | Endoplasmic reticulum |
| EVH1 | Enabled/VASP homology-1 |
| FRET | Fluorescence resonance energy transfer |

| | |
|---|---|
| GC | Guanylyl cyclase |
| HEK-293 | Human Embryonic Kidney-293 |
| HEPES | N-(2-hydroxyethyl)piperazine-N'-2-ethanesulfonic acid |
| IgG | Immunoglobulin G |
| $IP_3$ | Inositol-1, 4, 5-trisphosphate |
| $IP_3R$ | Inositol-1, 4, 5-trisphosphate receptor |
| LC/MS/MS | Tandem mass spectrometry with a nanoscale liquid chromatography |
| LTD | Long-term depression |
| LTP | Long-term potentiation |
| MAGUK | Membrane-associated guanylate kinase |
| MAP kinase | Mitogen-activated protein kinase |
| MES | 2-(*N*-morpholino)ethanesulfonic acid |
| mGluR | Metabotropic glutamate receptors |
| MPB | Biotin maleimide |
| NAADP | Nicotinic acid adenine dinucleotide phosphate |
| NCX | $Na^+/Ca^{2+}$-exchanger |
| NCKX | $Na^+/Ca^{2+}+K^+$-exchanger |
| NCKX2-FLAG | N-terminal FLAG-tagged rat brain $Na^+/Ca^{2+}+K^+$-exchanger 2 |
| NMDA | N-methyl-D-aspartate |
| nNOS | Neuronal nitric oxide synthase |
| PBS | Phosphate buffered saline |
| PCR | Polymerase chain reaction |
| PDE | Phosphodiesterase |
| PDZ | PSD-95, Discs-large, ZO-1 |
| PF | Parallel fibre |
| PHB | Prohibitin homology domain |
| PI | Phosphatidylinositol |
| $PIP_2$ | Phosphatidylinositol 4, 5-bisphosphate |
| PKA | Protein kinase A |
| PKC | Protein kinase C |

| | |
|---|---|
| PLB | Phospholamban |
| PLC | Phospholipase C |
| PLM | Phospholemman |
| PMCA | Plasma membrane $Ca^{2+}$-ATPase |
| PMSF | Phenylmethanesulphonyl fluoride |
| PSD | Postsynaptic density |
| PSD-95 | Postsynaptic density-95 |
| RIPA | Radio-immunoprecipitation assay |
| RNA | Ribonucleic acid |
| ROC | Receptor-operated channels |
| ROS | Rod outer segment |
| RT-PCR | Reverse-transcription-coupled polymerase chain reaction |
| RyR | Ryanodine receptor |
| SAP-90 | Synapse-associated protein 90 |
| SDS | Sodium dodecyl sulfate |
| SDS-PAGE | Sodium dodecyl sulfate polyacrylamide gel electrophoresis |
| SERCA | Sarco-endoplasmic reticulum $Ca^{2+}$-ATPase |
| SH3 | Src Homology 3 |
| siRNA | Small interfering ribonucleic acid |
| SLC | Solute carrier |
| SLN | Sarcolipin |
| SNP | Single nucleotide polymorphism |
| SOC | Store-operated channels |
| SR | Sarcoplasmic reticulum |
| SynGAP | Synaptic Ras GTPase-activating protein |
| TfR | Transferrin receptor |
| TM | Transmembrane |
| Tris | Tris(hydroxymethyl)aminomethane |
| TRPC | Transient receptor potential channel |
| VGCC | Voltage-gated $Ca^{2+}$ channel |
| XIP | Exchanger inhibitory peptide |

*"...that is, that man everywhere and at all times, whoever he may be, has preferred to act as he chose and not in the least as his reason and advantage dictated. And one may choose what is contrary to one's own interests, and sometimes one positively ought (that is my idea). One's own free unfettered choice, one's own caprice, however wild it may be, one's own fancy worked up at times to frenzy - is that very 'most advantageous advantage' which we have overlooked, which comes under no classification and against which all systems and theories are continually being shattered to atoms... What man wants is simply independent choice, whatever that independence may cost and where it may lead. And choice, of course, the devil only knows what choice."*

***Fyodor Dostoyevsky***

# CHAPTER ONE

## Literature Review and Introduction

## 1.1 Intracellular Calcium Homeostasis and Signalling

Calcium ($Ca^{2+}$) is one of the most ubiquitous and versatile intracellular signaling molecules and is known to regulate diverse cellular processes, such as fertilization, proliferation, secretion, muscle contraction, neuronal function, retinal light transduction, vesicle trafficking, and apoptosis (13-15, 229). In all cases the $Ca^{2+}$ signalling process is triggered by a rise in the intracellular $Ca^{2+}$ concentration ($[Ca^{2+}]_i$). That this seemingly simple process can give rise to such a wide variety of events depends on the different sensitivity of cells to complex spatial and temporal information, as well as the speed and amplitude of the $Ca^{2+}$ signals. Hence, it is essential for cells to adopt various mechanisms to maintain adequate $Ca^{2+}$ homeostasis, thus preventing unwanted signals and protecting them from toxic $Ca^{2+}$ overload. Unlike other second messengers and signalling molecules, $Ca^{2+}$ is not metabolized. Therefore, any $Ca^{2+}$ that enters the cytoplasm during a given signalling event must be removed from the cytoplasm to maintain homeostasis. A range of specialized $Ca^{2+}$ transport systems in the plasma membrane, the endoplasmic reticulum/sarcoplasmic reticulum (ER/SR), and mitochondria are responsible for precisely controlling the intracellular $Ca^{2+}$ concentration. These systems, along with many related secondary signalling cascades and effector molecules, account for the incredible specificity and versatility of $Ca^{2+}$ signalling. $Na^+/Ca^{2+}$ -exchangers, located in the plasma membranes of most cells, are key players in intracellular $Ca^{2+}$ homeostasis, actively transporting $Ca^{2+}$ ions out of the cytoplasm to the extracellular environment in response to the rise in $[Ca^{2+}]_i$. One particular member of this multigene family, the $K^+$-

dependent $Na^{+}/Ca^{2+}$-exchanger, NCKX2, which is abundantly expressed in brain neurons, is the subject of this thesis.

### *1.1.1 Key Players in Intracellular $Ca^{2+}$ Homeostasis*

There are a wide range of $Ca^{2+}$ handling proteins that perform specialized functions and display distinctive expression patterns and characteristic sub-cellular localization (12, 14, 15). These include the $Ca^{2+}$ channels and pumps found in the plasma membrane and in the membranes of the intracellular organelles such as ER/SR or mitochondria, $Ca^{2+}$ transporters/exchangers, and cytosolic $Ca^{2+}$ binding proteins. $Ca^{2+}$ channels, pumps, and transporters are primarily involved in generating and/or terminating a particular $Ca^{2+}$ signal by the opening and closing of their pores, thereby allowing the movement of $Ca^{2+}$ ions across the membrane. The opening/closing of these channels, pumps, and transporters can be regulated by changes in membrane potential, ligand binding, intracellular store emptying, or by second messenger molecules like inositol-1, 4, 5-trisphosphate ($IP_3$) (14, 15). A $Ca^{2+}$ signal generated by these mechanisms is then recognized by various $Ca^{2+}$ sensitive processes, which translate this signal into appropriate cellular responses. Cytosolic $Ca^{2+}$ binding proteins mainly act as sensor and effector molecules whose functions are tightly regulated by their direct interaction with $Ca^{2+}$ ions. Some of these $Ca^{2+}$ binding proteins are also known to be effective as intracellular $Ca^{2+}$ buffers, keeping $[Ca^{2+}]_i$ at its normal, sub-μM range with their high-affinity $Ca^{2+}$ binding sites.

In electrically excitable cells, voltage-gated $Ca^{2+}$ channels (VGCCs) are the major routes for $Ca^{2+}$ entry from the extracellular environment. This is a large family with distinctive pharmacological, biophysical, and regulatory properties, and includes the L-type channels found in cardiac myocytes and the P/Q-type channels found in neurons (35, 68, 124, 243). VGCCs exist as heteromers composed of a pore-forming α subunit and auxiliary β, $\alpha_2\delta$, and γ subunits. These auxiliary subunits act as regulators of VGCC function. Varying combinations of different α and auxiliary subunit isoforms further contribute to the diversity and heterogeneity of the VGCC family, implying that different types of cells may require a distinct VGCC to oversee a specific function.

In addition to the VGCC that sense changes in membrane potential, another family of $Ca^{2+}$ channels respond to the presence of specific ligands/agonists. These receptor-operated $Ca^{2+}$ channels (ROC) are comprised of functionally and structurally diverse non-specific cation channels, such as the N-methyl-D-aspartate (NMDA) receptors found in neuronal dendritic spines (21, 54, 73). The NMDA receptor belongs to a family of ionotropic glutamate-gated receptor channels, and is the primary $Ca^{2+}$ influx mechanism in many excitatory glutamatergic postsynapses of the central nervous system (CNS). $Ca^{2+}$ that enters the postsynaptic dendritic spine through the NMDA receptor is known to assume critical roles in modulating synaptic plasticity and excitatory synaptic transmission (21, 54). Purinergic (P2) receptors that bind to the extracellular nucleotides are another example of ROC (31, 147). These receptors are divided into two classes, the G protein-coupled P2Y receptors and the ionotropic P2X receptors, which are further divided into several subclasses (147). The metabotropic P2Y receptors are activated by

ATP and other naturally occurring nucleotides, and the activated P2Y receptors have been found to regulate a large variety of neuronal ion channels including the VGCC and $K^+$ channels (116). The P2X receptors, upon ATP-binding, undergo a rapid conformationcal change that allows the passage of $Ca^{2+}$ and other monovalent cations through the channel pore, resulting in membrane depolarization (213). The various purinergic receptor subtypes are widely distributed throughout the CNS, smooth muscle, endothelium, and immune cells. It is now well documented that in the mammalian CNS, P2 receptors carry out many important functions, from fast synaptic transmission, the release of neurotransmitters, differentiation and neurite growth (31, 116, 222).

Another type of $Ca^{2+}$ channel located in the plasma membrane senses the depletion of $Ca^{2+}$ from the internal stores associated with the ER/SR. The opening of such store-operated channels (SOC) causes an influx of $Ca^{2+}$ from the extracellular environment, which is then used to refill the depleted internal $Ca^{2+}$ stores (166, 211). Although SOCs and the associated $Ca^{2+}$ current through the plasma membrane are believed to be essential to a number of cellular processes, including the majority of signalling cascades found in sensory neurons, the precise identity of the SOC and the mode of its activation still remain elusive. Recently, the Orai family has emerged as the best molecular candidate for an essential component of the SOC, while the STIM (stromal interaction molecule) family of proteins appear to be essential for the ER/SR signal leading to activation of SOC (179, 237). STIM, a single spanning membrane protein found in the ER, senses ER luminal [$Ca^{2+}$], and through reorganization and clustering, it transduces information directly to the plasma membrane. Orai is a four

transmembrane spanning protein found in the plasma membrane and is thought to function as a $Ca^{2+}$ selective channel that is gated through its interaction with the store-activated ER $Ca^{2+}$ sensor (105).

Transient receptor potential (TRP) cation channels are six transmembrane spanning proteins expressed in almost all tissues and cell types, and comprise a diverse group of non-selective $Ca^{2+}$ permeable channels that bear structural similarities to *Drosophila* TRP channels (48, 195, 212). The TRP superfamily is divided into seven subfamilies based on their sequence homology and functional similarities, and display varying degrees of $Ca^{2+}$ conduction specificity over other monovalent cations. Different TRP channels also appear to be activated by distinct mechanisms, which include pathways that engage phospholipase C (PLC), binding of diacyl glycerol (DAG), lipid mediators (arachidonic acid), mechanical stimuli, and store depletion (195). Although a single defining characteristic of TRP channel function has not yet identified, they are known to play critical roles in sensory physiology, especially in the perception of a wide range of physical and chemical stimuli (195). However, whether TRP proteins are components of SOC, and their relation to recently discovered Orai/STIM, still remain highly controversial issues.

$Ca^{2+}$ is released from intracellular stores like the ER/SR by the action of specialized intracellular $Ca^{2+}$ release channels such as the inositol-1, 4, 5-trisphosphate receptor ($IP_3R$) and the ryanodine receptor (RyR) (71, 73, 283). $IP_3R$ is the predominant intracellular $Ca^{2+}$ release channel in non-excitable and secretory cells, and is activated by

the binding of $IP_3$ generated during a G-protein coupled receptor signalling event. Once $IP_3$ is bound, $IP_3R$ permits the flow of $Ca^{2+}$ down its concentration gradient from the ER to the cytoplasm, thereby rapidly increasing $[Ca^{2+}]_i$. Three isoforms of $IP_3R$ have been identified (type-1, -2, and -3 $IP_3R$), each with different $IP_3$ binding affinity. Among these, $IP_3R1$ is the most widely expressed and is found in all tissues and all developmental stages (192). The RyR is a large homotetrameric protein expressed in almost all cell types, and is the primary intracellular $Ca^{2+}$ release channel in striated muscles where it is most densely populated (71). Three RyR isoforms (RyR1, 2, and 3) are expressed in mammals, with a distinct isoform-dependent and tissue-specific expression pattern and equally distinct modes of activation (71, 283, 307). RyR1 is the predominant isoform expressed in skeletal muscles, where its activity is directly coupled to the skeletal muscle voltage-sensor, voltage-gated L-type $Ca^{2+}$ channels. The skeletal muscle L-type $Ca^{2+}$ channel forms a physical protein-protein contact with the large cytoplasmic domain of the underlying RyR1 within a narrow gap between the plasma membrane and the SR membrane, such that every other RyR1 is associated with four L-type $Ca^{2+}$ channels in a cluster. Depolarization of the cell membrane causes conformational changes in the L-type $Ca^{2+}$ channel and ultimately leads to the activation of RyR1 (71). RyR2 is the major isoform in cardiac muscle, but unlike RyR1 in skeletal muscles, physical protein-protein contact with the L-type $Ca^{2+}$ channel is not important for the activation of RyR2. Instead, RyR2 in cardiac muscles is activated by $Ca^{2+}$ entering the cytoplasm through the action of L-type $Ca^{2+}$ channels in a process known as $Ca^{2+}$-induced $Ca^{2+}$-release (CICR) (Figure 1-1) (14, 71, 256, 283).

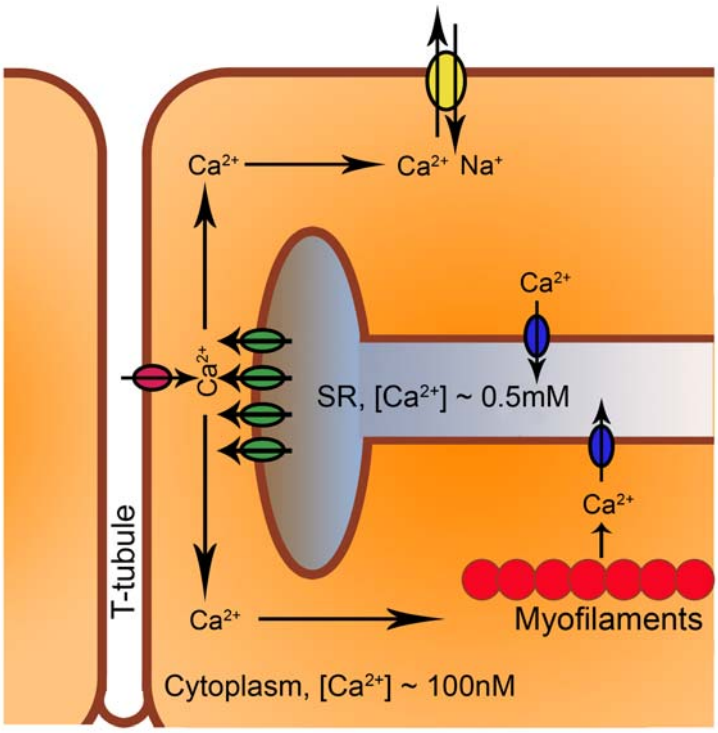


**Figure 1-1. $Ca^{2+}$ Signalling and E-C Coupling in Cardiac Ventricular Myocytes.** The depolarization of the ventricular sarcolemma causes the influx of $Ca^{2+}$ ions through the VGCC (purple) located in the T-tubule, increasing $[Ca^{2+}]_i$ in the dyadic junction enough to initiate CICR. Opening of RyR2 (green) in the jSR by a CICR mechanism then allows even more $Ca^{2+}$ ions to be released from the SR. This released $Ca^{2+}$ diffuses toward and binds to the contractile machinery (troponin C) and myocyte contraction begins. During the relaxation period, bound $Ca^{2+}$ is released and either pumped back to the SR by the action of SERCA (blue) or transported out of the myocyte by NCX (yellow) located in the sarcolemma away from the dyadic junction.

In addition to the ER/SR, other sites for the intracellular storage and release of $Ca^{2+}$ have been described. These storage sites include the mitochondria, the nucleus, and various acidic compartments such as lysosomes (260). Mitochondria are thought to act as passive $Ca^{2+}$ sinks, sequestering $Ca^{2+}$ upon its release from the ER or its influx from the extracellular environment, and slowly releasing $Ca^{2+}$back to the cytoplasm once the initial signal has been terminated. The role of the mitochondria as a $Ca^{2+}$ sink is apparent in cardiac myocytes, where the mitochondrial $Ca^{2+}$ level oscillates in response to the cellular $Ca^{2+}$ spikes required for muscle contraction (257). Mitochondria may also perform a spatial buffering role in cells, preventing potential global $[Ca^{2+}]_i$ rises from entering regions rich in mitochondria (224). $Ca^{2+}$ uptake plays a number of roles inside the mitochondria, since some of the metabolic enzymes and metabolite carries within the mitochondria require $Ca^{2+}$ for their activity (260). Although much attention has been directed toward investigations into the mechanisms of nuclear $Ca^{2+}$ regulation, there is still controversy concerning both the source and the nature of the $Ca^{2+}$ signals occurring in the nucleoplasm (1, 24). The nuclear envelope contains the same pumps and channels present in the ER/SR. Whether uptake and release can be triggered independently via signals from the nuclear side of the envelope is controversial. It does appear, however, that the nuclear envelope may slow down the propagation of an intracellular $Ca^{2+}$ wave into the nucleus, thereby generating a domain of lower $[Ca^{2+}]_i$ in the nucleus (1). The physiological role of nuclear $Ca^{2+}$ seems to vary in different cell types, but it has been proposed that nuclear $Ca^{2+}$ is involved in specific processes such as gene transcription, development, and protein transport across the nuclear envelop (1). Acidic compartments like lysosomes and lysosome-like granules have been identified as intracellular $Ca^{2+}$

stores which are only sensitive to nicotinic acid adenine dinucleotide phosphate (NAADP) (46). NAADP is one of the key second messengers that initiates the mobilization of intracellular $Ca^{2+}$ in various cell types (234, 259). However, the molecular nature of the NAADP-sensitive $Ca^{2+}$ uptake and release mechanisms in these acidic compartments are not well understood at this moment.

While these various $Ca^{2+}$ channels are all involved in the initiation of the $Ca^{2+}$ signalling cascade by increasing $[Ca^{2+}]_i$, $Ca^{2+}$ pumps and exchangers actively clear the cytoplasm of the $Ca^{2+}$ introduced during the initiation event. These $Ca^{2+}$ pumps and exchangers include plasma membrane $Ca^{2+}$-ATPase (PMCA) and $Na^{+}/Ca^{2+}$-exchanger (NCX) in the plasma membrane, and sarco/endoplasmic reticulum $Ca^{2+}$-ATPase (SERCA) in the ER/SR. PMCA is the primary $Ca^{2+}$ efflux mechanism in a variety of cell types. In non-excitable cells, it is often the only $Ca^{2+}$ extrusion system, whereas in excitable cells it shares this role with NCX (314). Four different isoforms of PMCA are encoded by four different genes, with tissue specific patterns of expression (28). PMCA1 and PMCA4 are expressed in almost all cells and tissues at similar levels, while PMCA2 and PMCA3 have more restricted patterns of expression. Recent studies using knockout mice have also established unique roles for PMCA genes in, among other things, hearing, cerebellar function, and sperm motility (28). SERCA pumps $Ca^{2+}$ ions released to the cytoplasm by the opening of RyR or $IP_3R$ back to the internal store, and, just like RyR, its isoform expression is highly tissue-specific: SERCA1a is mainly expressed in fast twitch skeletal muscles, SERCA2a in cardiac muscles, SERCA2b is ubiquitously expressed in all cells, and SERCA3 in non-muscle cells including platelets (76, 256). PMCA and

SERCA belong to the P-type ATPase family of proteins that utilize the energy stored in ATP to transport ions against their electrochemical gradient. PMCA pumps one $Ca^{2+}$ ion out of the cell during each ATP hydrolysis cycle, whereas SERCA transports two $Ca^{2+}$ ions back to the ER/SR per ATP molecule hydrolyzed (76, 227, 314). The crystal structures of some of the P-type ATPases have been determined (217, 226), amongst which that of SERCA has been most extensively studied (217, 218, 284, 292-295), allowing a glimpse into the exquisite details and precise workings of the pump.

Unlike PMCA, which has high $Ca^{2+}$ affinity but relatively low turnover rate (~100 $Ca^{2+}$ ions per second), plasma membrane $Na^{+}/Ca^{2+}$-exchangers display low $Ca^{2+}$ affinity, but a much faster rate of transport - a property highly valuable to a system that needs to clear large amounts of $Ca^{2+}$ very quickly, such as in electrically excitable cells (23). The mammalian $Na^{+}/Ca^{2+}$-exchanger is comprised of two different families: the $K^{+}$-independent $Na^{+}/Ca^{2+}$-exchanger (NCX) and the $K^{+}$-dependent $Na^{+}/Ca^{2+}$-exchanger (NCKX) families. The cardiac isoform of NCX (NCX1) and NCKX1 from bovine rod photoreceptors are by far the most extensively studied exchangers in each family (23, 263). These proteins will be discussed in further detail in the following section.

There are more than 200 cytosolic $Ca^{2+}$ binding proteins encoded by the human genome, a plethora that emphasizes the importance of such proteins in normal cellular functions (14). These $Ca^{2+}$ binding proteins are divided into two general classes: $Ca^{2+}$ buffers and $Ca^{2+}$ sensors/effectors (90, 97). Intracellular $Ca^{2+}$ buffers bind to $Ca^{2+}$ ions that enter the cell during the initiation of a signalling event, leaving only a small fraction

of free $Ca^{2+}$ ions available in the cytoplasm and thereby preventing a toxic $Ca^{2+}$ overload. Some well-known cytosolic $Ca^{2+}$ buffers include calbindin and parvalbumin, members of the EF-hand family of $Ca^{2+}$ binding proteins responsible for shaping $Ca^{2+}$ transients in many cell types, including fast-twitch muscles and the Purkinje neurons of the CNS (97, 271). Calreticulin and calsequestrin are major ER/SR $Ca^{2+}$ buffering chaperones that are not only involved in ER/SR luminal $Ca^{2+}$ handling, but are also responsible for aiding proper folding of ER/SR proteins during their synthesis (96). $Ca^{2+}$ sensors and effectors link the chemical signal of elevated $[Ca^{2+}]_i$ to a wide range of biochemical responses, such as $Ca^{2+}$ sensitive enzymatic processes (protein kinase C), muscle contraction (troponin C), neurotransmitter release (synaptotagmin), and gene expression (cAMP-response element binding-binding protein, CREB-binding protein). For example, calmodulin (CaM), one of the most well known $Ca^{2+}$ sensors, undergoes a pronounced conformational change upon the binding of $Ca^{2+}$ to its four EF-hand motifs, which then activates various downstream effectors like $Ca^{2+}$/calmodulin-dependent protein kinase (CaMK) (14, 15).

Altogether, the presence of a vast range of distinctive $Ca^{2+}$ handling proteins conveys the vigilance of cells in maintaining proper $Ca^{2+}$ homeostasis. Moreover, by selectively expressing certain types of proteins and confining those involved in a similar signalling pathway within a small microdomain, cells are able to discern various different $Ca^{2+}$ signals and correctly interpret them to produce appropriate $Ca^{2+}$-dependent cellular processes. Given the universality of $Ca^{2+}$ as a signalling molecule, such ability is

essential for proper cellular function, as will be clearly demonstrated by the description of $Ca^{2+}$ handling in cardiac myocytes and neuronal cells in the following sections.

### *1.1.2 Calcium Homeostasis and Signalling in Cardiac Myocytes*

The importance of proper $Ca^{2+}$ homeostasis is perhaps most thoroughly documented in the electrical activity of the mammalian heart, in which $Ca^{2+}$ is not only directly involved in the shaping of the action potential, but is also a key activator of the contractile myofilaments (12, 14, 16, 184, 283, 308). Indeed, numerous pieces of evidence accumulated over time suggest that abnormal fluctuations in $[Ca^{2+}]_i$ and/or the handling of intracellular $Ca^{2+}$ play a major role in the development of human heart failure (39). Cardiac excitation-contraction coupling (E-C coupling) refers to the process in which the electrical excitation of myocytes leads to the contraction of a heart (16). Mammalian ventricular myocytes, unlike those of other species, are distinguished by an extensive transverse tubule (T-tubule) system that allows effective $Ca^{2+}$ signalling by forming a network of membranes within the myocytes, thereby positioning various $Ca^{2+}$ handling proteins in close proximity to one another (Figure 1-1) (283). In addition, the membranes of the SR (junctional SR, jSR) are juxtaposed with the T-tubule. Together they form a membrane structure known as the dyadic junction, where the $Ca^{2+}$ signal is mobilized and contraction is triggered. This rather peculiar structural organization of the T-tubule and jSR in the ventricular myocyte is responsible for the successful synchronization of $Ca^{2+}$ release within the myocytes and the unified contraction of the ventricle, as described below in detail (Figure 1-1).

At rest, $[Ca^{2+}]_i$ in the ventricular myocyte is maintained at around 100nM (15). Upon depolarization of the sarcolemma, VGCCs located in the T-tubule membrane open and allow an influx of $Ca^{2+}$ ions from the extracellular environment. This results in a small increase in $[Ca^{2+}]_i$ in the dyadic junction, which, in turn, triggers the underlying SR $Ca^{2+}$ release channels, RyR2, to release a much larger amount of $Ca^{2+}$ from the SR via a $Ca^{2+}$-induced $Ca^{2+}$-release (CICR) mechanism (16, 308). CICR elevates the global $[Ca^{2+}]_i$ to approximately 1.0μM, the released $Ca^{2+}$ binding to troponin C in the myofilaments and activating myocardial contraction. Muscle relaxation is initiated by the dissociation of bound $Ca^{2+}$ from troponin C followed by its removal from the cytoplasm. The majority of the $Ca^{2+}$ signal is actively pumped back into the SR by the action of SERCA distributed over the non-junctional regions of the SR, whereas the $Ca^{2+}$ that entered the cytoplasm through VGCCs is transported back to the extracellular milieu by NCX (Figure 1-1) (12, 14, 16, 39). In ventricular myocytes, NCX, and not PMCA, is the primary $Ca^{2+}$ extrusion system found in the sarcolemma (23, 115, 263, 303).

### *1.1.3 Calcium Homeostasis and Signalling in Neurons*

In neurons, $Ca^{2+}$ ions are responsible for carrying out a large variety of highly specific and localized functions, such as remodelling of the synaptic organization, changes in synaptic plasticity, gene expression, and the release of neurotransmitters. Neurons are distinguished by a highly polarized morphology that includes spiny/aspiny dendrites, a cell body (soma), an axon, and presynaptic axonal terminals. This distinctive geometry gives neurons a spatial advantage that allows them to exquisitely decipher and compartmentalize different types of $Ca^{2+}$ signal, depending on where these signals are

initiated, how far they travel within a neuron, and how close the $Ca^{2+}$ channels are to the various $Ca^{2+}$ sensors/effectors found throughout the neuron (5, 12, 22, 57).

At the presynaptic axonal terminal, $Ca^{2+}$ entry to the cytoplasm through VGCC is essential in regulating neurotransmitter release. These $Ca^{2+}$ channels open rapidly upon depolarization of the membrane, and the resulting $Ca^{2+}$ influx is immediately coupled to vesicle fusion, releasing neurotransmitters into the synaptic cleft with only microseconds of delay after the initial elevation of the local $[Ca^{2+}]_i$ in the presynaptic terminal (175). This short delay is possible because the $Ca^{2+}$ sensors that trigger vesicle fusion and neurotransmitter release are located proximally to the $Ca^{2+}$ channels. Synaptotagmin, a protein with a single transmembrane domain and two high affinity $Ca^{2+}$ binding domains, is the $Ca^{2+}$ sensor for the rapid and synchronous release of neurotransmitters from the active zone in the presynaptic terminal, where neurotransmitter containing vesicles are docked at and/or hemifused with the plasma membrane, ready to undergo membrane fusion upon receiving a proper signal (56, 175, 255). Synaptotagmin interacts with membrane phospholipids in a $Ca^{2+}$-dependent manner, coupling the rise in local $[Ca^{2+}]_i$ to neurotransmitter release. However exactly how $Ca^{2+}$-bound synaptotagmin and its interaction with membrane phospholipids facilitates the fusion and eventual release of neurotransmitters is not fully understood. It appears that by binding to phospholipids, the $Ca^{2+}$-bound synaptotagmin displaces complexin, a component of the SNARE complex that serves to clamp the vesicles in the hemifused state at the active zone (92, 175, 290). Displacing complexin seems to “unlock” those vesicles from the hemifused state so that the final fusion process can proceed and the neurotransmitters can be released.

The formation of similar $Ca^{2+}$ microdomains is also apparent in postsynaptic dendritic spines. Dendritic spines are small, mushroom-shaped compartments extending from the dendritic shaft and form the receiving ends of almost all excitatory synapses in the mammalian CNS (132, 262). They contain a variety of intracellular organelles, including elements of actin-based cytoskeletons, mitochondria, and smooth ER, providing them with the means necessary to function as independent and semiautonomous units (132). A typical presynaptic axonal terminal forms a synapse with only one or two of the many dendritic spines of a postsynaptic neuron, thus allowing an individual postsynaptic neuron to communicate with virtually thousands of different presynaptic neurons (97). Therefore, the spines represent basic units of neuronal signal integration in which separate and independent $Ca^{2+}$ signalling events can be observed taking place in each spine almost all the time, displaying different time courses and amplitudes, and dictating different functional outcomes within a neuron (21, 22).

The channels and receptors involved in $Ca^{2+}$ influx are localized in the postsynaptic dendritic spines within a region known as the postsynaptic density (PSD) (Figure 1-2), which is visible under the electron microscope as an electron-dense thickening of the postsynaptic membrane (132). PSDs are directly juxtaposed with the active zone of the presynaptic axonal terminal, and occupy around 10% of the spine surface (21). Gathering evidence indicates that in addition to the channels and receptors, PSDs assemble a complex of signalling molecules and $Ca^{2+}$ sensors/effectors that influence the function of these channels and receptors. The protein-protein interactions in

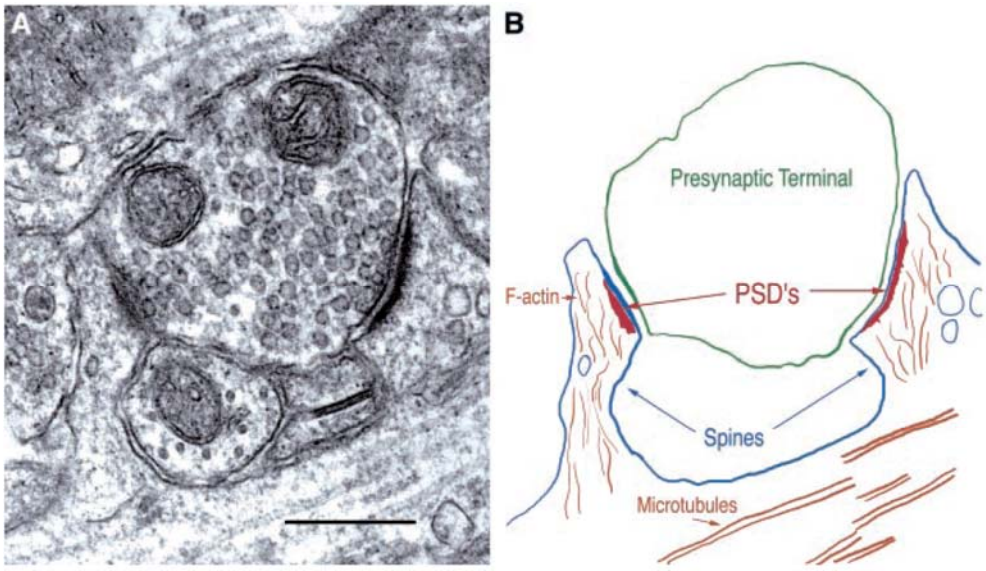


**Figure 1-2. Postsynaptic Densities (PSDs) of the Postsynaptic Dendritic Spines.** (A) A presynaptic axonal terminal is shown at the centre which is forming glutamatergic synapses with two postsynaptic dendritic spines. Little vesicles containing glutamate are observed clustering at the site of synaptic contact. Scale bar = 400nm. (B) Tracing of (A) identifying the synaptic structures observed including actin cytoskeletons and microtubules. The figure is taken from (132).

PSDs are mediated by several scaffolding proteins that maintain these signalling complexes, localizing individual $Ca^{2+}$ signalling events within the dendritic spines (132).

A major PSD scaffolding protein is postsynaptic density-95 (PSD-95), a member of the membrane-associated guanylate kinase (MAGUK) family which comprises four closely related proteins: PSD-95/SAP-90 (synapse-associated protein 90), PSD-93/chapsyn-110, SAP102 and SAP97 (132, 137). These proteins are characterized by five protein-interaction domains, including three amino-terminal PDZ (PSD-95, Discs-large, ZO-1) domains followed by a Src Homology 3 (SH3) domain and a guanylate kinase-like (GK) domain homologous to yeast guanylate kinase, but lacking enzymatic activity (21, 132, 137). The first two PDZ domains of PSD-95 are known to bind tightly to the C-terminal tail of one of the subunits of the NMDA receptor (151, 210). In addition, other synaptic proteins, such as neuronal nitric oxide synthase (nNOS) and synaptic Ras GTPase-activating protein (SynGAP), the function of which is regulated by cytosolic $Ca^{2+}$, are thought to interact with the remaining PDZ domains of PSD-95, thereby localizing those proteins in close vicinity to the NMDA receptors (27, 41, 138). Moreover, PSD-95 is also able to oligomerize by N-terminal “head-to-head” interactions, a self-association which would enhance the clustering of its interaction partners (137).

Homer, another scaffolding protein of the PSD first identified as an immediate early gene dynamically responsive to synaptic activity, is known to interact with the G-protein coupled metabotropic glutamate receptors (mGluR) (26). The Homer family of proteins contain an N-terminal enabled/VASP homology (EVH1) domain that recognizes

a -P-P-X-X-F- motif and a C-terminal coiled-coil domain that mediates self-multimerization. The C-terminal domain is absent in the original immediate-early gene form of Homer (Homer 1a) (311). Homer proteins in the PSD act as tethers that physically connect mGluRs with the underlying $IP_3R$, promoting the localization of $Ca^{2+}$ signalling complexes. Homers are also known to interact with a number of other $Ca^{2+}$ signalling proteins, such as TRPC channels, RyRs, and some of the L-type $Ca^{2+}$ channels in the PSD (311). Scaffolding proteins of the PSD like PSD-95 and Homer therefore form essential elements that effectively organize $Ca^{2+}$ microdomains within the postsynaptic dendritic spines to maximize the efficiency of the various $Ca^{2+}$ signals observed at these sites.

$Ca^{2+}$ enters the cytoplasm of the postsynaptic dendritic spine through three different pathways depending on the type of neuron and the manner in which the spine membrane of a particular neuron is depolarized: VGCC, NMDA receptors, and from intracellular stores via $IP_3R$ (22). VGCCs, and especially the high-voltage activated P/Q-type $Ca^{2+}$ channels, are the primary $Ca^{2+}$ influx mechanism in the spines of the Purkinje neurons of the mammalian cerebellum (269). The opening of these $Ca^{2+}$ channels requires α-amino-3-hydroxy-5-methyl-4-isoxazolepropionic acid (AMPA) type receptor-mediated membrane depolarization (67). AMPA receptors open to allow $Na^{+}$ influx in response to binding of the neurotransmitter glutamate released from parallel fibres (PF) that form synapses with spines of Purkinje neurons (Figure 1-3).

**Figure 1-3. Postsynaptic $Ca^{2+}$ Signalling in Purkinje Neurons.** Upon activation of parallel fibres that forms synapses with spines of Purkinje neurons, the neurotransmitter glutamate (black dots) is released, which binds and activates the AMPA receptor (red). Opening of the AMPA receptor causes the influx of $Na^{+}$ down its electrochemical gradient, which results in postsynaptic membrane depolarization as indicated in the cartoon. VGCC (purple) opens its pore in response to the membrane depolarization, allowing $Ca^{2+}$ ions to enter the cytoplasm of the postsynaptic dendritic spine. $[Ca^{2+}]_i$ is also raised by the action of mGluR1 (pink). Glutamate binding to mGluR1 causes activation of the G-protein (dark grey), which in turn stimulates the plasma membrane bound PLC (sky blue) to produce the soluble intracellular messenger $IP_3$. $IP_3$ then diffuses across the cytoplasm and binds $IP_3R$ (green) located in the ER, resulting in the release of $Ca^{2+}$ from the intracellular stores. The rise in $[Ca^{2+}]_i$ in the dendritic spine does not contribute to the global increase in $[Ca^{2+}]_i$, but rather has a local effect, such regulation of the AMPA receptor density at the spines, or modulation of long-term depression and long-term potentiation of excitatory synaptic transmission. $Ca^{2+}$ extrusion mechanisms such as NCX (yellow), PMCA (orange), and SERCA (blue) are also available to bring the elevated $[Ca^{2+}]_i$ back to its resting level.

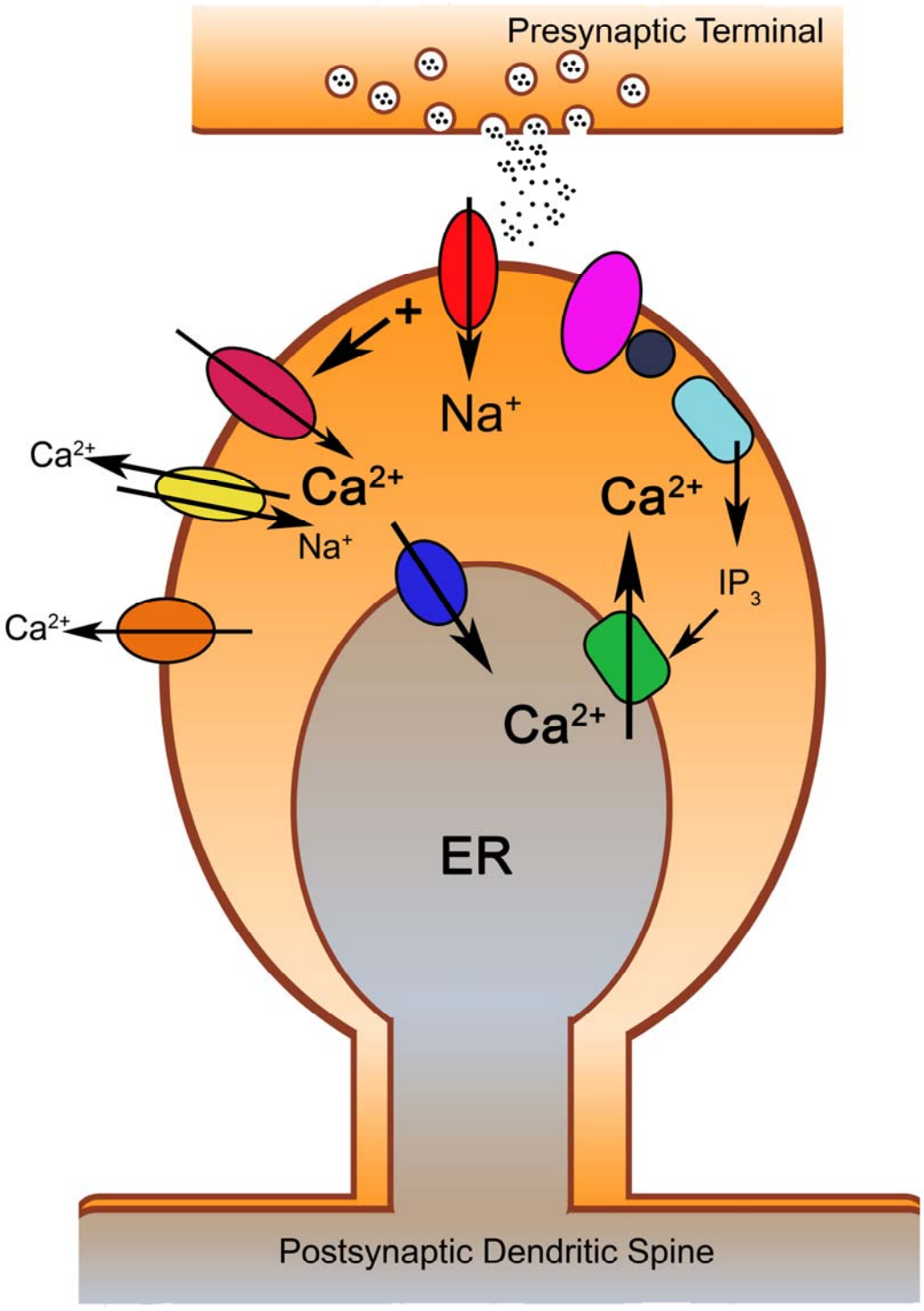
Presynaptic Terminal
+
Na+
Ca2+
Ca2+
Na+
Ca2+
Ca2+
IP3
Ca2+
ER
Postsynaptic Dendritic Spine

The observation that the expression of mGluR1 is particularly high at the PF synapses of Purkinje neurons (289) suggests that the transient increase in $[Ca^{2+}]_i$ observed there without changes in the membrane potential is due to the activation of mGluR1 by glutamate. So activated, mGluR1 produces $IP_3$, which diffuses to and opens the $IP_3R$, causing $Ca^{2+}$ release from the ER (Figure 1-3). Interestingly, the rise in $[Ca^{2+}]_i$ in the spines of the Purkinje neurons caused by the activation of VGCC or the $IP_3R$ does not contribute to the propagation of electrical signals through the dendrites and cell body, and is therefore strictly non-electrical in its impact (67). The potential role of these local postsynaptic $Ca^{2+}$ signals induced by the activation of mGluR1 or VGCC include the regulation of AMPA receptor density at the spines and modulating the long-term depression (LTD) and the long-term potentiation (LTP) of excitatory synaptic transmission important for motor learning and memory formation (150).

NMDA receptors, one of the most abundant proteins found in PSDs, are the major $Ca^{2+}$ influx mechanism of many excitatory postsynaptic dendritic spines in the mammalian CNS, including neurons of the hippocampus in which the NMDA receptor mediated $Ca^{2+}$ signalling pathway and the formation of a multi-molecular signalling complex is essential for changes in synaptic plasticity and long-term potentiation (LTP) (132). The opening of the NMDA receptors requires strong membrane depolarization, provided by the activation of the AMPA-type receptors, to relieve the voltage-sensitive block by extracellular $Mg^{2+}$, along with the binding of glutamate (97). Once open, the $Ca^{2+}$ that flows through the NMDA receptors acts on several different $Ca^{2+}$ effector molecules, such as $Ca^{2+}$/calmodulin-dependent protein kinase II (CaMKII), synGAP, and

nNOS which reside in the PSD by virtue of their interaction with the scaffolding protein PSD-95 (Figure 1-4).

CaMKII, a multifunctional serine/threonine kinase, is the most abundant signalling molecule found in the PSD, and is a primary target for $Ca^{2+}$ entering through the NMDA receptor (50). Several pieces of evidence suggest that CaMKII interacts with the cytosolic tails of the NMDA receptor subunit, thereby providing the docking sites for CaMKII in the PSDs (11, 164, 285). Interestingly, the activation of CaMKII also increases the affinity of CaMKII for NMDA, conferring a potential positive feedback mechanism and implying a role for CaMKII activation in the generation of LTP (164). Once activated, CaMKII plays diverse roles in regulating the NMDA receptor mediated $Ca^{2+}$ signalling pathways, which include phosphorylation of AMPA-type receptors and inhibition of SynGAP (50, 132).

SynGAP, another major component of PSDs in hippocampal neurons, is a synaptic GTPase-activating protein for Ras. It is known to interact with each of the three PDZ domains of PSD-95 through its C-terminal -Q-T-R-V motif, thereby positioning itself closely to the GTP-bound form of Ras, which it inactivates (41, 138). The GTP-bound form of Ras is known to activate the mitogen-activated protein kinase (MAP kinase) cascade, which in turn modulates the formation of excitatory postsynaptic potentials (EPSPs) and mediates cellular remodelling (132). The activity of SynGAP is itself inhibited by phosphorylation by CaMKII, suggesting that activation of the NMDA receptor could cause the inhibition of SynGAP and subsequently activate the MAP kinase

**Figure 1-4. Postsynaptic $Ca^{2+}$ Signalling in Hippocampal Neurons.** In hippocampal neurons of the mammalian CNS, the NMDA receptors (red) comprise the major $Ca^{2+}$ influx pathway. They are concentrated in the PSD of these neurons, and upon their activation by the neurotransmitter glutamate (black dots), $Ca^{2+}$ enters the spines and acts on several $Ca^{2+}$ effector molecules tightly organized in the PSD by scaffolding proteins like PSD-95 (light blue). These $Ca^{2+}$ effector molecules include CaMKII (purple), nNOS (orange), as well as synGAP (dark grey). The action of $Ca^{2+}$ on these effector molecules in turn results in appropriate postsynaptic responses like LTP and neuronal synaptic remodelling, by modulating downstream signalling events such as the MAPK cascade. The elevated $[Ca^{2+}]_i$ is then brought back to the resting state by $Ca^{2+}$ extrusion by NCX (yellow) and PMCA (dark orange), as well as $Ca^{2+}$ sequestration into the internal stores (ER) by SERCA (blue).

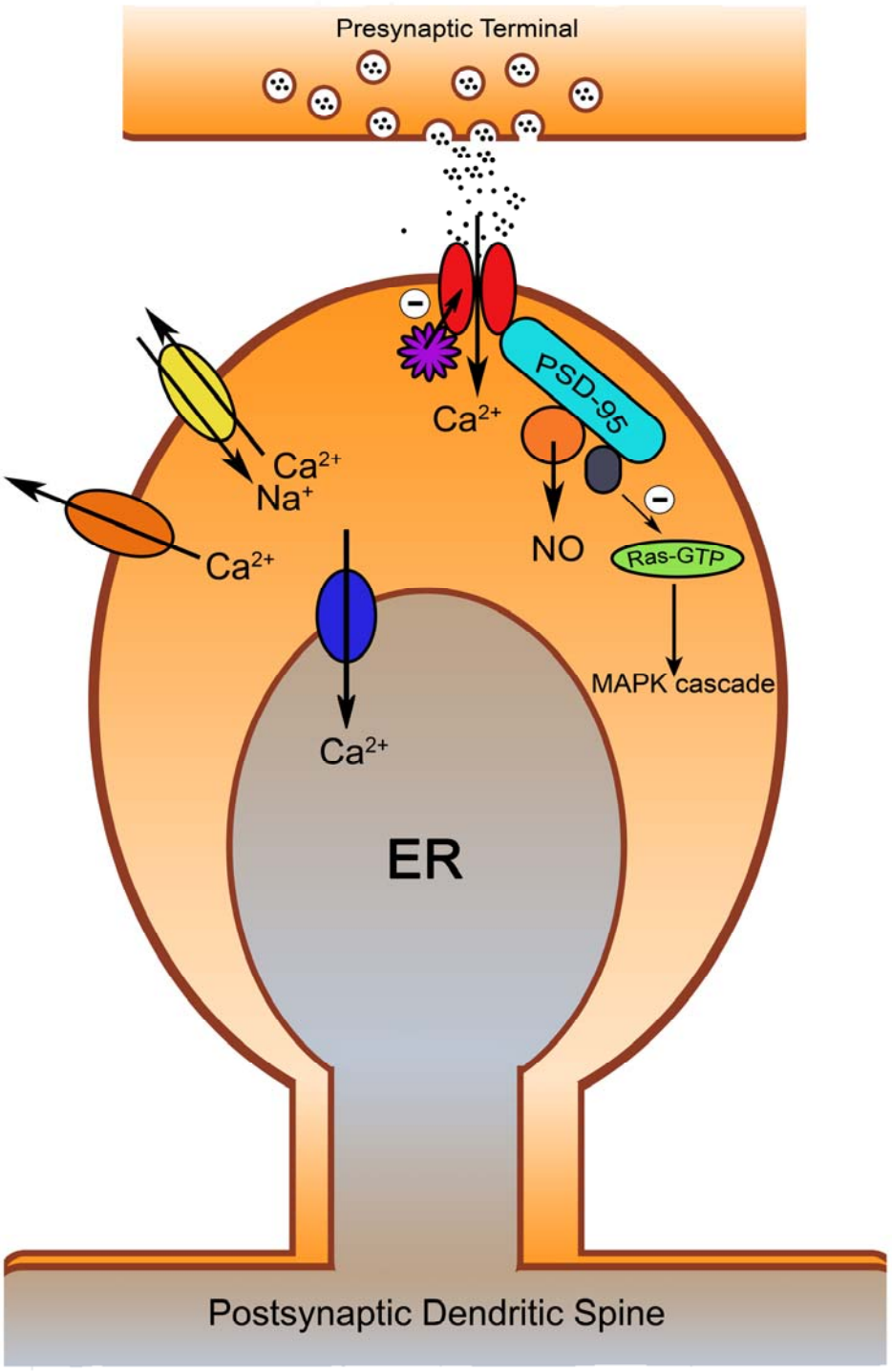
Presynaptic Terminal
PSD-95
Ca2+
Ca2+
Na+
Ca2+
NO
Ras-GTP
MAPK cascade
Ca2+
ER
Postsynaptic Dendritic Spine

pathway. nNOS, which catalyzes the formation of nitric oxide from L-arginine, has been shown to interact with the second PDZ domain of PSD-95 through its own N-terminal PDZ domain (27). This arrangement positions nNOS, whose function is regulated by $Ca^{2+}$/CaM, in close proximity to the NMDA receptor in the PSDs, thereby selectively coupling the production of nitric oxide to $Ca^{2+}$ influx through the NMDA receptor (21, 27). Altogether, the formation of the NMDA receptor signalling complex via protein-protein interactions mediated by scaffolding proteins like PSD-95 effectively translates the rapid rise in $[Ca^{2+}]_i$ into appropriate postsynaptic responses like LTP and neuronal synaptic remodelling.

Several $Ca^{2+}$ extrusion mechanisms also function in postsynaptic dendrites to bring the elevated $[Ca^{2+}]_i$ back to its resting state (Figure 1-4). When $[Ca^{2+}]_i$ reaches the micromolar range, SERCA pumps $Ca^{2+}$ into the ER, while NCX actively transports $Ca^{2+}$ across the postsynaptic membrane. PMCA, also found in the postsynaptic dendrites and in the spines, only makes a significant contribution to $Ca^{2+}$ clearance at low to moderate post synaptic $[Ca^{2+}]_i$ (less than 500nM), concentrations of $Ca^{2+}$ that are too low to result in any significant NCX activity. At higher $[Ca^{2+}]_i$, when NCX is active, the relatively low turnover of PMCA prevents it from making a major contribution to $Ca^{2+}$ clearance.

### 1.2 $Na^+/Ca^{2+}$-Exchangers

First identified in squid axons and cardiac myocytes in 1968 and 1969 (6, 254), where it plays a key role in plasma membrane $Ca^{2+}$ flux, the $Na^+/Ca^{2+}$-exchanger is also

known to be present in many other cell types, including neurons, glia, and smooth muscle cells. It is also involved in trans-epithelial $Ca^{2+}$ re-absorption in the kidney, neurotransmitter release from nerve terminals, and the release of insulin from pancreatic β-cells (23). There are two different NCX protein families: one that is dependent on $K^+$ (NCKX), and another $K^+$-independent exchanger (NCX) (302, 303). Both exchanger families are antiporters that transport $Ca^{2+}$ ions in exchange for $Na^+$ ions, the direction of the flux being determined by the relative electrochemical gradients of $Na^+$ and $Ca^{2+}$ ions (23, 61, 79, 159). In the case of the $K^+$-dependent exchanger, $K^+$ is co-transported with $Ca^{2+}$ in exchange for $Na^+$ ions (37, 63, 270). The $Ca^{2+}$ efflux mode in both $K^+$-dependent and -independent exchangers is known as the forward mode of the exchanger.

The $Na^+/Ca^{2+}$-exchanger was first cloned in 1990 from canine heart (205), and since then close to two decades of extensive research, employing the techniques of molecular biology, electrophysiology, and calcium imaging, have provided a detailed understanding of its function and regulatory properties. However, the three-dimensional structure of the full exchanger is not yet clearly understood, although the crystal structure of the regulatory cytosolic $Ca^{2+}$ binding domains of NCX1 was recently solved (106, 209). Moreover, the quaternary structure of the exchanger, and how this structure is related to the transport function and regulatory properties of the exchanger, have not been studied in detail.

*1.2.1 Superfamilies, Isoforms, and Splice Variants of $Na^+/Ca^{2+}$-Exchangers*

As mentioned above, the mammalian $Na^+/Ca^{2+}$-exchanger can be divided into two different protein families based upon the ion transport specificities of the molecules: the $Na^+/Ca^{2+}$-exchanger (NCX) family and the $Na^+/Ca^{2+}+K^+$-exchanger (NCKX) family (303). So far, three NCX and five NCKX genes have been identified. Each isoform is the product of a different gene, some of which are able to undergo alternative splicing. The genes that code for the NCX family of proteins belong to the solute carrier 8 (*SLC8*), whereas those of the NCKX family of proteins belong to another gene family, solute carrier 24 (*SLC24*) (303). Both *SLC8* and *SLC24* in turn belong to a superfamily of related $Ca^{2+}$/cation transporter genes, the *CaCA* superfamily (32, 248), which also contains three other branches, one characterized by the bacterial transporter YRBG, one by the plant $Ca^{2+}$/anion exchanger (CAX), and another by the less well characterized $Ca^{2+}$/cation exchanger (CCX), also referred to as NCLX or NCKX6.

The *CaCA* superfamily of exchangers is distinguished by a highly conserved overall membrane topology consisting of two clusters of putative hydrophobic transmembrane domains separated by a cytosolic loop of varying length. The number of hydrophobic transmembrane helices in each cluster ranges between four and six. In some cases an extra N-terminal helix presumed to form a signal peptide is also observed. However, the most distinctive feature that defines the *CaCA* superfamily is the presence of a signature amino acid sequence motif found within each hydrophobic transmembrane cluster called the α-repeat (272, 303). These α-repeats contain amino acids that are essential for the transport function of both NCX and NCKX families of proteins, and are

thought to associate with one another to form the ion binding pocket and pore of the exchangers (121, 141-143, 206, 240, 250, 251). This intra-molecular homology of the α-repeats together with the repeated pattern of hydrophobicity within these exchangers suggests an evolutionary gene duplication event.

The majority of genes in the NCX (*SLC8*) and NCKX (*SLC24*) families are expressed in animals, many in mammals. There are three known mammalian genes in the NCX family, *SLC8A1*, *SLC8A2*, *SLC8A3*, each producing distinct isoforms of NCX: NCX1 (*SLC8A1*), NCX2 (*SLC8A2*), and NCX3 (*SLC8A3*). Among these, the *NCX1* gene (205) was the first to be cloned and is known to be highly expressed in cardiac muscle, brain, and kidney, and to a lesser extent in many other tissues. NCX2 (171) and NCX3 (114) are expressed predominantly in brain and skeletal muscle; their molecular properties have not been investigated as thoroughly as those of NCX1. The locations of both mouse and human *NCX* genes have been determined, revealing that the NCX family of genes is dispersed over different chromosomes in both cases. In the mouse, the genes for *ncx1*, *ncx2*, and *ncx3* are found on chromosomes 17, 7, and 12 (114), while in the human they are found on chromosomes 2p22.1 (153), 19q13.2 (136), and 14q24.2 (81), respectively. The human *NCX1* gene consists of 12 exons spread over 400kb on chromosome 2, and together with *NCX2,* contains an unusually long 1.8kb exon 2 that codes for the N-terminal two-thirds of the protein sequence, including most of the intracellular loop (153). Interestingly, this single exon is broken into several exons by the insertion of introns in the *NCX3* gene (81).

Investigations on *NCX1* expression in various tissues have reported a major full-length mRNA transcript of 7.0kb that is highly expressed in many tissues, along with minor transcripts of ~13.0kb and ~4.0kb and a relatively abundant, ubiquitously expressed, and unpolyadenylated transcript of 1.8kb (145, 149, 162, 205, 312). An unusual circularized exon 2 transcript encoding a truncated NCX1 protein corresponding to the 1.8kb mRNA transcript has been reported by the Lytton Lab. It produced a 70kDa protein with partial $Na^+/Ca^{2+}$ exchanger activity when the linear version was prepared and transfected into Human Embryonic Kidney-293 (HEK-293) cells (170). The fact that the truncated protein was functional despite lacking the C-terminal hydrophobic domain, including the second α-repeat, implies that either the C-terminal end of the exchanger is not important for transport which would be inconsistent with a large body of mutagenesis work (204), or that two N-terminal halves might arrange themselves as a dimer in the membrane to form an ion transport pathway, suggesting that the NCX molecule might form a dimer or a higher-order oligomer in its physiological environment.

The human *NCX1* gene contains two regions of alternative splicing flanking the long exon 2 (23). The first site is found in the 5´-untranslated region of the transcript before the start of the open reading frame, and therefore does not affect the sequence or structure of the encoded exchanger. Three different and mutually exclusive non-coding initiating exons present in the 5´-untranslated region of the transcript are known as 1-Ht, 1-Kc, and 1-Br (202, 266). Three independent tissue-specific promoters upstream of each 5´-untranslated region exon drive and regulate the expression of *NCX1* in different tissues. Specifically, the *NCX1* transcript containing 1-Ht is known to be selectively

expressed in the heart, 1-Kr in the kidney, while 1-Br is expressed everywhere else, and especially in the brain (202). Therefore, the use of independent promoters bestows the means to selectively regulate gene expression according to tissue-specific physiological needs.

The second region of alternative splicing lies within the coding sequence of *NCX1* and is responsible for creating diverse splice variant protein isoforms. This region is found within the large intracellular loop of the exchanger that connects the two hydrophobic domains. Two mutually exclusive (exons A and B) and four cassette exons (exons C, D, E, and F) combine to produce multiple NCX1 isoforms with differing cytosolic loop lengths and structures (146, 162, 241). The splice variants of *NCX1* containing one of the two mutually exclusive exons, exon A, appear to be present exclusively in excitable cells, such as heart, skeletal muscle, and neuronal tissues, while those containing exon B seem to be mainly expressed in non-excitable cells and other tissues (162, 241, 303). The predominant isoform of *NCX1* found in heart consists of the exons A, C, D, E, and F, and is denoted NCX1.1. By comparison, the *NCX1* isoforms found in brain contain exons A and D (NCX1.4) or A, D and F (NCX1.5), and the kidney isoforms contain exons B and D (NCX1.3) or B, D and F (NCX1.7). No discernable differences in the tissue-specific expression pattern of the four cassette exons have been observed. Unlike *NCX1*, *NCX2* does not seem to undergo alternative splicing events (241). When expressed, *NCX2* forms a protein with an apparent molecular weight of 100kDa (303). *NCX3*, on the other hand, shows tissue-specific alternative splicing of three different exons, the genomic organization of which is still under investigation. The

comparison with *NCX1* suggests that *NCX3* might have similar exon organization, including the possible presence of the two mutually exclusive exons and a cassette exon homologous to exon C of *NCX1* (219, 241).

### *1.2.2 Structure of the $Na^+/Ca^{2+}$-Exchanger Protein, NCX1*

NCX1 is composed of 970 amino acids, with an N-terminal signal peptide of 32 amino acids and a single oligosaccharide attached to Asn9 of the processed protein, thus placing the N-terminus of the protein in the extracellular environment. Neither glycosylation nor cleavage of the signal peptide seem to alter the behaviour and function of NCX1 (80, 178). The mature protein has a predicted molecular mass of 108kDa, but migrates on SDS-PAGE as three bands with apparent molecular masses of 70kDa, 120kDa, and 160kDa under reducing conditions (205). The 120kDa band corresponds to the mature protein while the 70kDa band is a proteolytic fragment of the 120kDa band and is partially active (230, 261). The nature of the 160kDa band is currently not well understood, although several studies suggest that it might reflect the presence of an intramolecular disulfide bond (263), or be the product of heat-induced protein aggregation.

The initial topological organization of the exchanger, based on hydropathy analysis, predicted 12 transmembrane (TM) segments, including a signal peptide and a central large intracellular loop (205). Subsequently, cysteine scanning mutagenesis, cysteine modification susceptibility analysis, and epitope tagging experiments on recombinantly expressed NCX1 have revealed that the exchanger protein contains 9 TM

domains and an intracellular loop of about 550 amino acids (Figure 1-5) (120, 206). The N-terminus of the mature protein is extracellular, while the C-terminus is thought to be intracellular. Deletion studies on the large intracellular loop suggested that it is not required for transport function, since a mutant lacking a considerable portion of the loop region retained exchanger activity (189). Instead, it is involved in various regulatory events, such as $Na^+$ dependent inactivation, phosphorylation, and regulatory $Ca^{2+}$ binding (59, 108, 188, 231, 263). Ion translocation across the membrane is conferred by the transmembrane segments, which presumably assemble within the membrane to form ion binding sites and the transport pathway, although not much is known about their precise structural and functional nature.

Within the transmembrane regions, there are two segments that display internal sequence homology known as the α-repeats, the signature sequences of the CaCA superfamily (32, 272). The initial hydropathy analysis of the NCX1 sequence that predicted a 12 TM structure located the first α-repeat (α-1 repeat) in TM2-3 and the second α-repeat (α-2 repeat) in TM8-9, including the loops connecting these TMs, thereby placing both the α-repeats facing the extracellular side of the membrane (205, 272). The more recent and widely accepted topological model with 9 TM structure suggests that the α-repeats are oriented in opposite directions with respect to the membrane, with the α-2 repeat facing the cytosolic environment (Figure 1-5) (120, 206). This model introduces surprising asymmetry between the N-terminal half and the C-terminal half of the exchanger, and different structures near the two α-repeats. Studies using cysteine mutagenesis and disulfide cross-linking with a cysteine-less mutant form

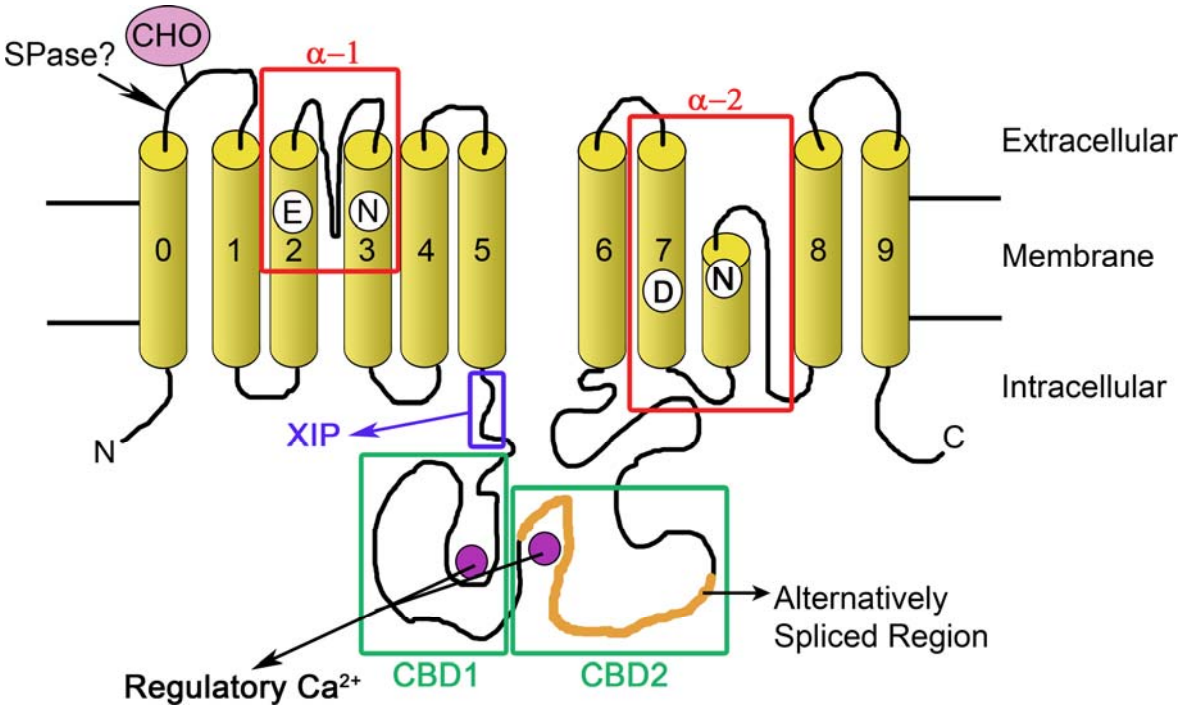


**Figure 1-5. Topology Model of NCX1.** NCX1 is composed of 10 TM segments including the N-terminal signal peptide (TM0). Putative signal peptidase cleavage site is indicated with the arrow. Also shown here are the single N-linked glycosylation site (CHO, purple) in the N-terminal extracellular loop, long cytosolic loop containing exchanger inhibitory peptide (XIP) and two CBDs, as well as the two α-repeats with the location of the critical amino acids. The alternatively spliced region in the cytosolic loop (orange) is also highlighted.

of NCX1 proposed that TM7 is close to TM3 near the intracellular side of the plasma membrane and to TM2 near the extracellular surface (240), bringing the two oppositely oriented α-repeats into proximity. A more recent study on the helix packing of NCX1 places TM1 and TM2 close to TM6, thereby locating the helices flanking the α-repeats in close proximity as well (250). Altogether, these data suggest the presence of an ion transport pathway formed by the two α-repeats. This concept is also supported by the conserved sequence of the α-repeats, and by mutagenesis experiments demonstrating the essential nature of many amino acids within these regions (60, 208, 220, 240). The precise amino acids involved in the ion binding sites within the α-repeats, and the ways in which they can accommodate one $Ca^{2+}$ ion and three to four $Na^{+}$ ions in a mutually exclusive manner remain to be investigated.

The long central intracellular loop of NCX1 is thought to regulate the function of the exchanger, but is not essential for ion exchange itself. It is located between TM5 and TM6 and contains several different regulatory motifs, including the exchanger inhibitory peptide (XIP) region and two $Ca^{2+}$-binding domains, CBD1 and CBD2 (Figure 1-5) (18, 106, 205, 207, 209, 303). The XIP region, found in the N-terminal end of the loop and comprising residues 251-270, is so named because the addition of a synthetic peptide bearing the same amino acid sequence was shown to significantly inhibit exchanger function (207). Recently, the crystal and NMR structures of both CBD1 and CBD2 have been solved (Figure 1-6) (18, 106, 209). These domains display an immunoglobulin fold with a β-sandwich motif, formed by two antiparallel β-sheets composed of seven β-strands. CBD1 contains a $Ca^{2+}$ binding site in the distal loops of the β-sandwich, where

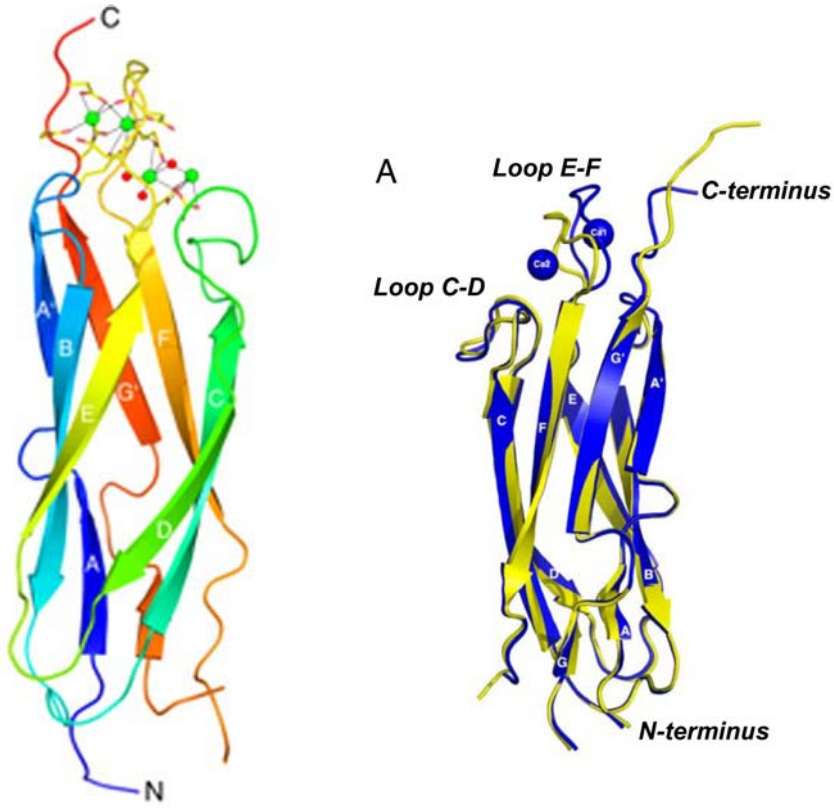


**Figure 1-6. Structure of the $Ca^{2+}$ Binding Domains of NCX1.** Ribbon representation of both CBD1 (left) and CBD2 (right) of NCX1 taken from (209) and (18), respectively. The seven β-strands of CBD1 are coloured from the N-terminus in blue to the C-terminus in red, and four $Ca^{2+}$ ions are represented as green circles (left). Shown right is the structural alignment of $Ca^{2+}$-bound (blue) and $Ca^{2+}$-free (yellow) structures of CBD2. Here, $Ca^{2+}$ is shown as blue spheres.

a series of acidic residues are involved in coordinating four $Ca^{2+}$ ions with high affinity (209). The binding of the $Ca^{2+}$ ions seems to induce a considerable conformational change within CBD1, the process of which is believed to impart the regulatory effect of cytosolic $Ca^{2+}$ on the exchanger activity. CBD2 is thought to bind two $Ca^{2+}$ ions with relatively low affinity and smaller conformational consequences (18, 106). These two CBDs in turn are believed to come together and pack in an antiparallel fashion with the $Ca^{2+}$ binding site of CBD1 pointing into the cytoplasm and away from the plasma membrane.

### *1.2.3 Function of the $Na^+/Ca^{2+}$-Exchanger, NCX1*

The $Na^+/Ca^{2+}$ exchanger was initially thought to transport three $Na^+$ in exchange for one $Ca^{2+}$ (232, 244, 245), but some recent studies suggest that four $Na^+$ may be transported in exchange for one $Ca^{2+}$ (61, 79). Yet another study conducted by the Hilgemann group proposed the exchange of one $Ca^{2+}$ and one $Na^+$ for one $Ca^{2+}$ (a $Na^+$ conducting mode) or three $Na^+$ (a net $2Na^+/1Ca^{2+}$ exchange) at a low rate in addition to one $Ca^{2+}$ for three $Na^+$ to explain the apparent discrepancies in the stoichiometry (130), but at present the issue on the correct ion transport stoichiometry is not clearly resolved. NCX1 activity is quite sensitive to mutations in the conserved α-repeat region (60, 121, 203). Mutations in the hydrophilic residues lining the two α-repeats of NCX1 were shown to significantly reduce or completely inhibit $^{45}Ca^{2+}$ uptake activity when the mutants were expressed in *Xenopus* oocytes (203). Furthermore, there is evidence to suggest that the cytoplasmic end of TM2 of NCX1, and especially a threonine residue at position 103 which when mutated to valine increases the apparent affinity of the

exchanger for intracellular $Na^+$, might be directly involved in the translocation of $Na^+$ ions (60). Two key acidic residues, Glu113 and Asp814 (one from each α-repeat), are conserved among all of the exchangers, and also found to be essential for the transport function of the exchanger. Mutations at these residues completely eliminate exchanger activity (203).

In addition, the function of the exchanger is regulated by several factors, such as the substrate $Na^+$ and $Ca^{2+}$ ions, ATP, phosphatidylinositol 4,5-bisphosphate ($PIP_2$), and other acidic phospholipids. High $[Na^+]_i$ inhibits exchanger activity by the process known as $Na^+$-dependent inactivation (108, 111). It is characterized by a rapid exponential decay of the peak outward current to a steady-state level induced by the application of high $[Na^+]$ to the cytosolic surface in an inside-out giant excised patch (111). $Na^+$-dependent inactivation does not depend on changes in the membrane potential, but it could be regulated by intracellular pH, regulatory $Ca^{2+}$, or by ATP (111). It was initially speculated that the inactivation occurs following the binding of $Na^+$ ions to the ion transport site oriented toward the cytoplasm, from which the exchanger can either translocate the bound $Na^+$ across the plasma membrane or transition into an inactive conformation (111, 263). Alternatively, $Na^+$-dependent inactivation might occur at a site distinct from the ion transport site (59). $Na^+$-inactivation appears to involve the XIP region discussed above, because mutations in this region alter the characteristics of $Na^+$-dependent inactivation, some relieving inactivation and some enhancing it (187).

While high $[Na^+]_i$ inhibits the exchanger, intracellular $Ca^{2+}$ ions that bind to the two CBDs found in the cytosolic loop of NCX1 activate the exchanger (42, 108). These activating $Ca^{2+}$ ions are not transported. The effect of regulatory $Ca^{2+}$ was first noted in the dialyzed squid giant axon (58) and later in giant excised patches (107, 108), in which the outward $Na^+/Ca^{2+}$ exchange current (the reverse mode of the exchanger) was activated by a sub-micromolar concentration of internal free $Ca^{2+}$ within seconds. Mutated analysis indicates that $Ca^{2+}$ binding to CBD1 is essential for activation of the exchanger, and CBD2 also plays a role in this process (18, 110, 165, 209, 221). In addition to activating the exchanger, $Ca^{2+}$ also alleviates $Na^+$-dependent inactivation, a process that may involve $Ca^{2+}$ binding to CBD2 (110, 209). Exchangers encoded by alternatively spliced transcripts containing the mutually exclusive "B" exon do not exhibit this $Ca^{2+}$-dependent alleviateion of $Na^+$-inactivation, as a result of the replacement of a critical Asp by an Arg residue within the $Ca^{2+}$ binding side of CBD2 (65). Structural data on the two CBDs seem to suggest a large conformational change in the intracellular loop as the means by which regulatory $Ca^{2+}$ activates the transporter (18, 209, 221). However, the precise molecular workings of the $Ca^{2+}$-induced activation of the exchanger are not well understood.

It was noted in giant patch preparations that ATP is another important regulator of exchanger activity (108, 110). Its major influence seems to be to render the exchanger much less sensitive to $Na^+$-dependent inactivation. This is caused by the hydrolysis of ATP to generate $PIP_2$ from phosphatidylinositol (PI) (109). The cationic XIP region has been implicated as being responsible for the $PIP_2$-mediated activation of the exchanger,

by directly and specifically interacting with anionic $PIP_2$ in the plasma membrane (98), a plausible notion considering the proposed localization of the XIP region to the lipid-membrane interface.

### *1.2.4 Physiological Roles of the $Na^+/Ca^{2+}$-Exchangers*

$Na^+/Ca^{2+}$ exchanger activity is almost omnipresent and plays an important role in normal cellular physiology. In the mammalian heart, where the exchanger density is high (250~400 exchanger molecules/$\mu m^2$ of plasma membrane) (172), NCX1 is the key $Ca^{2+}$ extrusion mechanism. The magnitude of the initial $Ca^{2+}$ influx from the extracellular milieu that triggers CICR varies from species to species, ranging from approximately 8% in rats to close to 30% of the total $Ca^{2+}$ transient in rabbits and humans (16). An equal fraction of $Ca^{2+}$ is therefore extruded from the cell by the action of the $Na^+/Ca^{2+}$-exchangers while the reminder is returned to the SR. Any perturbation in exchanger activity would be expected to change this homeostasis and thus bring about changes in $[Ca^{2+}]_i$ and SR $Ca^{2+}$ loading and consequent changes in heart function. In addition, $Ca^{2+}$ extrusion via the cardiac specific isoform, NCX1, is electrogenic, transporting a positive charge (carried by $Na^+$ ions) across the plasma membrane and thereby depolarizing the membrane. This electrogenic property of the exchanger may contribute to the size, shape, and length of the cardiac action potential. Interestingly, the thermodynamic driving force during the peak plateau phase of the cardiac action potential actually favours the reverse mode of the exchanger, bringing $Ca^{2+}$ ions into the cell (16, 23). The extent to which this $Ca^{2+}$ entry significantly affects cardiac E-C coupling is controversial, particularly since the exact ionic concentrations, their diffusion limits, and the intracellular buffering

capacity are all extremely hard to measure with certainty, thereby making it almost impossible to precisely understand the ionic environment the exchanger is exposed to during each heartbeat.

The importance of NCX1 activity to normal cardiac function was demonstrated in mice in which the global knockout of *ncx1* led to an embryonically lethal phenotype caused by developmental cardiac abnormalities (43, 152, 305). However, closer examination suggested that the observed embryonic lethality might not be due to the perceived cardiac developmental failure, but rather due to the lack of an organized vasculature in the yolk sacs as a result of the *ncx1* gene knockout (44). Using Cre/loxP technology, cardiac-specific *ncx1* knockout mice were recently generated in which up to 90% of cardiac myocytes were completely devoid of NCX1 protein expression and exchanger function (102). Interestingly, these cardiac-specific knockout mice lived to adulthood with only minor reduction in cardiac function, which eventually contributed to the slow progression of cardiac hypertrophy and ultimately led to heart failure as the animals aged. No drastic compensatory changes in the myocardium to the absence of the exchanger protein were observed, implying a remarkable adaptability of the cardiomyocytes to maintain normal cardiac function.

When myocytes from these knockout mice were isolated and used for further studies, a significant reduction in the L-type $Ca^{2+}$ channel current without any loss of VGCC protein expression was apparent. Patch-clamping studies revealed a decrease of more than 50% in the L-type $Ca^{2+}$ channel current and an increase in the inactivation

kinetics in knockout myocytes compared to wild type myocytes. Furthermore, this phenomenon could be normalized by dialysis with bis-(*o*-aminophenoxy)ethane-N,N,N´,N´-tetraacetic acid (BAPTA), indicating that the elevated level of subsarcolemmal $[Ca^{2+}]_i$ caused by the absence of NCX1 inactivates some L-type $Ca^{2+}$ channels (236). In addition to the reduced L-type $Ca^{2+}$ channel current, a shortened and more rapidly repolarising cardiac action potential was observed in cardiac-specific knockout mice, which appeared to result from an increase in the hyperpolarizing $K^+$ current (outward $I_{to}$ current), itself resulting from upregulation of the $I_{to}$ generating voltage-gated $K^+$ channel subunit $K_v4.2$ and the $K^+$ channel interacting protein (KChIP) (236). Thus the mechanisms that underlie adaptation to loss of NCX include a shortened cardiac action potential and rapid inactivation of the L-type $Ca^{2+}$ channel which leads to significantly lower trans-sarcolemmal $Ca^{2+}$ flux without any apparent change in SR $Ca^{2+}$ release, implying a gain of E-C coupling. How the gain of E-C coupling is achieved has not been fully investigated, although longer residence of $Ca^{2+}$ in the dyadic junction is a likely contributor.

NCX1 also plays an important role in heart failure (23). The levels of NCX protein and mRNA are elevated in congestive heart failure (23, 72). At the same time, the levels of SERCA and phospholamban expressions are reduced. Together, these changes result in the reduced amplitude, altered shape, and slowed relaxation of the $Ca^{2+}$ transients observed in heart failure (215, 309). Unloading of the SR $Ca^{2+}$ store occurs due to decreased expression of SERCA as well as increased expression and function of NCX1 which competes with SERCA for cytosolic $Ca^{2+}$ during muscle relaxation, leading to the

systolic/diastolic dysfunction noted in heart failure (17). The up-regulation of NCX1 also generates both early and delayed after-depolarizations, due to increased depolarizing current carried by elevated exchanger activity, which can trigger arrhythmogenic action potentials (181, 215, 309).

The physiological role of $Na^+/Ca^{2+}$-exchanger activity in brain has not been examined in as much detail as that in heart. All three isoforms of the NCX family are present throughout the brain and isoform-specific localization has been studied using *in situ* hybridization and immunohistochemistry (223, 253). These data indicate relatively high levels of expression for NCX1 and NCX2, with lower and more selective expression for NCX3 (223). As in the heart, experimental evidence suggests that the role of the exchangers in the neurons of the central nervous system, and especially in the synaptic regions of dendrites where the exchangers are preferentially localized, is to extrude $Ca^{2+}$ following its entry, thereby rapidly and effectively terminating $Ca^{2+}$-mediated signalling events (180). More detailed analysis of the differential distribution of these isoforms in neurons, as well as their sub-cellular localization, is required to understand their distinctive physiological roles.

The broad and high expression pattern displayed by NCX2 in the brain suggests that NCX2 might exert an important role in neuronal $Ca^{2+}$ homeostasis and function. To define the physiological function of NCX2, *ncx2* gene knockout mice were generated that exhibited delayed $Ca^{2+}$ clearance following depolarization in hippocampal pyramidal neurons, enhanced short term neuronal plasticity, and a shift from long-term depression

toward long-term potentiation (123). Overall, these knockout mice displayed enhanced learning and memory, mental tasks that require the function of the hippocampus. This suggests that NCX2 has a prominent role in synaptic $Ca^{2+}$ clearance.

*NCX* gene products are also found in other types of tissues like smooth muscles and the kidney. In smooth muscles, modulating $Na^{+}/Ca^{2+}$ exchanger activity with a selective NCX inhibitor KB-R7943 was shown to have a significant consequence on agonist-induced contraction (62, 112, 163). It appears that conditions that drive the reverse mode of the exchanger, such as SR store depletion and functional coupling with increased $Na^{+}$ flux through canonical TRP channels, lead to an increase in $Ca^{2+}$ influx and subsequent enhancement of agonist-induced contractions. However, because no reliable correlation between inhibition of exchanger function and changes in cytosolic $[Ca^{2+}]_i$ has been observed, it has been hypothesized that $Ca^{2+}$ flux through the exchanger in smooth muscle is tightly linked to changes in SR $Ca^{2+}$ content (23, 196). Recently, $Ca^{2+}$ entry into vascular smooth muscle cells via the NCX1.3 splice variant has been implicated in blood pressure control (119). Using the NCX1 inhibitor SEA0400 that preferentially blocks $Ca^{2+}$ entry, Iwamoto et al. (119) showed that the drug lowered blood pressure in salt-sensitive hypertensive rat models but not in salt-insensitive hypertensive rat models, suggesting that salt-sensitive hypertension is triggered by $Ca^{2+}$ entry through NCX1 in atrial smooth muscle. In the kidney, NCX1 is essential for the reabsorption of $Ca^{2+}$ in distal nephron segments, where its expression on the basolateral membranes is high (247). NCX1 drives transepithelial $Ca^{2+}$ transport, and thus is involved in systemic $Ca^{2+}$ regulation rather than altering the intracellular $[Ca^{2+}]$, as in all other tissues.

## 1.3 $K^+$-Dependent $Na^+/Ca^{2+}$-Exchangers

$K^+$-dependent $Na^+/Ca^{2+}$-exchanger activity was first identified in, and the transcript successfully cloned from, rod photoreceptor outer segments (37, 52, 246, 270). The sequence revealed that the $K^+$-dependent $Na^+/Ca^{2+}$-exchanger was evolutionarily related to the $K^+$-independent $Na^+/Ca^{2+}$ -exchangers, NCX, as evident in their signature α-repeats and topological similarities (32). Since then molecular cloning and database mining have revealed a family of NCKX genes, although detailed studies on each isoform have lagged behind those of the $K^+$-independent (NCX) $Na^+/Ca^{2+}$-exchanger family. NCKX proteins are expressed in many different cell types and perform diverse and often isoform-specific cellular functions, such as visual signal transduction, postsynaptic neuronal $Ca^{2+}$ clearance, and skin pigmentation (91, 156).

### *1.3.1 Isoforms and Splice Variants of $K^+$-Dependent $Na^+/Ca^{2+}$-Exchangers*

So far, five different NCKX genes have been identified and successfully cloned. The NCKX (*SLC24*) family of proteins has a transport stoichiometry of one $Ca^{2+}$ and one $K^+$ in exchange for four $Na^+$ ions (37, 63), the direction of the ion transport depending on the electrochemical gradients of the ions. It consists of proteins homologous to the bovine rod outer segment NCKX (NCKX1), the major $Ca^{2+}$ extrusion system in photoreceptors and a critical component of visual transduction. Homology-based cloning and database mining yielded four other family members, NCKX2, 3, 4, and 5 (154, 156, 169, 297). Five human NCKX genes, denoted *SLC24A1* (298), *SLC24A2* (238), *SLC24A3* (154), *SLC24A4* (169), and *SLC24A5* (156) code for each of the five NCKX proteins, which

exhibit relatively high sequence similarity, especially between the NCKX1/NCKX2 and NCKX3/NCKX4 pairs. The protein sequence of NCKX5 falls slightly closer to the NCKX3/NCKX4 pair. Overall, the sequence similarity observed among NCKX proteins is highest in the hydrophobic domains. The differences in the protein sequences and the lengths of the proteins lie within the intracellular loop, where alternative splicing patterns are noted in some members of the family. In addition, NCKX1, the largest NCKX protein with 1199 amino acids (for bovine rod NCKX1), contains a long N-terminal extracellular hydrophilic segment that is heavily glycosylated. This hydrophilic segment is either absent from or much shorter in other members of the family. Due to the extensive glycosylation, NCKX1 has an apparent molecular weight of ~220kDa when analyzed on a protein polyacrylamide gel, although the calculated molecular weight is only ~130kDa (52, 246).

Fluorescent *in situ* hybridization and radiation hybrid mapping analyses of the human *NCKX1* gene indicated its location on human chromosome 15q22 (299). The human *NCKX1* gene encodes a protein comprising 1081 amino acids and displaying 64.3% overall sequence identity with the bovine rod NCKX1(298). The human *NCKX1* gene contains a total of 10 exons, and, just like *NCX1*, displays an unusually long exon 2 containing approximately two thirds of the protein sequence, followed by four small cassette-like exons (exons 3-6) coding for the beginning of a long intracellular loop (299). The discovery of the human *NCKX1* gene with or without exon 3 suggests the possibility of an alternative splicing event, the consequence of the inclusion of the exon 3 being the introduction of a short stretch of amino acids at the N-terminal side of the

intracellular loop (246, 298, 299). In addition, analyses of rat eye mRNA using RT-PCR revealed four alternatively spliced variants of *NCKX1*, formed by either including or excluding four cassette-like alternatively spliced exons A-D, which correspond to exons 3-6 of the human *NCKX1* gene (235). Unlike the rather broad expression pattern displayed by different isoforms of *NCX1*, the expression of all *NCKX1* splice variants is restricted to the retinal rod outer segments (235, 238, 246). Although all splice variants were successfully delivered to the cell surface and exhibited $K^+$-dependent $Na^+/Ca^{2+}$ exchange activity when transiently transfected into HEK-293 cells, precisely why these different isoforms of NCKX1 are expressed in the rod photoreceptors remains to be investigated.

The second member of the NCKX family, *NCKX2*, was first cloned and isolated from rat brain with a homology-based approach using the cloned bovine *NCKX1* gene sequence (297). The rat *NCKX2* gene codes for a protein of 670 amino acids including the N-terminal signal peptide with a calculated molecular weight of 75kDa, while the expressed and processed protein runs at ~70kDa on a protein polyacrylamide gel. Northern blot analysis showed that the major transcript of 10.5kb was present in all regions of the brain, including the cerebral cortex, cerebellum, brainstem, and midbrain. Alternative splicing of the rat *NCKX2* gene is also observed, producing a slightly shorter protein that lacks 17 amino acids within the long intracellular loop. The discovery of the human *NCKX2* gene from the retina by homological cloning places it on chromosome 9p22 (238). The human *NCKX2* gene codes for a protein of 661 amino acids and has an overall 89.6% identity with the rat brain NCKX2. In addition, the human *NCKX2* gene is

subject to alternative splicing at exactly the same position as the rat *NCKX2* gene, resulting in inclusion or exclusion of the same 17 amino acid segment with only one amino acid change (238).

Subsequent cloning of the mammalian *NCKX3* (154), *NCKX4* (169), and *NCKX5* (156) completed the NCKX family. The human *NCKX3* gene is composed of 17 exons spread over 500kb and is localized on chromosome 20p11 (154). Interestingly, the long exon that codes for the first two thirds of the protein sequence found in *NCX1*, *NCX3*, *NCKX1*, and *NCKX2* is missing in the *NCKX3* gene, and there seems to be no evidence of alternative splicing of the gene. The human *NCKX3* codes for a protein of 644 amino acids, and is highly expressed in brain and moderately in other tissues. When expressed in HEK-293 cells, $K^+$ dependent $Na^+/Ca^{2+}$ exchange activity typical of the NCKX family of proteins was observed, confirming that the *NCKX3* gene indeed codes for a $K^+$-dependent $Na^+/Ca^{2+}$-exchanger. The human *NCKX4* gene encodes a protein of 605 amino acids, and is more closely related to NCKX3 than NCKX2 or NCKX1 (169). It is localized on chromosome 14q32, and consists of 18 exons spread over 174kb. The long exon 2 is also absent from the *NCKX4* gene, as with the *NCKX3* gene, and, with the exception of the exon 1/2 boundary, all the other exon junctions found in the *NCKX4* gene are identical to those of the *NCKX3* gene. Northern blot analysis of RNA samples from different rat tissues suggests that the *NCKX4* transcript is highly expressed in all regions of the brain, and in the aorta, lung, and thymus. Further analysis by *in situ* hybridization indicated robust expression of *NCKX4* transcripts in the CA1, CA3, and

dentate gyrus neurons of the hippocampus, in the Purkinje cells of the cerebellum, and in all regions of the thalamus (169).

### *1.3.2 Structure of $K^+$-Dependent $Na^+/Ca^{2+}$-Exchanger Proteins*

$K^+$-dependent $Na^+/Ca^{2+}$ exchanger proteins display an overall membrane topology reminiscent of $K^+$-independent $Na^+/Ca^{2+}$-exchangers (Figure 1-7). They are thought to have 11 TM segments (TM0-TM10), the first segment of which (TM0) is cleaved by signal peptidase during the post-translational processing event (127). Like the NCX proteins, NCKX proteins possess an extracellular domain at the N-terminus of the mature protein which contains at least one glycosylation site, although this region is generally longer in NCKX proteins than in the NCX proteins. The extracellular domain is then followed by a cluster of five putative TM segments (TM1-TM5), a long cytosolic loop of varying length, and another cluster of five proposed TM segments (TM6-TM10). Glycosylation scanning mutagenesis and cysteine accessibility analyses on recombinant NCKX2 suggest that both the N-terminal and C-terminal ends of the mature protein are located in the extracellular environment (33, 143). It is noteworthy that this topology puts the location of the C-termini of NCKX and NCX proteins on opposite sides of the plasma membrane. This structural difference may be related to their different ion binding and ionic specificities, although further experiments will be required to confirm this theory. Considering the similarity of the overall topology and the high sequence identity in the TM regions, it seems likely that the structure discussed above is shared by all members of the NCKX family (Figure 1-7).

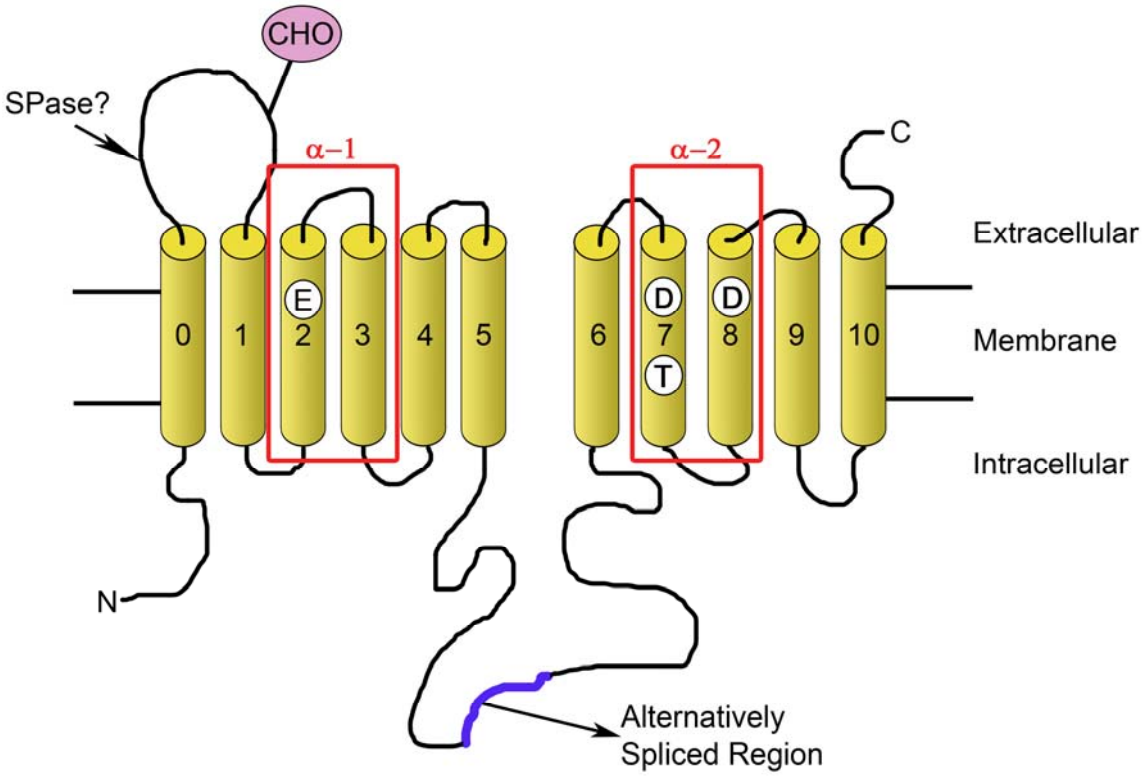


**1-7. Topology Model of NCKX2.** The experimental evidence suggests that NCKX2 is composed of 11 TM including the N-terminal signal peptide (TM0) that is cleaved at the proposed signal peptidase recognition site (indicated by the arrow). As in Figure 1-5, the important regions (N-terminal glycosylation site, alternatively spliced region, two α-repeats as well as the critical amino acid residues) are highlighted.

Just as in NCX1, the two α-repeats of NCKX2 are oriented toward opposite sides of the plasma membrane (Figure 1-7) (142), and are found close to one another in the mature folded protein, bringing together two key functional residues within the two α-repeats (141). These key acidic residues, Glu188 and Asp548 found in TM2 and TM7 respectively, are thought to line the cation binding pocket of NCKX2 since elimination of the charge on either residue resulted in a nonfunctional exchanger (128). Moreover, Asp575 in TM8 appears to be essential for the $K^+$ dependence of exchanger function, because mutating this residue to the corresponding residue in NCX (Asn) renders NCKX2 $K^+$-independent (129). Evidence from disulfide cross-linking studies confirmed that these three residues, although far apart in the primary sequence, are juxtaposed in three dimensional space, and thus could form disulfide bonds when cysteine was introduced in their respective positions in a cysteine-less exchanger (141). However, it is not clear whether the α-repeats of NCKX proteins also form re-entrant loops like those of NCX1.

### *1.3.3 Function of $K^+$-Dependent $Na^+/Ca^{2+}$-Exchangers*

The apparent ion stoichiometry of the $K^+$-dependent $Na^+/Ca^{2+}$-exchangers of one $Ca^{2+}$ and one $K^+$ for four $Na^+$ was first described in studies on isolated bovine rod outer segments (37, 270). This apparent stoichiometry was later confirmed using recombinant NCKX1 and NCKX2 expressed either in insect High Five cells or HEK-293 cells using $^{45}Ca^{2+}$ uptake assays or by electrophysiological characterizations (63, 276, 288). In addition, both recombinant NCKX1 and NCKX2 appear to have similar affinities for their substrate ions $Ca^{2+}$ (1~2μM), $K^+$ (15~40mM), and $Na^+$ (20~60mM) (63, 238).

Recombinant NCKX3 and NCKX4 have also been shown to display $K^+$-dependent $Na^+/Ca^{2+}$ exchanger activity using fluorescence imaging, electrophysiology, and $^{45}Ca^{2+}$ uptake experiments (154, 169), and display similar affinities for $Ca^{2+}$ and $Na^+$ as NCKX2, but have a much higher apparent affinity for $K^+$ (~1mM) (302). Functional analysis of various mutant forms of NCKX2 revealed that Thr551 on TM7 was responsible for the lower apparent $K^+$ affinity found in NCKX2, since mutating this residue to alanine, the corresponding residue in NCKX4, bestowed a high apparent $K^+$ affinity onto NCKX2 similar to NCKX4 (302). Since removing a potential liganding residue increases apparent $K^+$ affinity, and since the most current model of NCKX2 topology suggests that Thr551 lies on the cytoplasmic side of the key liganding residues (Glu188, Asp 548, and Asp575), it is not likely that Thr551 is directly involved in the liganding of $K^+$ ions. Rather, it is plausible that the residue might reduce the conformational flexibility and the ion binding/liganding strengths of these critical residues, resulting in the lowered apparent $K^+$ affinity.

Very little is known about the functional regulation of NCKX family members as compared to what is known about NCX1. Regulation at the level of gene transcription has not been analyzed in detail and consequently, no information is available regarding the promoter regions of the genes, transcription factor binding, or the elements involved in tissue-specificity. As discussed above, NCKX1, 2, and 4 are found to be alternatively spliced, although no obvious functional differences among the splice variants have been noted and a detailed analysis of the differential regulation of these variants has not been performed (169, 238, 297).

Recombinant NCKX2 has recently been shown to be inactivated in a time- and $Na^+$-dependent manner, an event already well described in NCX1 where it is known as $Na^+$-dependent inactivation (2, 111). Further mutational analysis suggested that this inactivation requires the binding of $Na^+$ to its intracellular transport sites. However, it is currently not known whether the apparent $Na^+$-dependent inactivation process is an innate phenomenon universal to all members of the NCKX family. Although many specific sequence motifs, such as the CaMKII phosphorylation consensus motif and PKC phosphorylation sites, are present in the central cytosolic loop of the NCKX family, few studies have examined their potential regulatory properties. NCKX2 exchanger activity in HEK-293 cells was enhanced by stimulation with phorbol esters, whereas NCKX3 and 4 were unaffected (160). Moreover, this phorbol ester-induced stimulation was abolished by PKC inhibitors and significantly reduced when the dominant-negative form of PKCε (K437R) was overexpressed in HEK-293 cells. PKC stimulation also led to increased phosphorylation of NCKX2 when analyzed by immunoprecipitation of the exchanger. The stimulation of the exchanger function was also noted at the calyx of Held, a large presynaptic terminal in the central nervous system where NCKX2 is thought to be the major $Ca^{2+}$ extrusion system (160). Altogether the current data suggest that NCKX2 exchanger function can be modulated physiologically via direct phosphorylation by PKC.

### *1.3.4 Physiological Roles of $K^+$-Dependent $Na^+/Ca^{2+}$-Exchangers*

The role of NCKX1 in rod photoreceptor outer segments has been well defined. Here, NCKX1 is physically associated in a hetero-oligomeric complex with cyclic guanosine 3´:5´-monophosphate-gated channels (cGMP-gated channels), which are

constitutively open in the dark (126). The opening of the cGMP-gated channels allows both $Na^+$ and $Ca^{2+}$ entry from the extracellular environment, and the combined activities of NCKX1-mediated $Ca^{2+}$ extrusion and $Ca^{2+}$ entry through cGMP-gated channels in the dark sets the resting level of $[Ca^{2+}]_i$ at ~500nM. Upon illumination, a retinal G-protein coupled receptor, rhodopsin, binds to and thereby activates a G-protein transducin, which in turn activates membrane-bound cyclic nucleotide phosphodiesterase (PDE). The hydrolysis of cGMP by activated PDE follows, resulting in the closure of cGMP-gated channels and hyperpolarisation of the plasma membrane. This triggers a series of changes within the photoreceptors to reduce the release of the neurotransmitter glutamate at the synapse. In addition, the cGMP-gated channel closure upon illumination, combined with the continued activity of NCKX1, leads to net $Ca^{2+}$ efflux and a rapid decrease in $[Ca^{2+}]_i$. This drop in $[Ca^{2+}]_i$ is key to visual adaptation, because it activates guanylyl cyclase-activating proteins (GCAP), acidic $Ca^{2+}$-binding proteins, and causes substantial activation of the specialized photoreceptor guanylyl cyclase (GC). Activated GC in turn drives the resynthesis of cGMP, thereby allowing the subsequent re-opening of the cGMP-gated channels.

A similar process of visual adaptation is expected to happen in cone outer segments. Cone outer segments are less sensitive to light than rod outer segments, respond to broader light wavelengths, and display faster kinetics. Hence their $Ca^{2+}$ handling properties might be expected to differ. The discovery of NCKX2 expression in chicken cone photoreceptors implies that NCKX2 in cones assumes a role analogous to that carried out by NCKX1 in rod photoreceptors (238). However, studies on NCKX2

knockout mice did not find any deficit in cone function or cone number (168), suggesting that other $Ca^{2+}$ efflux mechanisms exist that can compensate for the loss of cone NCKX2 or that the aspects of cone function that depend upon NCKX2 activity were not investigated.

In neurons where NCKX2 is widely distributed and most abundant, it is believed to be essential in pre- and postsynaptic $Ca^{2+}$ clearance. The expression of several isoforms of both $K^+$-independent and $K^+$-dependent $Na^+/Ca^{2+}$-exchangers are noted in neurons. An attempt to measure the relative contributions of these various isoforms to neuronal $Ca^{2+}$ clearance in acute preparations of axon terminals from the rat posterior pituitary (neurohypophysis) showed $K^+$-dependent $Na^+/Ca^{2+}$ exchanger activity to be most prominent (161). More than 60% of $Ca^{2+}$ clearance in these nerve endings was attributed to $Na^+/Ca^{2+}$ exchange, especially when $[Ca^{2+}]_i$ was higher than 500nM, and ~90% was $K^+$-dependent (161). Furthermore, studies on supraoptic magnocellular neurosecretory cells (MNC) subsequently confirmed that NCKX2 was responsible for the majority of $Ca^{2+}$ clearance from the axon terminal, where its expression is almost exclusively localized. Mechanisms other than $Na^+/Ca^{2+}$ exchange are important for $Ca^{2+}$ clearance from other sub-cellular locations like somata (140). The evidence also suggests a prominent role for $K^+$-dependent $Na^+/Ca^{2+}$ exchange in $Ca^{2+}$ clearance from presynaptic terminals, as seen at the calyx of Held, the mammalian giant presynaptic terminal (139). Studies on hippocampal neurons also demonstrated major $K^+$-dependent $Na^+/Ca^{2+}$ exchanger activity (134, 135), altogether implying strongly that NCKX proteins play significant roles in neuronal $Ca^{2+}$ signalling and homeostasis. Along with NCKX2, both

NCKX3 and NCKX4 proteins are also expressed in neurons. However, no clear physiological roles for these exchanger isoforms are known to this date (182).

To address the physiological role of NCKX2 in neuronal $Ca^{2+}$ signalling, *nckx2* gene knockout mice have been generated by the Lytton laboratory with interesting consequences (168). Mice lacking the NCKX2 protein were viable, fertile, and morphologically indistinguishable from their wild type littermates. No significant compensation mechanism was noted, as none of the other NCX and NCKX proteins and other $Ca^{2+}$ transport proteins differed in their expression. Reduced neuronal $Ca^{2+}$ fluxes measured in the knockout mice indicated that NCKX2 was responsible for a substantial fraction of $K^+$-dependent $Na^+/Ca^{2+}$ exchanger activity in neurons. The most interesting observation was made in Shaffer collateral/CA1 synapses, where a compelling loss of LTP and an increase in LTD were found. This may be due to the loss of a postsynaptic $Ca^{2+}$ extrusion system, resulting in a sustained $[Ca^{2+}]_i$ elevation that would affect the delicate balance between protein kinase and phosphatase activation. Moreover, the changes in synaptic plasticity led to subtle, but specific, behavioural deficits in the performance of these mice on specific motor learning and memory tests that depended upon the benefit of prior experience. This suggests that NCKX2 might be essential in memory consolidation or retention. Further studies are required to identify the underlying mechanisms that lead to these distinct functional abnormalities in *nckx2* knockout mice.

The zebrafish ortholog of human *NCKX5* was recently identified as the gene mutated in the *golden* phenotype, characterized by a lack of proper skin pigmentation

(156). Further investigation into the presence of potential polymorphisms within the human *NCKX5* gene revealed a single nucleotide polymorphism (SNP) encoding either alanine or threonine at amino acid 111 in the human NCKX5 protein. Analysing the allele frequency among a population sample revealed striking polarity, with the $Thr^{111}$ being the dominant allele among the European-American population, and the ancestral $Ala^{111}$ among African, Indigenous American, and East Asian population samples (156).

Studies on human NCKX5 in cultured human epidermal melanocytes and in heterologous expression systems further confirmed its role in skin pigmentation (91). Knockdown of the *NCKX5* gene using an siRNA strategy in both human and mouse melanocytes significantly reduced melanin production, directly linking the *NCKX5* gene with normal melanogenesis. Heterologous expression of human *NCKX5* in insect High Five cells resulted in $K^+$-dependent $Na^+/Ca^{2+}$ exchanger activity, which was significantly reduced when the A111T mutant was expressed. Although the A111T polymorphism by itself does not fully explain the wide variation of skin, eye, and hair colour observed within the European-American population, and the mechanism linking NCKX5 function with melanosome biogenesis is not known, this finding adds a new physiological role for the NCKX family of proteins.

### 1.4 Quaternary Structure and Sub-cellular Localization of $Na^+/Ca^{2+}$-Exchangers

One of the most crucial elements in understanding ion channels and transporters is knowledge of how their structures relate to their function. Indeed, a complete

understanding of the nature of ion transport requires detailed three-dimensional structures of channels and transporters in their native environment. However, obtaining three-dimensional structural information of membrane proteins has been laborious, due to the difficulty both of isolating pure protein and of growing well-ordered crystals of these purified proteins. Thus, only few channel and transporter structures are known to date.

Nonetheless, it is not too difficult to imagine from a purely structural point of view that a majority of the membrane proteins form oligomers and/or interact with other proteins, since volume exclusion, protein localization, and orientation in the two-dimensional space of the membrane would enhance the likelihood of both self-association as well as heteromeric protein interaction (301). If so, these interactions would no doubt have physiological consequences. For example, self-association could be the essential step in forming a proper channel or a transporter in which the ion transport pathway is formed at the subunit interface, as observed in $K^+$ channels, in which the functional pore of the channel is formed by four usually identical subunits (94, 183). Moreover, protein-protein interaction could lead to enhancement or inhibition of a protein function, either by a conformational restraint imposed by the interaction or by a functional coupling between two interacting proteins, such as seen in the interaction between SERCA and phospholamban, in which direct protein-protein association has an inhibitory effect on the function of SERCA (4).

Protein-protein interaction is also a key mechanism in the sub-cellular localization and compartmentalization of a protein complex. Many proteins involved in a common

signalling pathway, such as the intracellular $Ca^{2+}$ signalling cascade, are known to form a macromolecular complex via protein-protein interactions involving scaffolding proteins, interaction domains, and in some instances specialized lipid microdomains (36, 137, 311). The formation of such microdomains is thought to be an essential mechanism by which cells effectively organize independent signalling events so that a particular signal only elicits the appropriate response. Therefore, information on a protein quaternary structure and sub-cellular localization, and their effect on protein function and cell physiology is important for a complete understanding of the structure-function relationships of channels and transporters.

### *1.4.1 Oligomerization of $Na^+/Ca^{2+}$-Exchangers*

Both NCKX1 and NCKX2 are thought to exist as higher-order oligomeric species when expressed in recombinant systems (33, 126, 273). For NCKX1, oligomerization was also noted in the plasma membrane of bovine rod outer segment (ROS) (273). Chemical cross-linking studies using purified bovine ROS membranes revealed that virtually all NCKX1 molecules in rod photoreceptors could be disulfide-bonded to dimers with an apparent molecular mass of ~490kDa, demonstrating for the first time that $K^+$-dependent $Na^+/Ca^{2+}$-exchangers may exist as a homodimer in the plasma membrane (273). Interestingly, cross-linking of detergent-solubilized NCKX1 failed to produce the homodimeric species. The calculated molecular mass of detergent-solubilized NCKX1, based on the biophysical parameters obtained from hydrodynamic analyses, also indicated that the exchanger exists primarily as a monomer when solubilized. However, hydrodynamic studies with cross-linked and solubilized NCKX1 did produce a dimeric

exchanger, suggesting that NCKX1 primarily behaves as a monomer upon solubilization with detergent, and that dimer formation is a dynamic process that can be easily disrupted by the detergent solubilization. NCKX1 expressed in High Five insect cells also formed dimeric species upon chemical cross-linking, and co-immunoprecipitation studies using NCKX1/NCKX2 chimeras subsequently revealed that the formation of a NCKX1 dimer relied upon the presence of a single cysteine residue in the large extracellular loop of NCKX1 (128).

The functional and physiological consequences of the dimerization of NCKX1 are not clearly understood. At present, it appears as though NCKX1 is functionally fully active as a monomer, since NCKX1 is predominantly reconstituted in the monomeric state, and the reconstituted exchanger has been shown to be fully active (52, 273). More recent findings using thiol-specific cross-linkers of different sizes and partial proteolysis of the exchanger imply that dimerization inhibits the transport function of NCKX1 (9). Thus, dimerization seems to regulate the exchanger function. Interestingly, the NCKX1 dimer was shown to interact with the cGMP-gated channel (274), and thus the dimerization of NCKX1 observed in the previous cross-linking studies may be due to the close proximity of the two NCKX1 molecules created by their strong affinity for the cGMP-gated channel. However, whether this hypothesis is true or whether dimerization is the essential prerequisite for channel-exchanger association remains to be answered.

Oligomerization of NCKX2 was first noted in co-immunoprecipitation studies using HEK-293 cells expressing two different recombinant NCKX2 proteins (33).

Subsequently, chemical cross-linking of NCKX2 revealed the formation of a higher molecular weight adduct with an apparent molecular weight greater than predicted for the NCKX2 dimer (126). Just as for NCKX1, the formation of the higher molecular weight adduct of NCKX2 was attributed to the presence of a single cysteine residue, which in NCKX2 is found in the central cytosolic loop. However, the precise molecular identity and the oligomeric state of the higher molecular weight adduct of NCKX2 are not known. The cysteine residue in the central cytosolic loop of NCKX2 is considered to be inaccessible to sulfydryl modifying agents in the resting state unless is it subjected to prior reduction (33). In addition, the reduction of this cysteine was shown to activate the exchanger, presumably by relieving a structural constraint (33). Altogether these data seem to indicate that potential protein-protein interactions mediated by the cysteine residue in the central cytosolic loop of NCKX2 might regulate its exchanger function. Further studies are required to resolve this issue.

Unlike NCKX1 and NCKX2, evidence for NCX oligomerization is more limited. When analyzed by SDS-PAGE and immunoblot under non-reducing conditions, recombinant NCX1 transiently expressed in HEK-293 cells was observed to migrate as a band with an apparent molecular weight of the exchanger dimer (170). Recently, chemical cross-linking using single-cysteine exchangers revealed the presence of the higher molecular weight species resembling the NCX1 dimer (170, 249). Subsequent pull-down experiments detected the self-association of NCX1, further supporting the formation of the NCX1 dimer. Interestingly, NCX1 dimers were only observed in pull-down experiments after cross-linking the exchangers, suggesting that the interaction

between NCX1 monomers might be weak and thus easily disrupted by detergent solubilization. A higher molecular weight adduct of NCX1 greater than the dimer was also noted, but the origin of this higher molecular weight adduct was not further investigated. Although this study was not able to determine the functional consequence of NCX1 dimerization, it presented the first biochemical data indicating that NCX can form oligomers in the membrane environment.

### *1.4.2 Protein-Protein Interaction of $Na^+/Ca^{2+}$-Exchangers*

Protein interactions are the key mechanisms used in the assembly of a cell's structural compartments, such as the cytoskeleton and the nuclear pore. In addition, they are crucial for the localization and functional regulation of many membrane proteins and transporters. These interactions are often mediated by scaffolding proteins via conserved, specialized domains that recognize specific binding sites in their partner (225, 291), coordinating the clustering of the receptors and channels in the plasma membrane as well as anchoring them to the cytoskeleton. As well, the function of many membrane transporters is influenced by their interaction with other proteins. This area of study is not well developed for $Na^+/Ca^{2+}$-exchangers, and investigating these interactions will be important to understanding their physiological roles.

Nonetheless, several interacting partners of NCX1 have been identified which appear to impart regulatory effects on the exchanger activity. One of the earliest observations that NCX1 preferentially localized to myocyte T-tubules (75) led to the discovery of the association between NCX1 and the cytoskeletal protein ankyrin (189).

Ankyrins are peripheral membrane proteins known to link several plasma membrane proteins and elements of the cytoskeleton. *In vitro* immunoprecipitation experiments confirmed that ankyrin directly binds to NCX1, thereby providing a potential mechanism for the specific localization of NCX1 in a limited environment within cardiac myocytes. Subsequently, studies using mice heterozygous for a null mutation in ankyrin-B further confirmed the presence of an NCX1, ankyrin-B, $Na^+/K^+$ ATPase, and $IP_3R$ complex in cardiac myocytes that is distinct from the classic VGCC/ryanodine receptor dyads found along the T-tubules (194). It is highly likely that the direct interaction between ankyrin-B and NCX1 is necessary for the proper expression, localization, and post-translational stability of the exchanger (55). Although the ankyrin binding site in NCX1 has not been identified, it would be reasonable to assume that the large cytosolic loop of NCX1 may be responsible. Since this region is known to be important for the functional regulation of the exchanger, it implies that ankyrin interactions here may also have functional consequences.

Evidence also suggests that NCX1 might interact with the actin cytoskeleton and that this interaction may influence its exchanger function. Recombinant NCX1 expressed in the plasma membrane of Chinese hamster ovary (CHO) cells was found to be associated with the underlying filamentous-actin (F-actin) cytoskeleton in regions of cell-to-cell contact. (51). Deletion of the central cytosolic loop of the exchanger disrupted this association, implying that it is mediated by the cytosolic loop domain. It appears that F-actin association with the exchanger also modulates allosteric $Ca^{2+}$ activation of exchanger activity, but whether this effect is due to a direct protein-protein interaction or

due to more indirect influences caused by the formation of a larger macromolecular complex is not clear at this moment and requires further detailed analyses.

Phospholemman (PLM), a small single transmembrane spanning protein, is a member of the FXYD family of ion transport regulators known to modulate $Na^+/K^+$ ATPase activity in numerous tissues and to be important for proper cardiac contractility (87). Overexpressing wild-type and mutant PLM in rat cardiac myocytes using adenoviral infection showed that phosphorylation at Ser68 in the cytosolic tail of PLM by PKA is critical in mediating PLM's effect on contractility, $[Ca^{2+}]_i$ transients, and $Na^+/Ca^{2+}$ exchanger activity (281). Follow up studies using HEK-293 cells co-expressing recombinant NCX1 and PLM, as well as studies using PLM knockout mice, further confirmed that PLM binds to NCX1 in two regions located in the cytosolic loop, and that phosphorylation at Ser68 of PLM inhibits exchanger function (306, 313). The phosphorylation of Ser68 also seems to relieve the inhibitory effect of PLM on $Na^+/K^+$ ATPases. Taken together, these data are consistent with the role of β-adrenergic agonists in facilitating $Ca^{2+}$ influx and enhancing cardiac contractility.

Yeast two-hybrid screening strategies have recently identified two more NCX1 interacting partners, calcineurin and 14-3-3 proteins (131, 239). Calcineurin is a $Ca^{2+}$-sensitive serine/threonine protein phosphatase, originally identified in mammalian brain (53). The interaction between the C-terminus of calcineurin and the cytoplasmic loop of NCX1 exerted an inhibitory effect on the exchanger function, and was enhanced in hypertrophic neonatal rat cardiac myocytes subjected to chronic phenylephrine treatment

(131). The 14-3-3 proteins are a family of conserved regulatory proteins abundantly expressed in almost all eukaryotic cells that are capable of binding a wide variety of phosphorylated proteins (300). Various isoforms of the 14-3-3 protein family are able to interact the cytosolic loop of NCX1, 2, and 3 in phosphorylation-dependent manner, resulting in the inhibition of the exchanger activity (239). However, the precise physiological implications of the interactions between the exchanger and calcineurin or the 14-3-3 proteins are yet to be understood.

Compared to NCX1, not much is known about the protein-protein interactions of $K^+$-dependent $Na^+/Ca^{2+}$-exchangers. The best described protein-protein interaction was observed between NCKX1 and cGMP-gated channels in the outer segments of rod photoreceptors as mentioned above (8, 9, 126, 273, 274). Studies using calmodulin affinity chromatography and chemical cross-linking revealed that the α-subunit of cGMP-gated channels is associated with exchanger monomers in the plasma membrane in a molar ratio of 1:2 (274). The binding of the exchanger was specific to the α-subunit but not to the β-subunit of the cGMP-gated channel, but which part of the exchanger interacted with the α-subunit of the channel was not known. It was speculated that the dimerization of NCKX1 might be a consequence of its strong association with cGMP-gated channels, since two exchanger monomers bind tightly to one cGMP-gated channel, placing them in close physical proximity (274). Moreover, both the interaction with cGMP-gated channels and dimerization seem to inhibit NCKX1 function. Whether the function of cGMP-gated channels is also regulated by this proposed interaction is not clearly understood at this moment.

When expressed in recombinant systems, both NCKX1 and NCKX2 were shown to interact with the α-subunit of cGMP-gated channels by thiol-specific cross-linking and co-immunoprecipitation experiments (126). The interaction between the exchanger and the channel did not seem to be mediated by the central cytosolic loop of the exchanger, since deletion of the cytosolic loop did not affect the ability of either NCKX1 or NCKX2 to pull down the α-subunit of cGMP-gated channels (126). Moreover, both NCKX1 and NCKX2 were able to interact with different α-subunits of cGMP-gated channels (α-1 and α-3), suggesting that the interaction was not restricted to certain protein isoforms and might be a general phenomenon shared by the NCKX and cGMP-gated channel isoforms expressed in other cell types. The physiological implications of the observed interaction require further investigation.

### *1.4.3 Lipid Rafts, Caveolae, and Sub-cellular Localization of $Na^+/Ca^{2+}$-Exchangers*

Lipid rafts are detergent resistant, liquid-ordered microdomains of the plasma membrane that are rich in cholesterol and sphingolipids (82, 216, 268). Caveolae are a subset of lipid raft microdomains that appear as vesicular invaginations of the plasma membrane (216). Since their discovery, lipid rafts and caveolae have been linked to a variety of cellular activities and biological processes, such as endo/exocytosis, apoptosis, cell adhesion, cell migration, and the sub-cellular localization of proteins involved in signal transduction pathways. Caveolin-1 was the first structural protein to be identified in the lipid raft microdomain, and is the hallmark that distinguishes caveolae from all other non-caveolar lipid raft microdomains (155, 258). It is a scaffolding protein of 176

amino acids that forms a hairpin-like structure within the membrane. Its oligomerization is what brings about the invagination characteristic of caveolae (82).

So far, three distinct caveolin genes have been identified by molecular cloning: caveolin-1, caveolin-2, and caveolin-3 (93, 267, 291). 22kDa caveolin-1 and 20kDa caveolin-2 are co-expressed in many cell types, but are especially abundant in adipocytes, endothelial cells, and fibroblastic cell types, whereas the expression of caveolin-3 is muscle specific (82). Both homo- and hetero-oligomerization of caveolins are known to occur *in vivo*, forming high molecular mass oligomers containing approximately 14 to 16 individual molecules (268). In addition, caveolin homo- and hetero-oligomers are thought to interact with glycosphingolipids of the plasma membrane (74). It is these oligomer/oligomer and oligomer/lipid interactions that result in the interlocking network of caveolin molecules, which in turn give rise to the characteristic invagination.

Many studies indicate that caveolins modify the function of a range of signalling proteins (82). The exact mechanisms underlying this modulation are not clearly understood, but one speculation is that caveolins interact directly with signalling proteins and regulate their activity. As well, it is possible that caveolins cluster other membrane proteins and signaling molecules together within sequestered microdomains, thereby localizing whichever signals these proteins mediate. In either way, the clustering and/or regulation of signalling proteins in the caveolar microenvironment would result in more rapid cross-talk and an increased efficiency of signal transmission (268). Several proteins, such as endothelial nitric oxide synthase (eNOS) and G-protein $\alpha$-subunits, have

been shown to bind directly to caveolins (45, 84). This interaction is thought to occur through a caveolin scaffolding domain composed of residues 82~102 of caveolin-1, which binds to a specific ϕXϕXXXXϕXXϕ motif in its interacting proteins, where ϕ is a Phe, Tyr, or Trp residue and X is any amino acid (268).

Despite over a decade of extensive investigation, skepticism about the precise properties of lipid rafts/caveolae and their physiological roles, and even of the existence of such lipid microdomains still persists. The most commonly used technique for raft detection and isolation, the density floatation method, exploits the resistance of the lipid rafts/caveolae microdomain to solubilization by cold, nonionic detergents (174). Despite its popularity and ease of use, the density floatation method is only indirect and thus subject to different interpretations (199). Moreover, much controversy surrounds the precise identity of the detergent insoluble complexes, the influence of the detergent on the structure and/or aggregation of the domain, and whether this complex actually exists in cell membranes prior to detergent extraction. Hence, names other than the lipid rafts/caveolae microdomains, like detergent-resistant membranes (191), have been used to describe the detergent insoluble complex. Nonetheless, thermodynamic considerations and studies using a model membrane system suggest that the formation of the so-called cholesterol-rich “liquid-ordered” plasma membrane microdomains are possible (199, 279). Altogether, caution is needed in interpreting the data obtained when detergent insolubility is used as the means to isolate the rafts and caveolae microdomains.

Mounting evidence suggests that lipid rafts/caveolar microdomains are also responsible for the compartmentalization of proteins involved in intracellular $Ca^{2+}$ signalling pathways (95, 118). The muscle specific isoform, caveolin-3, is expressed in the heart and localized in the cardiac sarcolemma, where it appears to assume an important role in normal cardiac function. Transgenic overexpression of caveolin-3 in the mouse heart results in cardiomyopathy (3), and caveolin-3 gene knockout results in cardiac hypertrophy, reduced cardiac shortening, as well as progressive cardiomyopathy (310). Moreover, proteins like PMCA, members of the TRP family of capacitative $Ca^{2+}$ entry channels, $IP_3R$, and PLCβ are abundant in caveolae, strengthening the argument that caveolae and cavolin-3 are important for the localization and compartmentalization of these $Ca^{2+}$ handling proteins in cardiac myocytes and this is essential for normal heart function (77, 118, 177, 296).

Recently, the interaction of NCX1 with caveolin proteins in bovine cardiac sarcolemmal vesicles has been examined (25, 36). Although NCX1 is mostly found in the T-tubules of the sarcolemma, whereas caveolins are predominantly found on the surface membrane of ventricular myocytes, there was considerable overlap between the expression patterns of these proteins (275). Three potential caveolin-binding motifs in NCX1 were identified and co-immunoprecipitated to test possible interactions between NCX1 and the three caveolin isoforms in sarcolemmal vesicle preparations. Interestingly, NCX1 was shown to associate with caveolin-3, but not with caveolin-1 or caveolin-2. Depleting the vesicle preparation of cholesterol using the detergent β-cyclodextrin decreased NCX1 transport activity as well as caveolin-3 co-precipitation with NCX1.

Another study using non-failing and failing human hearts also demonstrated NCX1 association with caveolin-3, as well as annexin A5, implying that the caveolar-based macromolecular complexes might exist in the heart, where the proteins involved in intracellular $Ca^{2+}$ homeostasis are found clustered together (34). A more recent study, however, has caste doubt onto the quantitative significance of the observed interactions between NCX1 and caveolin in heart (36).

Additionally, there is evidence to suggest an association of NCX1 with caveolin-1 and caveolin-2 in rat C6 glioma cells (38). All three proteins are endogenous to C6 glioma cells, which do not express caveolin-3. Using a detergent-free method to isolate lipid rafts and/or caveolar microdomains (282), co-fractionation of NCX1 with caveolin-1 and caveolin-2 was noted. Further examination using co-immunoprecipitation and confocal microscopy revealed co-association and co-localization of these proteins, implying a caveolar localization of NCX1 in C6 glioma cells. Moreover, a decrease in the exchanger activity was observed when the expression of either caveolin-1 or caveolin-2 was inhibited, indicating that the NCX1-caveolin interaction may be important for the regulation of NCX1 function. Altogether, studies on the sub-cellular localization of NCX1 suggest that it is localized to the caveolae and interacts with caveolin proteins.

## 1.5 Research Objectives

The overall objective of this dissertation is to gain better understanding of the quaternary structure and sub-cellular localization of the $K^+$-dependent $Na^+/Ca^{2+}$-

exchanger, NCKX2. NCKX2 in mammalian brain is known to exhibit a distinctive punctate pattern reminiscent of proteins with caveolar localization (168). Considering the interaction of NCX1 with caveolin-3 in cardiac myocytes and the significance of the lipid raft microdomains to the sub-cellular localization of many signalling molecules, it is of great interest to study whether NCKX2 is also localized to the lipid raft/caveolar domains and interacts with caveolins. ***Thus, the first objective of this dissertation is to study the sub-cellular localization of NCKX2 to the lipid raft and/or caveolae microdomain, as well as to investigate possible associations between caveolins and NCKX2.*** Whole rat brains were used to isolate detergent-resistant membranes containing lipid rafts and/or caveolar microdomains by cold Triton X-100 extraction and density floatation using sucrose density gradient centrifugation, after which the fractionation pattern of NCKX2 was investigated. Co-immunoprecipitation experiments were conducted to test the association between caveolins and NCKX2.

Although rod photoreceptor NCKX1 has been shown to dimerize in the plasma membrane and to interact with cGMP-gated channels (272, 273), the precise oligomeric state of NCKX2 and its functional significance has not been examined in detail. Thus, it is of interest to investigate whether NCKX2 also forms dimers or higher order oligomers in the plasma membrane, and whether such oligomerization would be essential for NCKX2 function. This study would provide valuable information about the structural features underlying the function of NCKX2. ***Therefore, the second objective of this dissertation is to determine the oligomerization state of NCKX2.*** Catalyzed oxidation of adjacent free sulfydryls to disulfide bonds using 1, 10-phenanthroline complexed copper

was carried out using recombinantly expressed NCKX2 and rat brain NCKX2. In addition, cysteine mutant forms of NCKX2 were expressed in HEK-293 cells and used for oxidation reactions to identify those free sulfydryls responsible for the formation of NCKX2 oligomers. Co-immunoprecipitation analysis was carried out to confirm the homo-oligomerization of NCKX2. Finally, Blue-Native Polyacrylamide Gel Electrophoresis was performed to examine the precise molecular composition of the NCKX2 oligomers.

Regulation of NCKX2 function by protein-protein interaction has not been studied in detail. Cross-linking analyses have revealed the presence of a higher molecular weight adduct of NCKX2 whose size was greater than predicted for a NCKX2 dimer (126). The formation of this high molecular weight adduct was dependent on the single cysteine residue in the central cytosolic loop of the exchanger, although this residue was not important for non-covalent homomeric association of NCKX2 (33, 126), suggesting that it mediated a heteromeric association of NCKX2. ***Therefore, the last objective of this dissertation is to identify the potential protein-protein interactions and associations of NCKX2.*** Immunoprecipitation of endogenous NCKX2 from rat brain synaptosomal membrane vesicles or recombinant NCKX2 expressed in HEK-293 cells was carried out along with protein SDS-PAGE and tandem mass spectrometry combined with nanoscale liquid chromatography to identify the potential interacting partner(s) of NCKX2. Once identified, their interaction was confirmed by co-immunoprecipitation analyses.

# CHAPTER TWO

## Experimental Procedures

## 2.1 Molecular Techniques

### *2.1.1 Reagents, DNA Constructs, and Antibodies*

All common chemicals and reagents used were of analytical grade or better and were purchased from BDH, Fisher, VWR, or Sigma unless indicated otherwise. All molecular procedures were carried out essentially according to previously established protocols and according to the manufacturer's guidelines and manuals. All the cDNA expression constructs used in this thesis (except caveolin-2) were prepared previously by former members of the Lytton laboratory. Construction of the wild-type rat brain NCKX2 cDNA in the pcDNA 3.1(+) vector (Invitrogen), the N-terminal FLAG-tagged NCKX2 cDNA in the pRc/CMV vector (Invitrogen), and the Cysteine-to-Alanine mutants of both FLAG-tagged and untagged NCKX2 cDNA in the pcDNA 3.1(+) vector were described in previous studies (33, 297). Construction of rat heart NCX1.1, and human SERCA2, both in the pcDNA 3.1(+) vector, has also been described in previous studies (61, 233). Rat caveolin-1 expression constructs were prepared by a former member of the Lytton laboratory by PCR-based on database sequence, as described below for caveolin-2.

Affinity-purified polyclonal PA1-926 antibody directed against amino acid residues 90~102 (DLNDKIRDYTPQP) of rat brain NCKX2 was purchased from Affinity Bioreagents, Inc. Polyclonal antibody F against rat brain NCKX2 was prepared at the Southern Alberta Cancer Research Centre Hybridoma and Antibody Facility by immunizing rabbits with a glutathione S-transferase fusion protein containing amino acid

residues 384~463 of rat brain NCKX2 (33). All other antibodies used were purchased from BDH, Sigma, Medicorp, or Affinity Bioreagents, Inc. unless indicated otherwise.

*2.1.2 Generation of the Rat Caveolin-2 Expression Constructs*

5'-end forward and 3'-end reverse primers (ATGGGGCTGGAGACCGAG and TCAGTTGTGGCTCAGTTGCA, respectively) based on the rat caveolin-2 sequence (AF439780) were designed and used to amplify the cDNA of rat caveolin-2 by reverse-transcription-coupled polymerase chain reaction (RT-PCR) using Superscript II Reverse Transcriptase (Invitrogen) and Expand High Fidelity PCR System (Roche Molecular Biochemicals) using total RNA isolated from rat cerebrum as the template. The RT-PCR reaction yielded a single band of 489bp, which was subsequently ligated into the *EcoRV*-site of pBluescript II SK (-) (Stratagene) using the Quick-stick DNA Ligation Kit (Bioline), and sequenced to confirm its identity. The cDNA clone was then digested with *HindIII* and *EcoRI*, and the excised region containing the coding sequence of rat caveolin-2 was ligated into the pcDNA 3.1 (-) vector (Invitrogen).

*2.1.3 Expression of DNA constructs in HEK-293 Cells*

Human embryonic kidney cells (HEK-293) were cultured in high glucose Dulbecco's modified Eagle's Medium supplemented with 10% fetal bovine serum, 2mM L-glutamine, 1.0% non-essential amino acids, and 1.0% penicillin/streptomycin (100U/mL and 100µg/mL respectively), and maintained in 5.0% $CO_2$ at 37.0ºC. Transfection of Qiagen-purified cDNA constructs into HEK-293 cells in 100mm plates was performed using a standard calcium phosphate precipitation protocol with 2×N,N-

bis(2-hydroxyethyl)-2-aminoethanesulfonic acid buffer (BES buffer) as described previously (297).

*2.1.4 Protein Separation by SDS-PAGE, Immunoblotting, and Gel Staining*

Proteins in postnuclear extracts, microsomal fractions, detergent solutions, and other samples were separated and then visualized by sodium dodecyl sulfate polyacrylamide gel electrophoreses (SDS-PAGE) followed by immunoblotting, Coomassie staining, or silver staining. For SDS-PAGE, samples were mixed with equal volumes of 4×SDS sample buffer (0.25M Tris(hydroxymethyl)aminomethane hydrochloride (Tris·HCl), pH 6.8, 8.0% (w/v) SDS, 40% glycerol, and 8.0% β-mercaptoethanol). Samples were then immediately loaded on a gel without heating or boiling to prevent hydrophobic membrane proteins from forming aggregates. For non-reducing SDS-PAGE, SDS sample buffer without 8.0% β-mercaptoethanol but containing all other reagents was mixed with the sample, and the electrophoresis was carried out as described above. In all cases, broad-range prestained protein molecular weight markers (New England Biolabs, Inc.) and/or unstained protein molecular weight standards (Bio-Rad) were used as the markers for protein molecular weight.

Proteins separated by SDS-PAGE were transferred to nitrocellulose membranes and immunoblotting was performed as described previously (33, 297). All solutions used in immunoblotting experiments were made in phosphate buffered saline (1×PBS, 130mM NaCl, 3.0mM KCl, 8.0mM $Na_2HPO_4 \cdot 7H_2O$, 2.0mM $KH_2PO_4$, pH 7.2) containing 0.1% polyethylene glycol sorbitan monolaurate (TWEEN® 20). Briefly, immediately after

transfer, nitrocellulose membranes were incubated in a blocking buffer containing 5.0% (w/v) skim milk in PBS with gentle rocking overnight at 4.0ºC. The membranes were then incubated with various primary antibodies and horseradish peroxidase-conjugated secondary antibodies. The membranes were washed with PBS·TWEEN® 20 three times between the antibody applications as well as after the incubation with the secondary antibodies. The antibody signal was detected using Pierce Super Signal Plus ECL reagents.

Coomassie Brilliant Blue staining was carried out by staining a gel in 0.25% w/v Coomassie Brilliant Blue G-250, 50% methanol, 10% glacial acetic acid for 30 to 60 minutes, and then destaining the gel overnight in destain solution (40% methanol and 10% glacial acetic acid) or until the background became clear. Silver staining of SDS-PAGE gels was performed using the mass spectrometry compatible SilverQuest Silver Staining Kit from Invitrogen by following the manufacturer's instructions.

*2.1.5 Oxidation of Thiol Groups using 1,10-phenanthroline-complexed Copper*

Catalyzed oxidation of adjacent free sulfydryl groups to disulfide bonds was performed on ice for 30 minutes using 1,10-phenanthroline-complexed copper (CuPhe, final concentration of 2.0mM $CuCl_2$, and 10mM 1,10-phenanthroline) in 30mM N-(2-hydroxyethyl)piperazine-N'-2-ethanesulfonic acid/potassium hydroxide buffer (HEPES/KOH buffer), pH 7.4 containing protease inhibitors aprotinin (10µg/mL), phenylmethanesulfonyl fluoride (PMSF, 0.1mM), and leupeptin (1.0µg/mL) (273). Stock solutions of 500mM $CuCl_2 \cdot 2H_2O$ in $H_2O$ and 500mM 1,10-phenanthroline in dimethyl

sulfoxide (DMSO) were used to make the working solution of CuPhe containing 2.0mM $CuCl_2 \cdot 2H_2O$ and 10mM 1,10-phenanthroline. All solutions were made freshly just prior to use. The reaction was started by adding an equal volume of chilled CuPhe solution to the HEK-293 cell microsome preparations, rat brain synaptosomal membrane vesicles (rat brain microsomes) or detergent solubilized preparations so that the final concentration of $CuCl_2 \cdot 2H_2O$ and 1, 10-phenanthroline would reach 1.0mM and 20mM respectively. After 30 minute incubation on ice, the reaction was terminated by adding ethylenediaminetetraacetic acid (EDTA) to a final concentration of 10mM. Control experiments were also performed as described above using 30mM HEPES/KOH solution without CuPhe but containing all other reagents listed.

All the samples were run on 7.5% SDS-PAGE gels in both reducing and non-reducing conditions and transferred to nitrocellulose membranes. Immunoblotting experiments were then carried out using M2 anti-FLAG antibody (0.5µg/mL, Sigma) or the polyclonal antibody F against rat brain NCKX2 (1:5000 dilution) to detect the presence of disulfide bond-dependent higher molecular weight species of NCKX2.

*2.1.6 Blue-Native Polyacrylamide Gel Electrophoresis*

BN-PAGE was performed essentially as described by Schägger and von Jagow (265) using detergent solubilized HEK-293 cell microsomes transiently expressing NCKX2-FLAG or the Cys395Ala mutants of NCKX2-FLAG (NCKX2-FLAG C395A). Briefly, HEK-293 cell microsomes were solubilized on ice for 30 minutes using an equal volume of BN gel solubilization buffer containing 2.0mM EDTA pH 8.0, 20mM bis(2-

hydroxyethyl)iminotris(hydroxymethyl)methane (Bistris) pH 7.0, 0.5M 6-aminohexanoic acid, 1.0% glycerol, and either 2.0% Triton X-100 or CHAPS, so that the final concentration of the detergent in a solution reached 1.0%. The solubilized samples were then centrifuged for 5 minutes at 4.0ºC at maximum speed (16,000*g*) and the supernatant containing the solubilized membrane fractions was collected. The solubilized microsomes were then exposed to varying amounts of SDS (2.0%, 1.0%, 0.5%, 0.25%, and 0.0% w/v final concentration in the BN Gel solubilization buffer) with or without 0.1M 1, 4-dithiothreitol (DTT) for 30 minutes at 37.0ºC. After SDS solubilization, the samples were mixed with BN Gel sample buffer (100mM Bistris, 500mM 6-aminohexanoic acid, pH7.0) containing CBB G250 (0.5% w/v final concentration) and loaded on a BN gradient gel (5.0%~15% continuous gradient). The BN-PAGE was run at 4ºC for 1h at 100V with a cathode buffer (50mM Tricine, 15mM Bistris) containing 0.02% (w/v) CBB G250. The cathode buffer was then replaced with one lacking CBB G250 and electrophoresis continued for 2~3h at 150V. High Molecular Weight Calibration Kit for Electrophoresis (Amersham Biosciences) was used as the molecular weight markers. A conversion factor of 1.8 was applied to correct the molecular weights of the marker proteins to account for the differential amount of CBB bound to membrane proteins, as compared to the soluble marker proteins (104). This was achieved by dividing the actual marker protein mass by 1.8, and using the calculated mass for calibration of NCKX2 run on BN-PAGE.

For immunoblotting experiments of BN-gels stained with CBB G250, the stained gels were soaked in 25mL cold immunoblot transfer buffer (25mM Tris, 190mM glycine,

20% methanol) containing 0.1% (w/v) SDS for at least 30 minutes, and the transfer to nitrocellulose membranes was carried out using transfer buffer containing 0.01% SDS for 1 hour at 100V at 4.0ºC. The nitrocellulose membranes containing the transferred proteins appeared quite blue, and were subsequently destained with 45% methanol and 10% glacial acetic acid until they appeared reasonably clear in order to remove excess CBB G250 which interferes with antibody binding to the proteins. Destained membranes were washed briefly with 1×PBS, and the immunoblotting experiments were performed as described in section 2.1.4. The M2 anti-FLAG monoclonal antibody was used as the primary antibody for these immunoblotting experiments.

## 2.2 Preparation of Cell Extracts and Plasma Membrane Vesicles Fractions

### *2.2.1 HEK-293 Cell Post-nuclear Extracts and Microsome Preparation*

Approximately 48 hours after HEK-293 cells were transfected in 100mm plates with appropriate Qiagen-purified expression plasmids, cells were harvested by washing twice with PBS pH 7.2 and then collected by scraping and centrifugation. The cells were then solubilized for 30 minutes in 100µL ice-cold lysis buffer containing 1.0% detergent (Triton X-100 or CHAPS), 0.14M NaCl, 25mM Tris·HCl pH 7.5, 10mM EDTA, 0.1mM PMSF, and 100U/mL aprotinin per P100 plate. Samples were then centrifuged for 5 minutes at 4ºC in a microfuge at maximum speed (16,000×*g*), and the supernatant containing the detergent solubilized post-nuclear extracts was collected and immediately frozen at -80ºC.

HEK-293 microsomal membrane fractions were isolated as previously described with only minor modifications (185, 252). Briefly, approximately 48 hours post-transfection, cells in five 100mm plates were washed twice with PBS, scraped from the dish, collected by centrifugation, and swollen in 2.0mL of 10mM Tris·HCl pH 7.5 and 0.5mM $MgCl_2$. Final concentrations of 100U/mL aprotinin and 0.1mM PMSF were added to the swollen cells immediately before they were homogenized with 40 strokes in a 7.0mL Dounce Homogenizer with a tight A pestle. 2.0mL of 0.5M sucrose, 10mM Tris·HCl pH 7.5, 40µM $CaCl_2$, and 0.3M KCl was added to the homogenate and the samples were further homogenized with 20 strokes with a tight A pestle. The suspension was centrifuged for 20 minutes at 8,000*g* (4.0ºC) to pellet nuclei and mitochondria. The supernatant (~3.0mL) was collected and added to an ultracentrifuge tube containing 0.9mL of ice-cold 2.5M KCl so that the final concentration of KCl was 0.6M. The suspension was centrifuged for 1 hour at 120,000*g* (4.0ºC) in a Sorvall Ti75 fixed angle rotor to pellet a crude microsomal membrane fraction. The microsomes were resuspended in 100~150µL of 0.25M sucrose, 10mM Tris·HCl pH 7.5, 20µM $CaCl_2$, and 0.15M KCl, snap-frozen in liquid $N_2$ and stored at -80ºC.

Concentrations of proteins present in HEK-293 cell post-nuclear extracts and microsomal membrane fractions were determined by the Bradford Dye Binding Assay (Bio-Rad) using bovine γ-globulin as a protein standard and following the manufacturer's instructions. SDS-PAGE and immunoblotting were performed to confirm that the proteins encoded by the transfected constructs were expressed.

*2.2.2 Preparation of Rat Brain Synaptosomal Membrane Vesicles*

3 month-old male Sprague Dawley rats were sacrificed in a $CO_2$ chamber and their brains were removed as quickly as possible. Isolation of the whole-brain synaptosomal membrane vesicles was usually carried out immediately after the dissection of the brain. Otherwise, the dissected brains were immediately frozen by dipping in liquid nitrogen and stored at -80ºC until required, at which time they were rapidly thawed in a 37ºC water bath, then chilled on ice. Protein yields and membrane fractionation characteristics were indistinguishable between material isolated from fresh or from frozen brain. The wet weight of the dissected whole rat brain ranged from 1.9g to 2.1g. All buffers used in the isolation procedure were prepared freshly just prior to use and contained protease inhibitors PMSF (0.1mM final concentration), aprotinin (100U/mL), and leupeptin (1.0µg/mL).

A dissected whole rat brain was coarsely minced with scissors in 10.0mL of ice-cold homogenization buffer (0.25M sucrose, 25mM Tris·HCl pH 7.5, 1.0mM EDTA) and was homogenized by 15 strokes in a 7.0mL Dounce Homogenizer with a loose B pestle followed by another 15 stroke homogenization with a tight A pestle on ice. The suspension was centrifuged for 5 minutes at 1,000*g* (4.0ºC) in a Beckman JA-20 rotor, and the supernatant was collected into a fresh tube and kept on ice. The pellet formed from the centrifugation was resuspended in 10mL homogenization buffer by homogenizing with a tight A pestle (15 strokes), and re-centrifuged for 5 minutes. The resulting supernatant was combined with the supernatant collected from the initial centrifugation, and centrifuged again for 20 minutes at 12,000*g* (4.0ºC) in a JA-20 rotor.

The supernatant formed from this centrifugation was discarded and the pellet was resuspended in 10mL of 5.0mM Tris·HCl pH 7.5 and incubated on ice for 30 minutes before it was homogenized with a tight A pestle (20 strokes). 2.13volumes of 50% (w/v) sucrose solution in 10mM Tris·HCl pH 7.5 were mixed with the resuspension, which was then transferred to a clear Type 70Ti ultracentrifuge tube (25×89mm PC/PPO, Nalgene), and overlaid with 28.5% and 10% (w/v) sucrose solution in 10mM Tris·HCl pH 7.5 in succession to form a step sucrose density gradient. Ultracentrifugation was carried out for 30 minutes at 85,000g (4.0ºC) using a Beckman Type 70Ti rotor with slow deceleration and no brake. After the ultracentrifugation, the two sucrose gradient interfaces were clearly visible. The top interface (10%/28.5% interface) containing mostly myelin was discarded, while the second interface enriched with the synaptosomal membrane fractions was collected and diluted with 3×volumes of water. The diluted synaptosomal membrane fraction was subjected to another round of ultracentrifugation for 1 hour at 150,000*g* (4.0ºC) in a Type 70Ti rotor, and the pelleted synaptosomal membrane vesicles were washed and resuspended in a small volume (500~700µL) of 50mM NaCl and 50mM Tris·HCl pH 7.5. Concentrations of proteins in resuspended synaptosomal membrane vesicles were determined by the Bradford Dye Binding Assay, and SDS-PAGE and immunoblotting were performed to confirm the enrichment of rat brain NCKX2 in the isolated synaptosomal membrane vesicles.

## 2.3 Immunoprecipitation

### *2.3.1 Co-immunoprecipitation of recombinant NCKX2 from HEK-293 Cells*

Co-immunoprecipitation of N-terminal FLAG-tagged rat brain NCKX2 (NCKX2-FLAG), untagged wild-type rat brain NCKX2, and Cys395Ala mutants of both FLAG-tagged and untagged rat brain NCKX2 transiently co-expressed in HEK-293 cells was carried out essentially as described previously with minor modifications (33). Chilled Radio-immunoprecipitation assay buffer (RIPA buffer) containing 1.0% detergents (Triton X-100 or CHAPS), 0.14M NaCl, 25mM Tris·HCl pH 7.5, 10mM EDTA, 0.1mM PMSF, and 100U/mL aprotinin were used throughout the experiment.

Briefly, 500µg~1.0mg HEK-293 cell microsomes isolated from cells transiently transfected with different recombinant rat brain NCKX2 constructs in varying combinations were solubilized in ice-cold RIPA buffer (1.0mL final volume) for 30 minutes on ice, centrifuged at maximum speed (16,000*g*) for 5 minutes (4.0ºC), and the supernatant containing the solubilized membranes was collected. 100µL of 20% (w/v) Protein A Sepharose CL-4B (Sigma) swollen in RIPA buffer was then added to the supernatant, and the samples were slowly rotated for 30 minutes at 4.0ºC followed by low speed centrifugation (800*g* for 2 minutes) to clear the supernatant of the proteins that would bind directly to the Sepharose beads and interfere with the data analyses. The precleared supernatant was then mixed with 5.0µg M2 anti-FLAG monoclonal antibody (Sigma) for 2 hours by slow rotation at 4.0ºC. The antibody bound FLAG-tagged rat brain NCKX2 proteins were then immunoprecipitated with 100µL of 20% Protein A

Sepharose overnight (slow rotation, 4.0ºC). The beads were washed three times with 1.0mL RIPA buffer containing 0.3% detergent by quickly vortexing and spinning at 800*g* for 2 minutes (4.0ºC). The Protein A Sepharose beads with bound proteins were transferred to a fresh microcentrifuge tube, collected by a final spin at 800*g* for 2 minutes (4.0ºC), and the bound proteins were detached and collected by adding 50µL 2×SDS sample buffer containing 6.0% (w/v) SDS and 5% β-mercaptoethanol and heating the samples to 65ºC for 5 minutes. The sample buffer containing immunoprecipitated proteins was frozen immediately at -80ºC until used.

*2.3.2 Immunoprecipitation of NCKX2-FLAG Using Anti-FLAG M2-affinity Gel*

Immunoprecipitation of N-terminal FLAG-tagged rat brain NCKX2 (NCKX2-FLAG) transiently expressed in HEK-293 cells using anti-FLAG M2 agarose affinity gel from Sigma was performed essentially as described above with some modifications. Briefly, HEK-293 cells transiently expressing NCKX2-FLAG were grown in 100mm plates and, 48 hours after transfection, they were washed twice with ice-cold PBS and solubilized in 1.0mL RIPA buffer containing 1.0% Triton X-100 per P100 plate for 1h on ice. Samples were then centrifuged at maximum speed (16,000*g*) for 5 minutes (4.0ºC), the supernatant containing solubilized membrane fractions was collected, and 100µL of pre-washed anti-FLAG M2-affinity gel was added to immunoprecipitate NCKX2-FLAG and its potential interacting partners from HEK-293 cells. HEK-293 cells transfected with the mammalian expression vector (pcDNA 3.1 (+)), rat NCX1.1, or untransfected HEK-293 cells were used as the negative controls for the NCKX2-FLAG immunoprecipitation to monitor any associated changes and/or differences in HEK-293 cells due to the

transient overexpression of the recombinant proteins, especially those of $Ca^{2+}$ handling membrane transporters. Catalyzed oxidation of adjacent free sulfydryls to disulfide bonds by 1,10-phenanthroline complexed copper (CuPhe) was carried out with the detergent solubilized samples for 30 minutes on ice before the addition of the anti-FLAG M2-affinity gel. The protocol for the CuPhe catalyzed oxidation of adjacent free sulfydryls to disulfide bond was described in detail in section 2.1.5. Upon the addition of the anti-FLAG M2-affinity gel, the samples were slowly rotated at 4.0ºC overnight, and the beads were washed three times with 1.0mL of ice-cold RIPA buffer containing 0.3% detergent followed by centrifugation of the samples at 800*g* for 2 minutes (4.0ºC). After the final wash in a fresh microcentrifuge tube, the anti-FLAG M2-affinity gel was collected and the bound proteins were detached from the anti-FLAG M2-affinity gel by adding 50µL 2×SDS sample buffer with 6.0% (w/v) SDS and 5% β-mercaptoethanol and heating the samples to 65ºC for 5 minutes.

Proteins in the immunoprecipitated samples were separated by SDS-PAGE (7.5% or 12.0%) and visualized using Coomassie Brilliant Blue staining or silver staining. Protein bands of interest were excised from the gel and sent to the Southern Alberta Mass Spectrometry (SAMS) Centre for Proteomics at the University of Calgary to be analyzed by a tandem mass spectrometry (LC/MS/MS) for their identification.

### *2.3.3 Immunoprecipitation of NCKX2 from Rat Brain Synaptosomal Membrane Vesicles*

Immunoprecipitation of endogenously expressed NCKX2 from rat brain synaptosomal membrane vesicles was carried out using polyclonal F antibody against rat

brain NCKX2. Synaptosomal membrane vesicles containing 1~10mg protein were solubilized in ice cold RIPA buffer containing 1.0% detergents (Triton X-100 or *n*-dodecyl *β*-D-maltoside) for an hour. Samples were then centrifuged at maximum speed (16,000*g*) for 5 minutes (4.0ºC) to remove insoluble material and the supernatant containing solubilized membrane proteins was precleared using 200µL 50% (w/v) Protein A Sepharose CL-4B (Sigma) washed and swollen in RIPA buffer by slowly rotating for 30 minutes at 4.0ºC. Precleared supernatant was then mixed with 0.5~1.0µL polyclonal F antibody overnight by slow rotation at 4.0ºC. The antibody bound NCKX2 proteins were then immunoprecipitated with 200µL 50% Protein A Sepharose by slow rotation for two hours at 4.0ºC, and the beads were washed three times with 1.0mL RIPA buffer with 0.3% detergent by quickly vortexing and spinning down at 800*g* for 2 minutes. Bound proteins were then detached from the beads by adding 50µL 2×SDS sample buffer with high [SDS] (6% w/v) and 5% β-mercaptoethanol, and heating the samples to 65ºC for 5 minutes as described before. Rabbit pre-immune serum was used as the negative control for immunoprecipitation by the polyclonal F antibody.

## 2.4 Isolation of Lipid Raft Microdomains and Analysis of Fractionated Proteins

### *2.4.1 Isolation of Lipid Rafts/Caveolae Microdomains from Whole Rat Brain*

Lipid rafts and/or caveolae microdomains from whole rat brain were isolated using conventional density floatation methods first described by the Lisanti group with several modifications (264). All solutions used in the isolation procedure were prepared freshly immediately prior to use and were made in MBS buffer containing 25.0mM 2-(*n*-

morpholino)ethanesulfonic acid sodium salt (MES sodium, pH 6.5) and 150mM NaCl. All the procedures were performed at 4.0ºC unless otherwise indicated.

3-month old male Sprague Dawley rats were sacrificed in a $CO_2$ chamber and their brains were removed as quickly as possible. The brain was then minced with scissors and 10.0mL ice cold homogenization buffer in MBS containing 2.0% Triton X-100 and the protease inhibitors (1.0mM $Na_3VO_4$, 1.0mM $Na_3MoO_4$, 1.0mM EDTA, 1.0mM PMSF, 1.0mg/mL leupeptin, and 1.0mg/mL aprotinin) were added to the minced brain. The samples were then homogenized by 10 strokes with a loose-fitting Dounce homogenizer followed by another 10 strokes with a tight-fitting homogenizer. 1.0 ~ 2.0mL of the homogenized samples were mixed with an equal volume of 80% (w/v) sucrose solution in MBS buffer containing protease inhibitors (see above), so that the final concentration of the sucrose and Triton X-100 in the sample mixture would reach 40% and 1.0%, respectively. The rest of the samples were immediately frozen in liquid nitrogen and kept at -80ºC until required. Protein yields and membrane fractionation characteristics were indistinguishable between material isolated from fresh or from frozen brain. The fresh or frozen/thawed homogenate was then transferred to a clear ultracentrifuge tube (Beckman Ultra-Clear™, 14×89mm), and was carefully overlaid with 30% (w/v) and 5.0% (w/v) sucrose solutions in MBS buffer containing protease inhibitors so that the 40%/30% sucrose interface was sufficiently separated from the 30%/5.0% interface and clearly visible. The gradient was centrifuged at 39,000rpm for 16~22h using a Beckman SW41 Ti swinging bucket rotor with slow deceleration and no brake, and fractions (~500µL each) were collected from the top of the gradient and

immediately frozen in liquid nitrogen and stored at -80ºC until necessary. The detergent resistant lipid rafts/caveolae microdomains were visible floating near the 30%/5.0% sucrose interface as thick, viscous, white, and cloudy material, and had to be physically broken into pieces to be collected. The protein content in the fractions collected after the centrifugation was analyzed using SDS-PAGE and immunoblotting, and the identity of caveolae was confirmed by the presence of caveolins detected by rabbit polyclonal anti-caveolin antibody (BDH) which recognizes both caveolin-1 and caveolin-2.

### *2.4.2 Co-association of Rat Brain NCKX2 and Caveolins*

The possibility of co-association between rat brain caveolins (caveolin-1 and caveolin-2) and NCKX2 in lipid rafts/caveolae microdomains was investigated using a co-immunoprecipitation technique essentially as described in Section 2.3 with only a few minor changes as described below. Rat whole brain lipid rafts/caveolae microdomains were isolated as described above, but instead of collecting fractions from the entire sucrose gradient, only the thick white lipid rafts/caveolae fractions floating at the 30%/5.0% sucrose interface were collected for co-immunoprecipitation purposes. The lipid rafts/caveolae fractions were solubilized in ice cold RIPA buffer containing either 1.0% Triton X-100 or 1.0% *n*-dodecyl *β*-D-maltoside for 2 hours, and polyclonal F antibody against rat brain NCKX2 or rabbit polyclonal anti-caveolin antibody (5.0µg) was used to pull down NCKX2 or caveolins from the lipid rafts/caveolae fractions, respectively. The rabbit pre-immune serum collected prior to the peptide injection for the production of the polyclonal F antibody and the rabbit IgG isotype for the polyclonal anti-caveolin antibody were used as the negative controls for the immunoprecipitation.

*2.4.3. Isolation of Lipid Rafts/Caveolae Microdomains from HEK-293 Cells*

Lipid rafts and/or caveolae microdomains from HEK-293 cells transiently expressing N-terminal FLAG-tagged rat brain NCKX2 alone or with rat caveolin-1, or with rat caveolin-1 and caveolin-2 were isolated using the density floatation method as described above. Fractions were collected after the centrifugation from the top of the gradient, run on SDS-PAGE, and immunoblotted using M2 anti-FLAG antibody, rabbit polyclonal anti-caveolin antibody, monoclonal anti-caveolin-1 antibody (C37210, BDH), and monoclonal anti-caveolin-2 antibody (BDH) to investigate sub-cellular localization of these proteins.

**2.5 Analysis of Proteins and Peptides by Mass Spectrometry**

The identification of the potential interacting partner(s) of rat brain NCKX2 visualized by Coomassie or silver staining of the SDS-PAGE gels containing immunoprecipitated samples was carried out using tandem mass spectrometry (MS/MS) combined with nanoscale liquid chromatography (LC) on either a QSTAR® Pulsar *i* Hybrid quadrupole time-of-flight mass spectrometer (Applied Biosystems/PE Sciex) or an Agilent MSD Ion Trap XCT interfaced with an Agilent 1100 series Nano LC system at the Southern Alberta Mass Spectrometry (SAMS) Centre for Proteomics, the University of Calgary, Calgary, AB. Briefly, either Coomassie or silver stained protein bands were excised from the SDS-PAGE gel, and placed in a high quality, low-retension 0.6mL snap-cap tube prewashed with 50% acetonitrile with 0.1% trifluoroacetic acid (TFA). These samples were digested with trypsin at the SAMS Centre, and injected into

the LC/MS/MS for further analyses. A 10 fmol bovine serum albumin (BSA) sample digested with trypsin was run as a standard prior to injecting any samples on the LC/MS/MS system.

MS/MS spectra were acquired by either the QSTAR® or XCT ion trap mass spectrometer from peptide ions isolated and fragmented inside the trap. The sequences of the parent peptides are inferred by matching the MS/MS spectra to protein sequence databases (NCBInr). Mascot based on a modified molecular weight search (MOWSE) scoring algorithm system from Matrix Science (www.matrixscience.com) (228) was used as the MS/MS ion search engine in the SAMS Centre.

# CHAPTER THREE

## Sub-cellular Localization of Rat Brain NCKX2

The aim of this study was to investigate the sub-cellular localization of rat brain NCKX2 within the lipid rafts and/or caveolae microdomains and its interaction with caveolins. As discussed in Chapter 1, the lipid rafts and/or caveolae microdomains are important in compartmentalizing proteins involved in signal transduction, including those essential for intracellular $Ca^{2+}$ signalling and homeostasis such as the L-type $Ca^{2+}$ channels (7, 125), $IP_3R$-like protein (78), NOS (84, 85), and PMCA (77). Studies conducted using cardiac myocytes showed the association between NCX1 and the muscle specific isoform of caveolin (caveolin-3) (25). In C6 glioma cells, endogenous NCX1 co-localized and interacted with endogenous caveolin-1 and caveolin-2 (38). These observations suggest caveolar localization of NCX1 and NCX1 interaction with caveolins in both cardiac myocytes and cells in brain.

In the postsynaptic dendrites of neurons in brain where NCKX2 proteins are abundantly expressed, the lipid rafts/caveolae microdomains are thought to be involved in regulated trafficking of postsynaptic membrane proteins such as AMPA receptors, maintenance of postsynaptic structural integrity, as well as synaptic clustering and targeting of the proteins important for formation of a normal synapse (103, 286). Unlike the cardiac isoform of NCX1, however, virtually nothing is known about the role of the lipid rafts/caveolae microdomains in organizing NCKX2 in neurons. Immuno-histochemical staining of rat hippocampal sections with affinity-purified anti-NCKX2 polyclonal antibody N2F displayed a distinctive punctate staining pattern which is similar to the staining pattern observed for proteins with caveolar localization (168). In addition, when expressed in HEK-293 cells, rat NCKX2 was observed at the cell surface in a

similar punctuate pattern resembling lipid raft structures (297). Moreover, the linear sequence of rat brain NCKX2 contains predicted caveolin-binding motif-like domains in the intracellular loops (Y365GKLKYY371 in the long intracellular loop, and W236WPLF240 between M3 and M4), suggesting a possible interaction between caveolins and rat brain NCKX2.

Therefore, it was of interest to investigate whether rat brain NCKX2 is localized in the lipid rafts and/or caveolae microdomains and if so, how this sub-cellular localization is achieved. To answer these questions, cold non-ionic detergent solubilization of the membranes followed by density floatation isolation of the lipid rafts and/or caveolae microdomains were performed using whole rat brain as well as HEK-293 cells transiently expressing N-terminal FLAG-tagged NCKX2 alone or with caveolins. Together with co-immunoprecipitation analyses, the data suggest that a significant portion of rat brain NCKX2 is preferentially localized in the non-caveolar lipid rafts. Rat brain NCKX2 was not observed in caveolae where caveolins were found. This was the first study that revealed selective localization of rat brain NCKX2 into non-caveolar lipid raft microdomains.

### 3.1 NCKX2 Is Found in the Lipid Rafts/Caveolae Microdomains in Rat Brain

To ascertain the sub-cellular localization of NCKX2 within lipid rafts and/or caveolae microdomains in rat brain, conventional cold non-ionic detergent solubilization of the membrane and density floatation methods were employed, the schematic of which

is shown in Figure 3-1 and the procedure described in Chapter 2.4. This method, which exploits the property of the lipid rafts and/or caveolae microdomains that renders them resistant to detergent solubility at low temperature, was chosen since it is one of the most widely used lipid raft/caveolae isolation techniques to date and is relatively simple and easy to perform. Furthermore, the identity of most of the lipid rafts/caveolae associated proteins as well as many known biophysical properties of the lipid rafts and/or caveolae microdomains have been determined through the successful utilization of density floatation methods (242, 277). Hence, an adult male rat was sacrificed and its brain quickly dissected, and the whole rat brain was solubilized in ice-cold homogenization buffer containing the non-ionic detergent Triton X-100 followed by density floatation centrifugation.

After centrifugation, the detergent-resistant membranes containing the lipid rafts/caveolae were clearly visible as viscous, white, cloudy material floating at the interface formed between 5% and 30% (w/v) sucrose layers. Instead of just isolating the detergent-resistant membranes containing the lipid rafts/caveolae, the entire gradient was fractionated and samples of each fraction were run on a SDS-PAGE gel followed by immunoblotting. In this way, not only could the proteins that preferentially localized to the lipid rafts/caveolae microdomains be identified, but also the detergent-soluble non-raft/non-caveolae associated proteins in the high density sucrose region (30% to 40% sucrose solution) could be included in the analysis. The separation of the detergent-soluble non-rafts/non-caveolae associated proteins from the isolated detergent-resistant membranes containing the lipid rafts/caveolae microdomains would then confirm the

**Figure 3.1 Schematic of the Isolation of Detergent-Resistant Membranes.** Cells and tissues were solubilized in cold non-ionic detergents such as Triton X-100 and subjected to density floatation centrifugation as shown in the diagram. The solubilized membranes were mixed with an equal volume of 80% sucrose solution and were placed at the bottom of a clear ultracentrifuge tube. The step sucrose gradients were prepared by layering an equal volume of 30% and 5.0% sucrose solutions on top of the 40% sucrose solution containing the solubilized membranes, and the samples were ultracentrifuged for 16 to 22 hours at 39,000rpm at 4.0ºC. The detergent-resistant membrane fractions were visualized as a thick cloudy white material floating at the 5%/30% sucrose interface. Detergent soluble proteins remained near the bottom of the tube in the 40% sucrose solution. Fractions were collected from the top of the tube by pipetting, and the protein contents within each fraction were analysed by SDS-PAGE and immunoblotting.

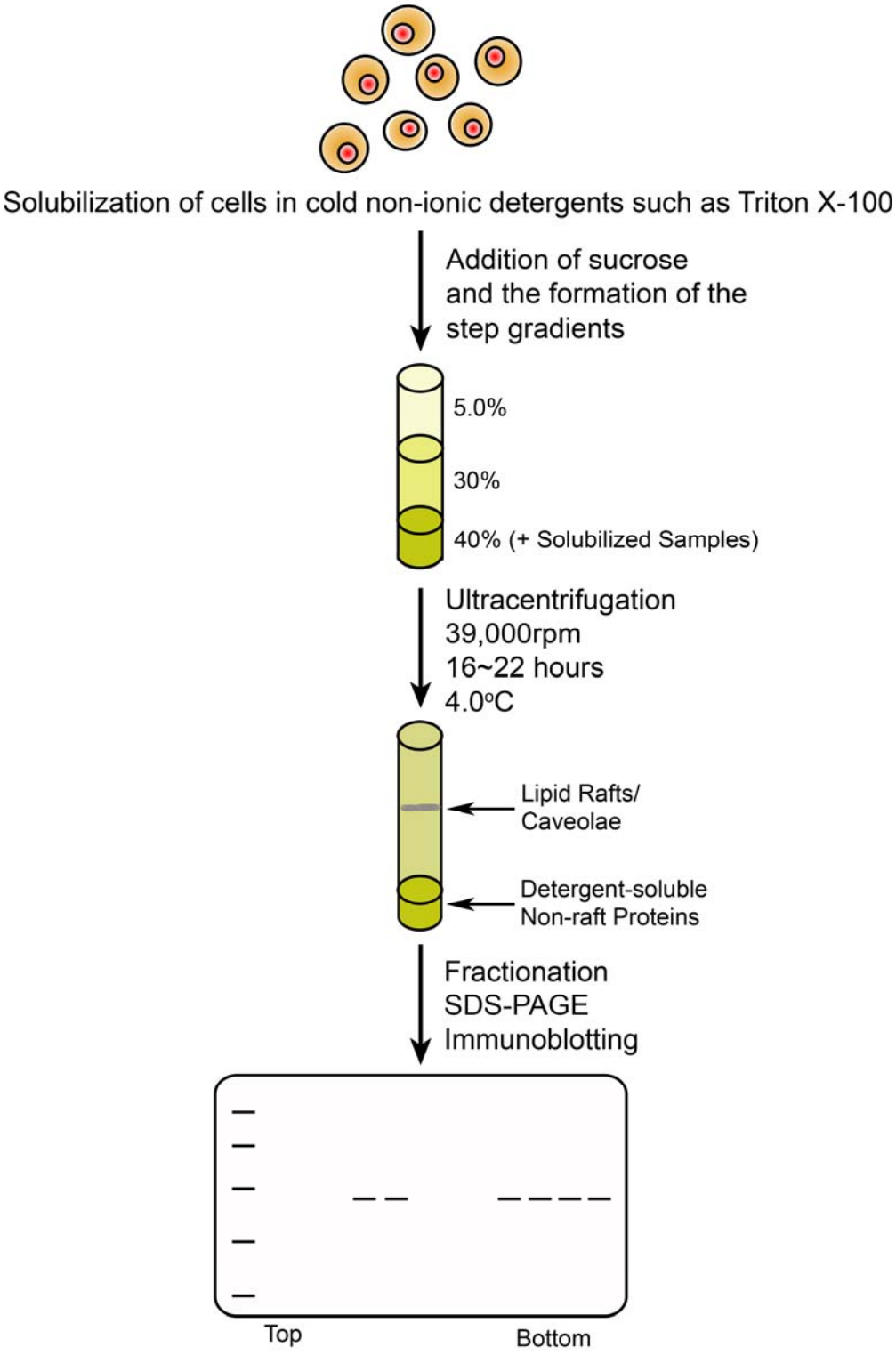
Solubilization of cells in cold non-ionic detergents such as Triton X-100
Addition of sucrose
and the formation of the
step gradients
5.0%
30%
40% (+ Solubilized Samples)
Ultracentrifugation
39,000rpm
16~22 hours
4.0°C
Lipid Rafts/
Caveolae
Detergent-soluble
Non-raft Proteins
Fractionation
SDS-PAGE
Immunoblotting
Top
Bottom

successful isolation of those microdomains from the detergent-solubilized membranes and proteins.

Figure 3-2 reveals a typical result obtained for such experiments. As seen in the topmost immunoblot probed with polyclonal F antibody against rat brain NCKX2, a significant amount of NCKX2 partitioned into fractions #11 and #12 located at the interface formed between 5% and 30% sucrose solutions where the detergent-resistant membranes containing the lipid rafts and/or caveolae were found. In all experiments performed, approximately 30 to 60% of total NCKX2 were localized to the detergent-resistant membranes. Caveolins, whose expression in neurons of the central nervous system is often debated (20, 83, 117), were clearly present and exclusively localized in the same fractions. The fact that caveolins were only found in these two fractions within which the detergent-resistant membranes were collected confirmed that these fractions were enriched with the lipid rafts/caveolae, and that rat brain NCKX2 localized into the lipid rafts/caveolae fraction. Some NCKX2 was also found in the high density sucrose region (30% and 40% sucrose), especially at the interface formed between 30% and 40% sucrose solutions, along with the brain specific β2 subunit of $Na^+/K^+$ ATPases (278). This suggested that a fraction of membrane lipid was still attached to these populations of proteins, making them more buoyant than fully detergent solubilized proteins. Transferrin receptor (TfR, Figure 3-2), a known non-raft/non-caveolae associated membrane protein, was excluded from the fractions which contained the lipid rafts/caveolae, and was instead found in the high density sucrose region (40%) as expected for detergent-solubilized membrane proteins.

**Figure 3-2. Isolation of Lipid Rafts/Caveolae Microdomains from Rat Brain.** Typical immunoblots displaying the sub-cellular localization pattern of a rat brain NCKX2 and other proteins. A whole rat brain was solubilized in 10mL buffer containing 1.0% (final concentration) cold Triton X-100, mixed with sucrose solution, and a small fraction was loaded at the bottom of a step sucrose gradient (5.0% and 30%) as described in Chapter 2. 500µL fractions were collected from the top of the gradient, and an equal volume of each fraction were mixed with SDS sample buffer and separated by SDS-PAGE (12%) followed by immunoblot analyses using appropriate antibodies against proteins of interest as listed in the figure. The fraction numbers and corresponding sucrose concentrations as well as the fractions containing the lipid rafts/caveolae are indicated at the bottom of the figure. Clathrin HC: clathrin heavy chain, $Na^+/K^+$ ATPase α: α subunit of $Na^+/K^+$ ATPase, $Na^+/K^+$ ATPase β: β2 subunit of $Na^+/K^+$ ATPase, TfR: transferrin receptor. All the antibodies used were monoclonal and were purchased from BDH, with the exception of the $Na^+/K^+$ ATPase α, antibody which was polyclonal and recognized all α subunits of $Na^+/K^+$ ATPase. This experiment was repeated more than 3 times and similar results were obtained each time.

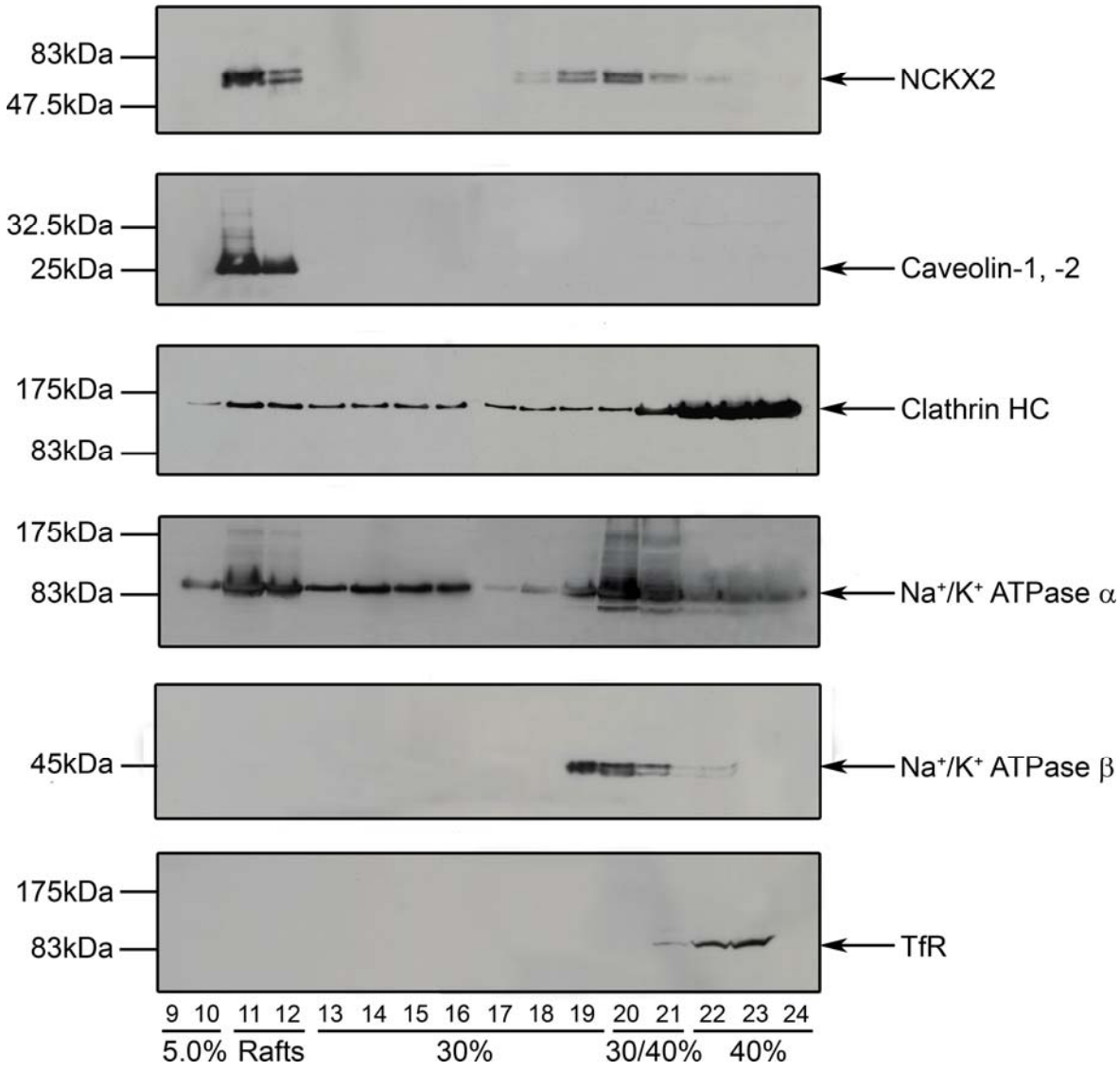
83kDa
47.5kDa
NCKX2
32.5kDa
25kDa
Caveolin-1, -2
175kDa
83kDa
Clathrin HC
175kDa
83kDa
Na+/K+ ATPase α
45kDa
Na+/K+ ATPase β
175kDa
83kDa
TfR
9 10 11 12 13 14 15 16 17 18 19 20 21 22 23 24
5.0% Rafts
30%
30/40%
40%

The heavy chain of clathrin (Clathrin HC, Figure 3-2), a fibrous protein that makes up clathrin coated pits formed during endocytosis and exocytosis, was observed evenly distributed in small amounts throughout the 5% and 30% sucrose interface and the 30% sucrose region, with a much greater concentration at the high density (40%) sucrose region. The partitioning of the majority of the clathrin heavy chain into the high density sucrose region suggested that most of the clathrin heavy chain was effectively solubilized by Triton X-100. The origin of the weaker band present in all fractions is not certain but may represent residual raft membrane-associated material. While the β2 subunit of $Na^+/K^+$ ATPases was concentrated within the interface formed between 30% and 40% sucrose solutions, the α subunits of $Na^+/K^+$ ATPases exhibited a broad distribution across the gradient, with a moderate enrichment in the two sucrose interfaces. Altogether, the data clearly revealed that a fraction of rat brain NCKX2 and caveolins were associated with the detergent-resistant membranes containing lipid rafts/caveolae microdomains.

## 3.2 NCKX2 Does Not Interact with Caveolins

### *3.2.1 NCKX2 Interaction with Caveolins in the Rat Brain Synaptosomal Membrane Vesicles and in the Rat Brain Crude Homogenates*

The previous experiment confirmed that a significant amount of NCKX2 in rat brain partitioned into the detergent-resistant membranes containing the lipid rafts and/or caveolae microdomains, the same fraction which contained caveolins. Found exclusively within caveolae, caveolins are not only responsible for the characteristic cave-like invagination of caveolae but also important as the scaffolds that hold many caveolae-

associated proteins in a multi-protein complex via protein-protein interaction. Therefore, the possibility of rat brain NCKX2 association with caveolins in caveolae was investigated by performing co-immunoprecipitation experiments using rat brain synaptosomal membrane vesicles as well as crude homogenates, prepared from whole rat brain, and the results are shown in Figures 3-3 and 3-4.

Unlike Triton X-100 or CHAPS, the non-ionic detergent *n*-dodecyl *β*-D-maltoside can effectively disrupt the lipid rafts/caveolae microdomains and solubilize proteins associated with the lipid rafts/caveolae (30, 167). Disruption of the lipid rafts/caveolae microdomain is required to investigate molecular interaction between two raft/caveolar proteins by co-immunoprecipitation. If the lipid raft/caveolae microdomain remained intact, immunoprecipitation of a raft/caveolae protein would result in the pull-down of the entire microdomain, by virtue of its detergent-resistant property. Therefore, any other raft/caveolar protein co-localized with the immunoprecipitated protein, regardless of their physical interaction, would be co-immunoprecipitated, making the data difficult to interpret. Thus, *n*-dodecyl *β*-D-maltoside was used to solubilize rat brain synaptosomal membrane vesicles for co-immunoprecipitation of rat brain NCKX2 and caveolins. As seen in Figure 3-3, immunoprecipitation of rat brain NCKX2 with polyclonal F antibody failed to pull down caveolins from the *n*-dodecyl *β*-D-maltoside solubilized rat brain synaptosomal membrane vesicles. The immunoblot of the rat brain synaptosomal membrane vesicles (+, Anti-Caveolin Blot, Figure 3-3) further revealed that the rat brain synaptosomal membrane vesicles contained low amounts of caveolins compared to the

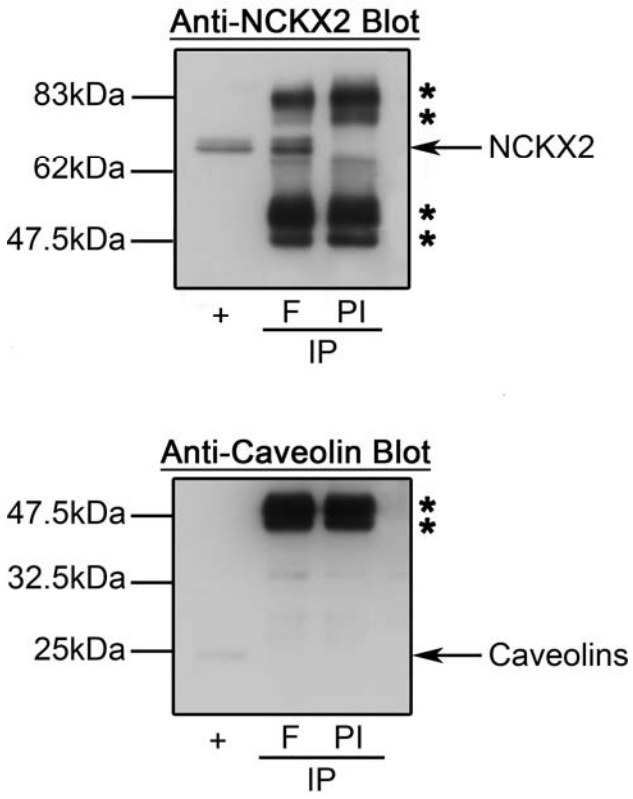


**Figure 3-3. Co-immunoprecipitation of NCKX2 and Caveolins from Rat Brain Synaptosomal Membrane Vesicles.** 1.0mg of rat brain synaptosomal membrane vesicle protein was solubilized in 1.0% *n*-dodecyl *β*-D-maltoside and immunoprecipitation was carried out using polyclonal antibody F against rat brain NCKX2 to investigate the potential association between caveolins and NCKX2. +: 20µg rat brain synaptosomal membrane vesicle protein, F: immunoprecipitation by polyclonal antibody F, PI: immunoprecipitation using pre-immune serum as a negative control for the F antibody. *Top*: immunoblot probed with the F antibody. *Bottom*: immunoblot probed with anti-caveolin polyclonal antibody (BDH). Asterisks indicate the position of immunoglobulin bands. The blots shown are representative of four independent experiments.

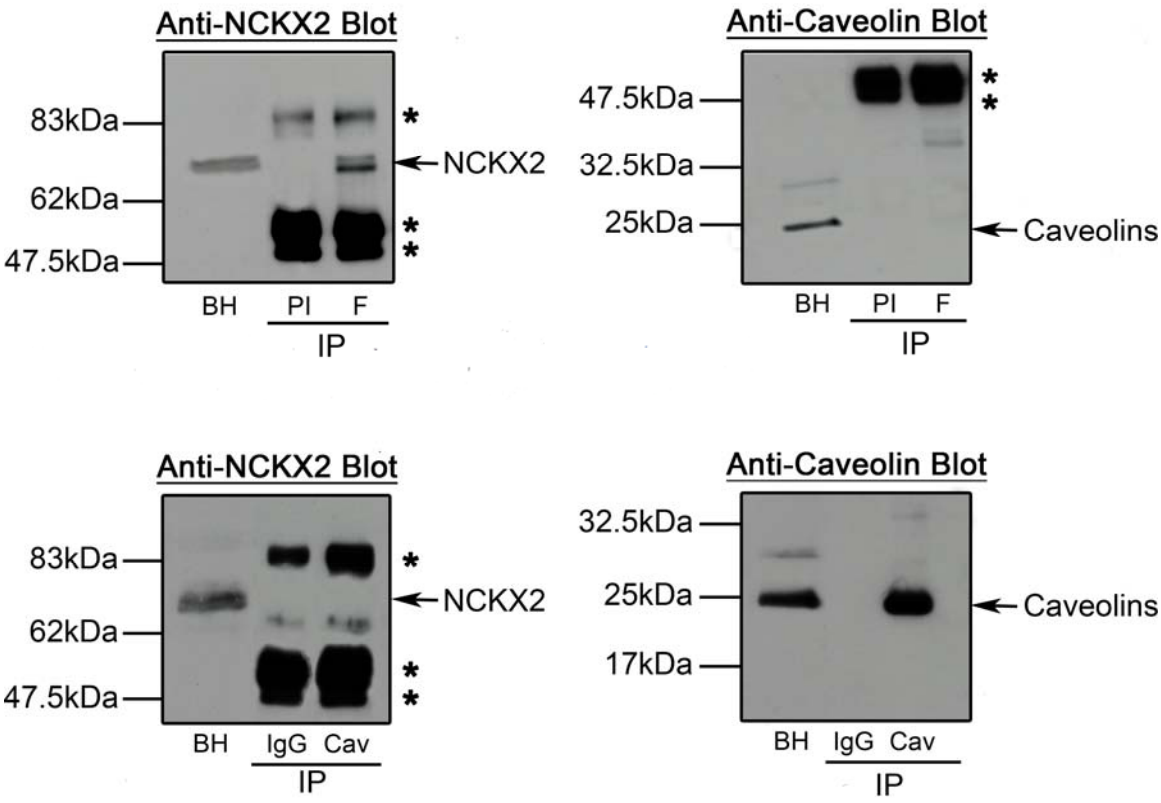


**Figure 3-4. Co-immunoprecipitation of NCKX2 and Caveolins from Rat Brain Crude Homogenates.** Rat brain crude homogenates were solubilized in 1.0% *n*-dodecyl *β*-D-maltoside and co-immunoprecipitation experiments were performed using polyclonal F antibody against rat brain NCKX2 and the monoclonal antibody against caveolin-1. *Top*: immunoprecipitation using polyclonal F antibody (F) and pre-immune serum (PI) as a negative control. *Bottom*: immunoprecipitation using monoclonal anti-caveolin-1 antibody (Cav) (BDH) and the IgG isotype (IgGκ) as a negative control. *Left*: immunoblots probed with polyclonal antibody F against rat brain NCKX2. *Right*: immunoblots probed with polyclonal anti-caveolin antibody. BH: 500µg brain homogenates. Asterisks indicate the position of immunoglobulin bands. The blots shown are representative of three independent experiments.

lipid raft preparations, as indicated by the weak labelling by the rabbit polyclonal anti-caveolin antibody on the immunoblot.

Figure 3-2 indicated that not all NCKX2 was present in the detergent-resistant membranes containing lipid raft/caveolae microdomains. Combined with the observation in Figure 3-3 that little or no caveolin was found in the brain synaptosomal membrane vesicles, it seemed possible that the isolated synaptosomes contained few if any lipid raft domains. Therefore, crude rat brain homogenates, a preparation containing both NCKX2 and caveolins, were used for co-immunoprecipitation analyses. As seen in Figure 3-4, the crude homogenates contained enough caveolins and NCKX2 to be detected by immunoblotting with the rabbit polyclonal anti-caveolin antibody and polyclonal F antibody against rat brain NCKX2. However, the immunoprecipitation of rat brain NCKX2 from the crude homogenates did not co-immunoprecipitate caveolins (Figure 3-4, top immunoblots). In the reverse experiment in which caveolins were immunoprecipitated using the rabbit polyclonal anti-caveolin antibody, NCKX2 was not co-immunoprecipitated (Figure 3-4, bottom immunoblots), providing further evidence that rat brain NCKX2 did not interact with caveolins.

### *3.2.2 NCKX2 Interaction with Caveolins in the Isolated Lipid Rafts/Caveolae Microdomains in Rat Brain*

Compared with the rat brain synaptosomal membrane vesicles that contained extremely low level of caveolins, and the crude brain homogenates in which NCKX2 and caveolins were found but not concentrated, the lipid rafts and/or caveolae microdomains

are highly enriched with both caveolins and NCKX2. Therefore, isolated lipid rafts/caveolae from the density floatation experiments were used for co-immunoprecipiation analyses. Similar to the previous results, rat brain NCKX2 did not associate with caveolins in the lipid rafts/caveolae microdomains as displayed in Figure 3-5. Immunoprecipitation of NCKX2 did not result in the co-immunoprecipitation of caveolins, and although both caveolin-1 and caveolin-2 were present in isolated lipid rafts/caveolae microdomains, neither associated with NCKX2.

Taken together, the co-immunoprecipitation experiments using solubilized rat brain synaptosomal membrane vesicles, rat brain crude homogenates, as well as isolated lipid rafts/caveolae demonstrated that rat brain NCKX2, although localized in the lipid rafts/caveolae microdomains, did not associate with caveolin-1 or caveolin-2. In addition, the caveolin immunoblot of the rat brain synaptosomal membrane vesicles in which NCKX2 was enriched (Figure 3-3) indicated that low levels of caveolins were present in the synaptosomal vesicles. This finding suggests that caveolins may be selectively lost during the synaptosomal membrane vesicle isolation procedure, or there may be little or no caveolins and caveolae formation at the neuronal synapses in the brain.

### 3.3 NCKX2 Is Localized in the Lipid Raft Microdomain Distinct from Caveolae

Intracellular $Ca^{2+}$ extrusion by NCKX2 is a major $Ca^{2+}$ clearance mechanism found in the neuronal synapses, in which NCKX2 is thought to be specifically localized

**Figure 3-5. Co-immunoprecipitation of NCKX2 and Caveolins from Rat Brain Detergent-Resistant Membranes.** The detergent-resistant membranes isolated as described in Chapter 2 were solubilized in cold 1.0% *n*-dodecyl *β*-D-maltoside and co-immunoprecipitation experiments were performed using polyclonal F antibody against rat brain NCKX2 and rabbit polyclonal anti-caveolin antibody to examine the potential association between the two proteins. F: immunoprecipitation using the polyclonal F antibody against NCKX2, PI: immunoprecipitation with the pre-immune serum as the negative control, Cav: immunoprecipitation using polyclonal anti-caveolin antibody, IgG: immunoprecipitation with the rabbit IgG isotype (IgGκ) of anti-caveolin antibody as the negative control. Each immunoblot was probed with the indicated antibody. From the top, polyclonal F antibody (for NCKX2), polyclonal anti-caveolin antibody, mouse monoclonal antibody against and specific to caveolin-1 (C37210, BDH) and mouse monoclonal antibody against caveolin-2 (BDH). Asterisks indicate the position of immunoglobulin bands. The blots shown are representative of four independent experiments.

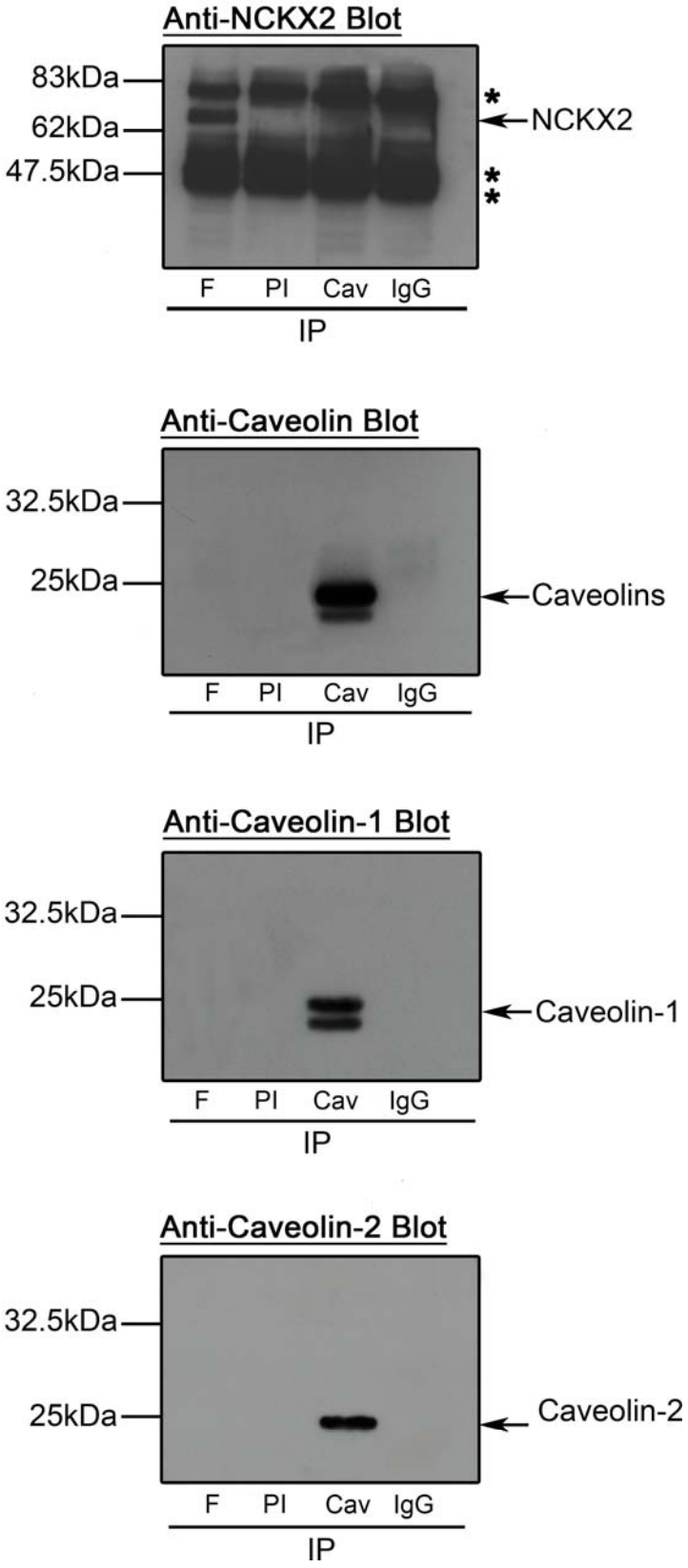
Anti-NCKX2 Blot
83kDa
62kDa
47.5kDa
NCKX2
F
PI
Cav
IgG
IP
Anti-Caveolin Blot
32.5kDa
25kDa
Caveolins
F
PI
Cav
IgG
IP
Anti-Caveolin-1 Blot
32.5kDa
25kDa
Caveolin-1
F
PI
Cav
IgG
IP
Anti-Caveolin-2 Blot
32.5kDa
25kDa
Caveolin-2
F
PI
Cav
IgG
IP

(139, 140). Since it appeared from the previous results that the same neuronal synapses might be devoid of caveolins and caveolae, and that rat brain NCKX2 did not associate with caveolins in the isolated lipid rafts/caveolae microdomain, it seemed possible that NCKX2 might be selectively found in the non-caveolar lipid raft microdomains and not in caveolae. To test whether rat brain NCKX2 displayed a distinct pattern of sub-cellular localization from caveolins, co-immunoprecipitation of rat brain NCKX2 and caveolins was performed using the isolated lipid rafts/caveolae microdomains in which the microdomain structure and the multi-protein complexes within the microdomain were not disrupted.

As seen Figure 3-6, immunoprecipitation of rat brain NCKX2 or caveolins in the isolated, intact lipid rafts/caveolae microdomain failed to co-immunoprecipitate the other, just as observed in the previous experiments. These data indicate that rat brain NCKX2 is localized in the lipid raft microdomains that are distinct from caveolae. Rat brain NCKX2 did not co-associate with caveolins not because there was a lack of a molecular interaction between the two proteins found in the same microdomains, but because they were found in different microdomains.

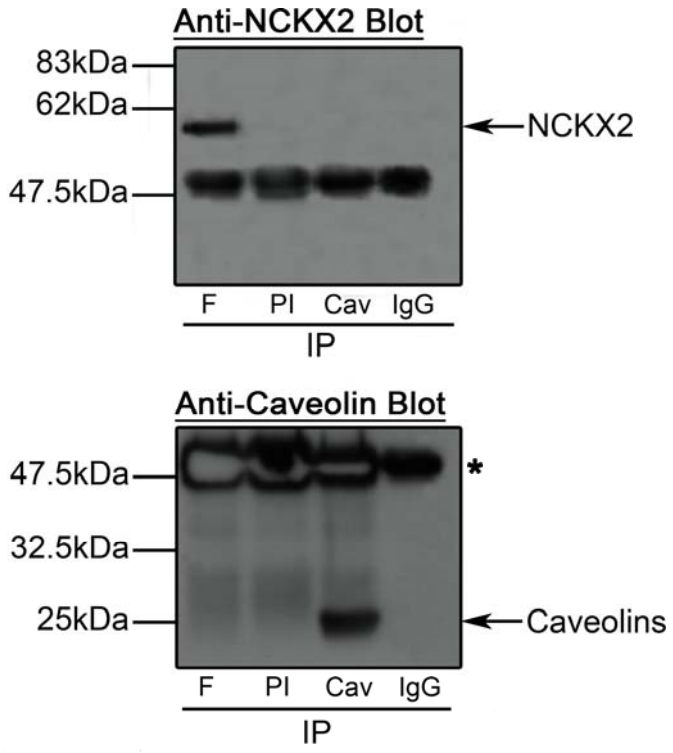


**Figure 3-6. Co-immunoprecipitation of NCKX2 and Caveolins from Rat Brain Detergent-Resistant Membranes Using Triton X-100.** Detergent-resistan t membranes isolated by density floatation were used for co-immunoprecipitation experiments to identify whether rat brain NCKX2 was localized in the lipid rafts microdomains distinct from caveolae. Ice-cold Triton X-100, which does not solubilize proteins from the detergent-resistant membranes, was used throughout the co-immunoprecipitation. The experiments were performed using polyclonal F antibody against rat brain NCKX2 and rabbit polyclonal anti-caveolin antibody. Asterisks indicate the position of immunoglobulin bands. The blots shown are representative of three independent experiments. See Figure 3-5 legend for more details.

## 3.4 Recombinant NCKX2 Behaves Differently from Rat Brain NCKX2

### *3.4.1 Effect of Non-ionic Detergents on the Sub-cellular Localization of NCKX2-FLAG in HEK-293 Cells*

Since the experiments described above revealed rat brain NCKX2 localization in the non-caveolar lipid raft microdomains, an attempt was made to investigate the molecular mechanisms that govern the observed sub-cellular localization pattern of rat brain NCKX2. For this, the N-terminal FLAG-tagged recombinant NCKX2 (NCKX2-FLAG) was transiently expressed in HEK-293 cells, which are known to be devoid of endogenous NCKX2 (G. Yang & J. Lytton, personal communication, data not shown). When ice-cold Triton X-100 was used to isolate the detergent-resistant membranes from these HEK-293 cells however, the protein did not partition into the detergent-resistant membranes containing the lipid raft microdomains (Figure 3-7). Instead, NCKX2-FLAG was highly enriched in the interface formed between 30% and 40% sucrose solutions and in the 40% sucrose region. However, when Triton X-100 was substituted with CHAPS, a milder non-ionic detergent than Triton X-100, NCKX2-FLAG exhibited a strikingly different pattern of sub-cellular localization. While found throughout the entire sucrose gradient, NCKX2-FLAG displayed the most intense labelling in the fractions that contained the detergent-resistant membranes including lipid rafts (fractions #2 and #3, Figure 3-7) and in the 30%/40% sucrose interface (fraction #7).

Neither caveolin-1 nor caveolin-2 was detected in HEK-293 microsomes by immunoblotting (data not shown), suggesting that little or no caveolins were

**Figure 3-7. Sub-cellular Localization of Recombinant NCKX2 in HEK-293 Cells.** Recombinant, N-terminal FLAG-tagged rat brain NCKX2 constructs were transiently expressed in HEK-293 cells and the detergent-resistant membranes were isolated as described in Chapter 2. The cells were solubilized with either ice-cold 1.0% Triton X-100 or 1.0% CHAPS (final concentration). After density floatation centrifugation, fractions were collected from the top of the gradient, run on an SDS-PAGE gel, and analyzed by immunoblot using monoclonal M2 anti-FLAG antibody or the monoclonal antibody against flotillin-2 (BDH). The blots shown are representative of four independent experiments.

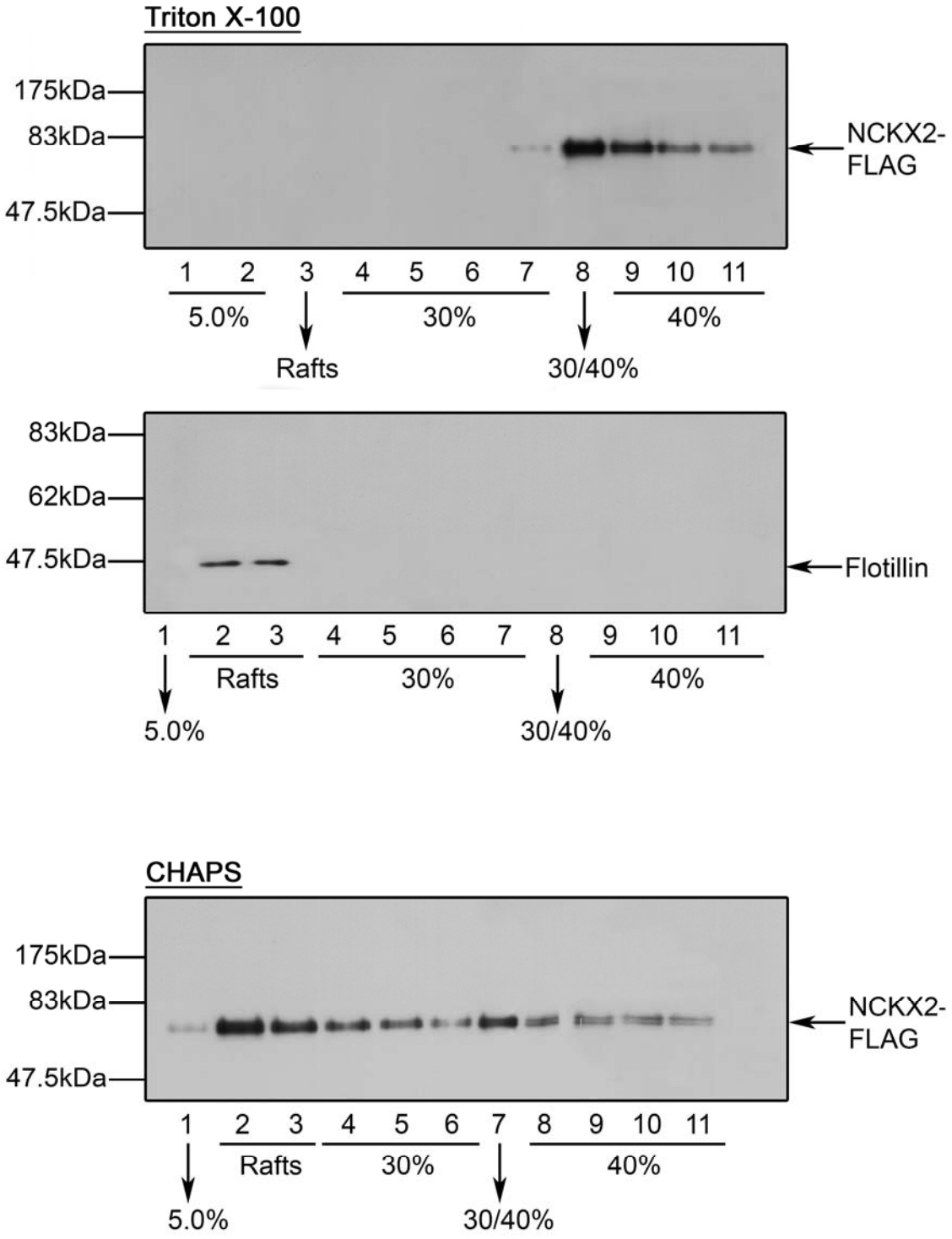
Triton X-100
175kDa
83kDa
47.5kDa
NCKX2-FLAG
1 2 3 4 5 6 7 8 9 10 11
5.0%
Rafts
30%
30/40%
40%
83kDa
62kDa
47.5kDa
Flotillin
1 2 3 4 5 6 7 8 9 10 11
5.0%
Rafts
30%
30/40%
40%
CHAPS
175kDa
83kDa
47.5kDa
NCKX2-FLAG
1 2 3 4 5 6 7 8 9 10 11
5.0%
Rafts
30%
30/40%
40%

endogenously expressed in HEK-293 cells. Flotillin, a non-caveolar lipid raft protein suggested to be a functional homolog of caveolins, is often used as a marker for non-caveolar lipid raft microdomains found in brain (304). Not only were flotillins endogenously expressed in HEK-293 cells, but they also partitioned into the fractions that were collected at the detergent-resistant interface formed between 5% and 30% sucrose solutions after density floatation isolation using Triton X-100 (Figure 3-7). This confirmed that the plasma membrane of HEK-293 cells contained non-caveolar lipid raft microdomains in which endogenous flotillins were localized. Taken together, the recombinant NCKX2-FLAG in HEK-293 cells behaved differently from the endogenous NCKX2 in rat brain in the density floatation analysis. Although non-caveolar lipid raft microdomains containing flotillins were present in HEK-293 cells, NCKX2-FLAG did not partition into the same lipid raft microdomains, unless the milder detergent, CHAPS, was used.

### *3.4.2 Effects of Caveolin Expression on the Sub-cellular Localization of NCKX2-FLAG in HEK-293 Cells*

When recombinant rat caveolin-1 and caveolin-2 were transiently co-expressed along with NCKX2-FLAG and the detergent resistant membranes containing lipid rafts/caveolae microdomains were isolated by density floatation using Triton X-100, NCKX2-FLAG was still found exclusively in the high density sucrose region (Figure 3-8). Although a minor amount of the recombinant caveolins were noted within the fraction that contained the detergent-resistant membranes containing the lipid rafts and/or caveolae microdomains, most of the recombinant caveolins transiently expressed in

HEK-293 cells were observed in the high density sucrose region (30%/40% interface and the 40% sucrose region). Just as for NCKX2, this pattern of sub-cellular localization of recombinant caveolins was different from what was seen in the rat brain. This could represent the pitfall of using a heterologous system in which transient transfection of a protein construct results in too much expression of the protein, thereby causing it to be found in the cellular compartment where it is not normally found.

Substituting CHAPS for Triton X-100 caused a drastic change in the fractionation pattern of both NCKX2-FLAG and recombinant caveolins when they were transiently co-expressed in HEK-293 cells (Figure 3-9). Unlike in Triton X-100, a fair amount of both NCKX2-FLAG and caveolins (caveolin-1 and caveolin-2) were observed in the detergent-resistant membranes containing the lipid rafts/caveolae microdomains. Caveolins were also noted throughout the entire sucrose gradient, whilst NCKX2-FLAG were shown to be found in the 30% sucrose region as well as the 30%/40% sucrose interface. This confirmed that the use of the non-ionic detergent CHAPS resulted in the shift of both NCKX2-FLAG and the recombinant caveolins to the detergent-resistant membranes. In addition, the sub-cellular localization of NCKX2-FLAG did not depend on the presence of caveolins, since the expression of caveolins did not influence the NCKX2-FLAG localization (Figures 3-8 and 3-9).

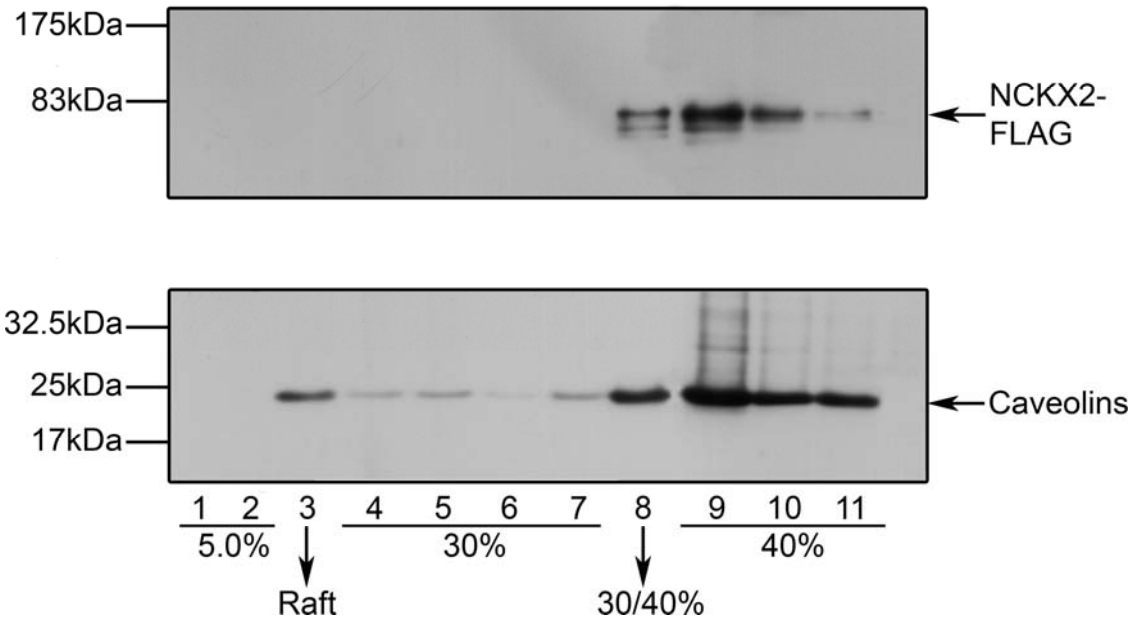


**Figure 3-8. Sub-cellular Localization of Recombinant NCKX2 and Recombinant Rat Caveolins in HEK-293 Cells – Triton X-100 Solubilization.** Recombinant, N-terminal FLAG-tagged rat brain NCKX2 and recombinant caveolin-1 and -2 constructs were transiently co-expressed in HEK-293 cells and the detergent-resistant membranes were isolated as described in Chapter 2 by solubilizing the cells with ice-cold 1.0% Triton X-100 (final concentration). After density floatation centrifugation, fractions were collected from the top of the gradient, run on an SDS-PAGE gel, and analyzed by immunoblot using monoclonal M2 anti-FLAG antibody (for NCKX2-FLAG) as well as rabbit polyclonal anti-caveolin antibody (for caveolins-1 and -2). The blots shown are representative of three independent experiments.

**Figure 3-9. Sub-cellular Localization of Recombinant NCKX2 and Caveolins in HEK-293 Cells – CHAPS Solubilization.** Recombinant, N-terminal FLAG-tagged rat brain NCKX2 and recombinant caveolin-1 and -2 constructs were co-expressed in HEK-293 cells and the detergent-resistant membranes were isolated as described in Chapter 2 by solubilizing the cells with ice-cold 1.0% CHAPS (final concentration). After density floatation centrifugation, fractions were collected from the top of the gradient, run on an SDS-PAGE gel, and analyzed by immunoblot using monoclonal M2 anti-FLAG antibody (for NCKX2-FLAG) as well as monoclonal anti-caveolin-1 and anti-caveolin-2 antibody. The blots shown are representative of five independent experiments.

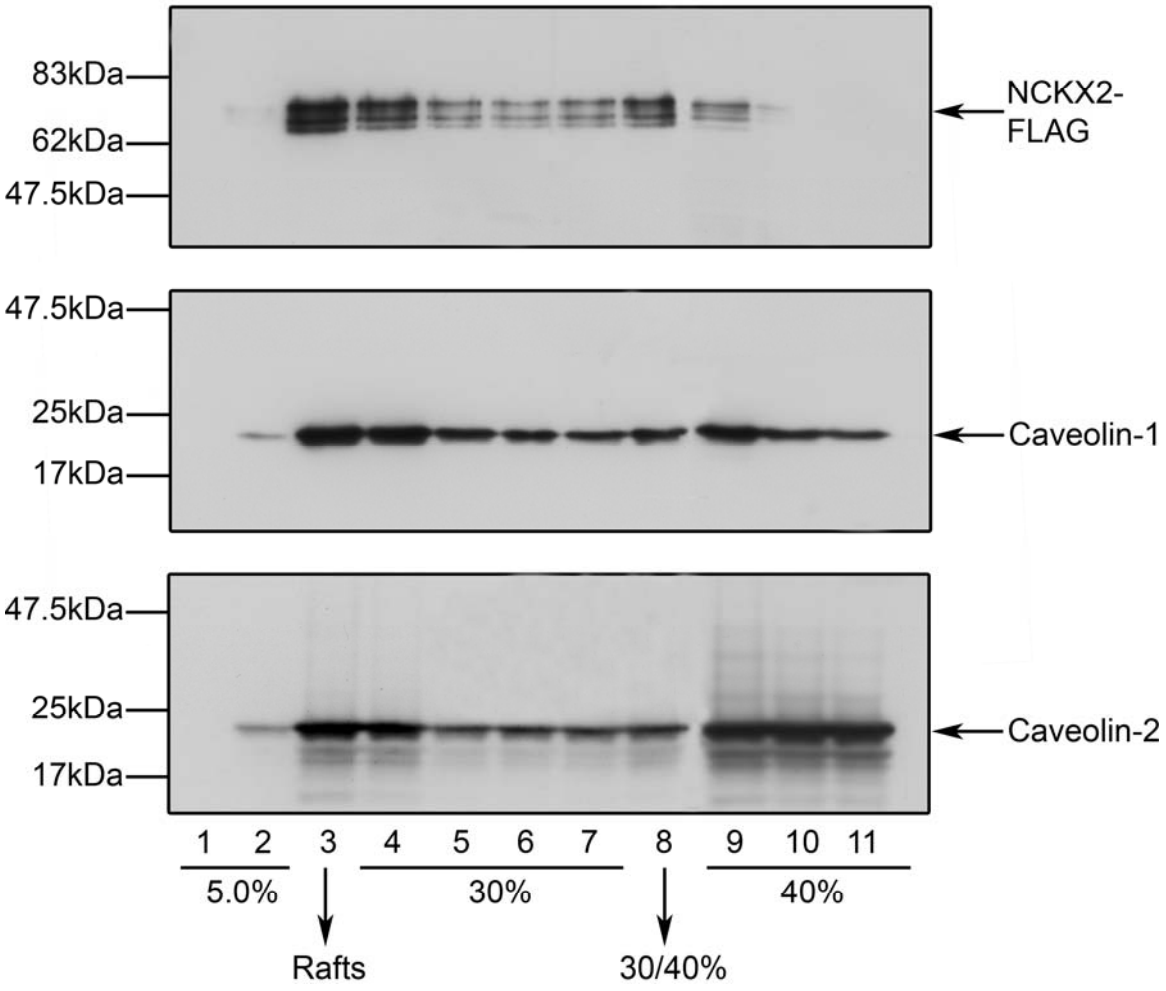
83kDa
62kDa
47.5kDa
NCKX2-FLAG
47.5kDa
25kDa
17kDa
Caveolin-1
47.5kDa
25kDa
17kDa
Caveolin-2
1 2 3 4 5 6 7 8 9 10 11
5.0%
30%
40%
Rafts
30/40%

### 3.5 Summary

Sub-cellular localization of NCKX2 into the lipid rafts and/or caveolae microdomains of rat brain was investigated using conventional density floatation methods, which effectively isolated the detergent-resistant membranes containing the lipid rafts/caveolae microdomains from the detergent soluble membranes and proteins. Approximately 30 to 60% of total rat brain NCKX2 was observed in the detergent-resistant membranes along with the resident caveolar protein, caveolin, which confirmed the sub-cellular localization of rat brain NCKX2 within the lipid rafts and/or caveolae microdomains of the rat brain neurons. A series of co-immunoprecipitation experiments subsequently revealed that rat brain NCKX2 is selectively and specifically localized to lipid rafts that are distinct from caveolae. The mutually exclusive pattern of the sub-cellular localization of the two proteins prevented their co-association even when the structure as well as the lipid and protein contents of the lipid rafts and/or caveolae microdomains were kept intact during co-immunoprecipitation. Recombinant NCKX2 in HEK-293 cells behaved remarkably differently from the endogenous rat brain NCKX2 during the density floatation analyses. The fractionation pattern of the recombinant NCKX2 depended upon the choice of the cold non-ionic detergent used during the procedure, rather than the presence of caveolins. The difference in the phospholipid composition of the plasma membranes of the rat brain neurons and HEK-293 cells, the respective complements of the endogenously expressed proteins, as well as any perturbation within HEK-293 cells due to the overexpression of recombinant NCKX2

could explain such differences in the behavior of the recombinant versus endogenous NCKX2.

# CHAPTER FOUR

## Oligomerization States of Rat Brain NCKX2

The objective of this project was to investigate the oligomeric state of rat brain NCKX2. Previous studies have demonstrated the possibility of formation of rat brain NCKX2 homo-oligomers by co-immunoprecipitating the wild-type and N-terminal FLAG-tagged rat brain NCKX2 (33). In addition, as described in Chapter 1, bovine rod NCKX1 forms a homodimer in the plasma membrane of the retinal rod photoreceptors, and this homo-dimerization has functionally important consequences in relation to its interaction with the α-subunit of the cGMP-gated channels (9, 273). Studies using heterologous systems (HEK-293 and High Five insect cells) stably expressing various combinations of recombinant, epitope-tagged chicken rod NCKX1, chicken cone NCKX2, and their deletion mutants and chimeras demonstrated an intermolecular association between chicken NCKX1 and NCKX2, potentially mediated by the interaction between the transmembrane domains of the respective exchangers (126). Although evidence for the co-association of NCKX2 has been presented, the precise molecular structure of this oligomeric complex was not clearly understood in detail, hence this aspect was investigated further in this study.

Catalyzed oxidation of adjacent free sulfydryls to disulfide bonds by 1, 10-phenanthroline-complexed copper (CuPhe), co-immunoprecipitation, as well as Blue Native Polyacrylamide Gel Electrophoreses (BN-PAGE) were employed to understand the oligomeric state of the recombinant rat brain NCKX2 expressed in HEK-293 cells. In addition, various cysteine-to-alanine mutants of the recombinant rat brain NCKX2 were used to investigate the region(s) of the rat brain NCKX2 that may be involved in oligomerization via disulfide linkages.

## 4.1 Free Sulfydryl-Dependent Formation of Higher Order Oligomers of NCKX2

### *4.1.1 Higher Order Oligomers of NCKX2-FLAG*

When microsomes were prepared under non-reducing conditions using HEK-293 cells over-expressing NCKX2-FLAG, and analyzed in the absence of reducing agent (β-ME) by SDS-PAGE followed by immunoblotting with monoclonal M2 anti-FLAG antibody, an intense monomeric band of NCKX2-FLAG at 75kDa (band a in Figure 4-1) was observed along with a very faint band at ~120kDa (band b), as well as two minor bands at ~150kDa (band c) and at ~200kDa (band d) (Figure 4-1). CuPhe-catalyzed reversible oxidation of adjacent free sulfydryls to disulfide bonds revealed the same four bands on the immunoblot, albeit with notably different relative intensities compared to those observed in the microsomes not subjected to oxidation by CuPhe. In the oxidized microsomes, the intensities of the monomeric 75kDa band as well as two higher molecular weight bands (120kDa and 150kDa) were significantly reduced and at times were only barely visible or not visible at all. Instead, the topmost 200kDa band showed the most intense labeling. In addition, when analyzed by densitometry, the intensity of the 200kDa band in the oxidized microsomes almost precisely matched the intensity of the monomeric 75kDa band in the microsomes that were not exposed to the catalyzed oxidation. This indicated that most of the NCKX2-FLAG monomers were oxidized to form the 200kDa oligomer (third and fourth lanes from left, Figure 4-1).

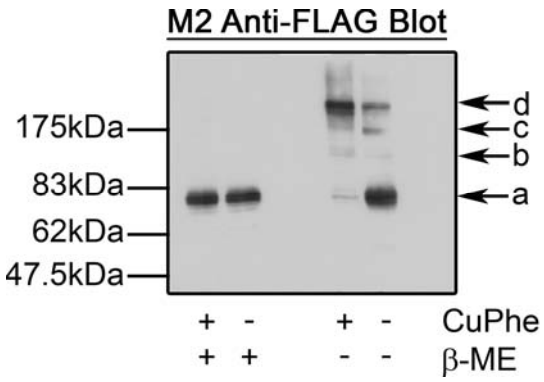


**Figure 4-1. Free Sulfydryl-Dependent Formation of Higher Order Oligomers of NCKX2-FLAG.** HEK-293 microsomes transiently expressing NCKX2-FLAG were subjected to CuPhe-catalyzed reversible oxidation of adjacent free sulfydryls to disulfide bonds as described in Chapter 2. The reaction was carried out for 30min on ice with (+) or without (-) the presence of CuPhe and terminated by the addition of EDTA. The reaction samples (+ CuPhe) were mixed with SDS-PAGE sample buffer and run on an SDS-PAGE gel under reducing (+ β-ME) and non-reducing (- β-ME) conditions. Separated proteins were transferred to nitrocellulose membranes, and immunoblotting was performed using M2 anti-FLAG antibody. The arrows (a, b, c, and d) indicate NCKX2-FLAG monomers (75kDa, a) as well as several higher order oligomeric species observed in non-reducing conditions. The blots shown are representative of seven independent experiments

Upon the addition of the reducing agent, β-mercaptoethanol, only the monomeric 75kDa band was labelled by the M2 anti-FLAG antibody, regardless of whether the CuPhe catalyzed oxidation reaction was carried out or not (left two lanes, Figure 4-1). This suggested that all disulfide bonds responsible for formation of the three higher molecular weight species of NCKX2-FLAG were reduced to free sulfydyls, and that the CuPhe-catalyzed oxidation was indeed completely reversible upon the introduction of the reducing agent. Taken together, this experiment revealed that, under non-reducing conditions, a considerable fraction of NCKX2-FLAG in HEK-293 microsomes exists as several oligomers, the formation of which is dependent upon the redox state of the sulfydryls of the exchanger. CuPhe-catalyzed oxidation of NCKX2-FLAG in HEK-293 microsomes resulted in almost a complete shift in labelling from the 75kDa NCKX2-FLAG monomer in the microsomes not subjected to the catalyzed oxidation to the 200kDa NCKX2-FLAG oligomer in non-reducing conditions. This indicates that the free sulfydryl(s) responsible for formation of the 200kDa oligomers of NCKX2-FLAG must not be occupied or modified prior to the reaction.

### *4.1.2 Cys395 and the Redox Dependent Formation of NCKX2-FLAG Oligomers*

The linear sequence of rat brain NCKX2 reveals a total of eight cysteine residues whose sulfydryls could be oxidized to form disulfide bonds responsible for the higher order oligomers of NCKX2-FLAG observed in Figure 4-1. The locations of these cysteine residues relative to the most current topology of rat brain NCKX2 are shown in Figure 4-2. All cysteine residues are highly conserved among different NCKX2 orthologs, and five of these that are found within or near the proposed transmembrane

domains of the exchangers (C3, C4, C6, C7, and C8, Figure 4-2) are also found in NCKX1. Despite their conserved nature, the precise role(s) of these cysteine residues in the exchanger structure and function are not well understood. Mutation analyses have shown that the two cysteines located on the extracellular side of the two transmembrane domains closest to the C-terminus of NCKX2 are essential for functional expression of recombinant rat brain NCKX2 in HEK-293 cells (33). However, generation of a partially functional cysteine-free human NCKX2 seemed to rule out the general importance of these two cysteine residues in NCKX2 function (144). Three other cysteine residues of rat brain NCKX2 are found in the hydrophilic loops of the exchanger, two in the N-terminal cytosolic segment and one in the middle of the large cytosolic loop. These cysteine residues are referred to using the following nomenclature, from the N-terminal end of the exchanger: Cys16 (C1), Cys24 (C2), Cys154 (C3), Cys224 (C4), Cys395 (C5), Cys614 (C6), Cys633 (C7), and Cys666 (C8) (Figure 4-2).

To identify the free sulfydryls of rat brain NCKX2 that are responsible for the redox dependent formation of the 200kDa oligomers of rat brain NCKX2 as well as the sulfydryls important for the other two higher-order oligomers (120kDa and 150kDa oligomers), various combined and single cysteine-to-alanine mutants of the N-terminal FLAG-tagged NCKX2 that were previously shown to be well expressed and functionally active in HEK-293 cells (C1-4A, C5A, and C1-5, 7A) were subjected to catalyzed oxidation by CuPhe as described before. As seen in Figure 4-3, NCKX2-FLAG C1-4A,

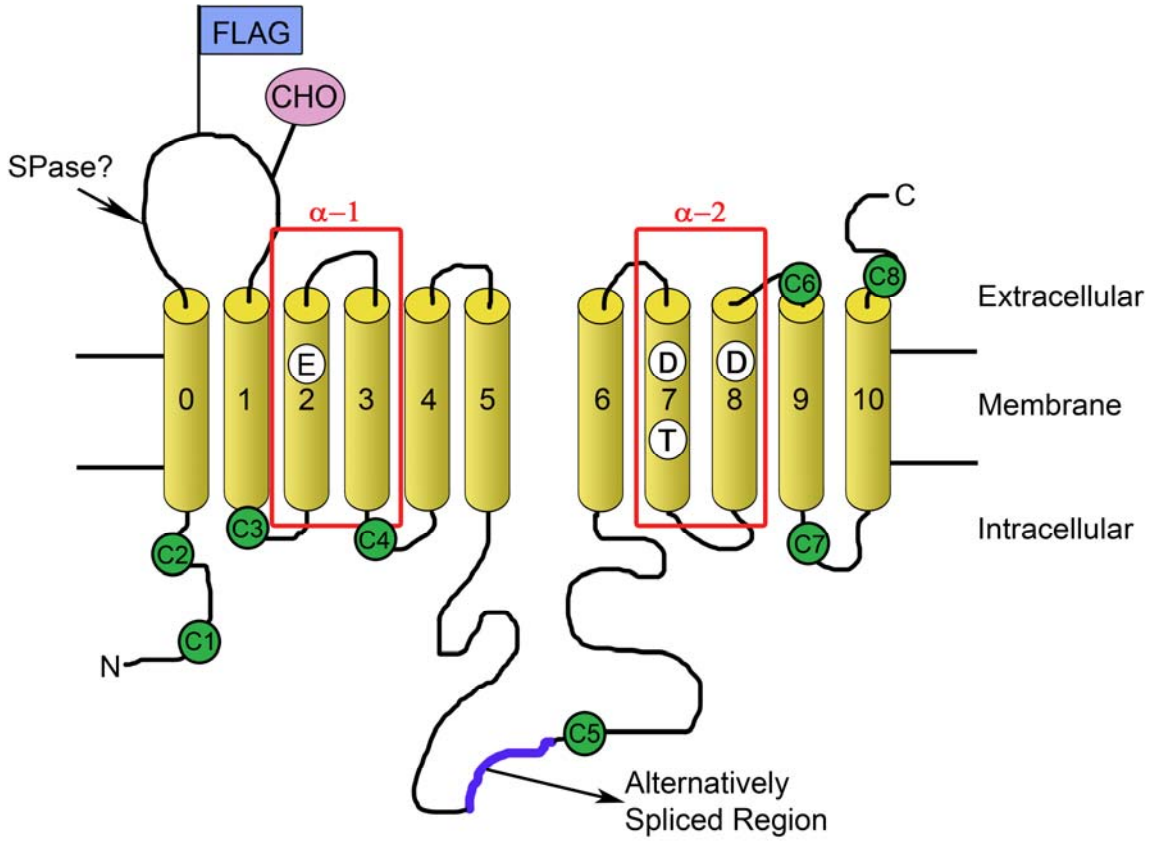


**Figure 4-2. Topology Diagram of NCKX2-FLAG and Its Native Cysteine Residues.** The locations of the eight native cysteine residues of rat NCKX2 are shown in the putative topology diagram presented in Figure 1-7. From the N-terminal end, those eight cysteines are: Cys16 (C1), Cys24 (C2), Cys154 (C3), Cys224 (C4), Cys395 (C5), Cys614 (C6), Cys633 (C7), and Cys666 (C8). The location at which the FLAG tag was inserted in the rat brain NCKX2 sequence is also indicated.

**Figure 4-3. Free Sulfydryl-Dependent Formation of Higher Order Oligomers of NCKX2-FLAG Cysteine-to-Alanine Mutants.** HEK-293 cells transiently expressing various NCKX2-FLAG cysteine-to-alanine mutants were subjected to CuPhe-catalyzed reversible oxidation as described in the legend to Figure 4-1, and the resulting immunoblots probed with M2 anti-FLAG antibody are shown. The top left immunoblot is the same as seen in Figure 4-1. NCKX2-FLAG C1-4A: cysteine-to-alanine mutant of NCKX2-FLAG in which the first four cysteine residues were mutated to alanine; NCKX2-FLAG C5A: cysteine-to-alanine mutant of NCKX2-FLAG in which only Cys395 (C5) was mutated to alanine; NCKX2-FLAG C1-5, 7A: cysteine-to-alanine mutant in which all cysteines except for Cys614 (C6) and Cys666 (C8) were mutated to alanine. The four bands are labelled as seen in Figure 4-1. The blots shown are representative of four independent experiments.

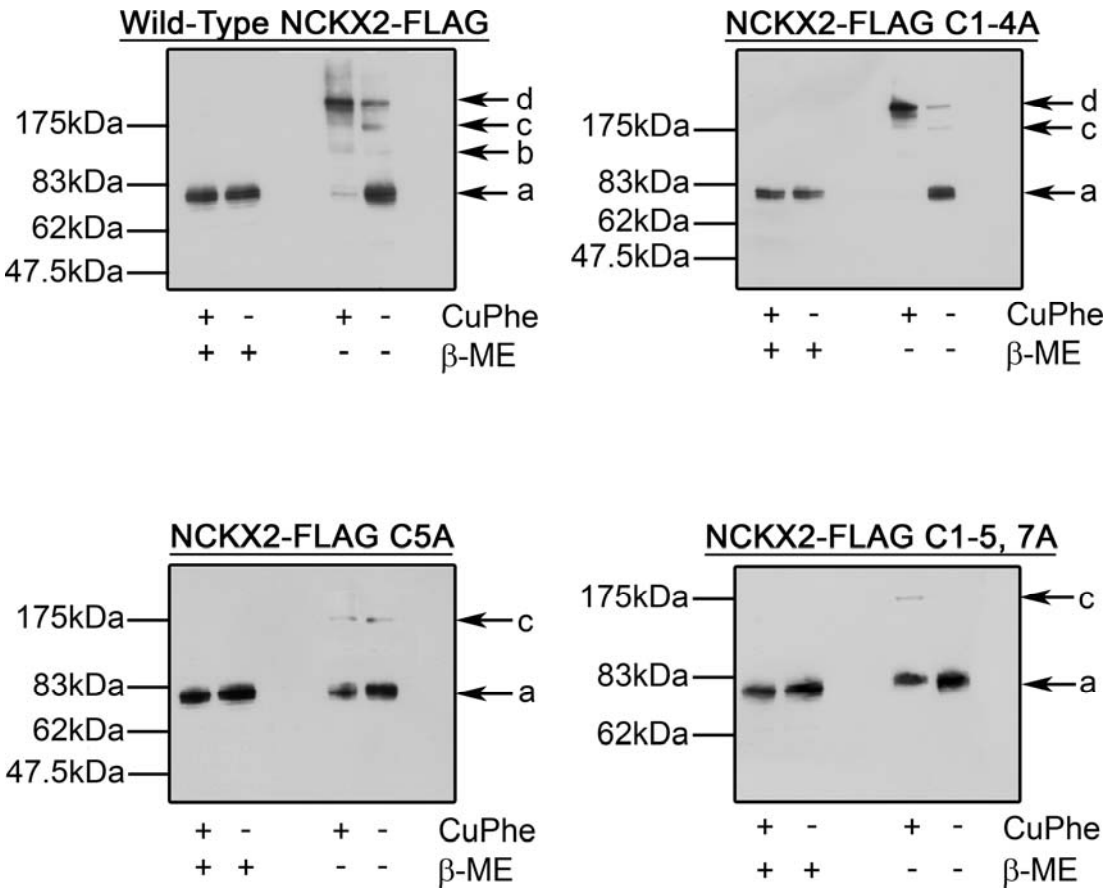
Wild-Type NCKX2-FLAG
175kDa
83kDa
62kDa
47.5kDa
d
c
b
a
+ - + - CuPhe
+ + - - β-ME
NCKX2-FLAG C1-4A
175kDa
83kDa
62kDa
47.5kDa
d
c
a
+ - + - CuPhe
+ + - - β-ME
NCKX2-FLAG C5A
175kDa
83kDa
62kDa
47.5kDa
c
a
+ - + - CuPhe
+ + - - β-ME
NCKX2-FLAG C1-5, 7A
175kDa
83kDa
62kDa
c
a
+ - + - CuPhe
+ + - - β-ME

in which the first four cysteine residues of rat brain NCKX2 were mutated to alanine, displayed a similar pattern of redox dependent formation of higher order oligomers as wild-type NCKX2-FLAG. Unlike wild-type NCKX2-FLAG, however, the faint 120kDa band that was occasionally observed in non-reducing conditions was completely absent in NCKX2-FLAG C1-4A or in the other cysteine-to-alanine mutants of NCKX2-FLAG tested, suggesting that the formation of this 120kDa oligomer of NCKX2-FLAG might depend on the presence of the first four cysteine residues of the exchanger.

Interestingly, CuPhe-catalyzed oxidation of NCKX2-FLAG C5A and NCKX2-FLAG C1-5, 7A did not result in the appearance of any 200kDa band, although the 150kDa band was visible. Importantly, the intensity of the 75kDa monomeric band was not significantly lower in the CuPhe treated samples compared to the untreated ones (Figure 4-3). This implies that Cys395, the single cysteine found in the long cytosolic loop of rat brain NCKX2, is essential for redox dependent formation of the 200kDa oligomers of NCKX2-FLAG in HEK-293 cell microsomes. Moreover, the data also suggest that the sulfydryl of Cys395 in HEK-293 cell microsomes must be unoccupied and/or unmodified in the isolated microsomes prior to oxidation so that they could be almost completely oxidized to produce the 200kDa oligomers of NCKX2-FLAG. Although a relatively minor species, the 150kDa oligomer of NCKX2-FLAG (band c in Figure 4-3) was observed in all mutants tested under non-reducing conditions. The presence of the 150kDa band was redox dependent since it was no longer visible when the reducing agent was introduced. The fact that this band was observed even in the HEK-293 cell microsomes transiently expressing NCKX2-FLAG C1-5, 7A suggested

that either or both of the remaining two cysteines, Cys614 (C6) and Cys666 (C8), were responsible for formation of the 150kDa oligomers of NCKX2-FLAG.

### *4.1.3 Detergent Solubilization and the Redox Dependent Formation of NCKX2-FLAG Oligomers*

The previous experiments using CuPhe to catalyze the oxidation of adjacent free sulfydryls to disulfide bonds were conducted using isolated HEK-293 microsomes not disrupted by the addition of detergent. To test the stability of the higher order oligomers of NCKX2-FLAG, HEK-293 microsomes transiently expressing wild-type or various cysteine-to-alanine mutants of NCKX2-FLAG were solubilized in ice-cold 1.0% Triton X-100 or 1.0% CHAPS (final concentration) for 30min just prior to the catalyzed oxidation by CuPhe. As seen in Figures 4-4 and 4-5, detergent solubilization of the HEK-293 microsomes did not significantly change the pattern of higher order oligomers of NCKX2-FLAG and its various cysteine-to-alanine mutants formed in non-reducing conditions by catalyzed oxidation. However, detergent solubilization had a mild oxidizing effect on the free sulfydryls of NCKX2-FLAG and NCKX2-FLAG cysteine mutants, resulting in a larger amount of the 200kDa oligomer without the catalyzed oxidation by CuPhe (Figures 4-4 and 4-5).

In summary, the catalyzed oxidation of free sulfydryls of NCKX2-FLAG to disulfide bonds in HEK-293 cell microsomes revealed the existence of several different higher order oligomers of NCKX2-FLAG. Cys395, found in the middle of the long cytosolic loop, was necessary for formation of the 200kDa oligomer of NCKX2-FLAG,

**Figure 4-4. Effect of Triton X-100 Solubilization on Free Sulfydryl-Dependent Formation of Higher Order Oligomers of NCKX2-FLAG.** HEK-293 microsomes transiently expressing NCKX2-FLAG or various cysteine-to-alanine mutants of NCKX2-FLAG were solubilized in ice-cold Triton X-100 (1.0% final concentration) for 30min just prior to CuPhe-catalyzed reversible oxidation reaction, and the resulting immunoblots probed with monoclonal M2 anti-FLAG antibody are shown. See Figure 4-3 legend for details. The blots shown are representative of three independent experiments.

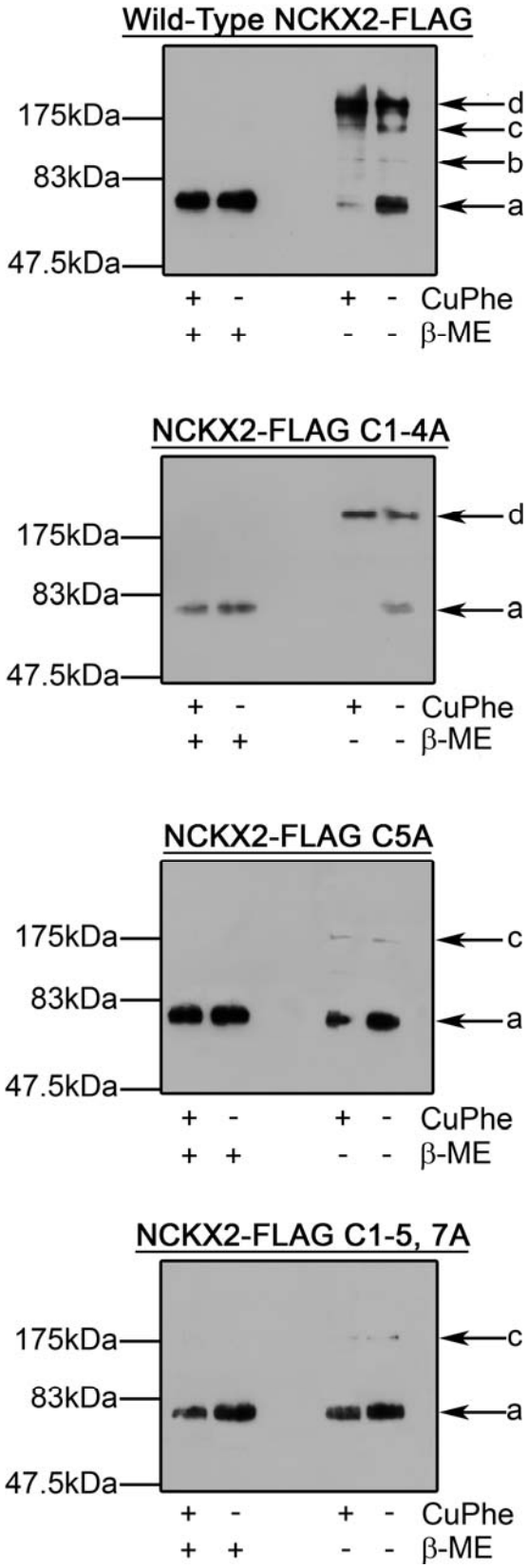
Wild-Type NCKX2-FLAG
175kDa
83kDa
47.5kDa
d
c
b
a
+ - + - CuPhe
+ + - - β-ME
NCKX2-FLAG C1-4A
175kDa
83kDa
47.5kDa
d
a
+ - + - CuPhe
+ + - - β-ME
NCKX2-FLAG C5A
175kDa
83kDa
47.5kDa
c
a
+ - + - CuPhe
+ + - - β-ME
NCKX2-FLAG C1-5, 7A
175kDa
83kDa
47.5kDa
c
a
+ - + - CuPhe
+ + - - β-ME

**Figure 4-5. Effect of CHAPS Solubilization on Free Sulfydryl-Dependent Formation of Higher Order Oligomers of NCKX2-FLAG.** HEK-293 microsomes transiently expressing NCKX2-FLAG or various cysteine-to-alanine mutants of NCKX2-FLAG were solubilized in ice-cold CHAPS (1.0% final concentration) for 30min just prior to CuPhe-catalyzed reversible oxidation, and the resulting immunoblots probed with the monoclonal M2 anti-FLAG antibody are shown. See Figure 4-3 legend for details. The blots shown are representative of three independent experiments.

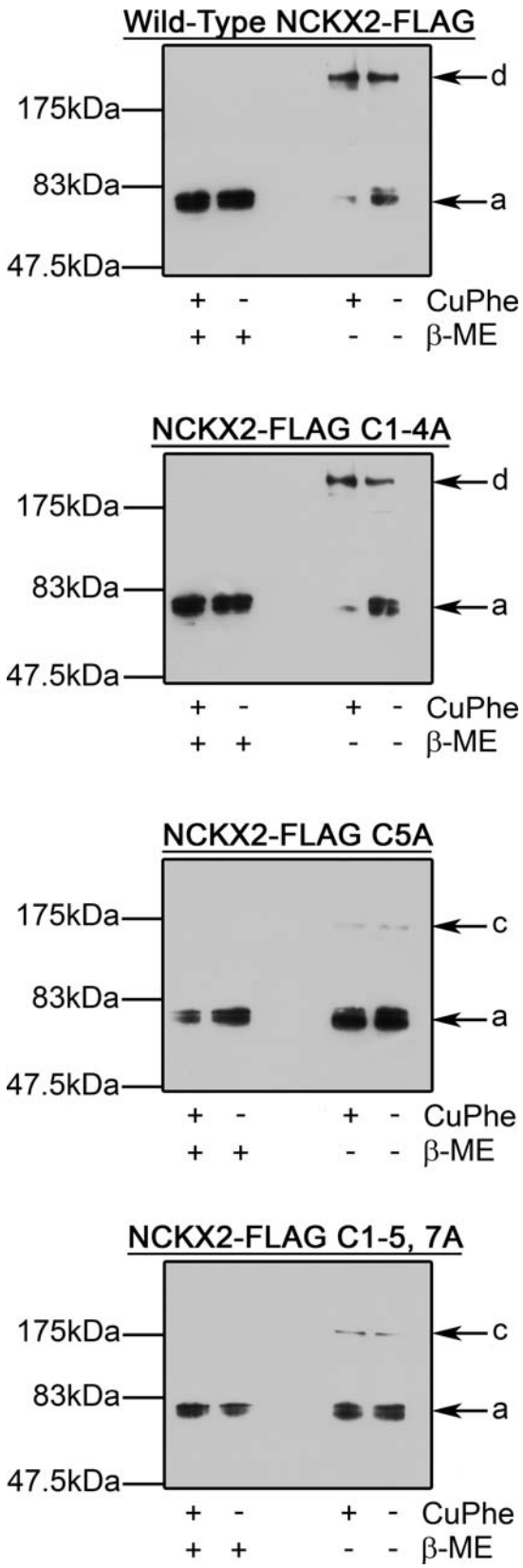
Wild-Type NCKX2-FLAG
175kDa
83kDa
47.5kDa
d
a
+ - + - CuPhe
+ + - - β-ME
NCKX2-FLAG C1-4A
175kDa
83kDa
47.5kDa
d
a
+ - + - CuPhe
+ + - - β-ME
NCKX2-FLAG C5A
175kDa
83kDa
47.5kDa
c
a
+ - + - CuPhe
+ + - - β-ME
NCKX2-FLAG C1-5, 7A
175kDa
83kDa
47.5kDa
c
a
+ - + - CuPhe
+ + - - β-ME

the highest order oligomer observed. The sulfydryl of Cys395 appeared to be mostly unoccupied or unmodified under non-reducing conditions, so that CuPhe-catalyzed oxidation of Cys395 would result in almost a complete shift of NCKX2-FLAG from its monomeric 75kDa form to the 200kDa oligomeric species via disulfide bond formation. A small fraction of NCKX2 was found as a 150kDa oligomer under non-reducing conditions in all the cysteine-to-alanine mutants of NCKX2-FLAG tested, indicating the remaining two cysteines of rat brain NCKX2, Cys614 and Cys666, were responsible for formation of the 150kDa oligomer. Detergent solubilization further oxidized the exchangers but nonetheless had no major impact on the pattern of higher oligomers of NCKX2-FLAG, suggesting that these higher order oligomers were stable in detergent solubilized membranes.

## 4.2 Homo-oligomerization of NCKX2

### *4.2.1 Co-immunoprecipitation of NCKX2*

The previous experiments demonstrated presence of the three different higher order oligomeric species of NCKX2-FLAG in non-reducing conditions, namely 120kDa, 150kDa, and 200kDa oligomers. Of these, formation of the 200kDa oligomer was dependent on the availability of the free sulfydryl in Cys395, the only cysteine found in the middle of the long cytosolic loop of rat brain NCKX2. To investigate whether all or any of these higher order oligomers could constitute homo-oligomers of rat brain NCKX2, co-immunoprecipitation experiments using HEK-293 microsomes transiently co-expressing two different recombinant rat brain NCKX2 constructs, N-terminal FLAG-

tagged rat brain NCKX2 and untagged rat brain NCKX2, were performed as described in Chapter 2, and the results are shown in Figure 4-6.

Briefly, equal amounts of DNA constructs encoding N-terminal FLAG-tagged and untagged rat brain NCKX2 were used to transfect HEK-293 cells. Two days post-transfection, microsomes were prepared and solubilized with the chosen detergents, and then immunoprecipitated using monoclonal M2 anti-FLAG antibody. The co-association of untagged rat brain NCKX2 in the immunoprecipitated samples was detected using affinity-purified PA1-926 antibody against rat brain NCKX2. The epitope for the affinity-purified PA1-926 antibody lies in the same N-terminal region of the exchanger in which the FLAG tag was inserted (Figure 4-2). The insertion of the FLAG tag replaced the epitope recognized by the PA1-926 antibody. Therefore, while the anti-FLAG antibody would only recognize NCKX2-FLAG, affinity-purified PA1-926 antibody would only detect the presence of wild-type untagged NCKX2. The antibody specificity can be seen in the lysate lanes of Figure 4-6.

As seen in the lysate lanes of Figure 4-6, both NCKX2-FLAG and untagged NCKX2 were expressed in HEK-293 cells, whether they were expressed alone or together. M2 anti-FLAG antibody successfully immunoprecipitated NCKX2-FLAG from the solubilized microsomes as expected, and also co-immunoprecipitated wild-type untagged NCKX2 when expressed together (Figure 4-6). The observation that wild-type untagged NCKX2 could be co-immunoprecipitated with NCKX2-FLAG clearly demonstrated that rat brain NCKX2 is able to form homo-oligomeric species. The use of

**Figure 4-6. Co-immunoprecipitation of Recombinant NCKX2 Expressed in HEK-293 Cells.** HEK-293 microsomes transiently expressing NCKX2-FLAG (F) and wild-type untagged NCKX2 (W) alone or together (F/W) were solubilized in RIPA buffer containing either 1% Triton X-100 (*top*) or 1% CHAPS (*bottom*) to investigate the homo-oligomerization of the NCKX2 proteins. Immunoprecipitation was performed using M2 anti-FLAG antibody, and the presence of NCKX2-FLAG in the immunoprecipitated sample (FLAG IP) was detected by M2 anti-FLAG antibody (anti-FLAG blot). The presence of the co-associated wild-type untagged NCKX2 was detected by the affinity-purified polyclonal PA1-926 antibody against NCKX2 (PA1-926 blot). The lysate samples contain aliquots of the solubilized microsomes just prior to the immunoprecipitation by M2 anti-FLAG antibody showing successful expression of the indicated DNA constructs as well as the absence of cross-reactivities of the antibodies. Asterisks indicate the position of immunoglobulin bands. The blots shown are representative of five independent experiments.

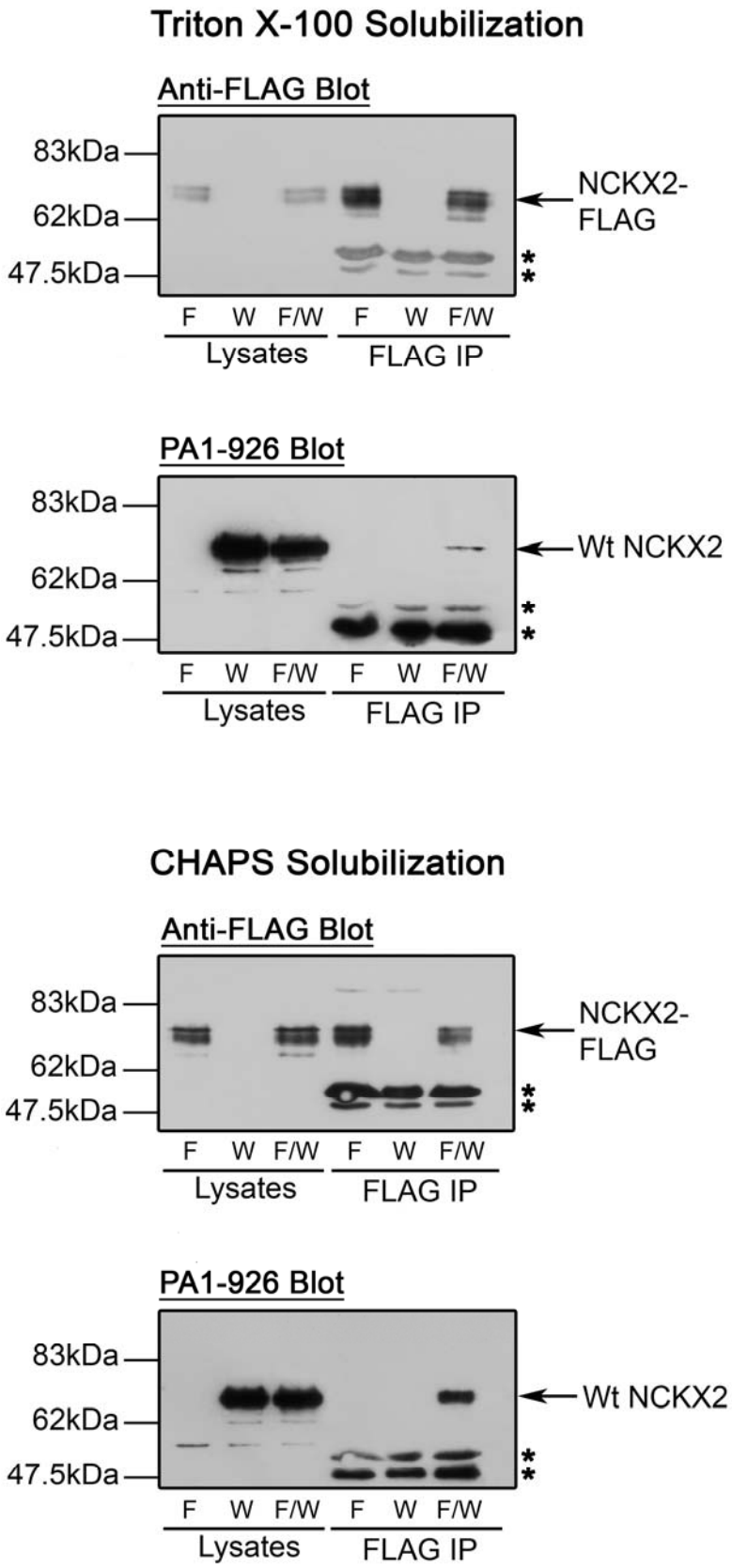
Triton X-100 Solubilization
Anti-FLAG Blot
83kDa
62kDa
47.5kDa
NCKX2-FLAG
**
F W F/W F W F/W
Lysates
FLAG IP
PA1-926 Blot
83kDa
62kDa
47.5kDa
Wt NCKX2
**
F W F/W F W F/W
Lysates
FLAG IP
CHAPS Solubilization
Anti-FLAG Blot
83kDa
62kDa
47.5kDa
NCKX2-FLAG
**
F W F/W F W F/W
Lysates
FLAG IP
PA1-926 Blot
83kDa
62kDa
47.5kDa
Wt NCKX2
**
F W F/W F W F/W
Lysates
FLAG IP

two different detergents (Triton X-100 and CHAPS) did not influence the overall co-immunoprecipitation results obtained, although the solubilization by CHAPS resulted in more co-immunoprecipitation of untagged NCKX2 compared to the solubilization by Triton X-100. These results suggest that some or even all of the higher order oligomers of NCKX2-FLAG seen in non-reducing conditions might represent a homo-oligomeric association.

### *4.2.2. Cys395 Is Not Necessary for the Homo-Oligomerization of NCKX2*

Since previous experiments (Figures 4-4 and 4-5) had indicated that a small fraction of NCKX2-FLAG exists as the Cys395-dependent 200kDa oligomer under detergent-solubilized conditions, it was possible that this oligomer was responsible for the observed co-immunoprecipitation of wild-type NCKX2 and NCKX2-FLAG. Therefore, the dependence of wild-type NCKX2/NCKX2-FLAG co-immunoprecipitation on the free sulfydryl of Cys395 was investigated next. Co-immunoprecipitation experiments were performed using NCKX2-FLAG C5A as well as untagged NCKX2 C5A constructs expressed in HEK-293 cells along with wild-type NCKX2-FLAG and untagged wild-type NCKX2. As seen in Figure 4-7, the absence of the free sulfydryl of Cys395 did not prevent co-immunoprecipitation of wild-type NCKX2 with NCKX2-FLAG and the efficiency of co-immunoprecipitation was not significantly influenced by the presence of this mutation in either or both tagged and/or untagged exchangers.

In contrast to the lack of any discernable effect of Cys395 mutation on the efficiency of co-immunoprecipitation of the recombinant exchangers, the choice of

**Figure 4-7. Co-immunoprecipitation of Recombinant NCKX2 and NCKX2 C395A Mutants Expressed in HEK-293 Cells.** HEK-293 microsomes transiently expressing various combinations of recombinant rat brain NCKX2 were solubilized in ice-cold RIPA buffer containing 1.0% CHAPS and co-immunoprecipitation experiments were performed using M2 anti-FLAG antibody. *Top*: immunoblot probed with M2 anti-FLAG antibody. *Bottom*: immunoblot probed with the affinity-purified polyclonal PA1-926 antibody against NCKX2. F: NCKX2-FLAG, FC5: NCKX2-FLAG C5A, Wt: untagged NCKX2, WtC5: untagged NCKX2 C5A. Asterisks indicate the position of immunoglobulin bands. See Figure 4-6 legend for more details. The blots shown are representative of five independent experiments.

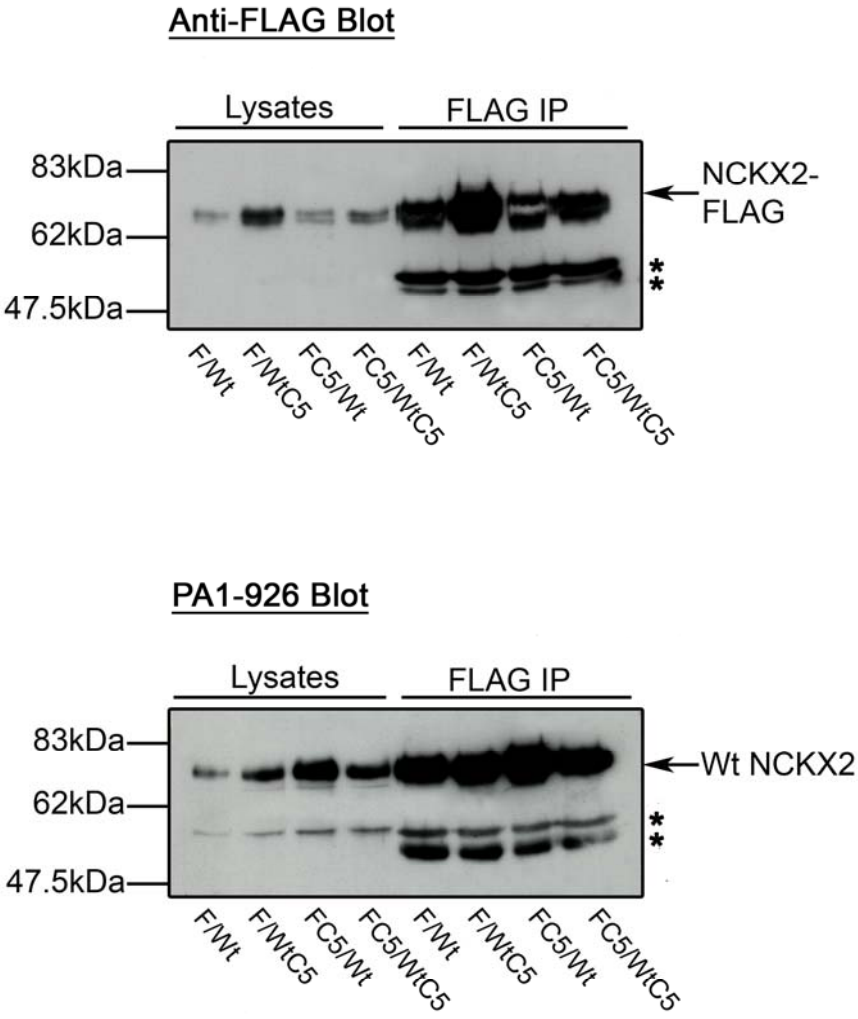
Anti-FLAG Blot
Lysates
FLAG IP
83kDa
62kDa
47.5kDa
NCKX2-
FLAG
**
F/Wt
F/WtC5
FC5/Wt
FC5/WtC5
F/Wt
F/WtC5
FC5/Wt
FC5/WtC5
PA1-926 Blot
Lysates
FLAG IP
83kDa
62kDa
47.5kDa
Wt NCKX2
**
F/Wt
F/WtC5
FC5/Wt
FC5/WtC5
F/Wt
F/WtC5
FC5/Wt
FC5/WtC5

**Figure 4-8. Co-immunoprecipitation of Recombinant NCKX2 C395A Mutants Expressed in HEK-293 Cells.** HEK-293 microsomes transiently co-expressing either tagged and untagged wild-type NCKX2 constructs (F/Wt), or tagged and untagged C5A mutants (FC5/WtC5) were solubilized in ice-cold RIPA buffer containing 1.0% CHAPS or 1.0% Triton X-100, the co-immunoprecipitation experiments were performed using M2 anti-FLAG antibody. *Top*: immunoblot probed with M2 anti-FLAG antibody. *Bottom*: immunoblot probed with the affinity-purified polyclonal PA1-926 antibody against NCKX2. F: NCKX2-FLAG, FC5: NCKX2-FLAG C5A, Wt: untagged NCKX2, WtC5: untagged NCKX2 C5A. Asterisks indicate the position of immunoglobulin bands. The blots shown are representative of four independent experiments.

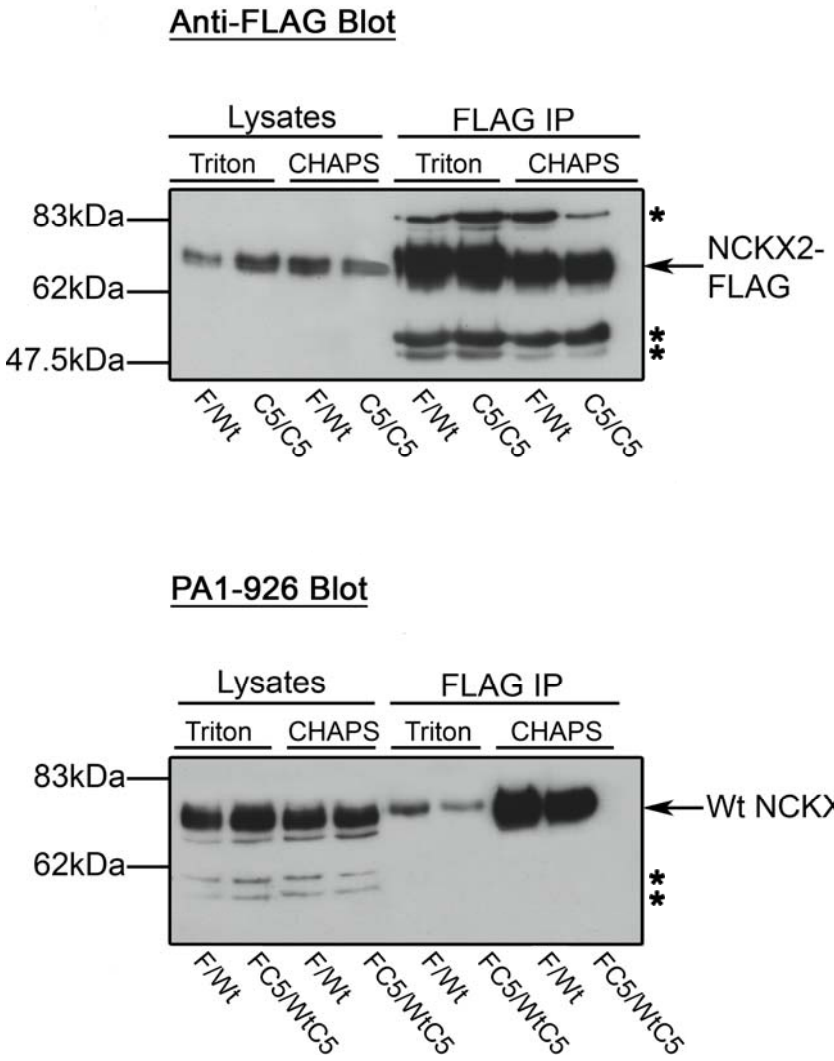
Anti-FLAG Blot
Lysates
FLAG IP
Triton
CHAPS
Triton
CHAPS
83kDa
62kDa
47.5kDa
NCKX2-
FLAG
F/Wt
C5/C5
F/Wt
C5/C5
F/Wt
C5/C5
F/Wt
C5/C5
PA1-926 Blot
Lysates
FLAG IP
Triton
CHAPS
Triton
CHAPS
83kDa
62kDa
Wt NCKX2
F/Wt
FC5/WtC5
F/Wt
FC5/WtC5
F/Wt
FC5/WtC5
F/Wt
FC5/WtC5

detergents had a notable effect, consistent with the data seen in Figure 4-8. When HEK-293 microsomes co-expressing NCKX2-FLAG and untagged NCKX2 were solubilized in 1.0% CHAPS, more untagged NCKX2 proteins were co-immunoprecipitated than when the same HEK-293 microsomes were solubilized using 1.0% Triton X-100 (F/Wt in Triton vs. CHAPS, PA1-926 blot, Figure 4-8). This was also true for the microsomes prepared from HEK-293 cells co-expressing two C395A mutants, NCKX2-FLAG C5A and untagged NCKX2 C5A (C5/C5 in Triton vs. CHAPS, PA1-926 blot, Figure 4-8). The type of detergent used did not influence the immunoprecipitation efficiency of the FLAG-tagged exchangers by the monoclonal M2 anti-FLAG antibody, as indicated by the comparatively equivalent labelling of the FLAG-tagged exchangers by the anti-FLAG antibody (Figure 4-8). These data demonstrate that recombinant NCKX2 proteins co-associate with one another in a complex that is not dependent on a covalent bond mediated by the formation of the disulfide bond between Cys395 residues of the exchanger monomers. The solubilization efficiencies of the detergent used in the experiments impacted the co-association efficiency of the exchanger monomer, while Cys395 mutation did not. This detergent effect was not due to incomplete solubilization of the exchanger proteins resulting in protein aggregates, since previous pilot experiments had demonstrated that NCKX2 proteins were completely soluble under the same conditions (1.0% Triton X-100 or 1.0% CHAPS), as defined by lack of sedimentation at 100,000*g* for one hour (data not shown). This detergent effect suggests that the interaction between the exchanger monomers lies within the portions of the transmembrane domains that interact with the detergent molecules.

## 4.3 Oligomeric State of Rat Brain NCKX2

The series of co-immunoprecipitation experiments described in sections 4.1 and 4.2 demonstrated that recombinant rat brain NCKX2 transiently expressed in HEK-293 cells formed homo-oligomers, and this homo-oligomeric association was driven by non-covalent interaction between the transmembrane domains of the exchanger monomers. The data also argued against the importance of the free sulfydryl of Cys395 in NCKX2 homo-oligomerization, although Cys395 was necessary for formation of the 200kDa oligomers of NCKX2-FLAG generated by CuPhe catalyzed or detergent induced oxidation of the adjacent free sulfydryls to disulfide bonds. To understand the precise oligomeric state of rat brain NCKX2, Blue-Native Polyacrylamide Gel Electrophoresis (BN-PAGE) was performed using HEK-293 microsomes transiently expressing NCKX2-FLAG or NCKX2-FLAG C5A. First developed by Schägger and von Jagow in 1991 (265), BN-PAGE uses the negatively charged dye Coomassie Brilliant Blue G250 (CBB G250) in place for SDS to impart negative charges necessary for the proteins to be resolved during electrophoresis. Since CBB G250 does not act as a detergent, it preserves the native structure of protein complexes thereby allowing high resolution separation of individual protein subunits and determination of the oligomeric state of a protein complex with relative ease and simplicity (47, 265, 287).

HEK-293 microsomes transiently expressing either NCKX2-FLAG or NCKX2-FLAG C5A were solubilized using 1.0% Triton X-100 or 1.0% CHAPS and then exposed to varying amounts of SDS with or without reducing agent (0.1M DTT). These

solubilized microsomes were run on a continuous BN gradient gel followed by immunoblotting using the monoclonal M2 anti-FLAG antibody, and the results are shown in Figures 4-9 and 4-10. In the absence of SDS (0% SDS) both NCKX2-FLAG and NCKX2-FLAG C5A were observed as higher order oligomers whose apparent size was greater than would have been expected for a NCKX2 dimer (band c, Figures 4-9 and 4-10). This was true regardless of the type of non-ionic detergent used to solubilize the HEK-293 cell microsomes, and was independent of the redox environment (absence or presence of DTT). Therefore, the data confirmed that both NCKX2-FLAG and NCKX2-FLAG C5A exist in an oligomeric complex in the plasma membrane, the quaternary structure of which is maintained even when they are solubilized by cold non-ionic detergents.

In Triton X-100 solubilized microsomes (Figure 4-9), the addition of 2.0% SDS and 0.1M DTT was sufficient to break all covalent and non-covalent interactions between both NCKX2-FLAG and NCKX2 C5A oligomers so that the only species observed on the immunoblots was the monomeric 75kDa exchanger (band a, +DTT blots, Figure 4-9). In the presence of 0.1M DTT, non-covalent association of the recombinant exchanger monomers was clearly seen as the formation of progressively higher order oligomers of NCKX2-FLAG and NCKX2-FLAG C5A with the decrease in SDS concentration, starting with what appears to be a dimeric 150kDa band of NCKX2-FLAG and NCKX2-FLAG C5A (band b, +DTT blots, Figure 4-9). The higher order oligomers of the recombinant exchangers with an apparent size greater than the NCKX2 dimer (band c) began to appear at lower SDS concentrations (0.25% SDS), eventually becoming the only

**Figure 4-9. Blue-Native Gel Electrophoresis and the Oligomeric State of Recombinant Rat Brain NCKX2 Solubilized in Triton X-100.** HEK-293 cell microsomes transiently expressing either NCKX2-FLAG or NCKX2-FLAG C5A were solubilized in 1.0% Triton X-100, and the solubilized microsomes were incubated in varying amounts of SDS in the presence (+DTT) or absence (-DTT) of 0.1M DTT. Solubilized microsomes were mixed with the BN sample buffer, run on a BN-PAGE gel, and analyzed by immunoblotting using the monoclonal M2 anti-FLAG antibody. The arrows indicate NCKX2-FLAG monomer (a), dimer (b), and oligomer (c), respectively. The actual molecular weights of the protein markers have been divided by a conversion factor of 1.8 (the adjusted, calculated, size is shown) to account for the differential binding of CBB dye to membrane proteins as compared to the soluble marker proteins as described in Chapter 2 (104). The blots shown are representative of three independent experiments.

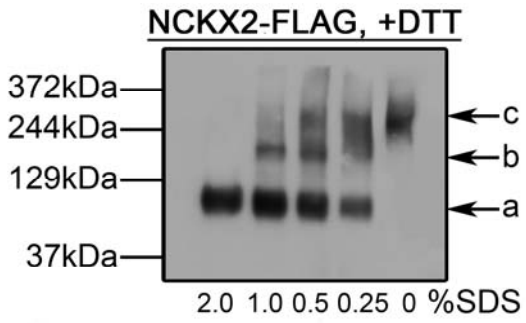
NCKX2-FLAG, +DTT
372kDa
244kDa
129kDa
37kDa
c
b
a
2.0 1.0 0.5 0.25 0 %SDS

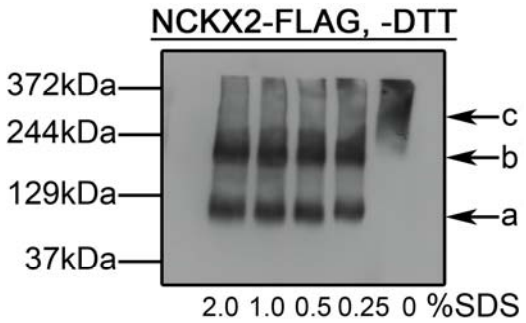
NCKX2-FLAG, -DTT
372kDa
244kDa
129kDa
37kDa
c
b
a
2.0 1.0 0.5 0.25 0 %SDS

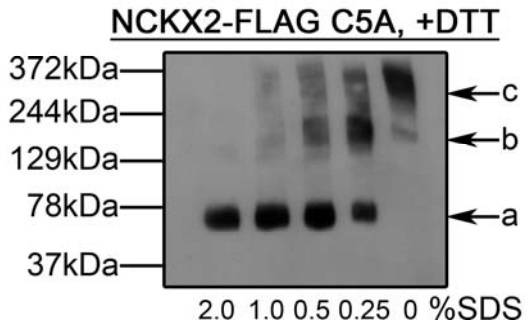
NCKX2-FLAG C5A, +DTT
372kDa
244kDa
129kDa
78kDa
37kDa
c
b
a
2.0 1.0 0.5 0.25 0 %SDS

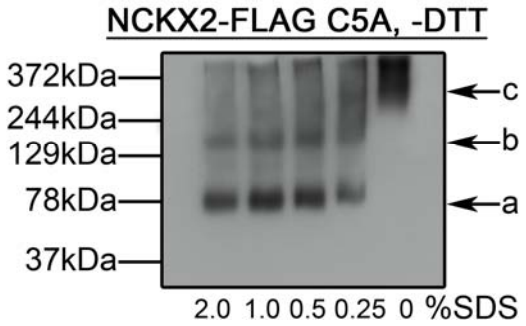
NCKX2-FLAG C5A, -DTT
372kDa
244kDa
129kDa
78kDa
37kDa
c
b
a
2.0 1.0 0.5 0.25 0 %SDS

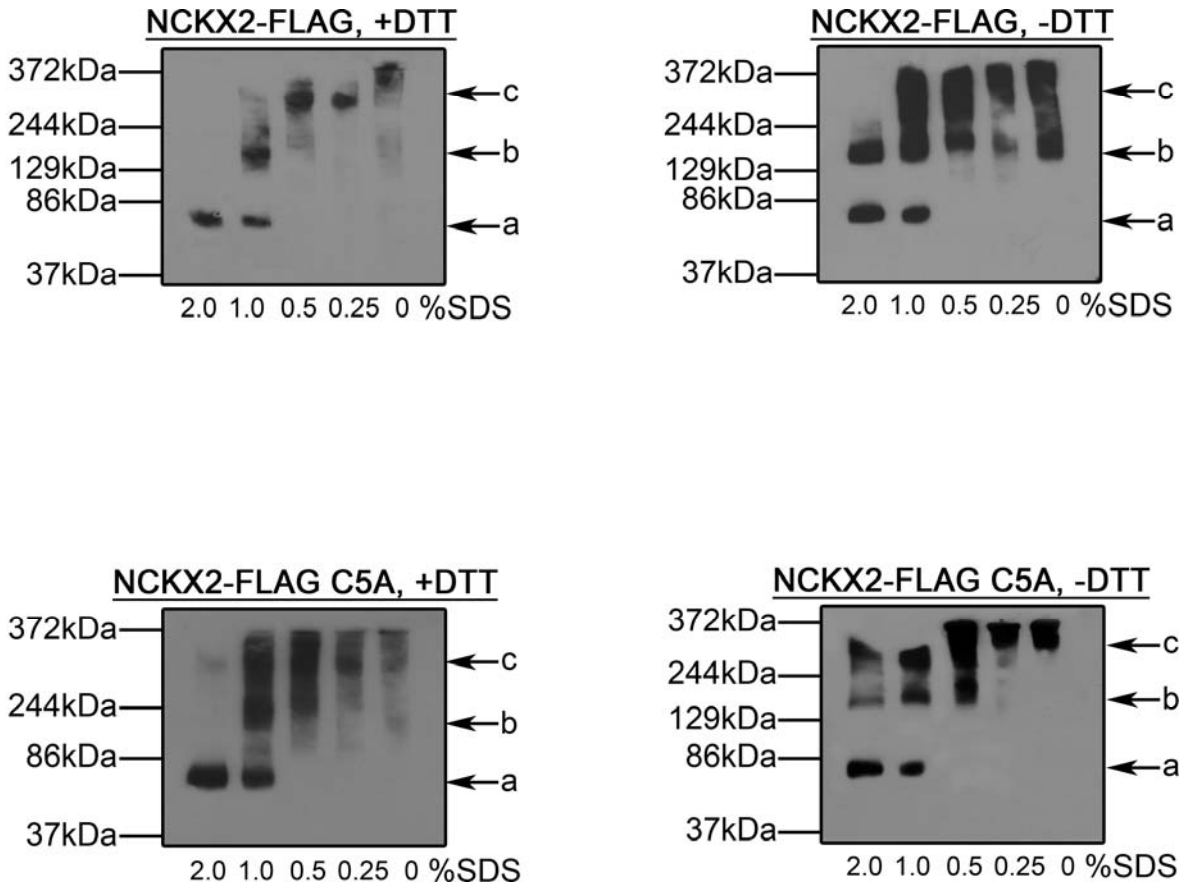


**Figure 4-10. Blue-Native Gel Electrophoresis and the Oligomeric State of Recombinant Rat Brain NCKX2 Solubilized in CHAPS.** HEK-293 cell microsomes transiently expressing either NCKX2-FLAG or NCKX2-FLAG C5A were solubilized in 1% CHAPS, and analysed on BN gels as described in the legend to Figure 4-9. The blots shown are representative of three independent experiments.

band observed in the absence of SDS as mentioned above. Some monomeric 75kDa exchanger band was clearly present at the lowest SDS concentration tested (0.25% SDS) and increased in intensity as the concentration of SDS increased, indicating that in the presence of Triton X-100 a low SDS concentration was sufficient to disrupt the non-covalent association between exchanger monomers.

In the absence of SDS, only higher order NCKX2 oligomers with an apparent size greater than the exchanger dimer were observed (band c, -DTT blots, Figure 4-9), independent of the presence of DTT. When the SDS concentration was raised in the absence of DTT, a large fraction of NCKX2-FLAG migrated as an apparent dimer of 150kDa, which was reduced to a monomer in the presence of DTT. Interestingly, the formation of this disulfide-dependent dimer was also seen for the NCKX2-FLAG C5A mutant, although at a much lower level than for NCKX2-FLAG. These data suggest the presence of two independent dimeric species under non-reducing conditions, one mediated via Cys395 and the other, a minor species that is independent of Cys395.

When 1.0% CHAPS was used to solubilize the HEK-293 microsomes, similar results were obtained (Figure 4-10). Just as with Triton X-100 solubilized microsomes, 2.0% SDS and 0.1M DTT were enough to break all interactions between the exchanger monomers so that only the monomeric 75kDa band was observed (band a, +DTT blots, Figure 4-10). The formation of progressively higher order oligomers of the recombinant exchangers was seen as the SDS concentration was decreased under reducing conditions, again reflecting the non-covalent association between exchanger monomers. Unlike

Triton X-100 solubilized microsomes, however, the 75kDa monomeric bands of NCKX2-FLAG and NCKX2-FLAG C5A were only present at higher SDS concentrations (2.0% and 1.0%) and disappeared as the SDS concentration was lowered. The requirement for higher SDS concentrations to dissociate NCKX2 oligomers in CHAPS compared to Triton X-100 suggests that the strength of the non-covalent association is dependent upon detergent properties. This result is consistent with the difference in co-immunoprecipitation efficiency observed earlier.

### 4.4 Summary

Recombinant rat brain NCKX2 transiently expressed in HEK-293 cells formed several higher order oligomers whose appearance on SDS-PAGE was dependent on the availability of free sulfydryls and the redox environment the exchangers were exposed to. In addition, the catalyzed oxidation of adjacent free sulfydryls to disulfide bonds by CuPhe revealed almost complete formation of a 200kDa oligomer of NCKX2-FLAG from the 75kDa monomer, and that the free sulfydryl of Cys395, the lone cysteine in the long cytosolic loop of rat brain NCKX2, was essential for the appearance of the 200kDa oligomers. However, co-immunoprecipitation experiments indicated that Cys395 was not essential for the exchanger homo-oligomerization. The choice of detergents had a large effect on co-immunoprecipitation efficiency, suggesting that NCKX2 homo-oligomerization was mediated by non-covalent association between the exchanger monomers, probably via hydrophobic interactions between the transmembrane domains. The BN-PAGE analysis of both NCKX2-FLAG and NCKX2-FLAG C5A also revealed

several higher order oligomers of NCKX2, including an apparent dimer and a higher order oligomer whose apparent molecular weight was greater than that of the exchanger dimer. Overall, the data suggest the existence in membranes from rat brain of an NCKX2 oligomeric species larger than a dimer, which may represent a homomeric tetramer, or a heteromeric species of uncertain composition.

# CHAPTER FIVE

## Rat Brain NCKX2 Protein-Protein Interaction

The aim of this study was to identify potential interacting partner(s) of rat brain NCKX2 and to understand the physiological and functional significance of the observed interactions. As discussed in Chapter 1, NCX1 is known to interact with several proteins, and these interactions are rapidly emerging as critical regulators of exchanger function (51, 173, 306). In addition, dimerization of bovine retinal rod NCKX1 and its interaction with the cGMP-gated channel are now well established by cross-linking and co-immunoprecipitation experiments in both endogenous and recombinant systems (126, 274). The evidence also suggests that the bovine rod NCKX1 and cGMP-gated channel interaction imparts a regulatory role on the exchanger function, stabilizing NCKX1 dimers and thereby inhibiting transport function (9). In the case of rat brain NCKX2, on the other hand, nothing about its association with other proteins has been reported.

CuPhe-catalyzed reversible oxidation of adjacent free sulfydryls to disulfide bonds using the N-terminal FLAG-tagged rat brain NCKX2 transiently expressed in HEK-293 cells described in the preceding chapter revealed the importance of the free sulfydryl of Cys395 in formation of the covalent 200kDa oligomer of NCKX2-FLAG, a size larger than expected for a dimer (Figures 4-3), as well as in the formation of a significant fraction of an apparent NCKX2 dimer observed by BN-PAGE (Figures 4-9 and 4-10). However, Cys395 was not necessary for the homo-oligomerization of NCKX2-FLAG as determined by co-immunoprecipitation, the interaction being primarily driven by a non-covalent association between exchanger monomers. These observations suggested the possibility of Cys395-mediated hetero-oligomerization of rat brain NCKX2

with an unidentified interacting partner resulting in the 200kDa oligomer of NCKX2-FLAG under non-reducing conditions.

Moreover, when intact rat brain synaptosomal membrane vesicles enriched with endogenous NCKX2 were run on a SDS-PAGE gel under non-reducing conditions followed by immunoblotting with the rabbit polyclonal antibody F against rat brain NCKX2, a unique band of an apparent molecular weight of 130kDa was noted (Figure 5-1). This band was not observed with NCKX2-FLAG in HEK-293 cells using polyclonal F antibody, which revealed the same oligomerization pattern as the M2 anti-FLAG antibody (Figure 4-1). Moreover, the 130kDa band was seen in addition to the same four oligomers of NCKX2-FLAG identified in HEK-293 cells (bands a to d, Figure 5-1), and the intensity of the labelling was stronger than any other higher order oligomers of rat brain NCKX2, except for the 75kDa monomer (Figure 5-1). This strongly indicated that endogenous rat brain NCKX2 might interact with a protein that is absent from the heterologous system and is only found within the neurons of rat brain. CuPhe catalyzed reversible oxidation of intact rat brain synaptosomal membrane vesicles did not change the labelling pattern, but resulted in a slight increase in the labelling intensity of the topmost 200kDa oligomeric band as well as the unique 130kDa band, and a moderate decrease in the labelling intensity of the monomeric 75kDa band. All in all, these experiments set the groundwork to identify the potential interacting partners of rat brain NCKX2.

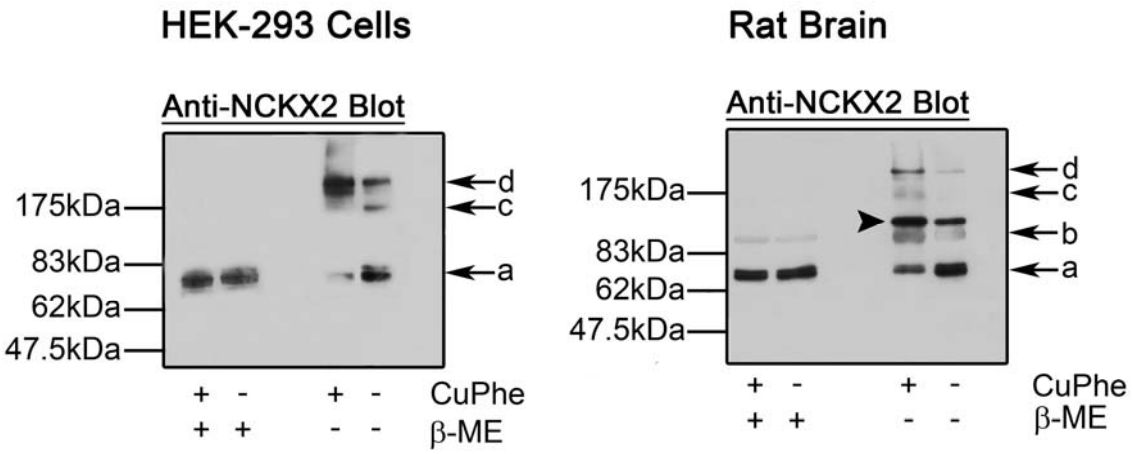


**Figure 5-1. Higher Order Oligomers of Rat Brain NCKX2.** Rat brain synaptosomal membrane vesicles enriched for endogenous NCKX2 were subjected to CuPhe-catalyzed reversible oxidation as described in Chapter 2, and the resulting immunoblot probed with rabbit polyclonal antibody F against rat brain NCKX2 is shown. The immunoblot presented on the left side displays free sulfydryl dependent formation of the higher order oligomers of N-terminal FLAG-tagged NCKX2 (NCKX2-FLAG) expressed in HEK-293 cells, probed with rabbit polyclonal antibody F. The arrows point to the NCKX2 monomer (band a, 75kDa) as well as higher order oligomers observed in non-reducing conditions (b, c, and d). The arrowhead in the immunoblot of rat brain NCKX2 indicates a novel band (~130kDa) unique to endogenous NCKX2 in the rat brain synaptosomal membrane vesicles that is absent from HEK-293 microsomes transiently expressing NCKX2-FLAG. The blots shown are representative of five independent experiments.

Immunoprecipitation of recombinant and endogenous NCKX2 using an appropriate antibody or agarose beads bearing covalently attached antibody followed by SDS-PAGE and visualization by gel staining were employed to co-immunoprecipitate any associated proteins. The identity of the associated proteins was determined by tandem mass spectrometry (MS/MS) combined with nanoscale LC analyses, and the robustness of the interaction was tested by co-immunoprecipitation, SDS-PAGE, and immunoblotting experiments.

## 5.1 Identification of Potential Interacting Partners of Rat Brain NCKX2

### *5.1.1 The Effect of Catalyzed Oxidation by CuPhe on NCKX2-FLAG Immunoprecipitation*

To identify novel potential interacting partners of rat brain NCKX2, HEK-293 cells transiently expressing the N-terminal FLAG-tagged NCKX2 (NCKX2-FLAG) were solubilized with ice-cold 1.0% Triton X-100, and NCKX2-FLAG was immunoprecipitated using anti-FLAG M2-affinity gel (Sigma). Anti-FLAG M2-affinity gel has the heavy chain of the monoclonal M2 anti-FLAG antibody covalently attached to agarose beads, thereby allowing the elution of the immunoprecipitated proteins without contamination by IgG aggregates, thus providing much cleaner resolution of the eluted proteins than conventional immunoprecipitation techniques using protein A or protein G. As seen in Figure 5-2, anti-FLAG M2-affinity gel was highly effective as a tool for the immunoprecipitation of NCKX2-FLAG expressed in HEK-293 cells, noted as a heavily stained 75kDa band on the Coomassie stained SDS-PAGE gels, absent from the vector

**Figure 5-2. Immunoprecipitation of NCKX2-FLAG Using Anti-FLAG M2-Affinity Gel.** HEK-293 cells transiently expressing rat brain NCKX2-FLAG, rat NCX1.1, human SERCA3, or cells transfected with the vector alone (pcDNA 3.1 (+), vector) were solubilized with 1.0% Triton X-100, and either treated with (+) or without (-) CuPhe. The solubilized cells were used to immunoprecipitate NCKX2-FLAG with anti-FLAG M2-affinity gel and the immunoprecipitated proteins were separated by SDS-PAGE (*top*:7.5%, *bottom*:12%), and were visualized by Coomassie Brilliant Blue (CBB) staining. For the bottom right immunoblot, an aliquot of CuPhe-treated, Triton X-100 solubilized HEK-293 cells expressing NCKX2-FLAG were collected and run on an SDS-PAGE followed by immunoblotting using M2 anti-FLAG antibody. The experiments shown are representative of three independent experiments.

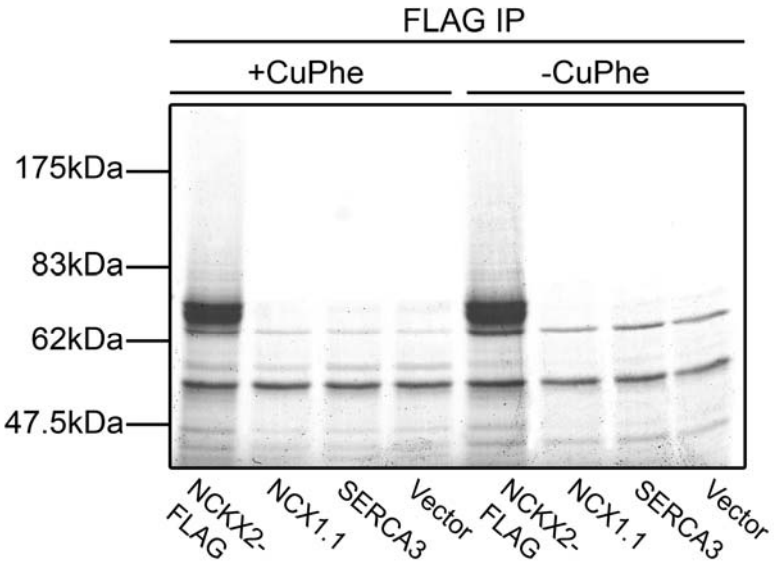
FLAG IP
+CuPhe
-CuPhe
175kDa
83kDa
62kDa
47.5kDa
NCKX2-FLAG
NCX1.1
SERCA3
Vector
NCKX2-FLAG
NCX1.1
SERCA3
Vector

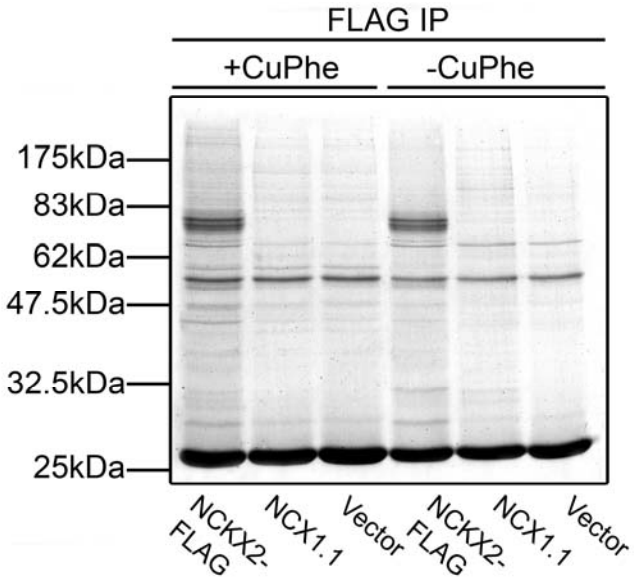
FLAG IP
+CuPhe
-CuPhe
175kDa
83kDa
62kDa
47.5kDa
32.5kDa
25kDa
NCKX2-FLAG
NCX1.1
Vector
NCKX2-FLAG
NCX1.1
Vector

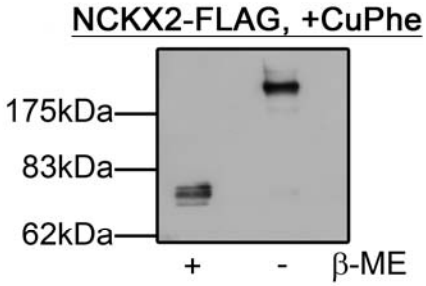
NCKX2-FLAG, +CuPhe
175kDa
83kDa
62kDa
+
-
β-ME

only, rat NCX1.1 or human SERCA3 transfection controls used. These transfection controls were selected to monitor any changes in protein expressions within HEK-293 cells due to transient over-expression of $Ca^{2+}$ handling membrane transporters that might interfere with the data interpretation. In addition, Coomassie stained gels showed no significant differences in the protein elution profiles after immunoprecipitation with anti-FLAG M2-affinity gel for HEK-293 cells transiently expressing rat NCX1.1, human SERCA3, or vector only (Figure 5-2).

Catalyzed oxidation of adjacent free sulfydryls to disulfide bonds using CuPhe just prior to the immunoprecipitation with anti-FLAG M2-affinity gel did not result in any discernable changes in the protein elution profiles of NCKX2-FLAG or of any other proteins compared with those that did not undergo catalyzed oxidation (+CuPhe vs. –CuPhe, Figure 5-2). CuPhe-catalyzed oxidation of NCKX2-FLAG, however, showed a shift of all 75kDa monomers to the 200kDa oligomer (Figure 5-1), which suggested that all NCKX2-FLAG monomers were engaged in the oligomeric association upon CuPhe-catalyzed oxidation. If this oligomeric association were to define a hetero-oligomeric complex of NCKX2-FLAG, then the complete nature of the oligomerization would suggest a molar stoichiometry of one exchanger molecule per one interacting partner, leading to the appearance of a novel interacting partner with an intensity similar to NCKX2-FLAG, when analyzed by Coomassie staining of a reducing SDS-PAGE gel following CuPhe-catalyzed oxidation and immunoprecipitation. The absence of any band with a comparable intensity to NCKX2-FLAG suggested that the 200kDa band as seen on the immunoblot of the non-reducing SDS-PAGE gel may correspond to a homo-

oligomeric species of NCKX2-FLAG with aberrant mobility, rather than to a heteromeric association as previously hypothesized. In addition, when NCKX2-FLAG in HEK-293 cell microsomes was analyzed with or without CuPhe-catalyzed oxidation using non-reducing SDS-PAGE gels followed by silver or Coomassie staining, unique NCKX2-associated bands were observed at 75kDa (-CuPhe) and at 200kDa (+CuPhe) which were both absent in the vector only transfected controls, consistent with the immunoblots (Figure 5-2),. However, when these bands were excised and subjected to LC/MS/MS, only NCKX2 could be confimed as present, suggesting the 200kDa oligomer may be a NCKX2 dimer displaying aberrant mobility on SDS-PAGE.

*5.1.2 Immunoprecipitation of the Recombinant Rat Brain NCKX2*

Careful analyses of the Coomassie stained SDS-PAGE gel revealed that the immunoprecipitation of NCKX2-FLAG resulted in the co-immunoprecipitation of several other proteins, as numerous protein bands appeared upon Coomassie staining (Figure 5-3). Although the staining intensities of these protein bands were not as strong as that of NCKX2-FLAG, nor were their abundances influenced by CuPhe-catalyzed oxidation, they could be distinguished clearly, and their co-immunoprecipitation was reproducible. Moreover, these protein bands were absent from all other control experiments including over-expression of other $Ca^{2+}$ transporters, suggesting that they might represent novel, meaningful, and physiologically relevant interacting partners for NCKX2-FLAG in HEK-293 cells. These protein bands were seen both in the lower molecular weight region and in the higher molecular weight region of the Coomassie stained SDS-PAGE gels.

**Figure 5-3. Immunoprecipitation of NCKX2-FLAG Using Anti-FLAG M2-Affinity Gel – Identification of Potential Interacting Partner(s) of NCKX2-FLAG.** HEK-293 cells transiently expressing rat brain NCKX2-FLAG, rat NCX1.1, human SERCA3, or cells transfected with the vector alone were solubilized in 1.0% Triton X-100 and the solubilized cells were subjected to immunoprecipitation using anti-FLAG M2-affinity gel as described in Chapter 2. Proteins eluted from the anti-FLAG M2-affinity gel by the addition of SDS sample buffer were resolved on an SDS-PAGE gel and visualized by staining the gel with CBB dye. Potential interacting partners of recombinant rat brain NCKX2-FLAG are indicated with the arrows (2 to 10) along with the intense NCKX2-FLAG signal. *Top*: 12% SDS-PAGE gel showing the potential interacting partners in the low molecular weight region. *Bottom*: 7.5% SDS-PAGE gel showing the potential interacting partners in the high molecular weight region. The experiments shown are representative of four independent experiments.

**Coomassie Brilliant Blue Staining**

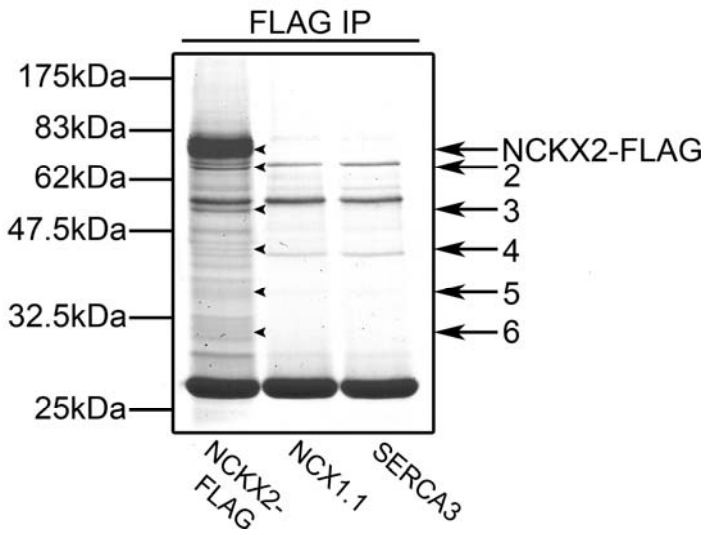


**Coomassie Brilliant Blue Staining**

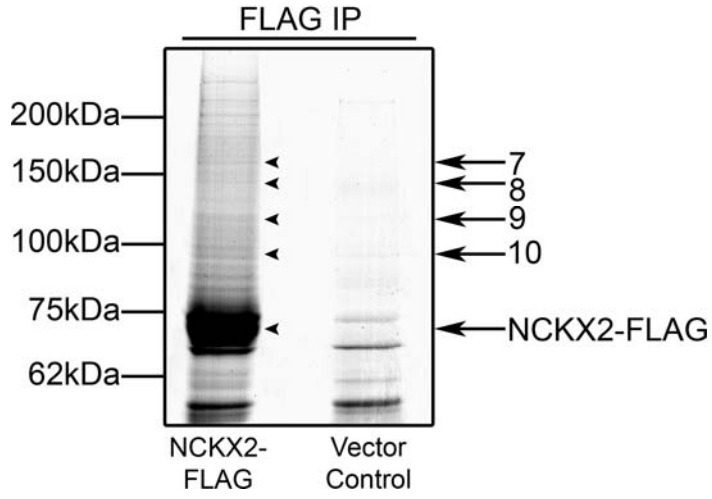

Consequently, several bands were excised from the gel as illustrated in Figure 5-3, and these bands were analyzed by LC/MS/MS as described in detail below.

### *5.1.3 Immunoprecipitation of Endogenous Rat Brain NCKX2*

To identify potential interacting partners of NCKX2 in rat brain, synaptosomal membrane vesicles were solubilized in ice-cold 1.0% Triton X-100 and NCKX2 enriched in the synaptosomal membrane vesicles was immunoprecipitated using the rabbit polyclonal F antibody against rat brain NCKX2. Although the polyclonal F antibody was highly sensitive and could be effectively used at a very high dilution during immunoblotting, the immunoglobulin bands represented a major contaminant during immunoprecipitation. In an effort to reduce the intensity of the immunoglobulin bands in these experiments, attempts were made to use either affinity-purified polyclonal F-antibody, or to covalently cross-link the antibody to agarose beads, both without success. The reasons for these failures are not clear, but may be due to destruction of the epitope recognition site by either procedure. In addition, elution conditions designed to prevent NCKX2 protein aggregation resulted in partial immunoglobulin aggregation which led to the appearance of immunoglobulin bands other than the expected 50kDa and 25kDa bands corresponding to the heavy and light chains, respectively. Therefore, it was necessary to identify those bands corresponding to the immunoglobulins amongst all other protein bands on Coomassie or silver stained SDS-PAGE gels to differentiate them from those protein bands brought down by their association with rat brain NCKX2. This was done by adding protein A Sepharose beads and the antibody to ice-cold RIPA buffer

containing 1.0% Triton X-100 in the absence of rat brain synaptosomal membrane vesicles, or by the use of an equivalent amount of pre-immune serum (Figure 5-4).

Upon careful inspection of the protein profile on the silver stained SDS-PAGE gels shown in Figures 5-4 and 5-5, several unique protein bands were shown to co-immunoprecipitate with rat brain NCKX2. These protein bands were absent from the control immunoprecipitation samples in which polyclonal F antibody against rat brain NCKX2 was replaced with pre-immune serum (Figure 5-5), or in which the rat brain synaptosomal membrane vesicles were omitted from the reaction (Figure 5-4). Just as in the previous experiments examining recombinant rat brain NCKX2 expressed in HEK-293 cells, these unique bands were excised and analyzed by LC/MS/MS. Unfortunately, the overwhelmingly strong immunoglobulin signals in the lower molecular weight region of the SDS-PAGE gel made the identification of any potential interacting partners with a molecular weight smaller than that of rat brain NCKX2 virtually impossible.

### *5.1.4 Mass Spectrometric Identification of Potential Interacting Partners of Rat Brain NCKX2*

Table 5-1 lists the identities, GI numbers, theoretical molecular weights of each of protein hits generated from LC/MS/MS of the protein bands, as well as the apparent molecular weights of corresponding bands on the SDS-PAGE gels, obtained from immunoprecipitation of recombinant rat brain NCKX2 transiently expressed in HEK-293 cells and endogenous rat brain NCKX2 enriched in synaptosomal membrane vesicle. Briefly, the excised Coomassie or silver stained protein bands were digested with trypsin

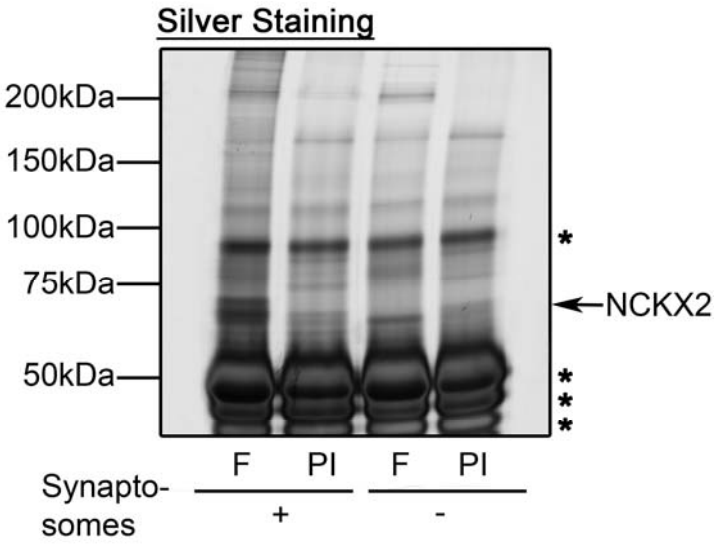


**Figure 5-4. Identification of Immunoglobulin Bands.** Protein A Sepharose beads were added to ice cold RIPA buffer containing 1.0% Triton X-100 and rabbit polyclonal F antibody against rat brain NCKX2 (F) or pre-immune serum (PI) in the presence or absence of rat brain synaptosomal membrane vesicles to identify protein bands resulting specifically from co-immunoprecipitation with rat brain NCKX2. The arrow indicates the silver staining of immunoprecipitated rat brain NCKX2. Asterisks indicate the position of immunoglobulin bands. The experiments shown are representative of four independent experiments.

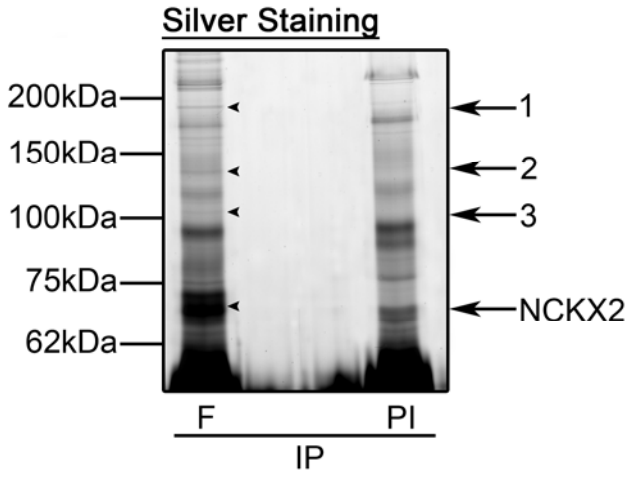


**Figure 5-5. Immunoprecipitation of Rat Brain NCKX2 and the Identification of Potential Interacting Partner(s).** Rat brain synaptosomal membrane vesicles enriched for endogenous NCKX2 were solubilized in 1.0% Triton X-100 and the immunoprecipitation experiment was carried out using polyclonal F antibody against rat brain NCKX2. Rabbit pre-immune serum (PI) was used as the negative control. Immunoprecipitated proteins were run on an SDS-PAGE gel and visualized by silver staining. Along with the strong signal obtained for rat brain NCKX2, bands corresponding to potential interacting protein(s) of rat brain NCKX2 are noted and were indicated with the arrows (1, 2, and 3). The experiments shown are representative of three independent experiments.

**Table 5-1. Identification of Potential Interacting Partners for Rat Brain NCKX2.** The unique protein bands that were observed in Coomassie Brilliant Blue stained or silver stained SDS-PAGE gels after the immunoprecipitation of recombinant NCKX2 (NCKX2-FLAG in HEK-293 cells, *top table*) or rat brain NCKX2 (in rat brain synaptosomal membrane vesicles, *bottom table*) were excised, digested with trypsin, and subjected to tandem mass spectrometry combined with nanoscale liquid chromatography (LC/MS/MS) analysis to find out their identities. The lists of the significant hits these analyses generated using Mascot based on a modified molecular weight search (MOWSE) scoring algorithm system from Matrix Science, their accession string, the theoretical molecular weight, and the observed molecular weight on the SDS-PAGE gels are shown. The numbers in the left column correspond to the numbers in Figure 5-3 (*top table*) and in Figure 5-5 (*bottom table*).

HEK-293 Cells

| Number | Protein Matches | GI Number | MW (kDa) | Observed MW (kDa) |
|---|---|---|---|---|
| 2 | Heat shock protein HSP70 | 188492 | 70 | 70 |
| 3 | β-tubulin | 1297274 | 51 | 50 |
| 4 | γ-actin | 178045 | 42 | 45 |
| 5 | Prohibitin-2 | 6005854 | 33 | 35 |
| 6 | Prohibitin-1 | 46360168 | 30 | 30 |
| 7 | SERCA2 | 4502285 | 111 | 160 |
| 8 | SERCA2 | 4502285 | 111 | 140 |
| 9 | $Na^+/K^+$ ATPase α | 179212 | 100 | 120 |
| 10 | Heat shock protein HSP90 | 306891 | 90 | 90 |

Rat Brain Synaptosomal Membrane Vesicles

| Number | Protein Matches | GI Number | MW (kDa) | Observed MW (kDa) |
|---|---|---|---|---|
| 1 | $Na^+/K^+$ ATPase α-3 subunit | 6978457 | 110 | 180 |
| 2 | Plasma membrane $Ca^{2+}$-transporting ATPase 1 (PMCA-1) | 14286099 | 140 | 125 |
| 3 | $Na^+/K^+$ ATPase α-1 chain precursor | 114373 | 114 | 110 |

into peptide fragments, and these fragments were analyzed by LC/MS/MS to obtain the sequences of each peptide fragment. Both trypsin digestion and LC/MS/MS were performed in the SAMS Centre. The acquired MS/MS spectra and peptide sequences were matched to a protein sequence database (NCBInr) leading to a successful identification of the potential interacting partners of NCKX2 in HEK-293 cells and in neurons of the rat brain. Mascot based on a modified molecular weight search (MOWSE) scoring algorithm system from Matrix Science (www.matrixscience.com) (228) was used for MS/MS ion search engine in the SAMS Centre.

In HEK-293 cells (Table 5-1), scaffolding proteins (prohibitins), cytoskeletal proteins (β-tubulin and γ-actin), transporters (SERCA2 and $Na^+/K^+$ ATPase α subunit), as well as chaperone proteins (HSP70 and 90) were identified as potential interacting partners of NCKX2-FLAG. In the case of rat brain synaptosomal membrane vesicles, all the protein bands identified plasma membrane $Ca^{2+}$ transporters and ion pumps, strongly implying that the association between NCKX2 and other $Ca^{2+}$ transporters might be of physiological significance. HSP70 and HSP90, stress proteins whose expression can be altered with environmental changes such as over-expression of a foreign protein like NCKX2-FLAG, were excluded from further analyses since their interaction with NCKX2-FLAG was considered to be most likely a consequence of over-expression. The association of rat brain NCKX2 with the other potential interacting partners was investigated further by co-immunoprecipitation as described in the following sections.

## 5.2 Recombinant Rat Brain NCKX2 and Prohibitins

### *5.2.1 Co-immunoprecipitation of NCKX2-FLAG and Prohibitins in HEK-293 Cells*

Prohibitins are highly conserved proteins found in eukaryotic cells that were initially identified as putative negative regulators of cell proliferation (193, 214), and inhibitors of the initiation of DNA synthesis (190), hence their name. Since then, prohibitins have been found to carry out a diverse range of physiological functions, including cell cycle regulation, suppression of oncogenesis, as well as inhibition of metabolism (193). The key function of prohibitins, however, is to act as membrane-bound chaperones, especially for mitochondrial proteins, preventing misfolding of newly synthesized proteins (193). Prohibitins are therefore known to reside mostly in mitochondria, but they have also been found in the nucleus and in the plasma membrane. Prohibitins may shuttle associated proteins and peptides between the plasma membrane and the membranes of mitochondria (148), and may have a role in transmembrane signal transduction. However, the precise function of prohibitins in the plasma membrane, where NCKX2 is localized, remains elusive. To investigate their interaction with recombinant rat brain NCKX2 transiently expressed in HEK-293 cells, co-immunoprecipitation experiments were performed using anti-FLAG M2-affinity gel.

As seen in Figure 5-6, immunoprecipitation of NCKX2-FLAG with anti-FLAG M2-affinity gel brought down endogenous prohibitins, which were not seen with either rat NCX1.1 or vector only controls. CuPhe-catalyzed oxidation was performed prior to immunoprecipitation to determine if such treatment would affect the co-

**Figure 5-6. Co-immunoprecipitation of NCKX2-FLAG and Prohibitins in HEK-293 Cells.** HEK-293 cells transiently expressing rat brain NCKX2-FLAG (F), rat NCX1.1 (N), or cells transfected with the vector alone (V) were solubilized with 1.0% Triton X-100, and treated with (+) or without (-)CuPhe. The solubilized cells were subjected to immunoprecipitation using anti-FLAG M2-affinity gel. Immunoprecipitated proteins were run on an SDS-PAGE gel followed by immunoblotting with M2 anti-FLAG antibody (*top*). The immunoblot was then stripped of the antibodies and reprobed with rabbit polyclonal anti-prohibitin antibody (BDH) (*bottom*). The ~75kDa bands observed in the anti-prohibitin blot are NCKX2-FLAG signals caused by the M2 anti-FLAG antibody not completely stripped off the immunoblot. Asterisks indicate the position of immunoglobulin bands. The blots shown are representative of two independent experiments

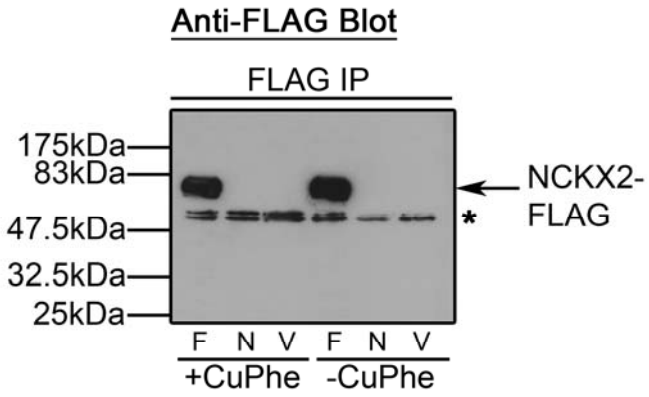
Anti-FLAG Blot
FLAG IP
175kDa
83kDa
47.5kDa
32.5kDa
25kDa
NCKX2-
FLAG
*
F N V F N V
+CuPhe -CuPhe

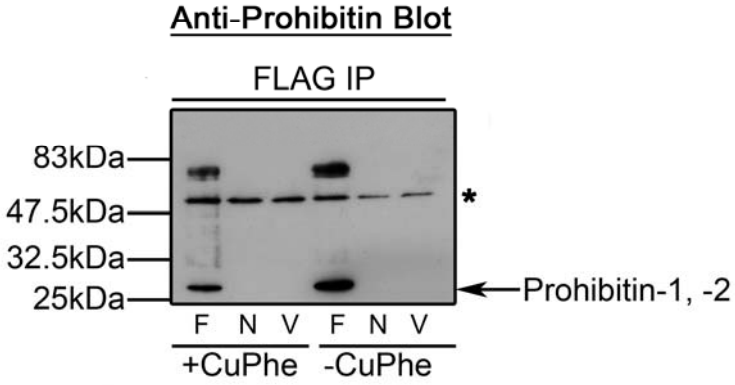
Anti-Prohibitin Blot
FLAG IP
83kDa
47.5kDa
32.5kDa
25kDa
*
Prohibitin-1, -2
F N V F N V
+CuPhe -CuPhe

immunoprecipitation of endogenous prohibitins and NCKX2-FLAG. Catalyzed oxidation by CuPhe did not enhance the co-immunoprecipitation of endogenous prohibitins and NCKX2-FLAG (Figure 5-6). Although the reverse experiment to test whether the prohibitin immunoprecipitation would result in co-immunoprecipitation of NCKX2-FLAG was not performed, these data nonetheless confirm the LC/MS/MS result and indicate that recombinant rat brain NCKX2-FLAG when expressed in HEK-293 cells associates with endogenous prohibitins.

### *5.2.2 Co-immunoprecipitation of Rat Brain NCKX2 and Prohibitins in Rat Brain Synaptosomal Membrane Vesicles*

Co-association of endogenously expressed rat brain NCKX2 and prohibitins in rat brain synaptosomal membrane vesicles was examined by co-immunoprecipitation analysis using the rabbit polyclonal F antibody against rat brain NCKX2 (Figure 5-7). Although prohibitins were present in the rat brain synaptosomal membrane vesicles, they failed to associate with rat brain NCKX2. This result was contrary to what was observed in the transfected HEK-293 cells. This suggested that either the interaction between prohibitins and NCKX2 in rat brain is less stable than it is in HEK-293 cells, or the interaction could be a phenomenon only found in the heterologous system expressing recombinant rat brain NCKX2. Alternatively, the association between endogenous prohibitins and NCKX2-FLAG observed in HEK-293 cells may represent a membrane compartment not present in the purified rat brain synaptosomal membrane vesicles.

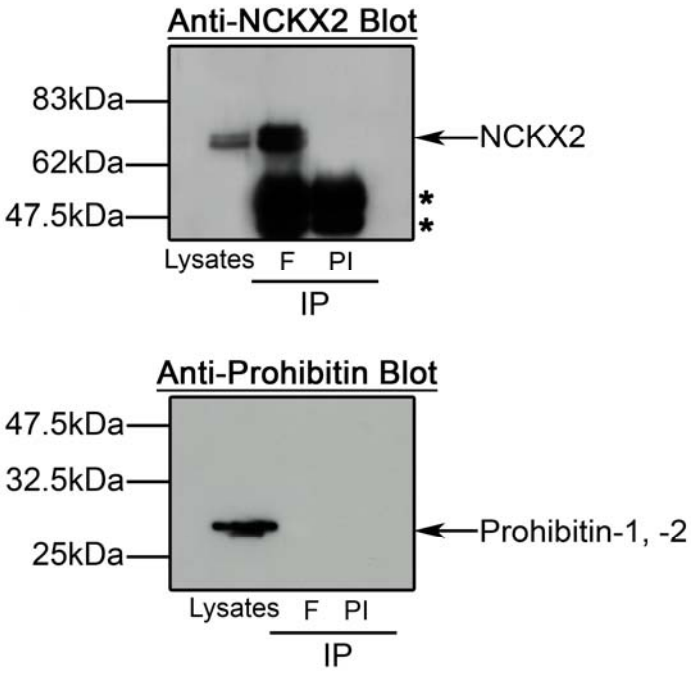


**Figure 5-7. Co-immunoprecipitation of Rat Brain NCKX2 and Prohibitins in Rat Brain Synaptosomal Membrane Vesicles.** Rat brain synaptosomal membrane vesicles enriched for endogenous NCKX2 were solubilized in ice-cold 1.0% Triton X-100 and rat brain NCKX2 was immunoprecipitated using rabbit polyclonal antibody F against NCKX2 (F). Rabbit pre-immune serum (PI) was used as a negative control. Bound proteins were eluted using SDS sample buffer, resolved on an SDS-PAGE gel followed by immunoblotting using polyclonal F antibody (*top*) and rabbit polyclonal anti-prohibitin antibody (*bottom*). Lysates represent samples of the Triton X-100 solubilized membrane vesicles just prior to immunoprecipitation. Asterisks indicate the position of immunoglobulin bands. The blots shown are representative of two independent experiments.

## 5.3 Rat Brain NCKX2 and Other Membrane Proteins

### *5.3.1 Sarco/Endoplasmic Reticulum $Ca^2$-ATPase Pumps (SERCA2)*

SERCA2, an isoform of sarco/endoplasmic reticulum $Ca^{2+}$-ATPase with the widest tissue distribution, was identified as one of the potential interacting partners of recombinant rat brain NCKX2 in HEK-293 cells (Table 5-1). Although SERCA2 is a SR/ER membrane protein, co-localization and functional coupling between $Na^+/Ca^{2+}$-exchangers and SERCA has been observed in smooth muscle cells, which suggested the possibility of a yet unidentified "molecular linkage" that physically connects exchangers with SERCA (196, 201). Moreover, the existence of plasma membrane-cytoskeleton-ER complexes in neurons and astrocytes results in the co-immunoprecipitation of rat brain NCX1 and SERCA2. Hence, a physical association between rat brain NCKX2 and SERCA2 seemed plausible.

The potential molecular association between SERCA2 and NCKX2 in rat brain synaptosomal membrane vesicles was examined by co-immunoprecipitation experiments. Both proteins were present in Triton X-100 solubilized rat brain synaptosomal membrane vesicles and were detected with the appropriate antibodies (Lysates, Figure 5-8), suggesting a possible plasma membrane/ER association. However, immunoprecipitation of rat brain NCKX2 by polyclonal F antibody did not result in the co-association of SERCA2. This result was inconsistent with the data obtained from LC/MS/MS using HEK-293 cells transiently expressing NCKX2-FLAG, implying that the interaction

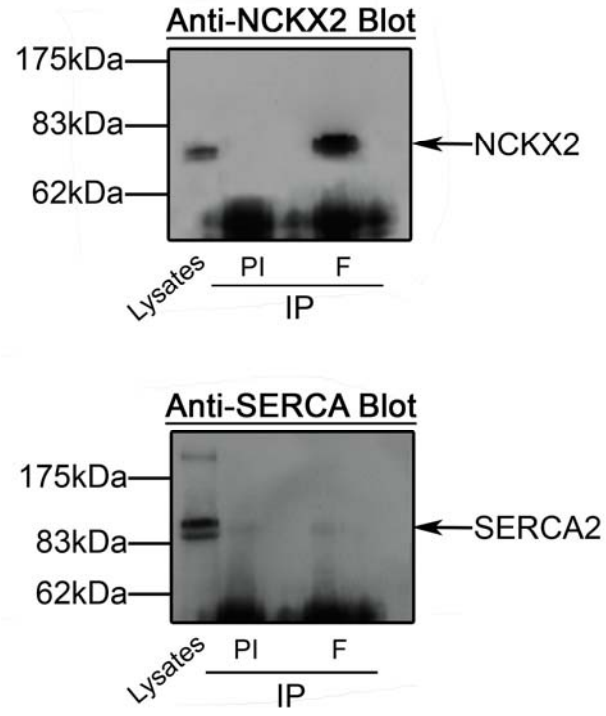


**Figure 5-8. Co-immunoprecipitation of Rat Brain NCKX2 and SERCA2 in Rat Brain Synaptosomal Membrane Vesicles.** Rat brain synaptosomal membrane vesicles enriched for NCKX2 were solubilized with ice-cold 1.0% Triton X-100 and immunoprecipitation of NCKX2 was carried out using rabbit polyclonal antibody F against rat brain NCKX2 (F). Rabbit pre-immune serum (PI) was used as a negative control. Bound proteins were eluted using SDS sample buffer, resolved on an SDS-PAGE gel followed by immunoblotting using polyclonal F antibody (*top*) or rabbit polyclonal antibody N1 against rat SERCA2 (*bottom*). Lysates represent samples of Triton X-100 solubilized membrane vesicles collected just prior to immunoprecipitation. The blots shown are representative of two independent experiments.

between NCKX2 and SERCA2 may be related to the transfected HEK-293 cell systems just as with NCKX2/prohibitin interactions.

### *5.3.2 Plasma Membrane $Ca^{2+}$-ATPase Pumps (PMCA)*

Molecular interaction between rat brain NCKX2 and the plasma membrane $Ca^{2+}$-ATPase pump (PMCA) observed by LC/MS/MS in rat brain samples was further investigated using co-immunoprecipitation as described above, and the results are displayed in Figure 5-9. The monoclonal anti-PMCA antibody that recognizes all four isoforms of PMCA (5F10, Affinity BioReagents) efficiently immunoprecipitated rat brain PMCA from the solubilized synaptosomal membrane vesicles, noted as an intense labelling of the 140kDa band (PMCA IP, anti-PMCA blot, Figure 5-9). However, immunoprecipitation of PMCA did not bring down rat brain NCKX2, nor did immunoprecipitation of NCKX2 result in co-association of PMCA. This result strongly suggests these two molecules do not associate to any appreciable extent.

### *5.3.3 The α subunit of $Na^+/K^+$ ATPase pumps*

The LC/MS/MS analyses revealed the α subunits of $Na^+/K^+$ ATPase as potential interacting partners of NCKX2 in both HEK-293 cells and rat brain (Table 5-1). Therefore, the association between the α subunits of $Na^+/K^+$ ATPase and rat brain NCKX2 were investigated by co-immunoprecipitation using rat brain synaptosomal membrane vesicles (Figure 5-10). All three proteins (α-1, α-3, and NCKX2) were detected in the Triton X-100 solubilized lysates of the synaptosomal membrane vesicles. In addition, both rat brain NCKX2 and the α-3 subunit of the $Na^+/K^+$ ATPase were

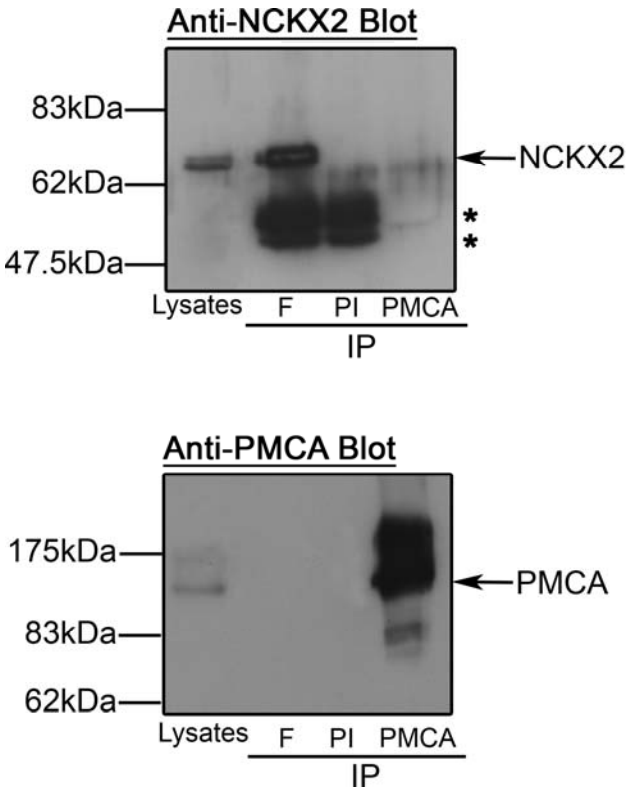


**Figure 5-9. Co-immunoprecipitation of Rat Brain NCKX2 and Plasma Membrane $Ca^{2+}$-Transporting ATPase (PMCA).** Rat brain synaptosomal membrane vesicles enriched for endogenous NCKX2 were solubilized with 1.0% Triton X-100 and immunoprecipitation was carried out using rabbit polyclonal F antibody against rat brain NCKX2 or monoclonal anti-PMCA antibody (BDH). Immunoprecipitated proteins were run on an SDS-PAGE gel followed by immunoblotting with the polyclonal F antibody (*top*) or the monoclonal anti-PMCA antibody (*bottom*). Asterisks indicate the position of immunoglobulin bands. The blots shown are representative of two independent experiments.

**Figure 5-10. Co-immunoprecipitation of Rat Brain NCKX2 and the α Subunits of $Na^+/K^+$ ATPases.** Rat brain synaptosomal membrane vesicles enriched for NCKX2 were solubilized with 1.0% Triton X-100 and immunoprecipitation was carried out using rabbit polyclonal F antibody against rat brain NCKX2 (F), monoclonal anti-$Na^+/K^+$ ATPase α-1 antibody (NKA $\alpha_1$), or monoclonal anti-$Na^+/K^+$ ATPase α-3 antibody (NKA $\alpha_3$) (BDH). Immunoprecipitated proteins were run on an SDS-PAGE gel followed by immunoblotting with polyclonal F antibody (*top*), monoclonal anti-$Na^+/K^+$ ATPase α-1 antibody (*middle*), and monoclonal anti-$Na^+/K^+$ ATPase α-3 antibody (*bottom*). Asterisks indicate the position of immunoglobulin bands. The blots shown are representative of two independent experiments

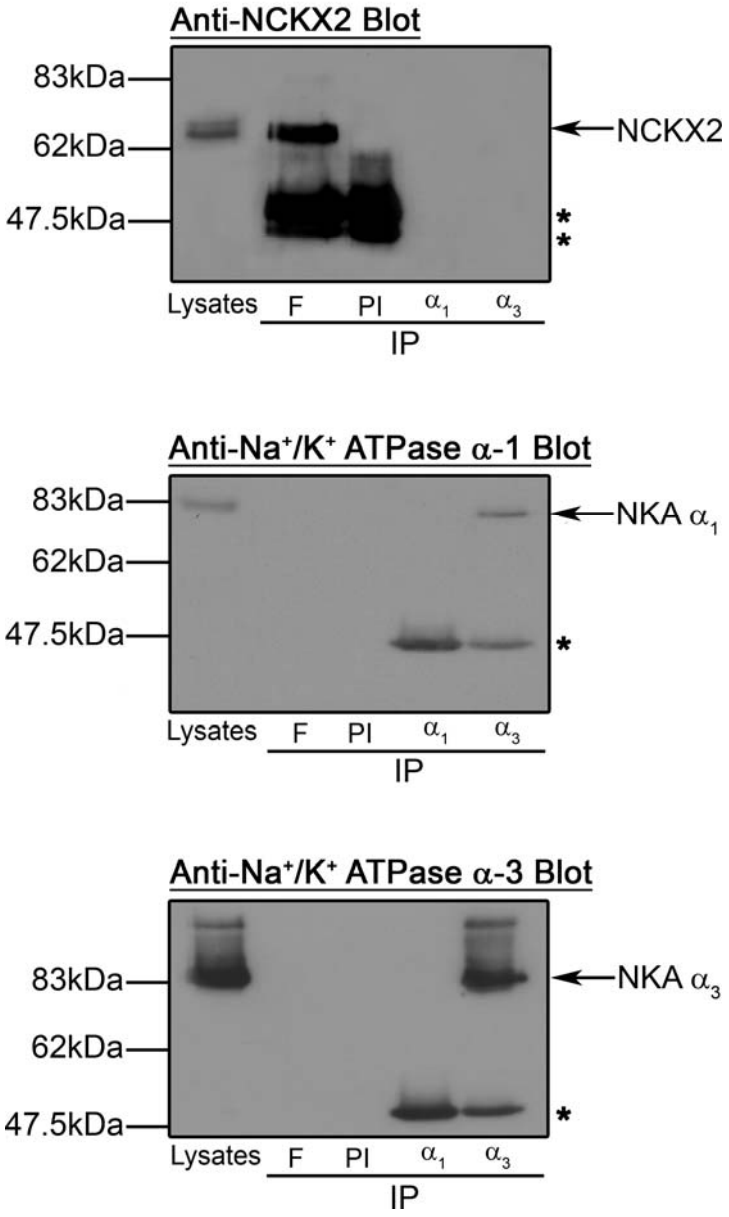
Anti-NCKX2 Blot
83kDa
62kDa
47.5kDa
NCKX2
*
*
Lysates
F
PI
α1
α3
IP
Anti-Na+/K+ ATPase α-1 Blot
83kDa
62kDa
47.5kDa
NKA α1
*
Lysates
F
PI
α1
α3
IP
Anti-Na+/K+ ATPase α-3 Blot
83kDa
62kDa
47.5kDa
NKA α3
*
Lysates
F
PI
α1
α3
IP

successfully immunoprecipitated by their respective specific antibodies. However, these two proteins did not co-immunoprecipitate as seen in Figure 5-10. Unfortunately, the monoclonal anti-$Na^+/K^+$ ATPase α-1 antibody failed to immunoprecipitate the α-1 subunit of $Na^+/K^+$ ATPase, and also appeared to react with the α-3 subunit of $Na^+/K^+$ ATPase, complicating the interpretation of the data on NCKX2-$Na^+/K^+$ ATPase α association.

**5.4 Summary**

In this chapter, potential interacting partners of rat brain NCKX2 were identified. The immunoprecipitation of recombinant rat brain NCKX2-FLAG transiently expressed in HEK-293 cells by anti-FLAG M2-affinity gel as well as the immunoprecipitation of the endogenously expressed rat brain NCKX2 from the rat brain synaptosomal membrane vesicles followed by SDS-PAGE, gel staining, and LC/MS/MS analyses both revealed a number of potential interacting partners. When these putative interactions were investigated further by co-immunoprecipitation followed by immunoblotting, only the association between prohibitins expressed in HEK-293 cells and NCKX2-FLAG was confirmed. The interactions between the $Ca^{2+}$ transporters and rat brain NCKX2 were not observed by immunoblotting after co-immunoprecipitation, undermining the data obtained from the mass spectrometric analyses. The reasons why such opposing results were obtained are not clear, but the different detection sensitivities of LC/MS/MS and immunoblotting, as well as different effects that chemicals and reagents such as detergents and staining materials used throughout the experiments might have on the

results obtained might account for some of the problems. Therefore, further studies are required to clarify this issue.

# CHAPTER SIX

## Discussion

Experiments described in this thesis have presented several interesting new findings regarding the sub-cellular and quaternary structure of rat brain NCKX2. The isolation of detergent-resistant membranes containing lipid rafts/caveolae microdomains from whole rat brain by density floatation and co-immunoprecipitation analyses revealed selective localization of rat brain NCKX2 into the lipid raft microdomains distinct from caveolae. In addition, catalyzed oxidation of adjacent free sulfydryls to disulfide bonds by CuPhe, NCKX2 co-immunoprecipitation, and BN-PAGE experiments demonstrated oligomerization of rat brain NCKX2 driven by non-covalent interaction between the exchanger monomers. The formation of a homo-oligomeric species of rat brain NCKX2 with an apparent molecular weight corresponding to a dimer as well as corresponding to a size greater than that of the exchanger dimer were also noted, although the precise oligomeric state and the nature of these species remains unclear. Several potential interacting partners of rat brain NCKX2 were identified by mass spectrometric analyses. However, these apparent interactions could not be confirmed in co-immunoprecipitation experiments, thereby making it difficult to draw convincing conclusions about the physiological relevance of the interactions observed by mass spectrometry. In this chapter, the significance of these results and the potential implications of these various findings on the structure and function of rat brain NCKX2 will be discussed in detail, along with future studies that would greatly aid in clarifying some of the issues brought up during the course of completing this thesis.

## 6.1 Sub-cellular Localization of Rat Brain NCKX2

A growing body of evidence has suggested that specific subsets of lipids can serve to organize the plasma membrane into discrete microdomains with specialized functions. This is a significant departure from the classical view of the lipid bilayer as a two-dimensional "fluid mosaic" first proposed by Singer and Nicolson in 1972 (280). The so-called "liquid-ordered" membrane microdomains, more commonly known as "lipid rafts," are enriched with cholesterol and sphingolipids, making them more ordered and buoyant than the rest of the plasma membrane. These microdomains are resistant to solubilization with cold non-ionic detergents, and from this observation the name "detergent-resistant membranes" was derived to collectively describe the plasma membrane microdomains isolated by non-ionic detergent solubilization followed by density floatation centrifugation (82, 199). The detergent-resistant membranes are thought to be composed of mixtures of different lipid rafts and caveolae. Caveolae are the subset of lipid rafts that appear as invaginations in the plasma membrane due to the oligomerization of one of their resident proteins, caveolin.

Many signalling proteins, including the proteins involved in intracellular $Ca^{2+}$ signalling and homeostasis, are selectively compartmentalized in lipid rafts/caveolae microdomains and this type of sub-cellular localization of the proteins is functionally important. In Chapter 3, rat brain NCKX2 was shown to be localized in lipid raft microdomains that are distinct from caveolae. This was the first study that addressed the preferential localization of this $Na^{+}/Ca^{2+}$-exchanger isoform to lipid rafts. It is likely that

the axonal terminals and the postsynaptic dendrites of neurons where rat brain NCKX2 is primarily localized might be devoid of caveolae and caveolins. Instead, lipid rafts may provide a platform for the organization of synaptic proteins such as PSD-95, NMDA receptors, and AMPA receptors. This could explain the selective localization of rat brain NCKX2 into the lipid raft microdomain and the subsequent failure of the exchanger to associate with caveolins (Figures 3-5 and 3-6).

### *6.1.1 Presence of Caveolae and Caveolins in Rat Brain*

In Chapter 3, isolation of the detergent-resistant membranes containing the lipid rafts/caveolae microdomains by density floatation from a whole rat brain convincingly demonstrated that caveolins were abundantly expressed in rat brain (Figure 3-2). The presence of caveolins and caveolae in brain has been vigorously debated by many researchers (20, 83, 117). However, it is now generally understood that although a small amount of caveolins are present in neuronal cells, they are primarily expressed in non-neuronal cells of the brain where they are the major constituents of caveolae, whereas non-caveolar lipid rafts are predominantly found in neurons (286). In addition, expression of caveolins is subject to temporal and spatial regulation, being up or down regulated during brain development and upon exposure to stress and mechanical injury (83, 186). The data presented in Chapter 3 support the robust expression of both caveolin-1 and caveolin-2 in rat brain, although the precise cellular location in which caveolins are expressed was not investigated.

The density floatation method used in the experiments described in Chapter 3 does not distinguish lipid rafts from caveolae within the detergent-resistant membranes. Use of whole rat brain would inevitably result in the isolation of various mixtures of the lipid rafts and caveolae from cells of both neuronal and non-neuronal origin. Based on previous studies, it is likely that the majority of caveolins are from the caveolar microdomains found in non-neuronal cells of brain such as astrocytes, glial cells, and endothelial cells (286). Labelling of caveolins by rabbit polyclonal anti-caveolin antibody was seen only weakly in rat brain synaptosomal membrane vesicles (Figure 3-3), whereas a relatively strong labelling of caveolins was observed in rat brain crude homogenates (Figure 3-4), supporting the non-neuronal origin of caveolins in rat brain. It is still plausible that caveolins and caveolae are present in neurons in places other than synaptic membranes, such as in axons or in the membranes of the neuronal cell body, and these neuronal caveolins are excluded from the synaptosomal membrane vesicle preparations. Therefore, further studies are required to identify the precise cellular and sub-cellular localization of caveolins in rat brain, especially within neurons.

### *6.1.2 The Lipid Raft Localization of Rat Brain NCKX2*

Figure 3-2 demonstrated that a significant amount of rat brain NCKX2 was found in the detergent-resistant membranes containing the lipid rafts/caveolae microdomains. The fact that the labelling of the transferrin receptors, well-known non-raft/non-caveolae associated membrane proteins, was observed exclusively at the higher density sucrose region where detergent solubilized membrane proteins were selectively partitioned confirms that the density floatation method and use of cold non-ionic detergent Triton X-

100 was effective in isolating the lipid rafts and/or caveolae microdomains with minimal contamination by other membrane fractions. These contaminants could include the membranes of the ER or incompletely solubilized plasma membranes that would be otherwise found in the high density sucrose region.

Whilst the existence of caveolins and caveolae in brain has been hotly debated, the presence of non-caveolar lipid raft microdomains in neurons has traditionally been associated with the axons and myelin membranes of neurons in which they were thought to be important as an axonal sorting mechanism (69, 157, 158). Mounting evidence also suggests the presence of lipid raft microdomains at the axonal terminals and the postsynaptic dendrites of neurons in which they were implicated in a variety of synaptic functions such as maintenance of synaptic morphology, trafficking, regulated exocytosis, and membrane fusion (66, 70, 88, 103, 286). Several well-known postsynaptic proteins including PSD-95, NMDA receptors, as well as AMPA receptors are thought to be localized within the lipid raft microdomains found in the postsynaptic dendritic plasma membranes, and it appears that their proper function is dependent on the association with the lipid rafts (19, 88, 103). Therefore, the majority of rat brain NCKX2 that is found in the detergent-resistant membranes is highly likely to be localized in the lipid raft microdomains found within the axonal terminals and the postsynaptic dendrites of neurons. Considering the low levels of caveolins in rat brain synaptosomal membrane vesicles and the failure of NCKX2 to co-associate with caveolins in all the membrane preparations tested (Figures 3-3, 3-4, and 3-5), rat brain NCKX2 is most likely localized to the non-caveolar lipid rafts of the synaptic membranes.

However, the strongest evidence that rat brain NCKX2 is found in the lipid raft microdomains and not in caveolae came from co-immunoprecipitation experiments using the isolated detergent-resistant membranes in ice-cold Triton X-100 (Figure 3-6). Unlike *n*-dodecyl *β*-D-maltoside, which is known to effectively disrupt and solubilize the detergent-resistant membranes, the use of ice cold Triton X-100 maintains the detergent-resistant membranes intact throughout the co-immunoprecipitation analyses, thereby allowing proteins localized in the same microdomain to be co-immunoprecipitated, regardless of the presence of any molecular interaction between these proteins. Although an appropriate positive control that demonstrates successful co-immunoprecipitation of caveolins and their known interacting partners, or proteins that are known to co-localize with caveolins would have been instrumental in making a definitive conclusion, the fact that rat brain NCKX2 did not co-immunoprecipitate caveolins in the detergent-resistant membranes using ice-cold Triton X-100 nonetheless suggested that NCKX2 preferentially localized into lipid rafts that are distinct from caveolae where caveolins are exclusively localized. The mechanisms responsible for preferentially targeting rat brain NCKX2 to non-caveolar lipid raft microdomains are not currently understood. It is possible that rat brain NCKX2 might interact with other non-caveolar lipid raft proteins and that this interaction might lead to the non-caveolar lipid raft localization.

In addition to the localization within the detergent-resistant membranes, a moderate amount of rat brain NCKX2 was found in the high density sucrose region (Figure 3-2), which suggested that the inclusion of rat brain NCKX2 in the lipid raft microdomains was not an all-or-none phenomenon as was the case with caveolins.

However, what causes rat brain NCKX2 to exhibit such a differential distribution pattern, and whether the different localization of rat brain NCKX2 directly translates into differences in exchanger function remains unknown.

*6.1.3 Effect of Non-ionic Detergents in the Isolation of Detergent-Resistant Membranes*

The majority of the studies on lipid rafts/caveolae microdomains in brain have used methods that exploit the insolubility of these fractions in cold non-ionic detergents (66). However, it has been argued that detergent resistance is an artificial and subjective phenomenon that does not provide any physiological insight (277). In addition, the assumption that cold non-ionic detergents can isolate the lipid rafts/caveolae microdomains in their native form has been criticized. There is evidence that indicates the composition of the lipid rafts/caveolae microdomains may vary depending on whether detergents are used to isolate these microdomains and which detergents are used for the procedure (29, 86, 100, 101, 113). Therefore, detergent-resistant membranes should not be assumed to represent biologically relevant lipid rafts and caveolae in their size, structure, or protein and lipid composition. Despite this caveat, most researchers still believe that the detergent-resistant membranes are the most accurate biochemical fraction that corresponds to lipid rafts/caveolae membrane domains (113).

Isolation of the detergent-resistant membranes from transfected HEK-293 cells clearly addressed these issues in several interesting ways (Figures 3-7, 3-8, and 3-9). NCKX2-FLAG transiently expressed in HEK-293 cells was completely absent from the detergent-resistant membranes regardless of the presence of caveolins, and even though

the presence of lipid rafts could be detected using the marker protein flotillin. This observation is consistent with the lack of an observed molecular interaction with caveolin, but inconsistent with the observation of raft-association of NCKX2 in brain membrane fractions. These differences could reflect inherent differences in the biophysical properties and the lipid composition of the plasma membranes between neurons in rat brain and HEK-293 cells. They could also imply the absence of some protein or lipid factor from HEK-293 cells that is necessary for NCKX2 localization to rafts in brain. Moreover, the fact that the use of CHAPS restored the presence of recombinant NCKX2 in detergent-resistant membranes (Figure 3-9) clearly demonstrates the dependence of the composition of the detergent-resistant membranes upon the choice of non-ionic detergents. In addition, the fact that the pattern of sub-cellular localization of recombinant caveolins was markedly different from what was seen in the rat brain regardless of the type of detergents used reflects the inherent problem associated with using a heterologous system (Figures 3-8 and 3-9). Transient transfection of recombinant caveolins resulted in over-expression of the protein otherwise absent from HEK-293 cells, which led to the observation of caveolins in the high sucrose regions where they are not normally found. Taken together, the results obtained in Chapter 3 revealed the structural complexity of plasma membranes of different cells/tissues, and the difficulty in using detergent-resistant membranes as the fraction representing functional rafts in biological systems.

*6.1.4 The Lipid Rafts, Caveolae, and $Na^+/Ca^{2+}$ Exchange*

In mammalian heart, an increasing amount of evidence points to a role of caveolae in organizing proteins important for intracellular $Ca^{2+}$ signalling and homeostasis. The importance of caveolin-3 in normal cardiac function is well understood, along with the localization of several $Ca^{2+}$ handling proteins such as PMCA, $IP_3R$, annexins, and NCX1 in caveolae (7, 99, 275, 310). In the case of NCX1, however, conflicting evidence regarding its caveolar localization and interaction with caveolins has been gathered. The initial studies conducted by Bossuyt *et al.* (25) found NCX1 in bovine sarcolemmal vesicles within caveolae. NCX1 was able to co-immunoprecipitate caveolin-3, but not caveolin-1 or caveolin-2. Soon after, NCX1 was found to form a $Ca^{2+}$-dependent trimolecular complex with annexin A5 and caveolin-3 in microsomal preparations obtained from human left ventricular myocardium (34). In addition, co-association of NCX1 with both caveolin-1 and caveolin-2 was noted in rat C6 glioma cells which do not express the muscle specific isoform caveolin-3 (38). Altogether these data suggest an interaction between NCX1 and caveolins and consequently a caveolar localization for NCX1 in both muscle and glioma cells.

In a recent study, however, Cavalli *et al.* argued that NCX1 in cardiac myocytes does not localize to caveolae and does not interact with caveolin-3 (36). Using both detergent and detergent-free methods to isolate lipid rafts/cavaolae microdomains, they concluded that the domain localization was dependent upon the solubilization methods and that the detergent-free carbonate based technique was inappropriate for the isolation of lipid rafts/caveolae microdomains, at least from rat heart. Interestingly, while these

findings contradict the previous results described above, this controversy is highly reminiscent of studies conducted on the lipid rafts/caveolae microdomain localization of $Na^+/K^+$ ATPases, in which use of different techniques as well as different tissues led to different conclusions regarding the sub-cellular localization of the catalytic subunits of $Na^+/K^+$ ATPases (66, 174, 176).

In this regard, the finding in Chapter 3 that rat brain NCKX2 is localized in the lipid raft microdomains distinct from caveolae is novel and unique since it is the first study conducted that revealed the selective localization of a $Na^+/Ca^{2+}$-exchanger to non-caveolar lipid rafts. This finding also implies that rat brain NCKX2 might be co-localized with other postsynaptic $Ca^{2+}$ handling proteins in the same set of lipid raft microdomains of the postsynaptic dendritic plasma membranes. It is likely that NCKX2 in the postsynaptic lipid raft microdomains might contribute to the formation of $Ca^{2+}$ microdomains along with NMDA receptors and AMPA receptors in which a local increase in $[Ca^{2+}]_i$ would be readily sensed by the exchanger, thereby influencing the local $Ca^{2+}$ dynamics and the efficiency of various $Ca^{2+}$ signalling events within the dendritic spines, such as LTP and neuronal synaptic remodelling. Co-localization studies using co-immunoprecipitation or immunofluorescence would be useful in understanding the role of lipid raft microdomains in the organization of postsynaptic $Ca^{2+}$ handling proteins.

## 6.2 Oligomeric State of Rat Brain NCKX2

Membrane channels and transporters, once correctly folded, may exist as monomers, dimers, and even higher order oligomers, and the formation of such quaternary structures could be important for proper function. For some proteins such as $K^+$ channels (64), tetramerization is an absolute prerequisite for functional channel formation, with each monomer equally contributing to the lining of the ion translocation pathway. For other proteins like $Na^+/K^+$ ATPases, the stable and correct folding and plasma membrane insertion of the catalytic subunit depends on the presence of the auxiliary subunit (122). In contrast, oligomerization has no known functional consequences for some other membrane proteins such as aquaporins (200). Although known to form oligomers, these proteins are fully capable of functioning as a monomer with each monomer capable of independently translocating substrate ions across the plasma membrane.

In Chapter 4, an analysis of the oligomeric state of rat brain NCKX2 was undertaken using CuPhe-catalyzed oxidation of adjacent free sulfydryls to disulfide bonds, co-immunoprecipitation, and BN-PAGE. NCKX2 oligomer formation depended upon hydrophobic interactions between the transmembrane domains of the exchanger. Further evidence from BN gels suggested the presence of a higher order oligomer of rat brain NCKX2 with an apparent molecular weight greater than expected for a dimer, but the precise composition of this higher order oligomer has yet to be defined. Another unresolved question concerns the role of Cys395 in the free sulfydryl-dependent

formation of the 200kDa oligomer of NCKX2 observed in SDS-PAGE gels, as well as the identity and composition of this oligomer. The evidence gathered so far is not sufficient to determine conclusively the nature of this oligomer. In addition, a minimal functional unit of rat brain NCKX2 cannot be determined from the data described in Chapter 4. Extrapolating from the studies conducted using bovine rod NCKX1 (9), it is tempting to speculate that independent ion transport pathways operate within each monomer. If this were true, NCKX2 oligomerization might confer a regulatory role on exchanger function.

### *6.2.1 Formation of the Rat Brain NCKX2 Dimer*

The evidence for rat brain NCKX2 homo-oligomerization was first observed when the N-terminal FLAG-tagged rat brain NCKX2 co-immunoprecipitated untagged recombinant rat brain NCKX2 transiently expressed in HEK-293 cells (33). In Chapter 4, dimerization of rat brain NCKX2 primarily driven by hydrophobic interactions was confirmed by co-immunoprecipitation as well as BN-PAGE. The observation that the choice of detergent influenced the efficiency of co-immunoprecipitation of untagged NCKX2 (Figure 4-6), and that this effect was independent of the presence of Cys395 (Figure 4-8), suggested that the primary force responsible for keeping the NCKX2 monomers together is non-covalent, presumably mediated mainly through the transmembrane domains, where detergents are known to have their largest effect. The association between NCKX2 monomers appeared relatively weak when assessed by co-immunoprecipitation experiments, and resulted in markedly decreased co-immunoprecipitation efficiency in the presence of the detergent Triton X-100 compared

to CHAPS (Figure 4-6). Regardless of the type of detergents used however, the overall immunoprecipitation efficiency of the NCKX2 monomers was low. It is possible that the oligomeric complex is only weakly associated together and dissociates during the washing step in the immunoprecipitation procedure. In addition, it is not clear what fraction of co-expressed proteins would exist as tagged/untagged oligomers as opposed to tagged/tagged and untagged/untagged oligomers. If a relatively low amount of tagged/untagged oligomers were formed, it would explain the relatively low co-immunoprecipitation efficiency. However, it would not explain the differences in the co-immunoprecipitation efficiency noted in the same set of HEK-293 microsomes solubilized using Triton X-100 or CHAPS.

Further experiments using BN-PAGE also revealed the presence of an apparent NCKX2 dimer (Figures 4-9 and 4-10). In the presence of reducing agent, the appearance of the apparent dimeric 150kDa band of NCKX2-FLAG depended on SDS concentration, suggesting that non-covalent forces hold native NCKX2 in an oligomeric state larger than a dimer. As these forces are disrupted by increasing SDS concentration, the complex first dissociates into dimers and then into monomers. In the absence of reducing agent, a substantial fraction of NCKX2-FLAG is covalently trapped as the dimer, even at high SDS concentrations. Similar results were also observed with NCKX2-FLAG C395A, although the amount of covalently trapped dimer was much less in this case. This is the first study to utilize BN-PAGE to examine the oligomeric state of NCKX2. Although previous studies using recombinant chicken cone NCKX2 expressed in HEK-293 cells or in insect High Five cells detected an NCKX2 adduct when analyzed by SDS-PAGE, it

was not clear that this adduct represented a NCKX2 dimer since its apparent molecular weight was larger than expected (126). The BN-PAGE analysis presented in Chapter 4 of this thesis strongly indicated that native rat brain NCKX2 forms a higher order oligomer, in a sequential oligomerization process, with dimerization as the initial step toward the formation of higher order species.

Interestingly, a fraction of the NCKX2 monomers are locked into an apparent dimeric complex, as seen in BN-PAGE gels as a 150kDa band observed in the absence of reducing agent (Figures 4-9 and 4-10), via a strong covalent disulfide bond that could not be disrupted by SDS. A similar pattern of SDS-independent dimeric/oligomeric state was observed in the NCKX2-FLAG C395A mutant. In that case, however, the amount of trapped dimer in the absence of SDS was far lower than the amount observed in wild-type NCKX2-FLAG. This result suggests that NCKX2 can be covalently linked into a dimer by two possible mechanisms: one requiring the free sulfydryl of Cys395, and the other independent of Cys395 but requiring other cysteine residues in NCKX2. The identity of the cysteine residue(s) responsible for stabilizing this alternate NCKX2 dimer is not known. Although disulfide bonds may trap a fraction of NCKX2 monomers as dimers, it is highly likely that the primary force that drives oligomerization of NCKX2 is non-covalent and hydrophobic since higher-order NCKX2 oligomers was observed independent of the presence of reducing agent. Therefore, intermolecular disulfide bond formation may be a secondary consequence of the dimerization of rat brain NCKX2, and its role could be restricted to structural stabilization of the NCKX2 dimer.

Recently, evidence that cardiac NCX1 could form a dimer has been presented using cross-linking and co-immunoprecipitation experiments similar to ones described in Chapter 4 (249). By re-introducing a single cysteine residue within the cysteine-less exchanger and performing CuPhe-catalyzed oxidation, free sulfydryl-dependent formation of the NCX1 dimer was noted. Dimer formation was both substrate and temperature dependent and seemed to occur along the transmembrane domains including parts of the two α repeats. Similar to what was observed for NCKX2 in Chapter 4, the interactions between NCX1 monomers was weak and easily disrupted by the detergent *n*-dodecyl-*β*-D-maltoside. In addition to the exchanger dimer, the formation of a higher order oligomer of NCX1 was also suggested. Along with the data presented in Chapter 4, the dimerization of NCX1 implies that dimerization/oligomerization might be a general structural phenomenon shared by all $Na^+/Ca^{2+}$-exchangers.

*6.2.2 Higher Order Oligomers of Rat Brain NCKX2*

As mentioned briefly above, rat brain NCKX2 can also exist as higher order oligomers whose apparent molecular weight is greater than that of the NCKX2 dimer. This was independently shown by CuPhe-catalyzed oxidation and by BN-PAGE analyses. CuPhe-catalyzed oxidation of adjacent free sulfydryls to disulfide bonds revealed the presence of a Cys395-dependent 200kDa NCKX2-FLAG oligomer observed on SDS-PAGE gels. In BN-PAGE experiments, NCKX2-FLAG displayed an apparent molecular weight of between ~250 and ~350kDa in the absence of SDS. Application of increasing SDS concentrations caused this larger species to progressively dissociate first into a ~150kDa band, and then into an NCKX2 monomer of 75kDa. Unfortunately,

smearing within the high molecular weight region of the BN gels made it difficult to clearly visualize and thereby obtain an accurate size and oligomeric state of the higher order oligomer of NCKX2-FLAG.

The data presented in Chapter 4 strongly and clearly demonstrate the presence of multiple oligomeric species of rat brain NCKX2. However, other than the NCKX2 dimer, the precise nature and oligomeric states of the other higher order species of rat brain NCKX2 remain to be resolved. It is not clear at this point whether all these oligomers represent strictly homo-oligomeric species of rat brain NCKX2, or whether some or all of these oligomers are involved in a heteromeric association, interacting with proteins other than NCKX2. In addition, the role of Cys395 in the formation of the higher order oligomers of NCKX2 is not well defined. It is obvious from the co-immunoprecipitation data presented in Chapter 4 that Cys395 is not necessary for dimerization, although the complete shift of the exchanger from the monomeric 75kDa band to the oligomeric 200kDa band observed on an SDS-PAGE gel upon oxidation by CuPhe was not possible without this cysteine. Further studies are required to identify the nature and the precise oligomeric state of the Cys395-dependent 200kDa oligomer of rat brain NCKX2.

### *6.2.3 Cys395 and the NCKX2 Oligomers*

One of the preliminary pieces of biochemical evidence in support of the oligomerization of rat brain NCKX2 was obtained simply by running a non-reducing SDS-PAGE gel using HEK-293 cell microsomes transiently expressing NCKX2-FLAG (Figure 4-1). The presence of several free sulfydryl-dependent higher order oligomers of

NCKX2-FLAG was observed, and CuPhe catalyzed oxidation further revealed the importance of Cys395 in formation of the 200kDa oligomer of NCKX2-FLAG (Figure 4-3). The fact that Cys395 is essential for the complete shift of NCKX2-FLAG on an SDS-PAGE gel from its monomeric 75kDa to the oligomeric 200kDa species upon CuPhe-catalyzed oxidation means that the sulfydryl of Cys395 is not modified or occupied under the non-reducing conditions of this experiment. This finding is in disagreement with a previous study that found Cys395 to be normally occupied in the resting condition in intact cells unless it was subjected to prior reduction (33). The use of intact whole HEK-293 cells in the cysteine-selective labelling as opposed to the HEK-293 microsomal preparation for CuPhe-catalyzed oxidation might explain this discrepancy. In addition, the membrane permeability of the biotin maleimide (MPB) used to selectively label the cysteine residues in the previous study is still debated (10). If in fact MPB displays poor membrane permeability, it could in turn lead to poor labelling of Cys395.

Detergent solubilization prior to CuPhe-catalyzed oxidation of NCKX2-FLAG in HEK-293 cell microsomes did not affect complete formation of the 200kDa oligomer. Detergent treatment had a mild oxidizing effect on the free sulfydryl of Cys395, however, resulting in a greater proportion of the 200kDa oligomer in the absence of CuPhe catalyzed oxidation. This effect is likely due to low levels of oxidizing compounds that are known to contaminate polyoxyethylene based detergents such as Triton X-100 (40). Moreover, the choice of detergent did not influence complete formation of the 200kDa oligomer of NCKX2-FLAG upon CuPhe-catalyzed oxidation. Taken together, the data presented in Chapter 4 suggest that the free sulfydryl of Cys395 is essential for complete

formation of the 200kDa oligomer of NCKX2-FLAG, the formation of which is independent of detergent solubilization.

Both co-immunoprecipitation and BN-PAGE experiments conclusively demonstrated that Cys395 is not necessary for the dimerization of rat brain NCKX2. Co-immunoprecipitation efficiency was not affected by the mutation in Cys395 (Figure 4-8), as suggested by the seemingly identical pattern of dimer formation in the BN-gels of NCKX2-FLAG and NCKX2-FLAG C5A (Figures 4-9 and 4-10). In addition, co-immunoprecipitation efficiency was dependent on the choice of detergents, suggesting that interactions between the exchanger monomers were weak and could be influenced by the detergent used for solubilization. BN-PAGE also confirmed the detergent-sensitive and weak dimer association, although in this case the addition of a low concentration of SDS was needed to observe a difference between the non-ionic detergents Triton X-100 and CHAPS. The apparent contradiction between the CuPhe-catalyzed oxidation data compared to the co-immunoprecipitation and BN-PAGE findings, suggest that the Cys395-dependent 200kDa oligomeric species seen on SDS-PAGE may not be an anomalously running NCKX2 dimer, but rather it could represent a NCKX2 hetero-oligomer with a combined apparent molecular weight of ~200kDa.

The hypothesis that Cys395 is involved in formation of a possible hetero-oligomeric complex of rat brain NCKX2 was tested in Chapter 5 by first exposing HEK-293 microsomes transiently expressing NCKX2-FLAG to CuPhe-catalyzed oxidation and then immunoprecipitating the exchanger, in hopes of observing the co-

immunoprecipitation of potential interacting partners that could be responsible for formation of the 200kDa oligomer of NCKX2. Since CuPhe-catalyzed oxidation of the exchanger consistently yielded a complete shift from its monomeric 75kDa size to the oligomeric 200kDa species, it was reasonable to assume that the exchanger would be involved in a protein interaction with a molecular stoichiometry of one exchanger vs. one interacting partner. If so, the interacting partner that co-associated with NCKX2 would appear as a protein band with relatively similar intensity as the NCKX2 band on an SDS-PAGE gel upon Coomassie staining. However, no such band was observed, as seen in Chapter 5 (Figure 5-2), although intense staining of the exchanger band was visible. It is possible that the predicted partner protein might have been present, but was either not well stained by Coomassie or was obscured by the NCKX2 band on the gel. On the other hand, this observation could suggest that the 200kDa oligomer of NCKX2-FLAG observed on SDS-PAGE gels upon CuPhe-catalyzed oxidation is a NCKX2 dimer that might run anomalously on the SDS-PAGE gel with the apparent molecular weight of ~200kDa. Indeed, BN-PAGE analysis of NCKX2-FLAG and NCKX2-FLAG C395A in the absence of reducing agent revealed the noticeable differences in the labelling intensities of the “locked” dimers of NCKX2-FLAG and NCKX2-FLAG C395A (Figures 4-9 and 4-10), strongly implying the presence of a second, perhaps different kind of NCKX2 dimer mediated by the disulfide bond formation between the two Cys395.

### *6.2.4 Oligomeric States of Rat Brain NCKX2*

Figure 6-1 decribes the possible multiple oligomeric states of rat brain NCKX2, based on the evidence gathered from the experiments described in this thesis. BN-PAGE

**Figure 6-1. Oligomeric States of Rat Brain NCKX2.** Cartoon representation of possible oligomeric states of rat brain NCKX2 based on the data obtained in Chapters 4 and 5. *Red line*: a disulfide bond, *SH*: free sulfydryl of Cys395, *yellow cylinder*: a NCKX2 monomer. In the presence of reducing agents (+DTT), rat brain NCKX2 monomers are non-covalently associated and exist as a higher order oligomer (A), potentially a tetramer. Upon the addition of SDS, non-covalently associated oligomers of NCKX2 start to break down, first to a dimer (B) and then into a monomer at higher SDS concentrations (C). In the absence of reducing agents (-DTT), some fraction of rat brain NCKX2 monomers forms a disulfide bond via free sulfydryls of adjacent Cys395 (D), or via cysteine residue(s) other than Cys395 (E) whose identity is not known at this moment, while most of rat brain NCKX2 monomers are still non-covalently associated (F). Addition of SDS in the absence of reducing agent leads to the formation of three different species of NCKX2 dimers (G); a non-covalently associated dimer (which subsequently dissociates to monomers at higher [SDS] as seen in (H)), a Cys395 disulfide-linked dimer which appears ~200kDa on SDS-PAGE gels, and a Cys395-independent disulfide-linked dimer which appears ~150kDa on SDS-PAGE gels (and is a minor species). CuPhe-catalyzed oxidation causes disulfide bond formation between all adjacent Cys395 within the tetrameric NCKX2 (I). Because a small fraction of NCKX2 tetramers are also disulfide linked by a non-Cys395 bond (J), SDS treatment of CuPhe cross-linked NCKX2 results in mostly 200 kDa dimers, but also a small fraction of a covalently linked tetramer (K).

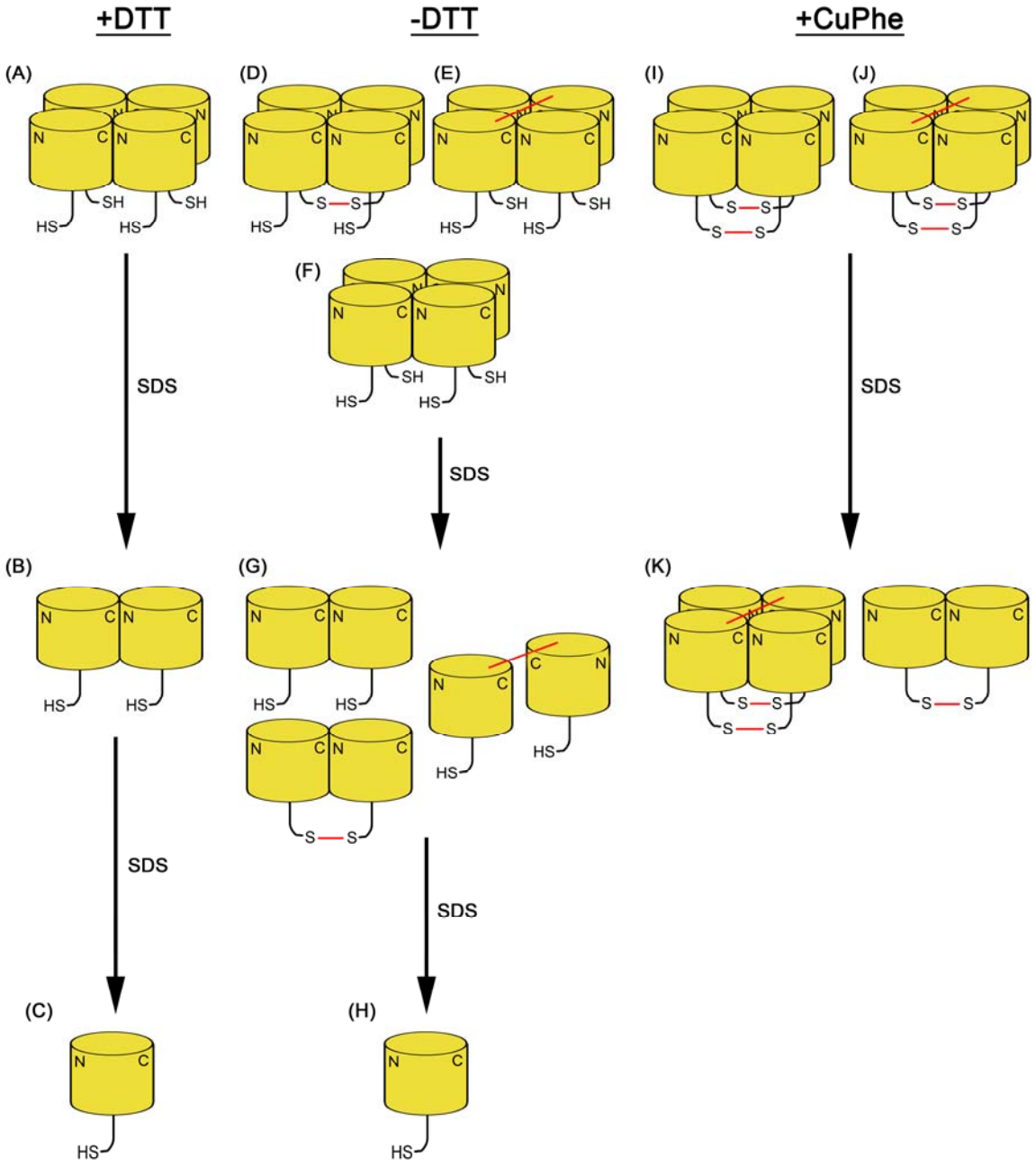
+DTT
-DTT
+CuPhe
(A)
(D)
(E)
(I)
(J)
(F)
SDS
SDS
SDS
(B)
(G)
(K)
SDS
SDS
(C)
(H)
N
C
HS
SH
S—S

analysis as well as non-reducing SDS-PAGE gels clearly demonstrated that native NCKX2 exists as a higher-order oligomer, possibly a tetramer, in the membrane formed as a dimer of dimers. The major driving force for the dimerization of rat brain NCKX2 is non-covalent and hydrophobic in its nature, but some fraction of these dimers is covalently linked via disulfide bond formation between two Cys395 residues (Figure 6-1). These Cys395-linked dimers of rat brain NCKX2 are noted as the ~150kDa band on BN-PAGE gels, and as the 200kDa band on non-reducing SDS-PAGE gels (Figures 4-1, 4-3, 4-9, and 4-10). Cys395-linked dimers of rat brain NCKX2 could exhibit aberrant mobility on non-reducing SDS-PAGE gels (200kDa) because the covalent cross-link, located in the middle of the protein, produces a species with larger cross-sectional size than a linear protein of similar mass.

In addition, the evidence also suggests that a low fraction of NCKX2 in the tetramer is covalently linked together into a dimer by cysteine residue(s) other than Cys395, linked possibly in a C-terminus to C-terminus anti-parallel orientation (Figure 6-1). This Cys395-independent, covalently associated NCKX2 dimer is seen as the 150kDa band in BN-PAGE gels with the NCKX2-FLAG C395A mutant (Figures 4-9 and 4-10), and as the 150kDa band in non-reducing SDS-PAGE gels (band c, Figures 4-1 and 4-3). Unlike the Cyc395 disulfide linked dimer, the C-terminally linked dimer has a more linear shape, and hence runs on SDS-PAGE in accordance with its actual size. Although the precise identity of the cysteine residue(s) responsible for the formation of this dimer is not known, it may involve free sulfydryls of Cys 614 (C6) and Cys666 (C8), since the 150kDa band was observed on non-reducing SDS-PAGE gels in the NCKX2-FLAG C1-

5, 7A mutant (Figure 4-3). Moreover, the relative labelling intensity of this 150kDa band was not affected by CuPhe-catalyzed oxidation, which suggests that the cysteine residue(s) in question might be buried in the membrane so that they are not easily accessible to free-sulfydryl modifying reagents like CuPhe.

Still, the oligomerization model shown in Figure 6-1 cannot explan the molecular nature of the 130kDa band of rat brain NCKX2 noted on non-reducing SDS-PAGE gels using rat brain synaptosomal membrane vesicles (Figure 5-1). This band was not observed with the recombinant rat brain NCKX2 in HEK-293 cells, and its labelling intensity was independent of CuPhe-catalyzed oxidation. This 130kDa oligomer of rat brain NCKX2 could represent the association between NCKX2 and an interacting partner, whose molecular identity remains unknown. If so, this novel interacting partner of rat brain NCKX2 is endogenous to neurons of rat brain but is not present in HEK-293 cells.

### 6.3 NCKX2 Protein-Protein Interactions

Protein-protein interactions are crucial in many aspects of biological function carried out by a cell. They are the mechanism used to maintain a cell's structural compartments such as the cytoskeleton and nuclear pore. They are essential for the integrity of many multiprotein enzymatic machineries such as RNA polymerases, and are the basis for the enzyme-protein substrate interactions important for catalysis. Last but not least, protein-protein interactions are the key mechanisms that physically tethers the

molecules involved in signal transduction pathways into sub-cellular microdomains. For most of the signalling proteins that are tethered this way, the protein-protein interactions often impart functional importance in addition to their role in protein scaffolding and organization. Some of these functionally important interactions are temporal and tightly regulated by the cell, only occurring when the need arises. On the other hand, some interactions are almost always required to maintain normal cell function. Therefore, investigation into the complex nature of the protein-protein interactions and their functional and physiological implications is critical to the understanding of the biological processes that govern living organisms.

The first line of evidence that indicated the presence of a potential hetero-oligomeric association of rat brain NCKX2 was presented in Chapter 4, which promptly led to a further investigation as described in Chapter 5. CuPhe-catalyzed oxidation of NCKX2 enriched in rat brain synaptosomal membrane vesicles revealed the presence of a novel ~130kDa band that was absent from HEK-293 cell microsomes transiently expressing recombinant NCKX2, further suggesting NCKX2 heteromerization. Here, mass spectrometric analyses revealed the identities of several highly interesting potential interaction partners of rat brain NCKX2, including cytoskeletal proteins, molecular chaperones, as well as $Ca^{2+}$ handling membrane proteins. However, subsequent co-immunoprecipitation experiment did not confirm the interaction between rat brain NCKX2 and most of these proteins. This suggests that NCKX2 protein-protein interactions might be weak and transient, such that the observation of specific partners is heavily dependent upon the conditions and techniques used to identify them.

*6.3.1 LC/MS/MS as a Tool for Identifying Interaction Partners*

Nanoscale liquid chromatography combined with tandem mass spectrometry (LC/MS/MS) has become one of the most versatile tools for peptide and protein identification. In combination with other more conventional biochemical techniques such as immunoprecipitation and SDS-PAGE, LC/MS/MS has proven to be a quick and easy means to accurately identify potential interacting partners of rat brain NCKX2, thereby providing a good starting ground for further investigation into the NCKX2 protein-protein interaction as seen in Chapter 5. LC/MS/MS was highly sensitive and was able to produce consistent peptide match and protein identification with good confidence and reproducibility, even with barely discernable Coomassie and silver stained bands. Concern over the use of silver staining and its compatibility with LC/MS/MS identification was minimized by using a commercially available mass spectrometry compatible silver staining kit (Invitrogen).

The major limitation associated with protein and peptide identification using a powerful technique such as LC/MS/MS was found in the initial immunoprecipitation procedure. Although the sample complexity was somewhat reduced by immunoprecipitating NCKX2 with an appropriate antibody, and several distinct and identifiable protein bands were observed upon gel staining, the resolution and sharpness of each band were still sub-optimal. Furthermore, when rat brain NCKX2 was immunoprecipitated using polyclonal F antibody against NCKX2, the intense staining of various immunoglobulins from the antibody itself further complicated the identification of co-immunoprecipitated protein bands. This was especially true for the lower molecular

weight region of the SDS-PAGE gel. Affinity-purified polyclonal F antibody was also used to immunoprecipitate rat brain NCKX2 in the hope of reducing the immunoglobulin bands, and improving the chance of detecting an interacting protein. Unfortunately, this attempt did not bring about the immunoprecipitation of rat brain NCKX2 and therefore this approach was not pursued further (data not shown). The reasons why this antibody failed to immunoprecipitate rat brain NCKX2 are not known.

### *6.3.2 Physiological Significance of NCKX2 Protein-Protein Interaction*

The list of potential interacting partners of rat brain NCKX2 identified by LC/MS/MS revealed some interesting trends (Table 5-1). These proteins could be divided into three major groups: molecular chaperones, cytoskeletal proteins, and membrane ion transporters. Identification of chaperones such as heat shock proteins as interacting partners of NCKX2 was made in HEK-293 cells. This was understandable considering the nature of the heterologous system which was forced to over-express the exogenously introduced proteins at high levels, causing the machinery involved in protein synthesis and folding to become saturated. Therefore, it is likely that some misfolded recombinant NCKX2 was bound to the heat shock proteins, resulting in their identification as interacting partners of NCKX2. This rationale was the basis for the decision not to test their interaction by co-immunoprecipitation.

The interaction between recombinant rat brain NCKX2 and endogenously expressed prohibitins in HEK-293 cells was confirmed by subsequent co-immunoprecipitation experiments. Considering its potential role as a molecular

chaperone, the interaction between prohibitins and NCKX2 might reflect that function as discussed above for the heat shock proteins. However, prohibitins are also thought to act as scaffolding proteins, belonging to the superfamily of PHB domain proteins which includes the resident lipid raft protein flotillin (193). The function of the highly conserved PHB domain is not fully understood, but it might constitute a lipid recognition motif, allowing its interaction partners to be preferentially partitioned into membrane microdomains such as lipid rafts and caveolae (193). Certainly, more studies are required to understand whether the perceived interaction between prohibitins and recombinant rat brain NCKX2 in HEK-293 cells has any implication in the sub-cellular localization of NCKX2. Co-immunoprecipitation experiments using rat brain synaptosomal membrane vesicles did not support the HEK-293 cell data (Figure 5-7) suggesting the interaction between prohibitins and NCKX2 might be present at non-synaptosomal sites in brain, or may only pertain to the heterologous system.

Although identified as potential interacting partners of rat brain NCKX2 by LC/MS/MS, none of the membrane $Ca^{2+}$ transporters or $Na^{+}/K^{+}$ ATPases co-immunoprecipitated with rat brain NCKX2 in solubilized synaptosomal membrane vesicles (Figures 5-8, 5-9, and 5-10). Considering their functional relationships, it is likely that rat brain NCKX2, along with membrane transporters such as PMCA, SERCA, and $Na^{+}/K^{+}$ ATPases, are clustered within membrane microdomains in the postsynaptic dendrites of neurons in rat brain. In addition, the fact that the observed apparent molecular weight of each potential interacting partner closely matched the theoretical molecular weight, and that these membrane transporters were identified in both

heterologous and endogenous systems suggests the legitimacy of their possible molecular association. Perhaps the differences in experimental design and conditions for LC/MS/MS and co-immunoprecipitation were responsible for such contradictory results. Co-immunoprecipitation was performed on a considerably smaller scale compared with NCKX2 immunoprecipitation that preceded LC/MS/MS, and this might explain the failure to observe any meaningful interaction between rat brain NCKX2 and membrane transporters by immunoblotting. It is possible that the interaction between rat brain NCKX2 and other proteins is a $Ca^{2+}$-dependent process. The concept was not tested in the experiments of this thesis, but warrants consideration for possible future directions. Also, the interaction between rat brain NCKX2 and other membrane transporters might be very weak and even transient, since those bands that were identified as ion transporters by Coomassie and silver staining were fairly faint in their labelling intensity compared to the labelling intensity of rat brain NCKX2. If this is true, the co-immunoprecipitation followed by immunoblotting might not be sensitive enough to detect such an interaction compared with the much more sensitive LC/MS/MS.

### 6.4 Future Studies

During the course of this work, several novel and interesting findings on the sub-cellular localization and quaternary structure of rat brain NCKX2 have been discovered. While these findings contributed to improving current knowledge of the exchanger structure, they also raised new questions regarding how newly discovered structural information might relate to the function of the exchanger. These issues include: 1)

identifying the role of lipid raft localization of rat brain NCKX2 and the factors causing such sub-cellular localization; 2) identifying the precise oligomeric state of rat brain NCKX2 and the role of Cys395; and 3) understanding the physiological relevance and potential functional implications of NCKX2 interaction with other proteins. Future studies that might help to address these issues are briefly discussed in this section, with hopes to attain more comprehensive understanding of the sub-cellular localization and quaternary structure of rat brain NCKX2.

### *6.4.1 Postsynaptic Lipid Rafts and Rat Brain NCKX2*

Although the data presented in Chapter 3 indicated that rat brain NCKX2 was localized in lipid raft microdomains of postsynaptic dendrites, the physiological significance of this sub-cellular localization and its contribution to neuronal intracellular $Ca^{2+}$ signalling are currently not well understood, necessitating further investigation into these matters. First of all, it would be helpful to confirm that postsynaptic $Ca^{2+}$ handling proteins are indeed organized into the same set of lipid raft microdomains, which would strengthen the hypothesis that the raft is the domain responsible for tethering of proteins involved in $Ca^{2+}$ signalling. The simplest way to test this hypothesis would be by performing co-immunoprecipitation of rat brain NCKX2 with postsynaptic $Ca^{2+}$ handling proteins such as PSD-95, NMDA receptors and AMPA receptors within the isolated detergent-resistant membrane fractions from synaptosomal membrane vesicles. As seen in Chapter 3, co-immunoprecipitation of these proteins in the presence of ice-cold Triton X-100 would indicate that they are found in the same set of lipid raft microdomains. Detailed immunocytochemical analysis using dual labelling with different fluorescent

antibodies and immunofluorescence, followed up with dual labelling using antibodies coupled to differentially sized gold-particles and electron microscopy, will confirm co-localization at synaptic sites. Once their co-localization is confirmed, more direct analyses using more sophisticated techniques like fluorescence resonance energy transfer (FRET) or single particle tracking could be used to determine if the distribution or motion of these proteins is consistent with clustering closer than would be expected for random distribution within the plasma membrane. To perform experiments such as these, explant culture or cultured neurons would be transfected using recombinant molecules tagged with fluorescent reporters. Work of this nature has been employed successfully to examine other post-synaptic proteins (89).

In addition, agents that are known to disrupt lipid raft microdomains such as β-cyclodextrin in combination with fluorescent $Ca^{2+}$ imaging in the neuronal culture could be used to address the role of lipid raft microdomains in intracellular $Ca^{2+}$ signalling and homeostasis. Cultured neurons will be loaded with the fluorescent $Ca^{2+}$ indicator fura-2, and the $K^+$-dependent fluctuations in $[Ca^{2+}]_i$ upon the application of the perfusion solution containing $Ca^{2+}$ and $K^+$ resulting from the exchanger working in reverse mode will be monitored in the presence and in the absence of β-cyclodextrin. If non-caveolar lipid raft localization of NCKX2 is indeed necessary for proper intracellular $Ca^{2+}$ homeostasis, then the disruption of the lipid rafts by β-cyclodextrin would manifest as notably different $[Ca^{2+}]_i$ fluctuation. β-cyclodextrin is considered to have a rather general effect on normal cellular functions other than disruption of lipid raft microdomains. If

this is true, then other methods such as blocking cholesterol biosynthesis or inhibiting cellular sphingolipid biosynthesis could be used instead.

If the importance of the lipid raft microdomain in the organization of postsynaptic $Ca^{2+}$ handling proteins and intracellular $Ca^{2+}$ signalling was confirmed, it would be important to determine how these proteins are localized within the lipid raft microdomains. Although caveolins are not found in postsynaptic dendrites, it is possible that other scaffolding proteins such as PSD-95 might be involved in holding these proteins together in the lipid raft, a hypothesis that could be easily tested by co-immunoprecipitation. It is also possible that co-localization is a $Ca^{2+}$-regulated event. In other words, changes in $[Ca^{2+}]_i$ might drive the formation of lipid raft-mediated microdomains that cluster membrane $Ca^{2+}$ handling proteins. This could be tested by density floatation analyses using synaptosomal membrane vesicles in the presence or absence of $Ca^{2+}$, and by observing changes in the protein contents of isolated detergent-resistant membranes. Both FRET and single particle tracking with or without the presence of $Ca^{2+}$ would also be able to confirm whether co-localization of the protein within lipid raft microdomains is $Ca^{2+}$ dependent.

Choosing a cell line that closely represents the cellular environments in which endogenous rat brain NCKX2 is found would also be helpful. The fact that recombinant rat brain NCKX2 displayed a markedly different detergent-resistant fractionation pattern in HEK-293 cells compared to the pattern seen in rat brain suggests that HEK-293 cells do not adequately represent the endogenous system in which NCKX2 is found.

Therefore, HEK-293 cells might not be the most suitable system to study NCKX2 sub-cellular localization, or any functional effect such sub-cellular localization might bring about. Primary cultured neurons such as the cultured hippocampal neurons or a cell line derived from a neuronal origin such as rat PC-12 cells in which NCKX2 proteins are endogenous expressed would represent possible alternatives.

*6.4.2 Determination of the Oligomeric State of Rat Brain NCKX2 and the Role of Cys395*

Despite their ease and simplicity, BN-PAGE and co-immunoprecipitation were insufficient to fully resolve the correct oligomeric state of the higher order oligomers of rat brain NCKX2. Therefore, analytical ultracentrifugation using sucrose gradients made with $H_2O$ and $D_2O$ and size exclusion chromatography of detergent-solubilized rat brain NCKX2 that measures biophysical parameters necessary to calculate hydrodynamic properties of the protein-detergent complex (49) would be helpful to determine the precise molecular weights and oligomeric states of the higher order oligomers of rat brain NCKX2. Unless the unknown NCKX2 interacting partners are of the same molecular weight as the NCKX2 monomer, the calculated molecular weight from these hydrodynamic parameters will be able to clarify the oligomeric state of rat brain NCKX2. If the interaction between exchanger monomers is weak and not stable enough to survive detergent solubilization, chemical cross-linking prior to detergent solubilization would be used to keep the higher order oligomers together throughout the experiments.

In addition, conducting the same hydrodynamic analyses after CuPhe-catalyzed oxidation using the Cys395 mutant form of recombinant rat brain NCKX2 will help to

understand the identity of the 200kDa oligomers of rat brain NCKX2 and the role of Cys395 in NCKX2 oligomerization. If the calculated molecular weight of the disulfide-bond induced recombinant NCKX2 oligomer is indeed 200kDa, and if this oligomer is absent in the Cys395 mutant form of the exchanger, this would indicate the presence of interacting partners of rat brain NCKX2 of about 130kDa in size. However, if the calculated molecular weight of the disulfide bond-induced recombinant exchanger oligomer would be 150kDa, this would suggest that the 200kDa oligomeric band on SDS-PAGE gels is the exchanger dimer running anomalously, and that Cys395 forms a disulfide bond with another exchanger monomer.

Techniques such as BN-PAGE, co-immunoprecipitation, analytical ultracentrifugation, as well as size exclusion chromatography require membrane proteins such as rat brain NCKX2 to be detergent solubilized prior to analysis. However, the structure of membrane proteins in detergent might not be biologically relevant. Radiation inactivation analysis using high-energy electrons could be useful, especially in defining the functional molecular mass of rat brain NCKX2. Vesicles obtained from HEK-293 cells transiently expressing recombinant NCKX2 proteins, or rat brain synaptosomal membrane vesicles, will be deep frozen and irradiated with an electron beam. After thawing the sample, the surviving NCKX2 activity after the irradiation will be measured using radioactive $Ca^{2+}$ uptake assays. Using the mathematical formula that defines the empirical relationship between functional molecular weight and radiation dose (133), the molecular weight of functional NCKX2 oligomers and the oligomeric state of functional NCKX2 in biological membranes could be identified. In addition, NCKX2 oligomers

could be covalently cross-linked in the membrane using commercially available cross-linking reagents such as a homobifunctional amine-reactive disuccinimidyl suberate (DSS). Both HEK-293 cell microsomes transiently expressing the recombinant NCKX2 proteins or rat brain synaptosomal membrane vesicles enriched with NCKX2 could be used for this type of experiments. Once cross-linked, these exchanger oligomers will be solubilized using detergents, and their sizes will be analyzed by various techniques described above, such as SDS-PAGE followed by immunoblotting, BN-PAGE, and analytical ultracentrifugation.

To test which free sulfydryls of rat brain NCKX2 are responsible for stabilizing the Cys395-independent exchanger dimer seen in non-reducing BN-PAGE gels (Figures 4-9 and 4-10), BN-PAGE using cysteine-to-alanine mutants of recombinant NCKX2 (C1-4A, C5, 7A, and C1-5, 7A) could be investigated. The absence of the dimeric 150kDa band on a non-reducing BN-gel at high SDS concentrations can be used to identify the free sulfydryls responsible for mediating the apparent dimer stabilization. If all the mutants tested would yield the dimeric 150kDa band, it would suggest that the free sulfydryl(s) responsible for the dimer stabilization were to be those of Cys 614 (C6) and Cys666 (C8), the two cysteins whose presence was essential for the expression of the recombinant NCKX2 in HEK-293 cells (33).

*6.4.3 Identification of NCKX2 interacting partners*

One of the biggest concerns surrounding identification of potential interacting partners of rat brain NCKX2 was the lack of agreement between the data obtained using

LC/MS/MS and using co-immunoprecipitation as seen in Chapter 5. Inherent differences in the two approaches combined with possible problems associated with weak or transitory interactions suggest that other methods should be employed. For example, yeast two-hybrid analysis is ideally suited to identifying low affinity interactions. For this, different hydrophilic loops of rat brain NCKX2 could be used to construct the binding domain-attached bait, and a rat brain cDNA library cloned into *GAL4*-activating domain vector used as the prey. The interaction will then be identified using X-α-Gal, causing positive yeast colonies to turn blue. In addition, bead-bound GST-fusion proteins containing different hydrophilic loops of NCKX2 could be used in combination with a protein extract from rat brain to identify possible interacting partners. This technique has the advantage of having a high concentration of the interacting portion of NCKX2, and the possibility of using a variety of mild conditions during the interaction phase to capture even the weakest and most transient interactions.

Some residual concern exists that the protein identifications determined by NCKX2 immunoprecipitation followed by LC/MS/MS could reflect artefacts of the procedure rather than true molecular interaction between the proteins. Aside from the follow up co-immunoprecipitation experiments used in this thesis, an alternative approach would be to use mouse brain extracts for the full immunoprecipitation experiments. In that case, the use of *nckx2* (-/-) knockout animals would serve as an ideal control to eliminate proteins that might be identified due to non-specific interactions associated with the immunoprecipitation technique.

In HEK-293 cells, prohibitins were shown to interact with recombinant NCKX2. As mentioned before, prohibitins contain a highly conserved PHB domain, a protein scaffolding domain also found in flotillin. Mounting evidence suggests a role of the PHB domain in lipid raft recruitment, allowing the localization of proteins that carry the PHB domain and their interaction partners within lipid rafts (197, 198). Considering the lipid raft localization of rat brain NCKX2, this finding is highly interesting and the NCKX2-prohibitin interaction might provide the mechanism for NCKX2 sub-cellular localization. This hypothesis could be tested by using siRNA to inhibit the expression of endogenous prohibitins in HEK-293 cells transiently expressing recombinant NCKX2 and investigating any changes in sub-cellular localization of the exchanger proteins by density floatation using CHAPS as compared to HEK-293 cells expressing prohibitins. If NCKX2 interaction with prohibitins in HEK-293 cells is indeed important for the sub-cellular localization of NCKX2, the knock-down of prohibitins would lead to the exclusion of NCKX2 from the detergent-resistant membranes.

## BIBLIOGRAPHY

1. Alonso, M.T., C. Villalobos, P. Chamero, J. Alvarez, and J. Garcia-Sancho (2006) Calcium microdomains in mitochondria and nucleus. *Cell Calcium* **40**(5-6): p. 513-525.
2. Altimimi, H.F. and P.P. Schnetkamp (2007) Na+-dependent inactivation of the retinal cone/brain Na+/Ca2+-K+ exchanger NCKX2. *J Biol Chem* **282**(6): p. 3720-3729.
3. Aravamudan, B., D. Volonte, R. Ramani, E. Gursoy, M.P. Lisanti, B. London, and F. Galbiati (2003) Transgenic overexpression of caveolin-3 in the heart induces a cardiomyopathic phenotype. *Hum Mol Genet* **12**(21): p. 2777-2788.
4. Asahi, M., H. Nakayama, M. Tada, and K. Otsu (2003) Regulation of sarco(endo)plasmic reticulum Ca2+ adenosine triphosphatase by phospholamban and sarcolipin: implication for cardiac hypertrophy and failure. *Trends Cardiovasc Med* **13**(4): p. 152-157.
5. Augustine, G.J., F. Santamaria, and K. Tanaka (2003) Local calcium signaling in neurons. *Neuron* **40**(2): p. 331-346.
6. Baker, P.F., M.P. Blaustein, A.L. Hodgkin, and R.A. Steinhardt (1969) The influence of calcium on sodium efflux in squid axons. *J Physiol* **200**(2): p. 431-458.
7. Balijepalli, R.C., J.D. Foell, D.D. Hall, J.W. Hell, and T.J. Kamp (2006) Localization of cardiac L-type Ca(2+) channels to a caveolar macromolecular signaling complex is required for beta(2)-adrenergic regulation. *Proc Natl Acad Sci U S A* **103**(19): p. 7500-7505.

8. Bauer, P.J. (2002) Binding of the retinal rod Na+/Ca2+-K+ exchanger to the cGMP-gated channel indicates local Ca(2+)-signaling in vertebrate photoreceptors. *Ann N Y Acad Sci* **976**: p. 325-334.

9. Bauer, P.J. and H. Schauf (2002) Mutual inhibition of the dimerized Na/Ca-K exchanger in rod photoreceptors. *Biochim Biophys Acta* **1559**(2): p. 121-134.

10. Bayer, E.A., M.G. Zalis, and M. Wilchek (1985) 3-(N-Maleimido-propionyl)biocytin: a versatile thiol-specific biotinylating reagent. *Anal Biochem* **149**(2): p. 529-536.

11. Bayer, K.U., P. De Koninck, A.S. Leonard, J.W. Hell, and H. Schulman (2001) Interaction with the NMDA receptor locks CaMKII in an active conformation. *Nature* **411**(6839): p. 801-805.

12. Berridge, M.J. (2006) Calcium microdomains: organization and function. *Cell Calcium* **40**(5-6): p. 405-412.

13. Berridge, M.J., M.D. Bootman, and P. Lipp (1998) Calcium--a life and death signal. *Nature* **395**(6703): p. 645-648.

14. Berridge, M.J., M.D. Bootman, and H.L. Roderick (2003) Calcium signalling: dynamics, homeostasis and remodelling. *Nat Rev Mol Cell Biol* **4**(7): p. 517-529.

15. Berridge, M.J., P. Lipp, and M.D. Bootman (2000) The versatility and universality of calcium signalling. *Nat Rev Mol Cell Biol* **1**(1): p. 11-21.

16. Bers, D.M. (2002) Cardiac excitation-contraction coupling. *Nature* **415**(6868): p. 198-205.

17. Bers, D.M., S. Despa, and J. Bossuyt (2006) Regulation of Ca2+ and Na+ in normal and failing cardiac myocytes. *Ann N Y Acad Sci* **1080**: p. 165-177.

18. Besserer, G.M., M. Ottolia, D.A. Nicoll, V. Chaptal, D. Cascio, K.D. Philipson, and J. Abramson (2007) The second Ca2+-binding domain of the Na+ Ca2+ exchanger is essential for regulation: crystal structures and mutational analysis. *Proc Natl Acad Sci U S A* **104**(47): p. 18467-18472.

19. Besshoh, S., D. Bawa, L. Teves, M.C. Wallace, and J.W. Gurd (2005) Increased phosphorylation and redistribution of NMDA receptors between synaptic lipid rafts and post-synaptic densities following transient global ischemia in the rat brain. *J Neurochem* **93**(1): p. 186-194.

20. Bickel, P.E., P.E. Scherer, J.E. Schnitzer, P. Oh, M.P. Lisanti, and H.F. Lodish (1997) Flotillin and epidermal surface antigen define a new family of caveolae-associated integral membrane proteins. *J Biol Chem* **272**(21): p. 13793-13802.

21. Blackstone, C. and M. Sheng (1999) Protein targeting and calcium signaling microdomains in neuronal cells. *Cell Calcium* **26**(5): p. 181-192.

22. Blackstone, C. and M. Sheng (2002) Postsynaptic calcium signaling microdomains in neurons. *Front Biosci* **7**: p. d872-885.

23. Blaustein, M.P. and W.J. Lederer (1999) Sodium/calcium exchange: its physiological implications. *Physiol Rev* **79**(3): p. 763-854.

24. Bootman, M.D., D. Thomas, S.C. Tovey, M.J. Berridge, and P. Lipp (2000) Nuclear calcium signalling. *Cell Mol Life Sci* **57**(3): p. 371-378.

25. Bossuyt, J., B.E. Taylor, M. James-Kracke, and C.C. Hale (2002) Evidence for cardiac sodium-calcium exchanger association with caveolin-3. *FEBS Lett* **511**(1-3): p. 113-117.

26. Brakeman, P.R., A.A. Lanahan, R. O'Brien, K. Roche, C.A. Barnes, R.L. Huganir, and P.F. Worley (1997) Homer: a protein that selectively binds metabotropic glutamate receptors. *Nature* **386**(6622): p. 284-288.

27. Brenman, J.E., D.S. Chao, S.H. Gee, A.W. McGee, S.E. Craven, D.R. Santillano, Z. Wu, F. Huang, H. Xia, M.F. Peters, S.C. Froehner, and D.S. Bredt (1996) Interaction of nitric oxide synthase with the postsynaptic density protein PSD-95 and alpha1-syntrophin mediated by PDZ domains. *Cell* **84**(5): p. 757-767.

28. Brini, M. (2008) Plasma membrane Ca(2+)-ATPase: from a housekeeping function to a versatile signaling role. *Pflugers Arch*.

29. Brown, D.A. and E. London (1998) Functions of lipid rafts in biological membranes. *Annu Rev Cell Dev Biol* **14**: p. 111-136.

30. Brown, D.A. and J.K. Rose (1992) Sorting of GPI-anchored proteins to glycolipid-enriched membrane subdomains during transport to the apical cell surface. *Cell* **68**(3): p. 533-544.

31. Burnstock, G. (2008) Purinergic signalling and disorders of the central nervous system. *Nat Rev Drug Discov* **7**(7): p. 575-590.

32. Cai, X. and J. Lytton (2004) The cation/Ca(2+) exchanger superfamily: phylogenetic analysis and structural implications. *Mol Biol Evol* **21**(9): p. 1692-1703.

33. Cai, X., K. Zhang, and J. Lytton (2002) A novel topology and redox regulation of the rat brain K+-dependent Na+/Ca2+ exchanger, NCKX2. *J Biol Chem* **277**(50): p. 48923-48930.

34. Camors, E., D. Charue, P. Trouve, V. Monceau, X. Loyer, F. Russo-Marie, and D. Charlemagne (2006) Association of annexin A5 with Na+/Ca2+ exchanger and caveolin-3 in non-failing and failing human heart. *J Mol Cell Cardiol* **40**(1): p. 47-55.

35. Catterall, W.A. (2000) Structure and regulation of voltage-gated Ca2+ channels. *Annu Rev Cell Dev Biol* **16**: p. 521-555.

36. Cavalli, A., M. Eghbali, T.Y. Minosyan, E. Stefani, and K.D. Philipson (2007) Localization of sarcolemmal proteins to lipid rafts in the myocardium. *Cell Calcium* **42**(3): p. 313-322.

37. Cervetto, L., L. Lagnado, R.J. Perry, D.W. Robinson, and P.A. McNaughton (1989) Extrusion of calcium from rod outer segments is driven by both sodium and potassium gradients. *Nature* **337**(6209): p. 740-743.

38. Cha, S.H., S.Y. Shin, S.Y. Jung, Y.T. Kim, Y.J. Park, J.O. Kwak, H.W. Kim, and C.K. Suh (2004) Evidence for Na+/Ca2+ exchanger 1 association with caveolin-1 and -2 in C6 glioma cells. *IUBMB Life* **56**(10): p. 621-627.

39. Chakraborti, S., S. Das, P. Kar, B. Ghosh, K. Samanta, S. Kolley, S. Ghosh, S. Roy, and T. Chakraborti (2007) Calcium signaling phenomena in heart diseases: a perspective. *Mol Cell Biochem* **298**(1-2): p. 1-40.

40. Chang, H.W. and E. Bock (1980) Pitfalls in the use of commercial nonionic detergents for the solubilization of integral membrane proteins: sulfhydryl oxidizing contaminants and their elimination. *Anal Biochem* **104**(1): p. 112-117.

41. Chen, H.J., M. Rojas-Soto, A. Oguni, and M.B. Kennedy (1998) A synaptic Ras-GTPase activating protein (p135 SynGAP) inhibited by CaM kinase II. *Neuron* **20**(5): p. 895-904.

42. Chernysh, O., M. Condrescu, and J.P. Reeves (2004) Calcium-dependent regulation of calcium efflux by the cardiac sodium/calcium exchanger. *Am J Physiol Cell Physiol* **287**(3): p. C797-806.

43. Cho, C.H., S.S. Kim, M.J. Jeong, C.O. Lee, and H.S. Shin (2000) The Na+ -Ca2+ exchanger is essential for embryonic heart development in mice. *Mol Cells* **10**(6): p. 712-722.

44. Cho, C.H., S.Y. Lee, H.S. Shin, K.D. Philipson, and C.O. Lee (2003) Partial rescue of the Na+-Ca2+ exchanger (NCX1) knock-out mouse by transgenic expression of NCX1. *Exp Mol Med* **35**(2): p. 125-135.

45. Chun, M., U.K. Liyanage, M.P. Lisanti, and H.F. Lodish (1994) Signal transduction of a G protein-coupled receptor in caveolae: colocalization of endothelin and its receptor with caveolin. *Proc Natl Acad Sci U S A* **91**(24): p. 11728-11732.

46. Churchill, G.C., Y. Okada, J.M. Thomas, A.A. Genazzani, S. Patel, and A. Galione (2002) NAADP mobilizes Ca(2+) from reserve granules, lysosome-related organelles, in sea urchin eggs. *Cell* **111**(5): p. 703-708.

47. Claeys, D., K. Geering, and B.J. Meyer (2005) Two-dimensional Blue Native/sodium dodecyl sulfate gel electrophoresis for analysis of multimeric proteins in platelets. *Electrophoresis* **26**(6): p. 1189-1199.

48. Clapham, D.E., L.W. Runnels, and C. Strubing (2001) The TRP ion channel family. *Nat Rev Neurosci* **2**(6): p. 387-396.

49. Clarke, S. and M.D. Smigel (1989) Size and shape of membrane protein-detergent complexes: hydrodynamic studies. *Methods Enzymol* **172**: p. 696-709.

50. Colbran, R.J. and A.M. Brown (2004) Calcium/calmodulin-dependent protein kinase II and synaptic plasticity. *Curr Opin Neurobiol* **14**(3): p. 318-327.

51. Condrescu, M. and J.P. Reeves (2006) Actin-dependent regulation of the cardiac Na(+)/Ca(2+) exchanger. *Am J Physiol Cell Physiol* **290**(3): p. C691-701.

52. Cook, N.J. and U.B. Kaupp (1988) Solubilization, purification, and reconstitution of the sodium-calcium exchanger from bovine retinal rod outer segments. *J Biol Chem* **263**(23): p. 11382-11388.

53. Crabtree, G.R. (2001) Calcium, calcineurin, and the control of transcription. *J Biol Chem* **276**(4): p. 2313-2316.

54. Cull-Candy, S., S. Brickley, and M. Farrant (2001) NMDA receptor subunits: diversity, development and disease. *Curr Opin Neurobiol* **11**(3): p. 327-335.

55. Cunha, S.R., N. Bhasin, and P.J. Mohler (2007) Targeting and stability of Na/Ca exchanger 1 in cardiomyocytes requires direct interaction with the membrane adaptor ankyrin-B. *J Biol Chem* **282**(7): p. 4875-4883.

56. DeBello, W.M., H. Betz, and G.J. Augustine (1993) Synaptotagmin and neurotransmitter release. *Cell* **74**(6): p. 947-950.

57. Delmas, P. and D.A. Brown (2002) Junctional signaling microdomains: bridging the gap between the neuronal cell surface and Ca2+ stores. *Neuron* **36**(5): p. 787-790.

58. DiPolo, R. (1979) Calcium influx in internally dialyzed squid giant axons. *J Gen Physiol* **73**(1): p. 91-113.

59. DiPolo, R. and L. Beauge (1991) Regulation of Na-Ca exchange. An overview. *Ann N Y Acad Sci* **639**: p. 100-111.

60. Doering, A.E., D.A. Nicoll, Y. Lu, L. Lu, J.N. Weiss, and K.D. Philipson (1998) Topology of a functionally important region of the cardiac Na+/Ca2+ exchanger. *J Biol Chem* **273**(2): p. 778-783.

61. Dong, H., J. Dunn, and J. Lytton (2002) Stoichiometry of the Cardiac Na+/Ca2+ exchanger NCX1.1 measured in transfected HEK cells. *Biophys J* **82**(4): p. 1943-1952.

62. Dong, H., Y. Jiang, C.R. Triggle, X. Li, and J. Lytton (2006) Novel role for K+-dependent Na+/Ca2+ exchangers in regulation of cytoplasmic free Ca2+ and contractility in arterial smooth muscle. *Am J Physiol Heart Circ Physiol* **291**(3): p. H1226-1235.

63. Dong, H., P.E. Light, R.J. French, and J. Lytton (2001) Electrophysiological characterization and ionic stoichiometry of the rat brain K(+)-dependent NA(+)/CA(2+) exchanger, NCKX2. *J Biol Chem* **276**(28): p. 25919-25928.

64. Doyle, D.A., J. Morais Cabral, R.A. Pfuetzner, A. Kuo, J.M. Gulbis, S.L. Cohen, B.T. Chait, and R. MacKinnon (1998) The structure of the potassium channel: molecular basis of K+ conduction and selectivity. *Science* **280**(5360): p. 69-77.

65. Dyck, C., A. Omelchenko, C.L. Elias, B.D. Quednau, K.D. Philipson, M. Hnatowich, and L.V. Hryshko (1999) Ionic regulatory properties of brain and

kidney splice variants of the NCX1 Na(+)-Ca(2+) exchanger. *J Gen Physiol* **114**(5): p. 701-711.

66. Eckert, G.P., U. Igbavboa, W.E. Muller, and W.G. Wood (2003) Lipid rafts of purified mouse brain synaptosomes prepared with or without detergent reveal different lipid and protein domains. *Brain Res* **962**(1-2): p. 144-150.

67. Eilers, J., G.J. Augustine, and A. Konnerth (1995) Subthreshold synaptic Ca2+ signalling in fine dendrites and spines of cerebellar Purkinje neurons. *Nature* **373**(6510): p. 155-158.

68. Evans, R.M. and G.W. Zamponi (2006) Presynaptic Ca2+ channels--integration centers for neuronal signaling pathways. *Trends Neurosci* **29**(11): p. 617-624.

69. Faivre-Sarrailh, C. and G. Rougon (1993) Are the glypiated adhesion molecules preferentially targeted to the axonal compartment? *Mol Neurobiol* **7**(1): p. 49-60.

70. Fallon, L., F. Moreau, B.G. Croft, N. Labib, W.J. Gu, and E.A. Fon (2002) Parkin and CASK/LIN-2 associate via a PDZ-mediated interaction and are co-localized in lipid rafts and postsynaptic densities in brain. *J Biol Chem* **277**(1): p. 486-491.

71. Fill, M. and J.A. Copello (2002) Ryanodine receptor calcium release channels. *Physiol Rev* **82**(4): p. 893-922.

72. Flesch, M., R.H. Schwinger, F. Schiffer, K. Frank, M. Sudkamp, F. Kuhn-Regnier, G. Arnold, and M. Bohm (1996) Evidence for functional relevance of an enhanced expression of the Na(+)-Ca2+ exchanger in failing human myocardium. *Circulation* **94**(5): p. 992-1002.

73. Foskett, J.K., C. White, K.H. Cheung, and D.O. Mak (2007) Inositol trisphosphate receptor Ca2+ release channels. *Physiol Rev* **87**(2): p. 593-658.

74. Fra, A.M., M. Masserini, P. Palestini, S. Sonnino, and K. Simons (1995) A photo-reactive derivative of ganglioside GM1 specifically cross-links VIP21-caveolin on the cell surface. *FEBS Lett* **375**(1-2): p. 11-14.

75. Frank, J.S., G. Mottino, D. Reid, R.S. Molday, and K.D. Philipson (1992) Distribution of the Na(+)-Ca2+ exchange protein in mammalian cardiac myocytes: an immunofluorescence and immunocolloidal gold-labeling study. *J Cell Biol* **117**(2): p. 337-345.

76. Frank, K.F., B. Bolck, E. Erdmann, and R.H. Schwinger (2003) Sarcoplasmic reticulum Ca2+-ATPase modulates cardiac contraction and relaxation. *Cardiovasc Res* **57**(1): p. 20-27.

77. Fujimoto, T. (1993) Calcium pump of the plasma membrane is localized in caveolae. *J Cell Biol* **120**(5): p. 1147-1157.

78. Fujimoto, T., S. Nakade, A. Miyawaki, K. Mikoshiba, and K. Ogawa (1992) Localization of inositol 1,4,5-trisphosphate receptor-like protein in plasmalemmal caveolae. *J Cell Biol* **119**(6): p. 1507-1513.

79. Fujioka, Y., M. Komeda, and S. Matsuoka (2000) Stoichiometry of Na+-Ca2+ exchange in inside-out patches excised from guinea-pig ventricular myocytes. *J Physiol* **523 Pt 2**: p. 339-351.

80. Furman, I., O. Cook, J. Kasir, W. Low, and H. Rahamimoff (1995) The putative amino-terminal signal peptide of the cloned rat brain Na(+)-Ca2+ exchanger gene (RBE-1) is not mandatory for functional expression. *J Biol Chem* **270**(32): p. 19120-19127.

81. Gabellini, N., S. Bortoluzzi, G.A. Danieli, and E. Carafoli (2002) The human SLC8A3 gene and the tissue-specific Na+/Ca2+ exchanger 3 isoforms. *Gene* **298**(1): p. 1-7.

82. Galbiati, F., B. Razani, and M.P. Lisanti (2001) Emerging themes in lipid rafts and caveolae. *Cell* **106**(4): p. 403-411.

83. Galbiati, F., D. Volonte, O. Gil, G. Zanazzi, J.L. Salzer, M. Sargiacomo, P.E. Scherer, J.A. Engelman, A. Schlegel, M. Parenti, T. Okamoto, and M.P. Lisanti (1998) Expression of caveolin-1 and -2 in differentiating PC12 cells and dorsal root ganglion neurons: caveolin-2 is up-regulated in response to cell injury. *Proc Natl Acad Sci U S A* **95**(17): p. 10257-10262.

84. Garcia-Cardena, G., P. Martasek, B.S. Masters, P.M. Skidd, J. Couet, S. Li, M.P. Lisanti, and W.C. Sessa (1997) Dissecting the interaction between nitric oxide synthase (NOS) and caveolin. Functional significance of the nos caveolin binding domain in vivo. *J Biol Chem* **272**(41): p. 25437-25440.

85. Garcia-Cardena, G., P. Oh, J. Liu, J.E. Schnitzer, and W.C. Sessa (1996) Targeting of nitric oxide synthase to endothelial cell caveolae via palmitoylation: implications for nitric oxide signaling. *Proc Natl Acad Sci U S A* **93**(13): p. 6448-6453.

86. Garner, A.E., D.A. Smith, and N.M. Hooper (2008) Visualization of detergent solubilization of membranes: implications for the isolation of rafts. *Biophys J* **94**(4): p. 1326-1340.

87. Garty, H. and S.J. Karlish (2006) Role of FXYD proteins in ion transport. *Annu Rev Physiol* **68**: p. 431-459.

88. Gaudreault, S.B., C. Chabot, J.P. Gratton, and J. Poirier (2004) The caveolin scaffolding domain modifies 2-amino-3-hydroxy-5-methyl-4-isoxazole propionate receptor binding properties by inhibiting phospholipase A2 activity. *J Biol Chem* **279**(1): p. 356-362.

89. Gerrow, K., S. Romorini, S.M. Nabi, M.A. Colicos, C. Sala, and A. El-Husseini (2006) A preformed complex of postsynaptic proteins is involved in excitatory synapse development. *Neuron* **49**(4): p. 547-562.

90. Gifford, J.L., M.P. Walsh, and H.J. Vogel (2007) Structures and metal-ion-binding properties of the Ca2+-binding helix-loop-helix EF-hand motifs. *Biochem J* **405**(2): p. 199-221.

91. Ginger, R.S., S.E. Askew, R.M. Ogborne, S. Wilson, D. Ferdinando, T. Dadd, A.M. Smith, S. Kazi, R.T. Szerencsei, R.J. Winkfein, P.P. Schnetkamp, and M.R. Green (2008) SLC24A5 encodes a trans-Golgi network protein with potassium-dependent sodium-calcium exchange activity that regulates human epidermal melanogenesis. *J Biol Chem*.

92. Giraudo, C.G., W.S. Eng, T.J. Melia, and J.E. Rothman (2006) A clamping mechanism involved in SNARE-dependent exocytosis. *Science* **313**(5787): p. 676-680.

93. Glenney, J.R., Jr. and D. Soppet (1992) Sequence and expression of caveolin, a protein component of caveolae plasma membrane domains phosphorylated on tyrosine in Rous sarcoma virus-transformed fibroblasts. *Proc Natl Acad Sci U S A* **89**(21): p. 10517-10521.

94. Gouaux, E. and R. Mackinnon (2005) Principles of selective ion transport in channels and pumps. *Science* **310**(5753): p. 1461-1465.

95. Gratton, J.P., P. Bernatchez, and W.C. Sessa (2004) Caveolae and caveolins in the cardiovascular system. *Circ Res* **94**(11): p. 1408-1417.

96. Groenendyk, J., J. Lynch, and M. Michalak (2004) Calreticulin, Ca2+, and calcineurin - signaling from the endoplasmic reticulum. *Mol Cells* **17**(3): p. 383-389.

97. Hartmann, J. and A. Konnerth (2005) Determinants of postsynaptic Ca2+ signaling in Purkinje neurons. *Cell Calcium* **37**(5): p. 459-466.

98. He, Z., S. Feng, Q. Tong, D.W. Hilgemann, and K.D. Philipson (2000) Interaction of PIP(2) with the XIP region of the cardiac Na/Ca exchanger. *Am J Physiol Cell Physiol* **278**(4): p. C661-666.

99. Head, B.P., H.H. Patel, D.M. Roth, N.C. Lai, I.R. Niesman, M.G. Farquhar, and P.A. Insel (2005) G-protein-coupled receptor signaling components localize in both sarcolemmal and intracellular caveolin-3-associated microdomains in adult cardiac myocytes. *J Biol Chem* **280**(35): p. 31036-31044.

100. Heerklotz, H. (2002) Triton promotes domain formation in lipid raft mixtures. *Biophys J* **83**(5): p. 2693-2701.

101. Heerklotz, H., H. Szadkowska, T. Anderson, and J. Seelig (2003) The sensitivity of lipid domains to small perturbations demonstrated by the effect of Triton. *J Mol Biol* **329**(4): p. 793-799.

102. Henderson, S.A., J.I. Goldhaber, J.M. So, T. Han, C. Motter, A. Ngo, C. Chantawansri, M.R. Ritter, M. Friedlander, D.A. Nicoll, J.S. Frank, M.C. Jordan,

K.P. Roos, R.S. Ross, and K.D. Philipson (2004) Functional adult myocardium in the absence of Na+-Ca2+ exchange: cardiac-specific knockout of NCX1. *Circ Res* **95**(6): p. 604-611.

103. Hering, H., C.C. Lin, and M. Sheng (2003) Lipid rafts in the maintenance of synapses, dendritic spines, and surface AMPA receptor stability. *J Neurosci* **23**(8): p. 3262-3271.

104. Heuberger, E.H., L.M. Veenhoff, R.H. Duurkens, R.H. Friesen, and B. Poolman (2002) Oligomeric state of membrane transport proteins analyzed with blue native electrophoresis and analytical ultracentrifugation. *J Mol Biol* **317**(4): p. 591-600.

105. Hewavitharana, T., X. Deng, J. Soboloff, and D.L. Gill (2007) Role of STIM and Orai proteins in the store-operated calcium signaling pathway. *Cell Calcium* **42**(2): p. 173-182.

106. Hilge, M., J. Aelen, and G.W. Vuister (2006) Ca2+ regulation in the Na+/Ca2+ exchanger involves two markedly different Ca2+ sensors. *Mol Cell* **22**(1): p. 15-25.

107. Hilgemann, D.W. (1989) Giant excised cardiac sarcolemmal membrane patches: sodium and sodium-calcium exchange currents. *Pflugers Arch* **415**(2): p. 247-249.

108. Hilgemann, D.W. (1990) Regulation and deregulation of cardiac Na(+)-Ca2+ exchange in giant excised sarcolemmal membrane patches. *Nature* **344**(6263): p. 242-245.

109. Hilgemann, D.W. and R. Ball (1996) Regulation of cardiac Na+,Ca2+ exchange and KATP potassium channels by PIP2. *Science* **273**(5277): p. 956-959.

110. Hilgemann, D.W., A. Collins, and S. Matsuoka (1992) Steady-state and dynamic properties of cardiac sodium-calcium exchange. Secondary modulation by cytoplasmic calcium and ATP. *J Gen Physiol* **100**(6): p. 933-961.

111. Hilgemann, D.W., S. Matsuoka, G.A. Nagel, and A. Collins (1992) Steady-state and dynamic properties of cardiac sodium-calcium exchange. Sodium-dependent inactivation. *J Gen Physiol* **100**(6): p. 905-932.

112. Hirota, S., E. Pertens, and L.J. Janssen (2007) The reverse mode of the Na(+)/Ca(2+) exchanger provides a source of Ca(2+) for store refilling following agonist-induced Ca(2+) mobilization. *Am J Physiol Lung Cell Mol Physiol* **292**(2): p. L438-447.

113. Hooper, N.M. (1999) Detergent-insoluble glycosphingolipid/cholesterol-rich membrane domains, lipid rafts and caveolae (review). *Mol Membr Biol* **16**(2): p. 145-156.

114. Hryshko, L.V., S. Matsuoka, D.A. Nicoll, J.N. Weiss, E.M. Schwarz, S. Benzer, and K.D. Philipson (1996) Anomalous regulation of the Drosophila Na(+)-Ca2+ exchanger by Ca2+. *J Gen Physiol* **108**(1): p. 67-74.

115. Hryshko, L.V. and K.D. Philipson (1997) Sodium-calcium exchange: recent advances. *Basic Res Cardiol* **92 Suppl 1**: p. 45-51.

116. Hussl, S. and S. Boehm (2006) Functions of neuronal P2Y receptors. *Pflugers Arch* **452**(5): p. 538-551.

117. Ikezu, T., H. Ueda, B.D. Trapp, K. Nishiyama, J.F. Sha, D. Volonte, F. Galbiati, A.L. Byrd, G. Bassell, H. Serizawa, W.S. Lane, M.P. Lisanti, and T. Okamoto (1998) Affinity-purification and characterization of caveolins from the brain:

differential expression of caveolin-1, -2, and -3 in brain endothelial and astroglial cell types. *Brain Res* **804**(2): p. 177-192.

118. Isshiki, M. and R.G. Anderson (2003) Function of caveolae in Ca2+ entry and Ca2+-dependent signal transduction. *Traffic* **4**(11): p. 717-723.

119. Iwamoto, T., S. Kita, J. Zhang, M.P. Blaustein, Y. Arai, S. Yoshida, K. Wakimoto, I. Komuro, and T. Katsuragi (2004) Salt-sensitive hypertension is triggered by Ca2+ entry via Na+/Ca2+ exchanger type-1 in vascular smooth muscle. *Nat Med* **10**(11): p. 1193-1199.

120. Iwamoto, T., T.Y. Nakamura, Y. Pan, A. Uehara, I. Imanaga, and M. Shigekawa (1999) Unique topology of the internal repeats in the cardiac Na+/Ca2+ exchanger. *FEBS Lett* **446**(2-3): p. 264-268.

121. Iwamoto, T., A. Uehara, I. Imanaga, and M. Shigekawa (2000) The Na+/Ca2+ exchanger NCX1 has oppositely oriented reentrant loop domains that contain conserved aspartic acids whose mutation alters its apparent Ca2+ affinity. *J Biol Chem* **275**(49): p. 38571-38580.

122. Jaunin, P., F. Jaisser, A.T. Beggah, K. Takeyasu, P. Mangeat, B.C. Rossier, J.D. Horisberger, and K. Geering (1993) Role of the transmembrane and extracytoplasmic domain of beta subunits in subunit assembly, intracellular transport, and functional expression of Na,K-pumps. *J Cell Biol* **123**(6 Pt 2): p. 1751-1759.

123. Jeon, D., Y.M. Yang, M.J. Jeong, K.D. Philipson, H. Rhim, and H.S. Shin (2003) Enhanced learning and memory in mice lacking Na+/Ca2+ exchanger 2. *Neuron* **38**(6): p. 965-976.

124. Jones, S.W. (1998) Overview of voltage-dependent calcium channels. *J Bioenerg Biomembr* **30**(4): p. 299-312.

125. Jorgensen, A.O., A.C. Shen, W. Arnold, A.T. Leung, and K.P. Campbell (1989) Subcellular distribution of the 1,4-dihydropyridine receptor in rabbit skeletal muscle in situ: an immunofluorescence and immunocolloidal gold-labeling study. *J Cell Biol* **109**(1): p. 135-147.

126. Kang, K., P.J. Bauer, T.G. Kinjo, R.T. Szerencsei, W. Bonigk, R.J. Winkfein, and P.P. Schnetkamp (2003) Assembly of retinal rod or cone Na(+)/Ca(2+)-K(+) exchanger oligomers with cGMP-gated channel subunits as probed with heterologously expressed cDNAs. *Biochemistry* **42**(15): p. 4593-4600.

127. Kang, K. and P.P. Schnetkamp (2003) Signal sequence cleavage and plasma membrane targeting of the retinal rod NCKX1 and cone NCKX2 Na+/Ca2+ - K+ exchangers. *Biochemistry* **42**(31): p. 9438-9445.

128. Kang, K.J., T.G. Kinjo, R.T. Szerencsei, and P.P. Schnetkamp (2005) Residues contributing to the Ca2+ and K+ binding pocket of the NCKX2 Na+/Ca2+-K+ exchanger. *J Biol Chem* **280**(8): p. 6823-6833.

129. Kang, K.J., Y. Shibukawa, R.T. Szerencsei, and P.P. Schnetkamp (2005) Substitution of a single residue, Asp575, renders the NCKX2 K+-dependent Na+/Ca2+ exchanger independent of K+. *J Biol Chem* **280**(8): p. 6834-6839.

130. Kang, T.M. and D.W. Hilgemann (2004) Multiple transport modes of the cardiac Na+/Ca2+ exchanger. *Nature* **427**(6974): p. 544-548.

131. Katanosaka, Y., Y. Iwata, Y. Kobayashi, F. Shibasaki, S. Wakabayashi, and M. Shigekawa (2005) Calcineurin inhibits Na+/Ca2+ exchange in phenylephrine-treated hypertrophic cardiomyocytes. *J Biol Chem* **280**(7): p. 5764-5772.

132. Kennedy, M.B. (2000) Signal-processing machines at the postsynaptic density. *Science* **290**(5492): p. 750-754.

133. Kepner, G.R. and R.I. Macey (1968) Membrane enzyme systems. Molecular size determinations by radiation inactivation. *Biochim Biophys Acta* **163**(2): p. 188-203.

134. Kiedrowski, L. (2004) High activity of K+-dependent plasmalemmal Na+/Ca2+ exchangers in hippocampal CA1 neurons. *Neuroreport* **15**(13): p. 2113-2116.

135. Kiedrowski, L., A. Czyz, G. Baranauskas, X.F. Li, and J. Lytton (2004) Differential contribution of plasmalemmal Na/Ca exchange isoforms to sodium-dependent calcium influx and NMDA excitotoxicity in depolarized neurons. *J Neurochem* **90**(1): p. 117-128.

136. Kikuno, R., T. Nagase, K. Ishikawa, M. Hirosawa, N. Miyajima, A. Tanaka, H. Kotani, N. Nomura, and O. Ohara (1999) Prediction of the coding sequences of unidentified human genes. XIV. The complete sequences of 100 new cDNA clones from brain which code for large proteins in vitro. *DNA Res* **6**(3): p. 197-205.

137. Kim, E. and M. Sheng (2004) PDZ domain proteins of synapses. *Nat Rev Neurosci* **5**(10): p. 771-781.

138. Kim, J.H., D. Liao, L.F. Lau, and R.L. Huganir (1998) SynGAP: a synaptic RasGAP that associates with the PSD-95/SAP90 protein family. *Neuron* **20**(4): p. 683-691.

139. Kim, M.H., N. Korogod, R. Schneggenburger, W.K. Ho, and S.H. Lee (2005) Interplay between Na+/Ca2+ exchangers and mitochondria in Ca2+ clearance at the calyx of Held. *J Neurosci* **25**(26): p. 6057-6065.

140. Kim, M.H., S.H. Lee, K.H. Park, W.K. Ho, and S.H. Lee (2003) Distribution of K+-dependent Na+/Ca2+ exchangers in the rat supraoptic magnocellular neuron is polarized to axon terminals. *J Neurosci* **23**(37): p. 11673-11680.

141. Kinjo, T.G., K. Kang, R.T. Szerencsei, R.J. Winkfein, and P.P. Schnetkamp (2005) Site-directed disulfide mapping of residues contributing to the Ca2+ and K+ binding pocket of the NCKX2 Na+/Ca2+-K+ exchanger. *Biochemistry* **44**(21): p. 7787-7795.

142. Kinjo, T.G., R.T. Szerencsei, and P.P. Schnetkamp (2007) Topologic investigation of the NCKX2 Na+/Ca2+-K+ exchanger alpha-repeats. *Ann N Y Acad Sci* **1099**: p. 34-39.

143. Kinjo, T.G., R.T. Szerencsei, R.J. Winkfein, K. Kang, and P.P. Schnetkamp (2003) Topology of the retinal cone NCKX2 Na/Ca-K exchanger. *Biochemistry* **42**(8): p. 2485-2491.

144. Kinjo, T.G., R.T. Szerencsei, R.J. Winkfein, and P.P. Schnetkamp (2004) Role of cysteine residues in the NCKX2 Na+/Ca(2+)-K+ Exchanger: generation of a functional cysteine-free exchanger. *Biochemistry* **43**(24): p. 7940-7947.

145. Kofuji, P., R.W. Hadley, R.S. Kieval, W.J. Lederer, and D.H. Schulze (1992) Expression of the Na-Ca exchanger in diverse tissues: a study using the cloned human cardiac Na-Ca exchanger. *Am J Physiol* **263**(6 Pt 1): p. C1241-1249.

146. Kofuji, P., W.J. Lederer, and D.H. Schulze (1994) Mutually exclusive and cassette exons underlie alternatively spliced isoforms of the Na/Ca exchanger. *J Biol Chem* **269**(7): p. 5145-5149.

147. Koles, L., S. Furst, and P. Illes (2007) Purine ionotropic (P2X) receptors. *Curr Pharm Des* **13**(23): p. 2368-2384.

148. Kolonin, M.G., P.K. Saha, L. Chan, R. Pasqualini, and W. Arap (2004) Reversal of obesity by targeted ablation of adipose tissue. *Nat Med* **10**(6): p. 625-632.

149. Komuro, I., K.E. Wenninger, K.D. Philipson, and S. Izumo (1992) Molecular cloning and characterization of the human cardiac Na+/Ca2+ exchanger cDNA. *Proc Natl Acad Sci U S A* **89**(10): p. 4769-4773.

150. Konnerth, A., J. Dreessen, and G.J. Augustine (1992) Brief dendritic calcium signals initiate long-lasting synaptic depression in cerebellar Purkinje cells. *Proc Natl Acad Sci U S A* **89**(15): p. 7051-7055.

151. Kornau, H.C., L.T. Schenker, M.B. Kennedy, and P.H. Seeburg (1995) Domain interaction between NMDA receptor subunits and the postsynaptic density protein PSD-95. *Science* **269**(5231): p. 1737-1740.

152. Koushik, S.V., J. Wang, R. Rogers, D. Moskophidis, N.A. Lambert, T.L. Creazzo, and S.J. Conway (2001) Targeted inactivation of the sodium-calcium exchanger (Ncx1) results in the lack of a heartbeat and abnormal myofibrillar organization. *Faseb J* **15**(7): p. 1209-1211.

153. Kraev, A., I. Chumakov, and E. Carafoli (1996) The organization of the human gene NCX1 encoding the sodium-calcium exchanger. *Genomics* **37**(1): p. 105-112.

154. Kraev, A., B.D. Quednau, S. Leach, X.F. Li, H. Dong, R. Winkfein, M. Perizzolo, X. Cai, R. Yang, K.D. Philipson, and J. Lytton (2001) Molecular cloning of a third member of the potassium-dependent sodium-calcium exchanger gene family, NCKX3. *J Biol Chem* **276**(25): p. 23161-23172.

155. Kurzchalia, T.V., P. Dupree, R.G. Parton, R. Kellner, H. Virta, M. Lehnert, and K. Simons (1992) VIP21, a 21-kD membrane protein is an integral component of trans-Golgi-network-derived transport vesicles. *J Cell Biol* **118**(5): p. 1003-1014.

156. Lamason, R.L., M.A. Mohideen, J.R. Mest, A.C. Wong, H.L. Norton, M.C. Aros, M.J. Jurynec, X. Mao, V.R. Humphreville, J.E. Humbert, S. Sinha, J.L. Moore, P. Jagadeeswaran, W. Zhao, G. Ning, I. Makalowska, P.M. McKeigue, D. O'Donnell, R. Kittles, E.J. Parra, N.J. Mangini, D.J. Grunwald, M.D. Shriver, V.A. Canfield, and K.C. Cheng (2005) SLC24A5, a putative cation exchanger, affects pigmentation in zebrafish and humans. *Science* **310**(5755): p. 1782-1786.

157. Ledesma, M.D., B. Brugger, C. Bunning, F.T. Wieland, and C.G. Dotti (1999) Maturation of the axonal plasma membrane requires upregulation of sphingomyelin synthesis and formation of protein-lipid complexes. *Embo J* **18**(7): p. 1761-1771.

158. Ledesma, M.D., K. Simons, and C.G. Dotti (1998) Neuronal polarity: essential role of protein-lipid complexes in axonal sorting. *Proc Natl Acad Sci U S A* **95**(7): p. 3966-3971.

159. Ledvora, R.F. and C. Hegyvary (1983) Dependence of Na+-Ca2+ exchange and Ca2+-Ca2+ exchange on monovalent cations. *Biochim Biophys Acta* **729**(1): p. 123-136.

160. Lee, J.Y., F. Visser, J.S. Lee, K.H. Lee, J.W. Soh, W.K. Ho, J. Lytton, and S.H. Lee (2006) Protein kinase C-dependent enhancement of activity of rat brain NCKX2 heterologously expressed in HEK293 cells. *J Biol Chem* **281**(51): p. 39205-39216.

161. Lee, S.H., M.H. Kim, K.H. Park, Y.E. Earm, and W.K. Ho (2002) K+-dependent Na+/Ca2+ exchange is a major Ca2+ clearance mechanism in axon terminals of rat neurohypophysis. *J Neurosci* **22**(16): p. 6891-6899.

162. Lee, S.L., A.S. Yu, and J. Lytton (1994) Tissue-specific expression of Na(+)-Ca2+ exchanger isoforms. *J Biol Chem* **269**(21): p. 14849-14852.

163. Lemos, V.S., D. Poburko, C.H. Liao, W.C. Cole, and C. van Breemen (2007) Na+ entry via TRPC6 causes Ca2+ entry via NCX reversal in ATP stimulated smooth muscle cells. *Biochem Biophys Res Commun* **352**(1): p. 130-134.

164. Leonard, A.S., I.A. Lim, D.E. Hemsworth, M.C. Horne, and J.W. Hell (1999) Calcium/calmodulin-dependent protein kinase II is associated with the N-methyl-D-aspartate receptor. *Proc Natl Acad Sci U S A* **96**(6): p. 3239-3244.

165. Levitsky, D.O., D.A. Nicoll, and K.D. Philipson (1994) Identification of the high affinity Ca(2+)-binding domain of the cardiac Na(+)-Ca2+ exchanger. *J Biol Chem* **269**(36): p. 22847-22852.

166. Lewis, R.S. (2007) The molecular choreography of a store-operated calcium channel. *Nature* **446**(7133): p. 284-287.

167. Li, S., K.S. Song, and M.P. Lisanti (1996) Expression and characterization of recombinant caveolin. Purification by polyhistidine tagging and cholesterol-dependent incorporation into defined lipid membranes. *J Biol Chem* **271**(1): p. 568-573.

168. Li, X.F., L. Kiedrowski, F. Tremblay, F.R. Fernandez, M. Perizzolo, R.J. Winkfein, R.W. Turner, J.S. Bains, D.E. Rancourt, and J. Lytton (2006) Importance of K+-dependent Na+/Ca2+-exchanger 2, NCKX2, in motor learning and memory. *J Biol Chem* **281**(10): p. 6273-6282.

169. Li, X.F., A.S. Kraev, and J. Lytton (2002) Molecular cloning of a fourth member of the potassium-dependent sodium-calcium exchanger gene family, NCKX4. *J Biol Chem* **277**(50): p. 48410-48417.

170. Li, X.F. and J. Lytton (1999) A circularized sodium-calcium exchanger exon 2 transcript. *J Biol Chem* **274**(12): p. 8153-8160.

171. Li, Z., S. Matsuoka, L.V. Hryshko, D.A. Nicoll, M.M. Bersohn, E.P. Burke, R.P. Lifton, and K.D. Philipson (1994) Cloning of the NCX2 isoform of the plasma membrane Na(+)-Ca2+ exchanger. *J Biol Chem* **269**(26): p. 17434-17439.

172. Li, Z., D.A. Nicoll, A. Collins, D.W. Hilgemann, A.G. Filoteo, J.T. Penniston, J.N. Weiss, J.M. Tomich, and K.D. Philipson (1991) Identification of a peptide inhibitor of the cardiac sarcolemmal Na(+)-Ca2+ exchanger. *J Biol Chem* **266**(2): p. 1014-1020.

173. Li, Z.P., E.P. Burke, J.S. Frank, V. Bennett, and K.D. Philipson (1993) The cardiac Na+-Ca2+ exchanger binds to the cytoskeletal protein ankyrin. *J Biol Chem* **268**(16): p. 11489-11491.

174. Lisanti, M.P., P.E. Scherer, J. Vidugiriene, Z. Tang, A. Hermanowski-Vosatka, Y.H. Tu, R.F. Cook, and M. Sargiacomo (1994) Characterization of caveolin-rich membrane domains isolated from an endothelial-rich source: implications for human disease. *J Cell Biol* **126**(1): p. 111-126.

175. Lisman, J.E., S. Raghavachari, and R.W. Tsien (2007) The sequence of events that underlie quantal transmission at central glutamatergic synapses. *Nat Rev Neurosci* **8**(8): p. 597-609.

176. Liu, L., K. Mohammadi, B. Aynafshar, H. Wang, D. Li, J. Liu, A.V. Ivanov, Z. Xie, and A. Askari (2003) Role of caveolae in signal-transducing function of cardiac Na+/K+-ATPase. *Am J Physiol Cell Physiol* **284**(6): p. C1550-1560.

177. Lockwich, T.P., X. Liu, B.B. Singh, J. Jadlowiec, S. Weiland, and I.S. Ambudkar (2000) Assembly of Trp1 in a signaling complex associated with caveolin-scaffolding lipid raft domains. *J Biol Chem* **275**(16): p. 11934-11942.

178. Loo, T.W., C. Ho, and D.M. Clarke (1995) Expression of a functionally active human renal sodium-calcium exchanger lacking a signal sequence. *J Biol Chem* **270**(33): p. 19345-19350.

179. Lorin-Nebel, C., J. Xing, X. Yan, and K. Strange (2007) CRAC channel activity in C. elegans is mediated by Orai1 and STIM1 homologues and is essential for ovulation and fertility. *J Physiol* **580**(Pt 1): p. 67-85.

180. Lorincz, A., B. Rozsa, G. Katona, E.S. Vizi, and G. Tamas (2007) Differential distribution of NCX1 contributes to spine-dendrite compartmentalization in CA1 pyramidal cells. *Proc Natl Acad Sci U S A* **104**(3): p. 1033-1038.

181. Lytton, J. (2007) Na+/Ca2+ exchangers: three mammalian gene families control Ca2+ transport. *Biochem J* **406**(3): p. 365-382.

182. Lytton, J., X.F. Li, H. Dong, and A. Kraev (2002) K+-dependent Na+/Ca2+ exchangers in the brain. *Ann N Y Acad Sci* **976**: p. 382-393.

183. MacKinnon, R. (2003) Potassium channels. *FEBS Lett* **555**(1): p. 62-65.

184. Marban, E. (2002) Cardiac channelopathies. *Nature* **415**(6868): p. 213-218.

185. Maruyama, K. and D.H. MacLennan (1988) Mutation of aspartic acid-351, lysine-352, and lysine-515 alters the Ca2+ transport activity of the Ca2+-ATPase expressed in COS-1 cells. *Proc Natl Acad Sci U S A* **85**(10): p. 3314-3318.

186. Masserini, M., P. Palestini, and M. Pitto (1999) Glycolipid-enriched caveolae and caveolae-like domains in the nervous system. *J Neurochem* **73**(1): p. 1-11.

187. Matsuoka, S., D.A. Nicoll, Z. He, and K.D. Philipson (1997) Regulation of cardiac Na(+)-Ca2+ exchanger by the endogenous XIP region. *J Gen Physiol* **109**(2): p. 273-286.

188. Matsuoka, S., D.A. Nicoll, L.V. Hryshko, D.O. Levitsky, J.N. Weiss, and K.D. Philipson (1995) Regulation of the cardiac Na(+)-Ca2+ exchanger by Ca2+. Mutational analysis of the Ca(2+)-binding domain. *J Gen Physiol* **105**(3): p. 403-420.

189. Matsuoka, S., D.A. Nicoll, R.F. Reilly, D.W. Hilgemann, and K.D. Philipson (1993) Initial localization of regulatory regions of the cardiac sarcolemmal Na(+)-Ca2+ exchanger. *Proc Natl Acad Sci U S A* **90**(9): p. 3870-3874.

190. McClung, J.K., D.B. Danner, D.A. Stewart, J.R. Smith, E.L. Schneider, C.K. Lumpkin, R.T. Dell'Orco, and M.J. Nuell (1989) Isolation of a cDNA that hybrid

selects antiproliferative mRNA from rat liver. *Biochem Biophys Res Commun* **164**(3): p. 1316-1322.

191. Melkonian, K.A., T. Chu, L.B. Tortorella, and D.A. Brown (1995) Characterization of proteins in detergent-resistant membrane complexes from Madin-Darby canine kidney epithelial cells. *Biochemistry* **34**(49): p. 16161-16170.

192. Mikoshiba, K. (2007) IP3 receptor/Ca2+ channel: from discovery to new signaling concepts. *J Neurochem* **102**(5): p. 1426-1446.

193. Mishra, S., L.C. Murphy, and L.J. Murphy (2006) The Prohibitins: emerging roles in diverse functions. *J Cell Mol Med* **10**(2): p. 353-363.

194. Mohler, P.J., J.Q. Davis, and V. Bennett (2005) Ankyrin-B coordinates the Na/K ATPase, Na/Ca exchanger, and InsP3 receptor in a cardiac T-tubule/SR microdomain. *PLoS Biol* **3**(12): p. e423.

195. Montell, C. (2005) The TRP superfamily of cation channels. *Sci STKE* **2005**(272): p. re3.

196. Moore, E.D., E.F. Etter, K.D. Philipson, W.A. Carrington, K.E. Fogarty, L.M. Lifshitz, and F.S. Fay (1993) Coupling of the Na+/Ca2+ exchanger, Na+/K+ pump and sarcoplasmic reticulum in smooth muscle. *Nature* **365**(6447): p. 657-660.

197. Morrow, I.C. and R.G. Parton (2005) Flotillins and the PHB domain protein family: rafts, worms and anaesthetics. *Traffic* **6**(9): p. 725-740.

198. Morrow, I.C., S. Rea, S. Martin, I.A. Prior, R. Prohaska, J.F. Hancock, D.E. James, and R.G. Parton (2002) Flotillin-1/reggie-2 traffics to surface raft domains

via a novel golgi-independent pathway. Identification of a novel membrane targeting domain and a role for palmitoylation. *J Biol Chem* **277**(50): p. 48834-48841.

199. Munro, S. (2003) Lipid rafts: elusive or illusive? *Cell* **115**(4): p. 377-388.

200. Murata, K., K. Mitsuoka, T. Hirai, T. Walz, P. Agre, J.B. Heymann, A. Engel, and Y. Fujiyoshi (2000) Structural determinants of water permeation through aquaporin-1. *Nature* **407**(6804): p. 599-605.

201. Nazer, M.A. and C. van Breemen (1998) Functional linkage of Na(+)-Ca2+ exchange and sarcoplasmic reticulum Ca2+ release mediates Ca2+ cycling in vascular smooth muscle. *Cell Calcium* **24**(4): p. 275-283.

202. Nicholas, S.B., W. Yang, S.L. Lee, H. Zhu, K.D. Philipson, and J. Lytton (1998) Alternative promoters and cardiac muscle cell-specific expression of the Na+/Ca2+ exchanger gene. *Am J Physiol* **274**(1 Pt 2): p. H217-232.

203. Nicoll, D.A., L.V. Hryshko, S. Matsuoka, J.S. Frank, and K.D. Philipson (1996) Mutagenesis studies of the cardiac Na(+)-Ca2+ exchanger. *Ann N Y Acad Sci* **779**: p. 86-92.

204. Nicoll, D.A., L.V. Hryshko, S. Matsuoka, J.S. Frank, and K.D. Philipson (1996) Mutation of amino acid residues in the putative transmembrane segments of the cardiac sarcolemmal Na+-Ca2+ exchanger. *J Biol Chem* **271**(23): p. 13385-13391.

205. Nicoll, D.A., S. Longoni, and K.D. Philipson (1990) Molecular cloning and functional expression of the cardiac sarcolemmal Na(+)-Ca2+ exchanger. *Science* **250**(4980): p. 562-565.

206. Nicoll, D.A., M. Ottolia, L. Lu, Y. Lu, and K.D. Philipson (1999) A new topological model of the cardiac sarcolemmal Na+-Ca2+ exchanger. *J Biol Chem* **274**(2): p. 910-917.

207. Nicoll, D.A. and K.D. Philipson (1991) Molecular studies of the cardiac sarcolemmal sodium-calcium exchanger. *Ann N Y Acad Sci* **639**: p. 181-188.

208. Nicoll, D.A., X. Ren, M. Ottolia, M. Phillips, A.R. Paredes, J. Abramson, and K.D. Philipson (2007) What we know about the structure of NCX1 and how it relates to its function. *Ann N Y Acad Sci* **1099**: p. 1-6.

209. Nicoll, D.A., M.R. Sawaya, S. Kwon, D. Cascio, K.D. Philipson, and J. Abramson (2006) The crystal structure of the primary Ca2+ sensor of the Na+/Ca2+ exchanger reveals a novel Ca2+ binding motif. *J Biol Chem* **281**(31): p. 21577-21581.

210. Niethammer, M., E. Kim, and M. Sheng (1996) Interaction between the C terminus of NMDA receptor subunits and multiple members of the PSD-95 family of membrane-associated guanylate kinases. *J Neurosci* **16**(7): p. 2157-2163.

211. Nilius, B. (2004) Store-operated Ca2+ entry channels: still elusive! *Sci STKE* **2004**(243): p. pe36.

212. Nilius, B., G. Owsianik, T. Voets, and J.A. Peters (2007) Transient receptor potential cation channels in disease. *Physiol Rev* **87**(1): p. 165-217.

213. North, R.A. and A. Verkhratsky (2006) Purinergic transmission in the central nervous system. *Pflugers Arch* **452**(5): p. 479-485.

214. Nuell, M.J., D.A. Stewart, L. Walker, V. Friedman, C.M. Wood, G.A. Owens, J.R. Smith, E.L. Schneider, R. Dell' Orco, C.K. Lumpkin, and et al. (1991) Prohibitin, an evolutionarily conserved intracellular protein that blocks DNA synthesis in normal fibroblasts and HeLa cells. *Mol Cell Biol* **11**(3): p. 1372-1381.

215. O'Rourke, B., D.A. Kass, G.F. Tomaselli, S. Kaab, R. Tunin, and E. Marban (1999) Mechanisms of altered excitation-contraction coupling in canine tachycardia-induced heart failure, I: experimental studies. *Circ Res* **84**(5): p. 562-570.

216. Okamoto, T., A. Schlegel, P.E. Scherer, and M.P. Lisanti (1998) Caveolins, a family of scaffolding proteins for organizing "preassembled signaling complexes" at the plasma membrane. *J Biol Chem* **273**(10): p. 5419-5422.

217. Olesen, C., M. Picard, A.M. Winther, C. Gyrup, J.P. Morth, C. Oxvig, J.V. Moller, and P. Nissen (2007) The structural basis of calcium transport by the calcium pump. *Nature* **450**(7172): p. 1036-1042.

218. Olesen, C., T.L. Sorensen, R.C. Nielsen, J.V. Moller, and P. Nissen (2004) Dephosphorylation of the calcium pump coupled to counterion occlusion. *Science* **306**(5705): p. 2251-2255.

219. On, C., C.R. Marshall, N. Chen, C.D. Moyes, and G.F. Tibbits (2008) Gene structure evolution of the Na+-Ca2+ exchanger (NCX) family. *BMC Evol Biol* **8**: p. 127.

220. Ottolia, M., D.A. Nicoll, and K.D. Philipson (2005) Mutational analysis of the alpha-1 repeat of the cardiac Na(+)-Ca2+ exchanger. *J Biol Chem* **280**(2): p. 1061-1069.

221. Ottolia, M., K.D. Philipson, and S. John (2004) Conformational changes of the Ca(2+) regulatory site of the Na(+)-Ca(2+) exchanger detected by FRET. *Biophys J* **87**(2): p. 899-906.

222. Pankratov, Y., U. Lalo, A. Verkhratsky, and R.A. North (2006) Vesicular release of ATP at central synapses. *Pflugers Arch* **452**(5): p. 589-597.

223. Papa, M., A. Canitano, F. Boscia, P. Castaldo, S. Sellitti, H. Porzig, M. Taglialatela, and L. Annunziato (2003) Differential expression of the Na+-Ca2+ exchanger transcripts and proteins in rat brain regions. *J Comp Neurol* **461**(1): p. 31-48.

224. Park, M.K., M.C. Ashby, G. Erdemli, O.H. Petersen, and A.V. Tepikin (2001) Perinuclear, perigranular and sub-plasmalemmal mitochondria have distinct functions in the regulation of cellular calcium transport. *Embo J* **20**(8): p. 1863-1874.

225. Pawson, T. and J.D. Scott (1997) Signaling through scaffold, anchoring, and adaptor proteins. *Science* **278**(5346): p. 2075-2080.

226. Pedersen, B.P., M.J. Buch-Pedersen, J.P. Morth, M.G. Palmgren, and P. Nissen (2007) Crystal structure of the plasma membrane proton pump. *Nature* **450**(7172): p. 1111-1114.

227. Penniston, J.T. and A. Enyedi (1998) Modulation of the plasma membrane Ca2+ pump. *J Membr Biol* **165**(2): p. 101-109.

228. Perkins, D.N., D.J. Pappin, D.M. Creasy, and J.S. Cottrell (1999) Probability-based protein identification by searching sequence databases using mass spectrometry data. *Electrophoresis* **20**(18): p. 3551-3567.

229. Petersen, O.H., M. Michalak, and A. Verkhratsky (2005) Calcium signalling: past, present and future. *Cell Calcium* **38**(3-4): p. 161-169.

230. Philipson, K.D., S. Longoni, and R. Ward (1988) Purification of the cardiac Na+-Ca2+ exchange protein. *Biochim Biophys Acta* **945**(2): p. 298-306.

231. Philipson, K.D., D.A. Nicoll, M. Ottolia, B.D. Quednau, H. Reuter, S. John, and Z. Qiu (2002) The Na+/Ca2+ exchange molecule: an overview. *Ann N Y Acad Sci* **976**: p. 1-10.

232. Pitts, B.J. (1979) Stoichiometry of sodium-calcium exchange in cardiac sarcolemmal vesicles. Coupling to the sodium pump. *J Biol Chem* **254**(14): p. 6232-6235.

233. Poch, E., S. Leach, S. Snape, T. Cacic, D.H. MacLennan, and J. Lytton (1998) Functional characterization of alternatively spliced human SERCA3 transcripts. *Am J Physiol* **275**(6 Pt 1): p. C1449-1458.

234. Pollak, N., C. Dolle, and M. Ziegler (2007) The power to reduce: pyridine nucleotides--small molecules with a multitude of functions. *Biochem J* **402**(2): p. 205-218.

235. Poon, S., S. Leach, X.F. Li, J.E. Tucker, P.P. Schnetkamp, and J. Lytton (2000) Alternatively spliced isoforms of the rat eye sodium/calcium+potassium exchanger NCKX1. *Am J Physiol Cell Physiol* **278**(4): p. C651-660.

236. Pott, C., X. Ren, D.X. Tran, M.J. Yang, S. Henderson, M.C. Jordan, K.P. Roos, A. Garfinkel, K.D. Philipson, and J.I. Goldhaber (2007) Mechanism of shortened action potential duration in Na+-Ca2+ exchanger knockout mice. *Am J Physiol Cell Physiol* **292**(2): p. C968-973.

237. Prakriya, M., S. Feske, Y. Gwack, S. Srikanth, A. Rao, and P.G. Hogan (2006) Orai1 is an essential pore subunit of the CRAC channel. *Nature* **443**(7108): p. 230-233.

238. Prinsen, C.F., R.T. Szerencsei, and P.P. Schnetkamp (2000) Molecular cloning and functional expression of the potassium-dependent sodium-calcium exchanger from human and chicken retinal cone photoreceptors. *J Neurosci* **20**(4): p. 1424-1434.

239. Pulina, M.V., R. Rizzuto, M. Brini, and E. Carafoli (2006) Inhibitory interaction of the plasma membrane Na+/Ca2+ exchangers with the 14-3-3 proteins. *J Biol Chem* **281**(28): p. 19645-19654.

240. Qiu, Z., D.A. Nicoll, and K.D. Philipson (2001) Helix packing of functionally important regions of the cardiac Na(+)-Ca(2+) exchanger. *J Biol Chem* **276**(1): p. 194-199.

241. Quednau, B.D., D.A. Nicoll, and K.D. Philipson (1997) Tissue specificity and alternative splicing of the Na+/Ca2+ exchanger isoforms NCX1, NCX2, and NCX3 in rat. *Am J Physiol* **272**(4 Pt 1): p. C1250-1261.

242. Raimondo, F., P. Ceppi, K. Guidi, M. Masserini, C. Foletti, and M. Pitto (2005) Proteomics of plasma membrane microdomains. *Expert Rev Proteomics* **2**(5): p. 793-807.

243. Randall, A. and C.D. Benham (1999) Recent advances in the molecular understanding of voltage-gated Ca2+ channels. *Mol Cell Neurosci* **14**(4-5): p. 255-272.

244. Reeves, J.P. and C.C. Hale (1984) The stoichiometry of the cardiac sodium-calcium exchange system. *J Biol Chem* **259**(12): p. 7733-7739.

245. Reeves, J.P. and J.L. Sutko (1980) Sodium-calcium exchange activity generates a current in cardiac membrane vesicles. *Science* **208**(4451): p. 1461-1464.

246. Reilander, H., A. Achilles, U. Friedel, G. Maul, F. Lottspeich, and N.J. Cook (1992) Primary structure and functional expression of the Na/Ca,K-exchanger from bovine rod photoreceptors. *Embo J* **11**(5): p. 1689-1695.

247. Reilly, R.F., C.A. Shugrue, D. Lattanzi, and D. Biemesderfer (1993) Immunolocalization of the Na+/Ca2+ exchanger in rabbit kidney. *Am J Physiol* **265**(2 Pt 2): p. F327-332.

248. Ren, Q., K. Chen, and I.T. Paulsen (2007) TransportDB: a comprehensive database resource for cytoplasmic membrane transport systems and outer membrane channels. *Nucleic Acids Res* **35**(Database issue): p. D274-279.

249. Ren, X., D.A. Nicoll, G. Galang, and K.D. Philipson (2008) Intermolecular cross-linking of Na+-Ca2+ exchanger proteins: evidence for dimer formation. *Biochemistry* **47**(22): p. 6081-6087.

250. Ren, X., D.A. Nicoll, and K.D. Philipson (2006) Helix packing of the cardiac Na+-Ca2+ exchanger: proximity of transmembrane segments 1, 2, and 6. *J Biol Chem* **281**(32): p. 22808-22814.

251. Ren, X., D.A. Nicoll, and K.D. Philipson (2007) Transmembrane segments I, II, and VI of the canine cardiac Na+/Ca2+ exchanger are in proximity. *Ann N Y Acad Sci* **1099**: p. 40-42.

252. Resh, M.D. and R.L. Erikson (1985) Highly specific antibody to Rous sarcoma virus src gene product recognizes a novel population of pp60v-src and pp60c-src molecules. *J Cell Biol* **100**(2): p. 409-417.

253. Reuter, H. and H. Porzig (1995) Localization and functional significance of the Na+/Ca2+ exchanger in presynaptic boutons of hippocampal cells in culture. *Neuron* **15**(5): p. 1077-1084.

254. Reuter, H. and N. Seitz (1968) The dependence of calcium efflux from cardiac muscle on temperature and external ion composition. *J Physiol* **195**(2): p. 451-470.

255. Rizo, J., X. Chen, and D. Arac (2006) Unraveling the mechanisms of synaptotagmin and SNARE function in neurotransmitter release. *Trends Cell Biol* **16**(7): p. 339-350.

256. Rizzuto, R. and T. Pozzan (2006) Microdomains of intracellular Ca2+: molecular determinants and functional consequences. *Physiol Rev* **86**(1): p. 369-408.

257. Robert, V., P. Gurlini, V. Tosello, T. Nagai, A. Miyawaki, F. Di Lisa, and T. Pozzan (2001) Beat-to-beat oscillations of mitochondrial [Ca2+] in cardiac cells. *Embo J* **20**(17): p. 4998-5007.

258. Rothberg, K.G., J.E. Heuser, W.C. Donzell, Y.S. Ying, J.R. Glenney, and R.G. Anderson (1992) Caveolin, a protein component of caveolae membrane coats. *Cell* **68**(4): p. 673-682.

259. Rutter, G.A. and E.A. Bellomo (2008) Ca2+ signalling: a new route to NAADP. *Biochem J* **411**(1): p. e1-3.

260. Ryan, M.T. and N.J. Hoogenraad (2007) Mitochondrial-nuclear communications. *Annu Rev Biochem* **76**: p. 701-722.

261. Saba, R.I., A. Bollen, and A. Herchuelz (1999) Characterization of the 70 kDa polypeptide of the Na/Ca exchanger. *Biochem J* **338 ( Pt 1)**: p. 139-145.

262. Sabatini, B.L., M. Maravall, and K. Svoboda (2001) Ca(2+) signaling in dendritic spines. *Curr Opin Neurobiol* **11**(3): p. 349-356.

263. Santacruz-Toloza, L., M. Ottolia, D.A. Nicoll, and K.D. Philipson (2000) Functional analysis of a disulfide bond in the cardiac Na(+)-Ca(2+) exchanger. *J Biol Chem* **275**(1): p. 182-188.

264. Sargiacomo, M., M. Sudol, Z. Tang, and M.P. Lisanti (1993) Signal transducing molecules and glycosyl-phosphatidylinositol-linked proteins form a caveolin-rich insoluble complex in MDCK cells. *J Cell Biol* **122**(4): p. 789-807.

265. Schagger, H. and G. von Jagow (1991) Blue native electrophoresis for isolation of membrane protein complexes in enzymatically active form. *Anal Biochem* **199**(2): p. 223-231.

266. Scheller, T., A. Kraev, S. Skinner, and E. Carafoli (1998) Cloning of the multipartite promoter of the sodium-calcium exchanger gene NCX1 and characterization of its activity in vascular smooth muscle cells. *J Biol Chem* **273**(13): p. 7643-7649.

267. Scherer, P.E., T. Okamoto, M. Chun, I. Nishimoto, H.F. Lodish, and M.P. Lisanti (1996) Identification, sequence, and expression of caveolin-2 defines a caveolin gene family. *Proc Natl Acad Sci U S A* **93**(1): p. 131-135.

268. Schlegel, A. and M.P. Lisanti (2001) Caveolae and their coat proteins, the caveolins: from electron microscopic novelty to biological launching pad. *J Cell Physiol* **186**(3): p. 329-337.

269. Schmolesky, M.T., J.T. Weber, C.I. De Zeeuw, and C. Hansel (2002) The making of a complex spike: ionic composition and plasticity. *Ann N Y Acad Sci* **978**: p. 359-390.

270. Schnetkamp, P.P., D.K. Basu, and R.T. Szerencsei (1989) Na+-Ca2+ exchange in bovine rod outer segments requires and transports K+. *Am J Physiol* **257**(1 Pt 1): p. C153-157.

271. Schwaller, B., M. Meyer, and S. Schiffmann (2002) 'New' functions for 'old' proteins: the role of the calcium-binding proteins calbindin D-28k, calretinin and parvalbumin, in cerebellar physiology. Studies with knockout mice. *Cerebellum* **1**(4): p. 241-258.

272. Schwarz, E.M. and S. Benzer (1997) Calx, a Na-Ca exchanger gene of Drosophila melanogaster. *Proc Natl Acad Sci U S A* **94**(19): p. 10249-10254.

273. Schwarzer, A., T.S. Kim, V. Hagen, R.S. Molday, and P.J. Bauer (1997) The Na/Ca-K exchanger of rod photoreceptor exists as dimer in the plasma membrane. *Biochemistry* **36**(44): p. 13667-13676.

274. Schwarzer, A., H. Schauf, and P.J. Bauer (2000) Binding of the cGMP-gated channel to the Na/Ca-K exchanger in rod photoreceptors. *J Biol Chem* **275**(18): p. 13448-13454.

275. Scriven, D.R., A. Klimek, P. Asghari, K. Bellve, and E.D. Moore (2005) Caveolin-3 is adjacent to a group of extradyadic ryanodine receptors. *Biophys J* **89**(3): p. 1893-1901.

276. Sheng, J.Z., C.F. Prinsen, R.B. Clark, W.R. Giles, and P.P. Schnetkamp (2000) Na(+)-Ca(2+)-K(+) currents measured in insect cells transfected with the retinal cone or rod Na(+)-Ca(2+)-K(+) exchanger cDNA. *Biophys J* **79**(4): p. 1945-1953.

277. Shogomori, H. and D.A. Brown (2003) Use of detergents to study membrane rafts: the good, the bad, and the ugly. *Biol Chem* **384**(9): p. 1259-1263.

278. Shyjan, A.W., C. Gottardi, and R. Levenson (1990) The Na,K-ATPase beta 2 subunit is expressed in rat brain and copurifies with Na,K-ATPase activity. *J Biol Chem* **265**(9): p. 5166-5169.

279. Simons, K. and W.L. Vaz (2004) Model systems, lipid rafts, and cell membranes. *Annu Rev Biophys Biomol Struct* **33**: p. 269-295.

280. Singer, S.J. and G.L. Nicolson (1972) The fluid mosaic model of the structure of cell membranes. *Science* **175**(23): p. 720-731.

281. Song, J., X.Q. Zhang, B.A. Ahlers, L.L. Carl, J. Wang, L.I. Rothblum, R.C. Stahl, J.P. Mounsey, A.L. Tucker, J.R. Moorman, and J.Y. Cheung (2005) Serine 68 of phospholemman is critical in modulation of contractility, [Ca2+]i transients, and Na+/Ca2+ exchange in adult rat cardiac myocytes. *Am J Physiol Heart Circ Physiol* **288**(5): p. H2342-2354.

282. Song, K.S., S. Li, T. Okamoto, L.A. Quilliam, M. Sargiacomo, and M.P. Lisanti (1996) Co-purification and direct interaction of Ras with caveolin, an integral

membrane protein of caveolae microdomains. Detergent-free purification of caveolae microdomains. *J Biol Chem* **271**(16): p. 9690-9697.

283. Song, L.S., S. Guatimosim, L. Gomez-Viquez, E.A. Sobie, A. Ziman, H. Hartmann, and W.J. Lederer (2005) Calcium biology of the transverse tubules in heart. *Ann N Y Acad Sci* **1047**: p. 99-111.

284. Sorensen, T.L., J.V. Moller, and P. Nissen (2004) Phosphoryl transfer and calcium ion occlusion in the calcium pump. *Science* **304**(5677): p. 1672-1675.

285. Strack, S. and R.J. Colbran (1998) Autophosphorylation-dependent targeting of calcium/ calmodulin-dependent protein kinase II by the NR2B subunit of the N-methyl- D-aspartate receptor. *J Biol Chem* **273**(33): p. 20689-20692.

286. Suzuki, T. (2002) Lipid rafts at postsynaptic sites: distribution, function and linkage to postsynaptic density. *Neurosci Res* **44**(1): p. 1-9.

287. Swamy, M., G.M. Siegers, S. Minguet, B. Wollscheid, and W.W. Schamel (2006) Blue native polyacrylamide gel electrophoresis (BN-PAGE) for the identification and analysis of multiprotein complexes. *Sci STKE* **2006**(345): p. pl4.

288. Szerencsei, R.T., C.F. Prinsen, and P.P. Schnetkamp (2001) Stoichiometry of the retinal cone Na/Ca-K exchanger heterologously expressed in insect cells: comparison with the bovine heart Na/Ca exchanger. *Biochemistry* **40**(20): p. 6009-6015.

289. Takechi, H., J. Eilers, and A. Konnerth (1998) A new class of synaptic response involving calcium release in dendritic spines. *Nature* **396**(6713): p. 757-760.

290. Tang, J., A. Maximov, O.H. Shin, H. Dai, J. Rizo, and T.C. Sudhof (2006) A complexin/synaptotagmin 1 switch controls fast synaptic vesicle exocytosis. *Cell* **126**(6): p. 1175-1187.

291. Tang, Z., P.E. Scherer, T. Okamoto, K. Song, C. Chu, D.S. Kohtz, I. Nishimoto, H.F. Lodish, and M.P. Lisanti (1996) Molecular cloning of caveolin-3, a novel member of the caveolin gene family expressed predominantly in muscle. *J Biol Chem* **271**(4): p. 2255-2261.

292. Toyoshima, C., M. Nakasako, H. Nomura, and H. Ogawa (2000) Crystal structure of the calcium pump of sarcoplasmic reticulum at 2.6 A resolution. *Nature* **405**(6787): p. 647-655.

293. Toyoshima, C. and H. Nomura (2002) Structural changes in the calcium pump accompanying the dissociation of calcium. *Nature* **418**(6898): p. 605-611.

294. Toyoshima, C., H. Nomura, and Y. Sugita (2003) Structural basis of ion pumping by Ca(2+)-ATPase of sarcoplasmic reticulum. *FEBS Lett* **555**(1): p. 106-110.

295. Toyoshima, C., H. Nomura, and T. Tsuda (2004) Lumenal gating mechanism revealed in calcium pump crystal structures with phosphate analogues. *Nature* **432**(7015): p. 361-368.

296. Trevino, C.L., C.J. Serrano, C. Beltran, R. Felix, and A. Darszon (2001) Identification of mouse trp homologs and lipid rafts from spermatogenic cells and sperm. *FEBS Lett* **509**(1): p. 119-125.

297. Tsoi, M., K.H. Rhee, D. Bungard, X.F. Li, S.L. Lee, R.N. Auer, and J. Lytton (1998) Molecular cloning of a novel potassium-dependent sodium-calcium exchanger from rat brain. *J Biol Chem* **273**(7): p. 4155-4162.

298. Tucker, J.E., R.J. Winkfein, C.B. Cooper, and P.P. Schnetkamp (1998) cDNA cloning of the human retinal rod Na-Ca + K exchanger: comparison with a revised bovine sequence. *Invest Ophthalmol Vis Sci* **39**(2): p. 435-440.

299. Tucker, J.E., R.J. Winkfein, S.K. Murthy, J.S. Friedman, M.A. Walter, D.J. Demetrick, and P.P. Schnetkamp (1998) Chromosomal localization and genomic organization of the human retinal rod Na-Ca+K exchanger. *Hum Genet* **103**(4): p. 411-414.

300. van Heusden, G.P. (2005) 14-3-3 proteins: regulators of numerous eukaryotic proteins. *IUBMB Life* **57**(9): p. 623-629.

301. Veenhoff, L.M., E.H. Heuberger, and B. Poolman (2002) Quaternary structure and function of transport proteins. *Trends Biochem Sci* **27**(5): p. 242-249.

302. Visser, F. and J. Lytton (2007) K+ -dependent Na+/Ca2+ exchangers: key contributors to Ca2+ signaling. *Physiology (Bethesda)* **22**: p. 185-192.

303. Visser, F., V. Valsecchi, L. Annunziato, and J. Lytton (2007) Exchangers NCKX2, NCKX3, and NCKX4: identification of Thr-551 as a key residue in defining the apparent K(+) affinity of NCKX2. *J Biol Chem* **282**(7): p. 4453-4462.

304. Volonte, D., F. Galbiati, S. Li, K. Nishiyama, T. Okamoto, and M.P. Lisanti (1999) Flotillins/cavatellins are differentially expressed in cells and tissues and form a hetero-oligomeric complex with caveolins in vivo. Characterization and epitope-mapping of a novel flotillin-1 monoclonal antibody probe. *J Biol Chem* **274**(18): p. 12702-12709.

305. Wakimoto, K., K. Kobayashi, O.M. Kuro, A. Yao, T. Iwamoto, N. Yanaka, S. Kita, A. Nishida, S. Azuma, Y. Toyoda, K. Omori, H. Imahie, T. Oka, S. Kudoh, O. Kohmoto, Y. Yazaki, M. Shigekawa, Y. Imai, Y. Nabeshima, and I. Komuro (2000) Targeted disruption of Na+/Ca2+ exchanger gene leads to cardiomyocyte apoptosis and defects in heartbeat. *J Biol Chem* **275**(47): p. 36991-36998.

306. Wang, J., X.Q. Zhang, B.A. Ahlers, L.L. Carl, J. Song, L.I. Rothblum, R.C. Stahl, D.J. Carey, and J.Y. Cheung (2006) Cytoplasmic tail of phospholemman interacts with the intracellular loop of the cardiac Na+/Ca2+ exchanger. *J Biol Chem* **281**(42): p. 32004-32014.

307. Wehrens, X.H., S.E. Lehnart, and A.R. Marks (2005) Intracellular calcium release and cardiac disease. *Annu Rev Physiol* **67**: p. 69-98.

308. Wier, W.G. and C.W. Balke (1999) Ca(2+) release mechanisms, Ca(2+) sparks, and local control of excitation-contraction coupling in normal heart muscle. *Circ Res* **85**(9): p. 770-776.

309. Winslow, R.L., J. Rice, S. Jafri, E. Marban, and B. O'Rourke (1999) Mechanisms of altered excitation-contraction coupling in canine tachycardia-induced heart failure, II: model studies. *Circ Res* **84**(5): p. 571-586.

310. Woodman, S.E., D.S. Park, A.W. Cohen, M.W. Cheung, M. Chandra, J. Shirani, B. Tang, L.A. Jelicks, R.N. Kitsis, G.J. Christ, S.M. Factor, H.B. Tanowitz, and M.P. Lisanti (2002) Caveolin-3 knock-out mice develop a progressive cardiomyopathy and show hyperactivation of the p42/44 MAPK cascade. *J Biol Chem* **277**(41): p. 38988-38997.

311. Worley, P.F., W. Zeng, G. Huang, J.Y. Kim, D.M. Shin, M.S. Kim, J.P. Yuan, K. Kiselyov, and S. Muallem (2007) Homer proteins in Ca2+ signaling by excitable and non-excitable cells. *Cell Calcium* **42**(4-5): p. 363-371.

312. Yu, A.S., S.C. Hebert, S.L. Lee, B.M. Brenner, and J. Lytton (1992) Identification and localization of renal Na(+)-Ca2+ exchanger by polymerase chain reaction. *Am J Physiol* **263**(4 Pt 2): p. F680-685.

313. Zhang, X.Q., B.A. Ahlers, A.L. Tucker, J. Song, J. Wang, J.R. Moorman, J.P. Mounsey, L.L. Carl, L.I. Rothblum, and J.Y. Cheung (2006) Phospholemman inhibition of the cardiac Na+/Ca2+ exchanger. Role of phosphorylation. *J Biol Chem* **281**(12): p. 7784-7792.

314. Zylinska, L. and M. Soszynski (2000) Plasma membrane Ca2+-ATPase in excitable and nonexcitable cells. *Acta Biochim Pol* **47**(3): p. 529-539.